Chapter 3

SPECTROSCOPY

Conveners: G. Bali, N. Brambilla, R. Mussa, J. Soto

Authors: G. Bali, D. Besson, A. Böhrer, N. Brambilla, P. Cooper, C. Davies, E. Eichten, S. Eidelman, R. Faustov, T. Ferguson, R. Galik, S. Godfrey, A. Kronfeld, P. Mackenzie, C. Morningstar, R. Mussa, V. Papadimitriou, A. Pineda, S. Ricciardi, J. -M. Richard, E. Robutti, J. Simone, T. Skwarnicki, J. Soto, G. Stancari, Yu. Sumino, J. Tseng, B. Yabsley, Z. Zhao

1 THEORY INTRODUCTION[1]

Most theorists agree that QCD alone should describe the spectroscopy of heavy quarkonium. Nevertheless, there are important difficulties to do so in practise. One can roughly distinguish between two approaches: the phenomenological and the theoretical one.

The phenomenological approach attempts to model what are believed to be the features of QCD relevant to heavy quarkonium with the aim to produce concrete results which can be directly confirmed or falsified by experiment and may guide experimental searches. The theoretical approach tries to describe heavy quarkonium with QCD based calculations and/or approximations.

The basic tools of the phenomenological approach are potential models, both non-relativistic and relativistic. The use of non-relativistic potential models is justified by the fact that the bottom and, to a lesser extent, the charm masses are large in comparison to $\Lambda_{\rm QCD}$, the typical hadronic scale. Hence a quantum mechanical description of the system based on two heavy quarks interacting through a suitable potential appears reasonable. The potential is usually chosen in a way that at short distances coincides with the weak coupling QCD one-gluon exchange Coulomb potential and in the long range it incorporates confinement, for instance, by including a linearly rising potential. Since relativistic effects appear to be sizable for some states, mostly in charmonium, models incorporating some relativistic kinematics are also being used. Different models of quark confinement may result in different classes of relativistic corrections. For states close to and beyond the two heavy-light meson threshold, the potential models have to be complemented with these extra degrees of freedom in order to account for possible mixing effects. Hybrid states which are expected from QCD should also be incorporated by hand. The phenomenological approaches will be described in Section 3.

The theoretical approach aims at obtaining the spectrum of heavy quarkonium from QCD. This is in principle more complicated than obtaining masses of light mesonic states since an additional large scale m, the mass of the heavy quark, enters the calculation. If we assume that m is much larger than any other scale in the system, in particular $\Lambda_{\rm QCD}$, the heavy quark and antiquark are expected to move slowly about each other at a relative velocity $v \ll 1$. The system becomes non-relativistic and hence splittings between states with the same quantum numbers are expected to be of size $\sim mv^2$ whereas hyperfine splittings are of order $\sim mv^4$, if one proceeds by analogy to QED bound states (where $v \sim \alpha$). If $v^2 \sim 0.1$, as expected in ground state bottomonium, a direct (lattice) QCD calculation requires a precision significantly better than 10 % to detect spin-averaged masses and of more than 1 % to resolve fine structure splittings. Moreover, all these scales have to be resolved on one and the same lattice, necessitating many lattice points. This is to be compared with light quarkonium where the splittings are a leading order effect. Consequently, calculating the heavy quarkonium spectrum from lattice QCD

[1] Author: J. Soto

requires a tremendous computational effort, which in some cases can be somewhat ameliorated with the introduction of anisotropic lattices, as discussed in Section 2.1.

Alternatively, it may be advisable to exploit the fact that m is large and v small before attempting the computation. This is most efficiently done using non relativistic effective field theories. The effective theory which takes into account that m is much larger than the remaining scales in the system is NRQCD [1–3]. Since $m \gg \Lambda_{QCD}$, NRQCD can be made equivalent to QCD at any desired order in $1/m$ and $\alpha_{\rm s}(m) \ll 1$ by enforcing suitable matrix elements to be equal at that order in both theories. One may then attempt a lattice calculation from NRQCD. What one gains now is that the spin independent splittings are a leading order effect rather than a v^2 one and the hyperfine splittings a v^2 correction (rather than v^4). See Section 2.2.1 for a detailed discussion of these calculations.

NRQCD, however, does not fully exploit the fact that v is small. In particular, gluons of energy $\sim mv$, the typical relative three-momentum of the heavy quarks, are still explicit degrees of freedom in NRQCD whereas they can never be produced at energies $\sim mv^2$. For lower lying states the scale mv corresponds both to the typical momentum transfer k (inverse size of the system) and to the typical relative three-momentum p. It is then convenient to introduce a further effective theory where degrees of freedom of energy $\sim k$ are integrated out. This EFT is called pNRQCD [4, 5], see Section 2.3. The degrees of freedom of pNRQCD depend on the interplay of the scales k, $E \sim mv^2$ and $\Lambda_{\rm QCD}$. The weak and strong coupling regimes are discussed respectively in Section 2.3.1 and 2.3.2. A related EFT for the weak coupling regime, called vNRQCD [6], will be discussed in Chapter 6 (Standard Model). Sum rules are also discussed in the same chapter in relation to the calculation of the lowest energy levels in the spectrum.

The distribution of the theory contributions is as follows. We begin with the theoretical approach and use the EFT philosophy as an organizing principle. We shall arrange the contributions according to the number of hypothesis that are done in order to obtain them from QCD. Hence, we shall start by contributions which rely on QCD only. Next we will discuss contributions which may be embraced by NRQCD, and finally contributions which may be embraced by pNRQCD. We would like to emphasize that, if the relevant hypothesis are fulfilled, (i) NRQCD and pNRQCD are equivalent to QCD, and (ii) each of these EFTs allows to factorize a relevant scale, which further simplifies calculations. All the states can in principle be studied from QCD, the main tool being lattice techniques. In practise, however, a number of limitations exists, which are described in Section 2.1. Except for very high excitations (particularly in charmonium) for which relativistic effects become important, these states can also be studied from NRQCD, the main tool being again lattice techniques, see Section 2.2. States below and not too close to open flavour threshold can also be studied using pNRQCD. A few of these, including the $\Upsilon(1S)$ and $\eta_b(1S)$, can be studied by means of analytical weak coupling techniques (Section 2.3.1). The remaining ones can be studied using pNRQCD in the strong coupling regime (Section 2.3.2), which needs as an input nonperturbative potentials to be calculated on the lattice. We continue next with the phenomenological approach, which mainly consist of a description of potential models (Section 3.1) and of approaches to open flavour thresholds (Section 3.3). The former provide good phenomenological descriptions for the states below open flavour threshold whereas the latter are important for a good description of excitations close or above the open flavour threshold, in particular of the recently discovered $X(3872)$ charmonium state. An effort has been made to link potential models to the theoretical approach. Double (and triple) heavy baryons are also discussed both in the theoretical (Sections 2.2.3, 2.3.4) and phenomenological approach (Section 3.4.2).

2 THEORETICAL APPROACH

2.1 Direct lattice QCD calculation[2]

2.1.1 Methods

(For an introduction to general QCD lattice methods cf. Chapter 1.) When simulating quarks with a mass m on a lattice with lattice spacing a, one will inevitably encounter ma [or $(ma)^2$] corrections, which are of order one, unless $m \ll a^{-1}$. The Fermilab group [7] have argued in favour of a re-interpretation of the clover action, suggesting that physical results can be obtained even for masses as large as $ma \approx 1$, see also Section 2.2.1 below. However, still one would either want to extrapolate such results to the continuum limit or at least put them into the context of an effective field theory with two large scales, in this case m and a^{-1}. If interpreted as an EFT, higher order terms have to be added and the matching coefficients to QCD have to be determined to sufficiently high order in perturbation theory, to reduce and estimate remaining systematic uncertainties.

In the quenched approximation, the condition $ma \ll 1$ can be realized for charm quarks; however, at present bottom quarks are still somewhat at the borderline of what is possible. One approach to tackle this problem is to introduce an anisotropy, with a temporal lattice spacing a_τ smaller than the spatial lattice spacing $a_\sigma = \xi a_\tau$, with parameter $\xi > 1$. The spatial lattice extent $L_\sigma a_\sigma$ has to be large enough to accommodate the quarkonium state (whose size is of order $r \simeq (mv)^{-1}$). With a sufficiently large a_σ this is possible, keeping the number of points L_σ limited, while the temporal lattice spacing can be chosen to be smaller than the quarkonium mass in question, $a_\tau < M^{-1}$, at relative ease. This means that anisotropic simulations are naively cheaper by a factor ξ^3, compared to the isotropic analogue with a lattice spacing $a = a_\tau$.

While at tree level the lattice spacing errors are indeed of $\mathcal{O}[(ma_\tau)^n]$, one loop corrections mean that there will still be $\mathcal{O}[\alpha_{\rm s}(ma_\sigma)^n]$ terms present: only to the extent to which $\alpha_{\rm s}\xi^n$ is small, the leading order lattice effects can be regarded as $\mathcal{O}[(ma_\tau)^n]$. Furthermore, the anisotropy parameter ξ has to be determined consistently for the quark and gluon contributions to the QCD action. Within the quenched approximation this problem factorizes: one can first "measure" the gauge anisotropy by determining the decay of purely gluonic spatial and temporal correlation functions. Subsequently, one can adjust the Fermionic anisotropy accordingly. This fine-tuning does not come for free, in particular if the number of adjustable parameters is larger than two. Consequently, no consistent nonperturbative $\mathcal{O}(a)$ improvement programme has been carried through so far, for non-trivial anisotropies. While there might be a net gain from using anisotropy techniques in the quenched approximation, the parameter tuning becomes much more delicate and costly once light sea quarks are included. In this case the numerical matching of the anisotropy for light Fermions cannot be disentangled from the gluonic one anymore.

2.1.2 Results with relativistic heavy quarks

We will first review results on the quenched bottomonium spectrum, before discussing charmonia in the quenched approximation, on anisotropic as well as on isotropic lattices and with sea quarks.

Only one bottomonium study with relativistic action has been performed so far [8], employing lattices with anisotropies $\xi = 4$ and $\xi = 5$, in the quenched approximation. In this case, the inverse lattice spacing, a_τ^{-1} was varied from 4.5 GeV up to about 10.5 GeV. The lattice extents were typically of size $L_\sigma a_\sigma \approx 1$ fm, however, they were not kept constant when varying a_τ such that finite size effects are hard to disentangle. The spatial lattice sizes are also dangerously close to the inverse confinement–deconfinement phase transition temperature (cf. Chapter 7). After using the $1^1P_1 - 1^3S_1$ splitting (identifying the 1^1P_1 mass with the spin averaged experimental $1^{\overline{3}}\overline{P}$ states) to set the lattice spacing and the 1^3S_1 to adjust the b quark mass, qualitative agreement with the spin-averaged experimental spectrum is observed.

[2] Author: G. Bali

Table 3.1: Charmonium results in the quenched approximation [9–12], where the scale is such that $r_0^{-1} = 394$ MeV. The purely statistical errors do not reflect the uncertainty in r_0, or due to quenching. All values are in units of MeV. Glueball masses [13–15] are included for comparison. The last three lines refer to spin-exotic (non-quark model) quantum numbers.

J^{PC}	state	CP–PACS	Columbia	QCD-TARO	experiment	glueballs
0^{-+}	η_c	3013 (1)	3014 (4)	3010 (4)	2980(1)	2500(40)
	η_c'	3739(46)	3707(20)		3654(10)	3500(60)
1^{--}	J/ψ	3085 (1)	3084 (4)	3087 (4)	3097	
	$\psi(2S)$	3777(40)	3780(43)		3686	3700(50)
1^{+-}	h_c	3474(10)	3474(20)	3528(25)	$m(1^3\overline{P})$=3525	2830(30)
	h_c'	4053(95)	3886(92)		—	
0^{++}	χ_{c0}	3408	3413(10)	3474(15)	3415(1)	1720(30)
	χ_{c0}'	4008(122)	4080(75)		—	2540(120)
1^{++}	χ_{c1}	3472 (9)	3462(15)	3524(16)	3511	
	χ_{c1}'	4067(105)	4010(70)		—	
2^{++}	χ_{c2}	3503(24)	3488(11)		3556	2300(25)
	χ_{c2}'	4030(180)			—	
2^{-+}	1^1D_2		3763(22)		—	2975(30)
					—	3740(40)
2^{--}	1^3D_2		3704(33)		$X(3872)$???	3780(40)
3^{--}	1^3D_3		3822(25)		—	3960(90)
3^{+-}	1^1F_3		4224(74)		—	3410(40)
3^{++}	1^3F_3		4222(140)		—	3540(40)
0^{+-}	H_0		4714(260)		—	4560(70)
1^{-+}	H_1		4366(64)		—	
2^{+-}	H_2		4845(220)		—	3980(50)

For the $1^3S_1 - 1^1S_1$ splitting, where one might hope finite size effects to largely cancel, the authors obtain the continuum extrapolated value of 59 ± 20 MeV. To leading order in pQCD, this splitting is expected to be proportional to the wave function density at the origin, multiplied by $\alpha_{\rm s}(\mu)$. Adjusting the lattice spacing from spin-averaged splittings amounts to matching the quenched lattice coupling to the phenomenological one at a low energy scale $\ll \mu$. In the quenched approximation $\alpha_{\rm s}(\mu)$ approaches zero faster as μ is increased and hence $\alpha_{\rm s}(\mu)$ will be underestimated: the quoted fine structure splitting represents a lower limit on the phenomenological one. Indeed, the analogous result for the charmonium case underestimates the known experimental number by a factor 1.25–1.5, when setting the scale in a similar way [9, 10].

Both, the Columbia group [11, 12] as well as the CP–PACS Collaboration [9] have studied the charmonium spectrum on anisotropic lattices. The same anisotropic clover quark action was used as for the bottomonium study discussed above, where the leading order lattice artefacts are expected to be of $\mathcal{O}(\alpha_{\rm s}a_\tau)$ and $\mathcal{O}(a_\tau^2)$. The CP–PACS Collaboration studied the anisotropy, $\xi = 3$, on a set of four inverse lattice spacings a_σ^{-1}, ranging from about 1 up to 2.8 GeV, on spatial volumes $(1.6\,\mathrm{fm})^3$. The Columbia group simulated four lattice spacings ranging from about 0.8 up to 2 GeV at anisotropy $\xi = 2$. They were able to vary their volume from 1.5 up to 3.3 fm and found finite volume effects to be below their statistical resolution.

We display the respective continuum-limit extrapolated results in Table 3.1. We also include results from the QCD–TARO collaboration [10], with $\xi = 1$. The quark mass is set such that the spin averaged $1\overline{S}$ state corresponds to 3067.6 MeV. (Note that the present phenomenological value is slightly higher than this.) For comparison we convert the Columbia results into units of $r_0^{-1} = 394$ MeV. This

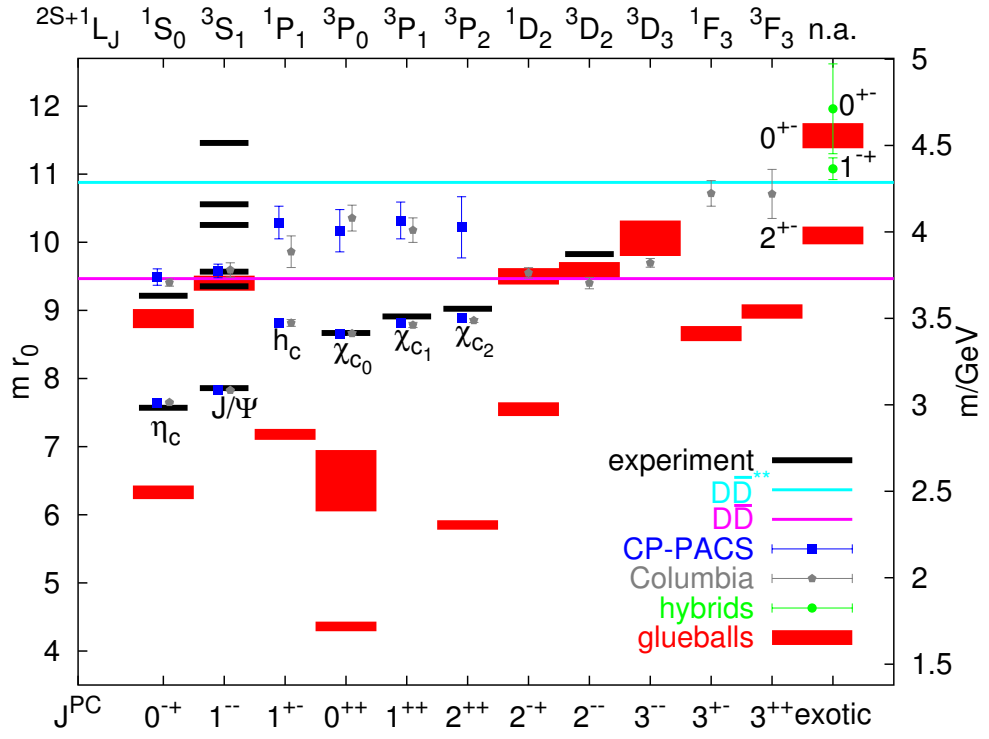

Fig. 3.1: The quenched charmonium spectrum (CP–PACS [9], Columbia [11, 12]), glueballs [13–15] and spin-exotic $c\bar{c}$-glue hybrids [12], overlayed with the experimental spectrum.

scale is implicitly defined through the static potential [16], $dV(r)/dr|_{r=r_0} = 1.65$. It cannot directly be obtained in experiment. However, r_0/a is easily and very precisely calculable in lattice simulations. In the quenched approximation we have to assume a scale error on spin averaged splittings of at least 10 %, on top of the errors displayed in the Table. We also include glueball masses [13–15] into the table. The last three lines incorporate spin-exotic J^{PC} assignments ($c\bar{c}g$ hybrid mesons).

The anisotropic results are also displayed in Fig. 3.1, borrowed from Ref. [17], where we plot the new $X(3872)$ state at $J^{PC} = 2^{--}$, however, this assignment is somewhat arbitrary. As can be seen, where overlap exists, the results from the three collaborations employing three different anisotropies are consistent with each other. All S- and P-wave fine structure splittings are underestimated, which is expected in the quenched approximation. The Columbia group [12] reported that the state created by the $J = 1$ D-wave operator rapidly converged towards the mass of the vector S-wave ground state. The same was observed in the case of the 2^{++} F-wave with respect to the χ_{c2} ground state: this indicates that the charm quark mass is too light for L to be a good quantum number.

That the charm mass is not particularly heavy, in comparison to typical scales of gluonic excitations, can also be seen from the overlap between the glueball and charmonium spectra. Once sea quarks are switched on, these glueballs will become unstable. However, the presence of a background of such excitations might very well affect spectrum and decays in some channels. For instance the dominant decay of a vector charmonium is into gluons, and it is quite conceivable that such a channel should also couple to would-be glueballs.

When performing the Wick contractions of propagators of flavour singlet states like charmonia, two contributions arise: a connected one, with quark and antiquark propagating alongside each other, and a disconnected (OZI suppressed) one, with annihilation and creation diagrams of $c\bar{c}$. In all charmonium simulations that have been performed so far, with two notable exceptions [18, 19], the disconnected diagram has been neglected. It is well known that OZI processes play a role within the light pseudoscalar

and scalar sectors. This has also been extensively studied on the lattice [20,21]. In the case of charmonia, in particular for S and D waves, substantial corrections due to mixing with intermediate gluonic states are a possibility, even within the quenched approximation. For states that are close to threshold, in addition mixing with two-meson states will occur, once sea quarks are included.

Charmonia have also been studied on isotropic lattices, within the quenched approximation [10, 18, 19, 22, 23], and with sea quarks [24]. The QCD–TARO collaboration [10] worked at tiny lattice spacings, ranging from about 2 GeV down to 5 GeV. The results are consistent with those obtained by the Columbia group [12] and by CP–PACS [9], but the use of an $\mathcal{O}(a)$ improved action allowed for a very well controlled continuum limit extrapolation. The quenched value, within the OZI approximation and using $r_0^{-1} = 394$ MeV to set the scale, is 77(2)(6) MeV, with all remaining systematic errors quoted. This value would increase by 15 % if the scale was set from the $1^3\overline{P} - 1\overline{S}$, still short of the experimental 117 MeV.

In an exploratory study, in which for the first time the diagram that contains disconnected quark loops has been included, McNeile and Michael [18] find evidence that while the position of the ground state vector state appears to be largely unaffected, the pseudoscalar mass is reduced by an amount of the order of 20 MeV with respect to the non-flavour singlet reference value. One explanation might be the background of glueballs, c.f. Fig. 3.1. A more recent study by QCD–TARO [19] confirms that the vector state remains largely unaffected. They rule out an increase of the pseudoscalar mass, however, a decrease by an amount of up to 20 MeV would not contradict their data.

First studies [24] utilizing the AsqTad staggered light quark action and approximating $2 + 1$ flavours of sea quarks by taking roots of the Fermionic determinant have been performed. The light quark mass was varied down to about $m_s/6$. The $\mathcal{O}(\alpha_s a)$ clover action, in the Fermilab heavy quark interpretation [7] was used. Extrapolating to physical sea quark mass, a hyperfine structure splitting of 97(2) MeV is obtained, see also Section 2.2.1 below. This is an increase of almost 40 %, over their quenched reference value. At least the latter would have been somewhat smaller if normalized with respect to r_0 rather than to the $\Upsilon' - \Upsilon$ splitting. However, OZI diagrams have been neglected and neither is the lattice spacing dependence resolved as yet. Clearly, a precision study of the charmonium spectrum requires not only sea quarks but also flavour singlet diagrams to be included.

2.2 NRQCD

NRQCD takes advantage that the masses of the charm and bottom quarks are much larger than $\Lambda_{\rm QCD}$ in order to build an EFT which is equivalent to QCD at any desired order in $1/m$ and $\alpha_s(m)$. Starting from NRQCD two approaches may be followed for spectrum computations: direct lattice calculations (Section 2.2.1) or further integration of the soft scale (the scale of the momentum transfer) to arrive at an EFT in which only the ultrasoft degrees of freedom remain dynamical, pNRQCD (Section 2.3). An introduction to NRQCD is given in Chapter 1, see also Refs. [25–27] for some introduction to the nonrelativistic EFT formulation. An introduction to lattice methods (quenched and unquenched) has been given in Chapter 1.

2.2.1 Lattice NRQCD calculations with light sea quarks[3]

The use of non-relativistic effective field theories permits the computer to handle only scales appropriate to the physics of the non-relativistic bound states without having to spend a lot of computer power on the large scale associated with the heavy quark mass which is irrelevant to the bound state dynamics. This makes the calculations more tractable so that many more hadron correlators can be calculated for better statistical precision. We will focus our discussion on the most recent calculations obtained within this approach, which include light sea quarks.

[3] Authors: C. Davies, A. Kronfeld, P. Mackenzie, J. Simone

On the lattice, heavy quark effects and discretisation effects are intertwined. One can treat them together by introducing an effective Lagrangian [28, 45]

$$\mathcal{L} = \; - \; \psi^\dagger \Bigg[\delta m + D_4 - \frac{\boldsymbol{D}^2}{2m} - \frac{c_4^{\rm lat}}{8m^3} \left(\boldsymbol{D}^2\right)^2 - \frac{w_1^{\rm lat} a^2}{6m} \sum_i D_i^4 - \frac{c_D^{\rm lat}}{8m^2} \left(\boldsymbol{D} \cdot g\boldsymbol{E} - g\boldsymbol{E} \cdot \boldsymbol{D}\right) - \frac{c_S^{\rm lat}}{8m^2} i\boldsymbol{\sigma} \cdot \left(\boldsymbol{D} \times g\boldsymbol{E} + g\boldsymbol{E} \times \boldsymbol{D}\right) - \frac{c_F^{\rm lat}}{2m} \boldsymbol{\sigma} \cdot g\boldsymbol{B} \Bigg] \psi + \cdots , \tag{3.1}$$

similar to the standard (continuum) NRQCD Lagrangian, but note that the derivative operators are 'improved' on the lattice to remove leading errors arising from the lattice spacing. See also the Section 3.2.3 "Heavy Quark Actions" in Chapter 1. We have omitted the term $\psi^\dagger m \psi$.

Compared to the NRQCD description of continuum QCD, an unimportant difference is the Euclidean metric (D_4 instead of $-iD_0$). Also, unlike in dimensional regularization, in lattice regularization the mass shift δm will in general be non-zero. However, this cancels from mass differences and decay amplitudes. Moreover, it can be determined nonperturbatively from the Υ dispersion relation. Obviously, terms accompanied by w_i are lattice specific. The essential difference is that the matching scale is provided by the lattice spacing: the short-distance coefficients $c_i^{\rm lat}$, $w_i^{\rm lat}$ and δm depend on am and on the details of the chosen discretisation. The matching of $c_i^{\rm lat}$ and $w_i^{\rm lat}$ is carried out to some accuracy in $\alpha_{\rm s}$. From Eq. (3.1) one sees that the most important matching condition is to identify the kinetic mass m with the heavy quark mass in the lattice scheme, and then tune the higher-dimension interactions.

One area of lattice QCD which has remained problematic is the handling of light quarks on the lattice. This is now being addressed successfully and is critical to obtaining precision results of use to experiment. In particular the problem is how to include the dynamical (sea) $u/d/s$ quark pairs that appear as a result of energy fluctuations in the vacuum. We can often safely ignore $c/b/t$ quarks in the vacuum because they are so heavy, but we know that light quark pairs have significant effects, for example in screening the running of the gauge coupling and in generating Zweig-allowed decay modes for unstable mesons.

Many calculations in the past have used the "quenched approximation," attempting to compensate sea quark effects by *ad hoc* shifts in the bare coupling and (valence) quark masses. The results then suffer from errors as large as 10–30%. The error of the quenched approximation is not really quantifiable and this is reflected by a lack of internal consistency when different kinds of hadrons are used to fix the bare parameters. This ambiguity plagues the lattice QCD literature.

The MILC Collaboration recently have produced ensembles of gluon field configurations which include 2 degenerate light sea quarks (u, d) and a heavier one (s) [30]. They rely on fast supercomputers and a new discretisation of the quark action: the improved staggered formalism [31]. At quark masses small enough for reliable chiral extrapolations, staggered Fermions appear much faster than any other formulation of lattice Fermions. However, each flavour of staggered quarks is included in the sea by taking the fourth root of the staggered determinant and there are still theoretical issues to be resolved about this. Taking the u and d masses the same makes the lattice calculation much faster and leads to negligible errors in isospin-averaged quantities. The sea s quark mass is chosen to be approximately correct based on earlier studies (in fact the subsequent analysis shows that it was slightly high and further ensembles are now being made with a lower value). The sea u and d quarks take a range of masses down as low as a sixth of the (real) m_s. Ensembles are available at two different values of the lattice spacing, 0.12 fm and 0.09 fm, and the spatial lattice volume is $(2.5\ {\rm fm})^3$, reasonably large. Analysis of hadronic quantities on these ensembles has been done by the MILC and HPQCD collaborations [29].

There are 5 bare parameters of QCD relevant to this analysis: $\alpha_{\rm s}$, $m_{u/d}$, m_s, m_c and m_b. Changing the bare $\alpha_{\rm s}$ changes the lattice spacing. It is important to fix these parameters with the masses of "gold-plated" hadrons, i.e., hadrons which are well below their strong decay thresholds. Such hadrons are well-defined experimentally and theoretically and should be accurately calculable in lattice QCD.

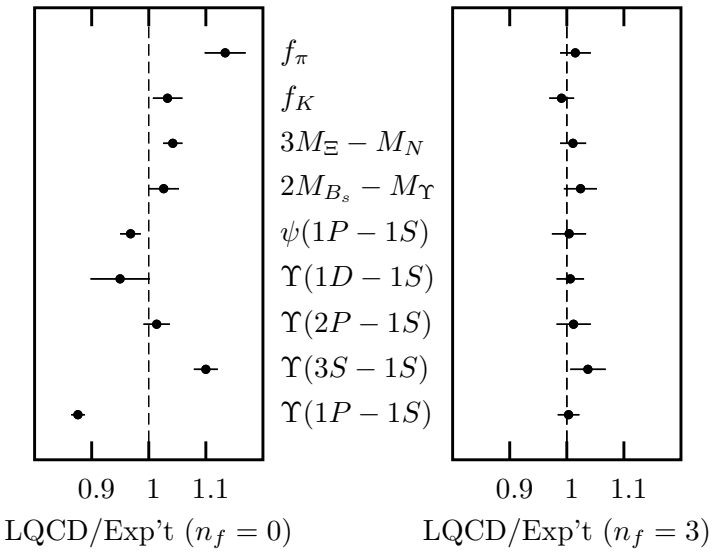

Fig. 3.2: Lattice QCD results divided by experiment for a range of "gold-plated" quantities which cover the full range of hadronic physics [29]. The unquenched calculations on the right show agreement with experiment across the board, whereas the quenched approximation on the left yields systematic errors of $\mathcal{O}(10\%)$.

Using them to fix parameters will then not introduce unnecessary additional systematic errors into lattice results for other quantities. This has not always been done in past lattice calculations, particularly in the quenched approximation. It becomes an important issue when lattice QCD is to be used as a precision calculational tool. We use the radial excitation energy in the Υ system (i.e., the mass splitting between the Υ' and the Υ) to fix the lattice spacing. This is a good quantity to use because it is very insensitive to all quark masses, including the b quark mass (experimental values for this splitting are very similar for charmonium and bottomonium) and so it can be determined without a complicated iterative tuning process. m_π, m_K, m_{D_s} and m_Υ are used to fix the quark masses. Thus, quarkonium turns out to be a central part in this study.

Once the Lagrangian parameters are set, we can focus on the calculation of other gold-plated masses and decay constants. If QCD is correct and lattice QCD is to work it must reproduce the experimental results for these quantities precisely. Figure 3.2 shows that this indeed works for the unquenched calculations with u, d and s quarks in the vacuum. A range of gold-plated hadrons are chosen which range from decay constants for light hadrons through heavy-light masses to heavy quarkonium. This tests QCD in different regimes in which the sources of systematic error are very different and stresses the point that QCD predicts a huge range of physics with a small set of parameters.

Refs. [24, 32–34] give more details on the quantities shown in Fig. 3.2. Here we concentrate on the spectrum of bottomonium and charmonium states, using, respectively, lattice NRQCD [35] and the Fermilab method for heavy quarks [7]. We include a brief discussion of the B_c mass, including the status of an ongoing unquenched calculation using the MILC ensembles.

Υ results with NRQCD

Figure 3.3(a) shows the radial and orbital splittings [33] in the $b\bar{b}$ (Υ) system for the quenched approximation (n_f = 0) and with the dynamical MILC configurations with 3 flavours of sea quarks. We use the standard lattice NRQCD effective theory for the valence b quarks [35], which takes advantage of the non-relativistic nature of the bound states. The lattice NRQCD action used here is accurate through v^4 where v is the velocity of the b quark in its bound state. It also includes corrections to remove discretisation errors at $\mathcal{O}(p^2a^2v^2) \sim \mathcal{O}(v^4)$, but does not include $\mathcal{O}(\alpha_s v^4)$ corrections to the coefficients c_i and

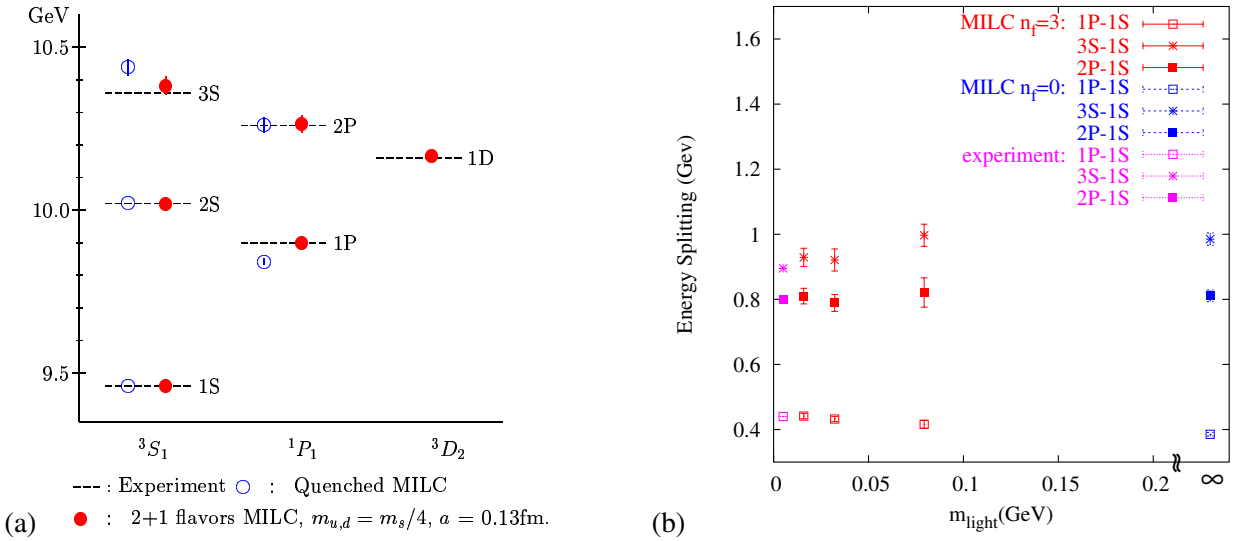

Fig. 3.3: Radial and orbital splittings in the Υ system from lattice QCD, using the $\Upsilon' - \Upsilon$ splitting and the Υ mass to fix the lattice spacing and the b-quark mass [33]. (a) Comparison of the quenched approximation (open circles) and QCD with u, d and s sea quarks (filled) circles. Note that the 1S and 2S levels are used to fix the b quark mass and lattice spacing respectively so are not predictions. (b) Dependence of the splittings as a function of the of the bare sea u/d quark mass.

w_i in Eq. (3.1), which are subleading. This means that spin-independent splittings, such as radial and orbital excitations, are simulated through next-to-leading-order in the velocity expansion and should be accurate to around 1%. Thus, these splittings provide a very accurate test not only of lattice QCD, but also of the effective-field theory framework. At present, the fine structure in the spectrum is only correct through leading-order [which is $\mathcal{O}(v^4)$ in this case] and more work must be done to bring this to the same level and allow tests against, for example, the splittings between the different χ_b states [33]. This is in progress. Systematic uncertainties due to such truncations have for instance been estimated in Ref. [36], based on lattice potentials.

The Υ system is a good one for looking at the effects of sea quarks because we expect it to be relatively insensitive to sea quark masses. The momentum transfer inside an Υ is larger than any of the u, d or s masses and so we expect the radial and orbital splittings to simply count the number of sea quarks once they are reasonably light. Figure 3.3(b) shows this to be true — the splittings are independent of the sea u/d quark mass in the region we are working in. Chiral extrapolation in the u/d quark mass is immaterial in this case. Therefore, the left-most lattice points in Fig. 3.3(b) are the ones used in Figs. 3.2 and 3.3(a).

ψ results with the Fermilab method

Figure 3.4 shows the spectrum of charmonium states below the $D\overline{D}$ threshold [24]. In this plot the lattice spacing was fixed from the $\Upsilon' - \Upsilon$ splitting (as above), and the c quark mass was tuned to get the D_s mass correct. Therefore, these results are obtained directly from QCD without adjusting any free parameters. For Fig. 3.4(a), the zero of energy has been moved to the spin-averaged mass $\bar{m}_\psi = \frac{1}{4}m_{\eta_c} + \frac{3}{4}m_{J/\psi}$.

These results are obtained using the Fermilab method [7] for the charmed quark. In this method one starts with Wilson Fermions, but the discretisation effects are controlled and understood using non-relativistic field theories, as in Eq. (3.1). The non-relativistic interpretation also has implications for how the action is improved. In the notation of Eq. (3.1) the chromomagnetic interaction is adjusted so that $c_F^{\rm lat}$ is correct at tree level. However, at higher order, there are $O[(m_c a)^2] \sim 10\%$ and $\mathcal{O}(\alpha_s)$ errors and

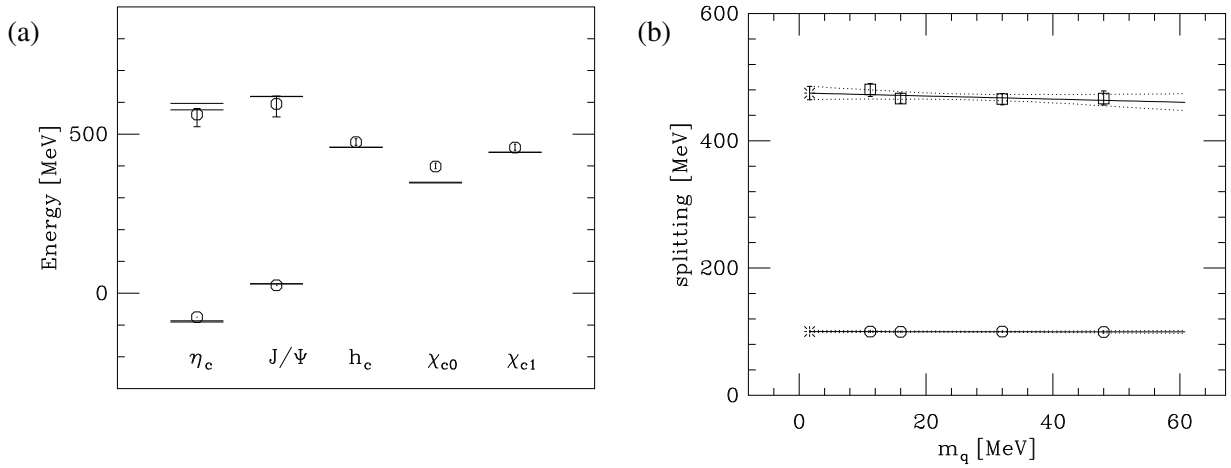

Fig. 3.4: Radial and orbital splittings in the charmonium system from lattice QCD with 3 light sea quarks, fixing the lattice spacing from the $\Upsilon' - \Upsilon$ splitting (as above), and the c quark mass from the D_s mass [24]. (a) Spectrum; (b) dependence on the sea quark mass.

some sign of these is seen in the mismatch with experiment of the hyperfine splitting in Fig. 3.4(a). In the past such discrepancies were masked by quenching errors, whereas now they can be resolved. Note that OZI violating contributions [18, 19] are also neglected currently. They are expected to be small but a decrease of up to 20 MeV in m_{η_c} is not ruled out.

The Fermilab action can be systematically improved, and the theoretical work needed is in progress. The most important new features are a one-loop calculation of the chromomagnetic coupling [37], and a systematic enumeration of all operators needed for improvement through v^6 [38].

B_c ground state

In 1998 the lowest-lying bound state of $\bar{b}c$ quarkonium was observed in semi-leptonic decays [39], yielding a mass of $m_{B_c} = 6.4 \pm 0.4$ GeV. A more precise measurement with hadronic decays is expected to come soon from Run II of the Tevatron, cf. Section 9. For lattice QCD, the B_c is a 'gold-plated' hadron and we have the opportunity to predict its mass ahead of experiment. Here we report on a preliminary lattice calculation, building on the progress detailed above. In previous quenched calculations accurate result could not be provided, due to the inconsistency of this approach described above.

The method used in the present study was developed in a quenched calculation [40], and follows almost immediately from Eq. (3.1). As long as one may use the effective Lagrangian to describe the charmed and bottom quarks on the lattice, the meson mass satisfies [28],

$$M_{1\,B_c} = m_{\bar{b}} + m_c + B_{B_c}, \tag{3.2}$$

where B_{B_c} is the binding energy of the B_c meson. The accuracy of the binding energy depends on how well the coefficients $c_i^{\rm lat}$ have been adjusted. The scheme- and scale-dependent quark masses cancel from the relation [40],

$$M_{1\,B_c} - \tfrac{1}{2}\left[M_{1\,\psi} + M_{1\,\Upsilon}\right] = B_{B_c} - \tfrac{1}{2}\left[B_\psi + B_\Upsilon\right]. \tag{3.3}$$

Note that within potential models flavour independence implies that this combination is small and positive [41,42]. One can now predict the B_c mass by adding back the experimental $\frac{1}{2}\left[M_\psi + M_\Upsilon\right]$. A variant of this technique is to use the D_s and B_s masses instead of (half the) quarkonium masses.

An unquenched lattice calculation has recently been carried out [43, 44], using the MILC ensembles discussed above. Analyses at two light sea quark masses and two values of the lattice spacing show

a consistent picture, as expected. Using the quarkonium baseline, Allison *et al.* find [43]

$$M_{B_c} = 6304 \pm 4 \pm 11^{+18}_{-\ 0}\ \mathrm{MeV}, \tag{3.4}$$

where the uncertainties are, respectively, from statistics (after chiral extrapolation), tuning of the heavy-quark masses, and heavy-quark discretization effects. The last is estimated from the mismatch of operators of order v^4 in the effective Lagrangian and are dominated by the relativistic correction $(\boldsymbol{D}^2)^2$. The estimate is guided by potential models (and is the only change from earlier conference reports [44]). The overall errors are so small because the lattice calculation has been set up to focus on the binding-energy difference, and raw uncertainties of several percent have been leveraged to the sub-percent level for the mass itself.

This result can be checked with the heavy-light baseline, $M_{B_c} = M_{D_s} + M_{B_s} + [B_{B_c} - (B_{D_s} + B_{B_s})]$, with somewhat larger uncertainties. Allison *et al.* find [43]

$$M_{B_c} = 6243 \pm 30 \pm 11^{+37}_{-\ 0}\ \mathrm{MeV}. \tag{3.5}$$

The systematic uncertainties are larger with the heavy-light baseline because there is less cancellation between the B_c quarkonium and the heavy-light D_s and B_s.

The dominant uncertainties can be reduced by choosing more highly-improved actions in lattice gauge theory, or by reducing the lattice spacing, as discussed in Ref. [43].

2.2.2 Heavy hybrids on the lattice[4]

QCD suggests the existence of mesonic states in which the valence quark-antiquark pair is bound by an *excited* gluon field. A natural starting point in the quest to understand such states is the heavy quark sector. The vastly different characteristics of the slow massive heavy quarks and the fast massless gluons suggest that such systems may be amenable to a Born–Oppenheimer treatment, similar to diatomic molecules. The slowly moving heavy quarks correspond to the nuclei in diatomic molecules, whereas the fast gluon and light-quark fields correspond to the electrons. At leading order, the gluons and light quarks provide adiabatic potentials $V_{Q\bar{Q}}(r)$, where r is the quark–antiquark separation, and the behavior of the heavy quarks is described by solving the Schrödinger equation separately for each $V_{Q\bar{Q}}(r)$. The Born–Oppenheimer approximation provides a clear and unambiguous picture of conventional and hybrid mesons: conventional mesons arise from the lowest-lying adiabatic potential, whereas hybrid mesons arise from the excited-state potentials.

The first step in a Born–Oppenheimer treatment of heavy quark mesons is determining the gluonic terms $V_{Q\bar{Q}}(r)$. Since familiar Feynman diagram techniques fail and the Schwinger–Dyson equations are intractable, the path integrals needed to determine $V_{Q\bar{Q}}(r)$ are estimated using Markov-chain Monte Carlo methods (Lattice QCD simulations). The spectrum of gluonic excitations in the presence of a static quark–antiquark pair has been accurately determined in lattice simulations [46, 47] which make use of anisotropic lattices, improved actions, and large sets of operators with correlation matrix techniques. These gluonic $V_{Q\bar{Q}}(r)$ levels may be classified by the magnitude Λ of the projection of the total angular momentum $\mathbf{J}_g$ of the gluon field onto the molecular axis, and by $\eta = \pm 1$, the symmetry under charge conjugation combined with spatial inversion about the midpoint between the quark and the antiquark. States with $\Lambda = 0, 1, 2, \ldots$ are denoted by $\Sigma, \Pi, \Delta, \ldots$, respectively. States which are even (odd) under the above-mentioned CP operation are denoted by the subscripts g (u). An additional $\pm$ superscript for the Σ states refers to even or odd symmetry under a reflection in a plane containing the molecular axis.

In the leading Born–Oppenheimer approximation, one replaces the covariant Laplacian $\boldsymbol{D}^2$ by an ordinary Laplacian $\boldsymbol{\nabla}^2$. The error that one makes is equivalent to $1/M_Q$ and $1/M_Q^2$ corrections [48] to $V_{Q\bar{Q}}$ that go beyond the LBO and are suppressed by a factor v^2, using perturbative NRQCD power

[4] Author: C. Morningstar

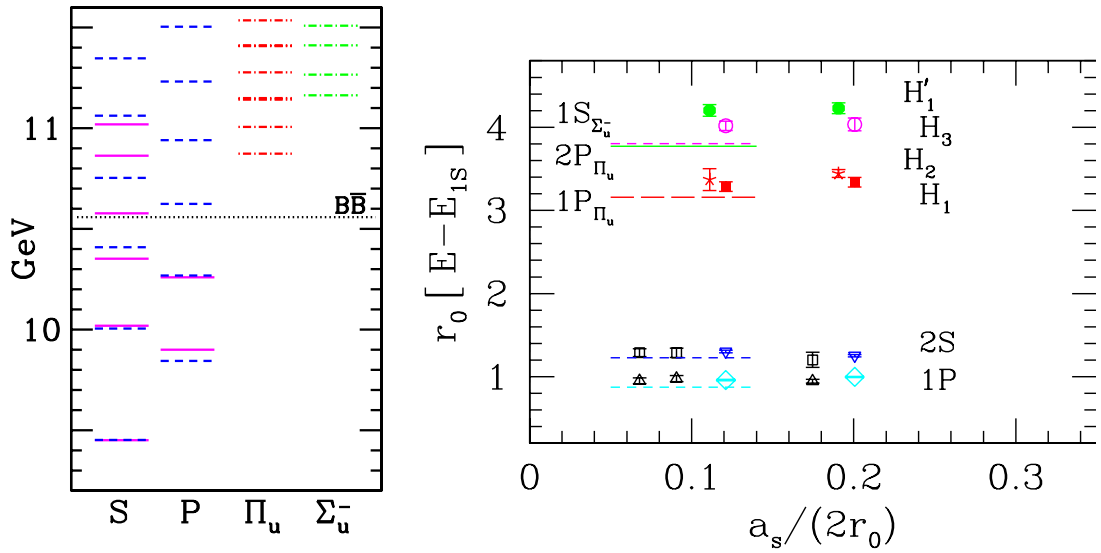

Fig. 3.5: (Left) The spectrum of conventional and hybrid heavy-quark mesons in the leading Born–Oppenheimer approximation and neglecting light quarks (from Ref. [46]). Conventional S and P states are shown, as well as hybrids based on the Π_u and Σ_u^- adiabatic surfaces. Solid lines indicate spin-averaged experimental measurements. (Right) Simulation results from Ref. [46] for two conventional and four hybrid bottomonium level splittings (in terms of $r_0^{-1} = 450$ MeV and with respect to the $1S$ state) against the lattice spacing a_s. Predictions from the leading Born–Oppenheimer calculation, shown as horizontal lines, reproduce all of the simulation results to within 10 %, strongly supporting the validity of a Born–Oppenheimer picture for such systems at leading order. Results from Ref. [49] using an NRQCD action with higher-order relativistic corrections are shown as hollow boxes and hollow upright triangles.

counting rules. The spin interactions of the heavy quarks are also neglected, and one solves the radial Schrödinger equation:

$$-\frac{1}{2\mu}\frac{d^2u(r)}{dr^2} + \left\{\frac{\langle \boldsymbol{L}^2_{Q\bar{Q}}\rangle}{2\mu r^2} + V_{Q\bar{Q}}(r)\right\} u(r) = E\, u(r), \tag{3.6}$$

where $u(r)$ is the radial wavefunction of the quark–antiquark pair and μ denotes the reduced mass. The expectation value in the centrifugal term is given in the adiabatic approximation by

$$\langle \boldsymbol{L}^2_{Q\bar{Q}}\rangle = L(L+1) - 2\Lambda^2 + \langle \boldsymbol{J}^2_g\rangle, \tag{3.7}$$

where $\langle \boldsymbol{J}^2_g\rangle = 0$ for the Σ_g^+ level and $\langle \boldsymbol{J}^2_g\rangle = 2$ for the Π_u and Σ_u^- levels.

The leading-order Born–Oppenheimer spectrum of conventional $\bar{b}b$ and hybrid $\bar{b}gb$ states (in the absence of light quarks) obtained from the above procedure is shown in Fig. 3.5. Below the $\overline{B}B$ threshold, the Born–Oppenheimer results agree well with the spin-averaged experimental measurements of bottomonium states (any small discrepancies essentially disappear once light quark loops are included). Above the threshold, agreement with experiment is lost, suggesting significant corrections either from mixing and other higher-order effects or (more likely) from light sea quark effects.

The validity of the Born–Oppenheimer picture relies on the smallness of mixing between states based on different $V_{Q\bar{Q}}(r)$. In addition, relativistic (including spin) corrections and radiation of colour neutral objects such as glueballs and mesons are neglected. In Ref. [46] the LBO level splittings have been compared with those determined from meson simulations using a non-relativistic (NRQCD) heavy-quark action. The NRQCD action included only a covariant temporal derivative and the leading covariant

kinetic energy operator; quark spin and $\boldsymbol{D}^4$ terms were neglected. Differences between the two results originate from both different $\mathcal{O}(1/M_Q)$ terms [48] and from the automatic inclusion of mixing effects between different adiabatic surfaces within the NRQCD simulations. Naively one might expect the former effect to be of $\mathcal{O}(v^2) \approx 10$ %. The level splittings (in terms of the hadronic scale r_0 and with respect to the $1S$ state) of the conventional $2S$ and $1P$ states and four hybrid states were compared (see Fig. 3.5) and indeed found to agree within 10%, strongly supporting the validity of the leading Born–Oppenheimer picture, at least in the absence of light sea quarks and spin-effects.

A very recent study [50] has demonstrated that the Υ ground state carries little admixture from hybrids, supporting the LBO, at least in the sector that is governed by the ground state potential. Using lowest-order lattice NRQCD to create heavy-quark propagators, a basis of unperturbed S-wave and $|1H\rangle$ hybrid states was formed. The $c_F \boldsymbol{\sigma} \cdot \boldsymbol{B}/2M_Q$ spin interaction was then applied at an intermediate time slice to compute the mixings between such states due to this interaction in the quenched approximation. Diagonalizing the resulting two-state Hamiltonian then yielded the admixtures of hybrid configuration in the Υ and η_b. For a reasonable range of c_F values, the following results were obtained: $\langle 1H|\Upsilon\rangle \approx 0.076-0.11$ and $\langle 1H|\eta_b\rangle \approx 0.13-0.19$. Hence, hybrid mixings due to quark spin effects in bottomonium are very small. Even in charmonium, the mixings were found not to be large: $\langle 1H|J/\Psi\rangle \approx 0.18 - 0.25$ and $\langle 1H|\eta_c\rangle \approx 0.29 - 0.4$. Investigations of the mixing of hybrid states with radially excited standard quarkonium states which are energetically closer and spatially more extended are certainly an exciting avenue of future research.

In the absence of light quark loops, one obtains a very dense spectrum of mesonic states since the $V_{Q\bar{Q}}(r)$ potentials increase indefinitely with r. However, the inclusion of light quark loops changes the $V_{Q\bar{Q}}(r)$ potentials. First, there are slight corrections at small r, and these corrections remove the small discrepancies of the leading Born–Oppenheimer predictions with experiment below the $B\overline{B}$ threshold seen in Fig. 3.5. For large r, the inclusion of light quark loops drastically changes the behavior of the $V_{Q\bar{Q}}(r)$ potentials: instead of increasing indefinitely, these potentials eventually level off at a separation above 1 fm when the static quark–antiquark pair, joined by gluonic flux, can undergo fission into $(Q\bar{q})(\bar{Q}q)$, where q is a light quark and Q is a heavy quark. Clearly, such potentials cannot support the populous set of states shown in Fig. 3.5; the formation of bound states and resonances substantially extending over 1 fm in diameter seems unlikely. A complete open-channel calculation taking the effects of including the light quarks correctly into account has not yet been done, but unquenched lattice simulations [51] show that the Σ_g^+ and Π_u potentials change very little for separations below 1 fm when sea quarks are included. This makes it conceivable that a handful of low-lying states whose wavefunctions do not extend appreciably beyond 1 fm in diameter may exist as well-defined resonances in nature.

In addition to such direct threshold effects there is the possibility of transitions between different adiabatic surfaces, mediated by radiation of pions and other light mesons or pairs of light mesons. A first lattice study of such effects has been performed by McNeile and Collaborators [52].

A recent quenched calculation [8] of bottomonium hybrids using a relativistic heavy-quark action on anisotropic lattices confirms the predictions of the Born–Oppenheimer approximation, but admittedly, the uncertainties in the simulation results are large. These calculations used a Symanzik-improved anisotropic gauge action and an improved Fermion clover action. Quenched results on Charmonium hybrids obtained by employing a relativistic quark actions [12] can be found in Fig. 3.1 and Table 3.1 in Section 2.1. The dominant decay channel for the lightest (1^{-+}) hybrid would be into a D and a $\overline{D}^{**}$ should it be heavier than the respective threshold, and radiation of a light pseudoscalar or scalar state if lighter.

A determination of the spectrum properly taking into account effects from light quarks is still needed. Taking the Born–Oppenheimer approximation beyond leading order is also a project for future work. Monte Carlo computations of relevant matrix elements involving the gauge field can not only facilitate the evaluation of higher-order terms in the Born–Oppenheimer expansion, but also provide valuable information on the production and decays of these novel states.

2.2.3 *QQq baryons on the lattice*[5]

While recent lattice results from several groups on three quark static potentials exist [53–57], no such potentials have been calculated for the situation containing two static sources at distance r, accompanied by a light quark, as yet. However, two groups have directly studied the situation for $Q = c$, within the quenched approximation, one employing the so-called D234 improved Wilson type action [58] as well as NRQCD [59] on anisotropic lattices and the UKQCD Collaboration employing the relativistic clover charm quark action [60].

In the NRQCD study [59] two lattice spacings, $a \approx 0.15\,\text{fm}, 0.22\,\text{fm}$ and four light quark masses have been realized and *bbq*, *ccq* as well as *bqq* and *cqq* baryons studied. No finite volume checks were performed and radiative corrections to the NRQCD matching coefficients ignored. In the UKQCD study [60] only one lattice spacing $a \approx 0.08$ fm and one volume, $La \approx 2$ fm were realized. The light quark masses scattered around the strange quark mass and both, singly and doubly charmed baryons were studied. All studies yield consistent results. The values quoted by UKQCD are [60],

$$\begin{aligned} \Xi_{cc} &= 3549(13)(19)(92)\,\text{MeV} \quad , \quad \Omega_{cc} = 3663(12)(17)(95)\,\text{MeV} \\ \Xi^*_{cc} &= 3641(18)(08)(95)\,\text{MeV} \quad , \quad \Omega^*_{cc} = 3734(14)(08)(97)\,\text{MeV}. \end{aligned} \tag{3.8}$$

The first errors are statistical, the second encapsulate uncertainties in the chiral extrapolations and fit ranges. The third error represents the uncontrolled systematics: finite a effects, finite volume effects and quenching, estimated by comparing the lattice Λ_c mass to the experimental result.

2.3 pNRQCD[6]

From the various dynamical scales that play a role in the heavy quarkonium systems, namely m, mv, mv^2 and $\Lambda_{\rm QCD}$, only the hard scale m has been factorized in NRQCD and becomes explicit in its Lagrangian. Only the fact that $m \gg mv, mv^2, \Lambda_{\rm QCD}$ is exploited but no use is made of the scale separation, $mv \gg mv^2$. A higher degree of simplification is achieved by building another effective theory, where degrees of freedom of order $\sim mv$ are integrated out as well, i.e., an EFT where only the ultrasoft degrees of freedom (with energies $\sim mv^2$) remain dynamical. In this way a big simplification is obtained and analytic calculations of the spectrum become feasible, at least in some dynamical regimes, at variance with NRQCD where the spectrum can only be obtained in a model independent way by Lattice calculation. pNRQCD [4, 5] takes advantadge of the fact that for many non-relativistic systems the scale associated to the size of the system $k \sim mv$ is much larger than the binding energy $E \sim mv^2$. Therefore it is possible to integrate out the scale of the momentum transfer k in a way such that pNRQCD is equivalent to NRQCD at any desired order in E/k, k/m and $\alpha_{\rm s}(\mu)$. Two dynamical situations may occur here: (1) k is much larger than $\Lambda_{\rm QCD}$, (2) k is of the order of $\Lambda_{\rm QCD}$. In the first case the matching from NRQCD to pNRQCD may be performed in perturbation theory, expanding in terms of $\alpha_{\rm s}$. In the second situation, the matching has to be nonperturbative, i.e., no expansion in $\alpha_{\rm s}$ is allowed. We will refer to these two limits as the weak and strong coupling regimes. Recalling that $k \sim r^{-1} \sim mv$, these two situations correspond to systems with inverse typical radius smaller or bigger than $\Lambda_{\rm QCD}$, or systems respectively dominated by the short range or long range (with respect to the confinement radius) physics. We will consider these two situations in the following two subsections.

2.3.1 *Weak coupling regime*[7]

When $k \gg E >\sim \Lambda_{\rm QCD}$, we are in the perturbative matching regime ($v \sim \alpha_{\rm s}(m\alpha_{\rm s})$). The scale $r \sim 1/(mv)$ is integrated out and the pNRQCD Lagrangian consists of a singlet and an octet wave function field interacting with respective potentials and coupled to ultrasoft gluons. The effective degrees

[5] Author: G. Bali

[6] Authors: N. Brambilla, J. Soto

[7] Authors: N. Brambilla, J. Soto

of freedom are: $Q\bar{Q}$ states (decomposed into a singlet and an octet wave function under colour transformations) with energy of order of the next relevant scale, $\Lambda_{\rm QCD}, mv^2$ and momentum $\mathbf{p}$ of order mv, plus ultrasoft gluons $A_\mu(\mathbf{R}, t)$ with energy and momentum of order $\Lambda_{\rm QCD}, mv^2$. All the gluon fields are multipole expanded (i.e., expanded in r). The Lagrangian is then an expansion in the small quantities $p/m, 1/(rm)$ and $\mathcal{O}(\Lambda_{\rm QCD}, mv^2) \times r$.

The pNRQCD Lagrangian is given at the next to leading order (NLO) in the multipole expansion by [5] (in the centre-of-mass system):

$$\mathcal{L}_{\rm pNRQCD} = {\rm Tr}\left\{ {\rm S}^\dagger \left(i\partial_0 - \frac{\mathbf{p}^2}{m} - V_s(r) - \sum_{n\geq 1} \frac{V_s^{(n)}}{m^n} \right) {\rm S} + {\rm O}^\dagger \left(iD_0 - \frac{\mathbf{p}^2}{m} - V_o(r) - \sum_{n\geq 1} \frac{V_o^{(n)}}{m^n} \right) {\rm O} \right\}$$
$$+ gV_A(r) {\rm Tr}\left\{ {\rm O}^\dagger \mathbf{r}\cdot\mathbf{E}\,{\rm S} + {\rm S}^\dagger \mathbf{r}\cdot\mathbf{E}\,{\rm O} \right\} + g\frac{V_B(r)}{2} {\rm Tr}\left\{ {\rm O}^\dagger \mathbf{r}\cdot\mathbf{E}\,{\rm O} + {\rm O}^\dagger {\rm O}\mathbf{r}\cdot\mathbf{E} \right\} - \frac{1}{4} F^a_{\mu\nu} F^{\mu\nu a}. \qquad (3.9)$$

The $V_{s,o}^{(n)}, V_A, V_B$ are potentials, which play the role of matching coefficients and contain the non-analytical dependence in r, to be calculated in the matching between NRQCD and pNRQCD. Poincaré invariance imposes relations among these matching coefficients [61]. To leading order in the multipole expansion, the singlet sector of the Lagrangian gives rise to equations of motion of the Schrödinger type. The other terms in Eq. (3.9) contain (apart from the Yang–Mills Lagrangian) retardation (or non-potential) effects that start at the NLO in the multipole expansion. At this order the non-potential effects come from the singlet-octet and octet-octet interactions mediated by an ultrasoft chromoelectric field.

Recalling that $r \sim 1/(mv)$ and that the operators count like the next relevant scale, $\mathcal{O}(mv^2, \Lambda_{\rm QCD})$, to the power of the dimension, it follows that each term in the pNRQCD Lagrangian has a definite power counting. As a consequence of this power counting the interaction of quarks with ultrasoft gluons is suppressed in the Lagrangian by a factor v (by gv if $mv^2 \gg \Lambda_{\rm QCD}$) with respect to the LO.

The various potentials in Eq. (3.9) have been calculated at different orders in the perturbative matching. V_s is known to two loops [$\mathcal{O}(\alpha_{\rm s}^3)$] [62, 63] as well as the leading log of the three loop contribution [64]. V_o is known to two loops (see York Schröder, private communications in Ref. [65]). $V_s^{(1)}$ is known to two loops [67] and $V_s^{(2)}$ to one loop [68]. V_A and V_B are known at tree level [5] (and are independent of r) and have no logs at one loop [70].

Note that the static limit of pNRQCD ($m \to \infty$) results in a nontrivial theory (unlike in pNRQED), since both singlet and octet fields remain dynamical and interact through ultrasoft gluons. The static energy of two infinitely heavy sources $V_{QCD}(r)$, which will be discussed below, can be obtained for small r. In fact, the coefficient of the infrared logarithmic contribution to $V_{QCD}(r)$ first pointed out in Ref. [71] was calculated using the static pNRQCD Lagrangian [64].

Given the Lagrangian in Eq. (3.9) it is possible to calculate the quarkonium energy levels. Contributions to the spectrum originate both in quantum mechanical perturbation theory and in the dynamics of ultrasoft gluons. The latter contributions contain nonperturbative effects and this will be discussed in the corresponding section below.

The static QCD potential[8]

For decades, the static QCD potential $V_{\rm QCD}(r)$, formally defined from an expectation value of the Wilson loop, has been widely studied for the purpose of elucidating the nature of the interaction between heavy quark and antiquark. The potential at short distances can be computed by perturbative QCD, whereas its long distance shape can be computed by lattice simulations. (See Sections 2.3.2 and 2.3.3 for lattice computations.)

[8] Author: Yu. Sumino

Computations of $V_{\rm QCD}(r)$ in perturbative QCD have a long history. The 1-loop and 2-loop corrections were computed in Refs. [72–74] and [62, 63, 75–78], respectively. The logarithmic correction at 3-loops originating from the ultrasoft scale was first pointed out in Ref. [71] and computed in Refs. [64, 79]. A renormalization-group (RG) improvement of $V_{\rm QCD}(r)$ at next-to-next-to-leading log (NNLL) was performed in Ref. [70].[9]

Since the discovery [83–85] of the cancellation of $\mathcal{O}(\Lambda_{\rm QCD})$ renormalons between $V_{\rm QCD}(r)$ and twice the quark pole mass[10], the convergence of the perturbative series improved drastically and much more accurate perturbative predictions of the potential shape became available. This feature indicates the validity of the renormalon dominance picture for the QCD potential and pole mass. According to this picture, a perturbative uncertainty of $V_{\rm QCD}(r)$, after cancelling the $\mathcal{O}(\Lambda_{\rm QCD})$ renormalon, is estimated to be $\mathcal{O}(\Lambda_{\rm QCD}^3 r^2)$ at $r \ll \Lambda_{\rm QCD}^{-1}$ [87].

An OPE of $V_{\rm QCD}(r)$ was developed within the pNRQCD framework [5]. In this framework, residual renormalons, starting from $\mathcal{O}(\Lambda_{\rm QCD}^3 r^2)$, are absorbed into the matrix element of a non-local operator (non-local gluon condensate). Then, in the multipole expansion at $r \ll \Lambda_{\rm QCD}^{-1}$, the leading nonperturbative contribution to the potential becomes $\mathcal{O}(\Lambda_{\rm QCD}^3 r^2)$ [5].

Several studies [78,88–91] showed that perturbative predictions for $V_{\rm QCD}(r)$ agree well with phenomenological potentials (determined from heavy quarkonium spectroscopy) and lattice calculations of $V_{\rm QCD}(r)$, once the $\mathcal{O}(\Lambda_{\rm QCD})$ renormalon is accounted for. Ref. [92] showed that also a Borel resummation of the perturbative series yields a potential shape in agreement with lattice results if the $\mathcal{O}(\Lambda_{\rm QCD})$ renormalon is properly treated. In fact the agreement holds within the expected $\mathcal{O}(\Lambda_{\rm QCD}^3 r^2)$ uncertainty.[11] These observations further support the validity of renormalon dominance and of the OPE for $V_{\rm QCD}(r)$.

Qualitatively, the perturbative QCD potential becomes steeper than the Coulomb potential as r increases (once the $\mathcal{O}(\Lambda_{\rm QCD})$ renormalon is cancelled). This feature can be understood, within perturbative QCD, as an effect of the *running* of the strong coupling constant [88, 89, 93].

Using a scale-fixing prescription based on the renormalon dominance picture, it was shown analytically [94] that the perturbative QCD potential approaches a "Coulomb+linear" form at large orders, up to an $\mathcal{O}(\Lambda_{\rm QCD}^3 r^2)$ uncertainty. The "Coulomb+linear" potential can be computed systematically as more terms of perturbative series are included via RG; up to NNLL, it shows a convergence towards lattice results.

Heavy quarkonium spectra [12]

In recent years, perturbative computations of the heavy quarkonium spectrum (an expansion in $\alpha_{\rm s}$ and $\ln\alpha_{\rm s}$) have enjoyed a significant development. A full computation of the spectrum up to $\mathcal{O}(\alpha_{\rm s}^4 m)$ was performed in Refs. [98, 99]. The spectra up to the same order for the system with unequal heavy quark masses and with non-zero quark mass in internal loops were computed, respectively, in Refs. [95, 97] and [77, 95]. Perturbative computations at higher orders were made possible by the advent of effective field theories such as pNRQCD [4, 5] or vNRQCD [6] and by the threshold expansion technique [100]. The $\mathcal{O}(\alpha_{\rm s}^5 m \ln\alpha_{\rm s})$ term originating from the ultrasoft scale was computed in Refs. [64, 69, 79]. Ref. [101, 102] resummed the $\alpha_{\rm s}^4 m(\alpha_{\rm s}\ln\alpha_{\rm s})^n$ terms. The full Hamiltonian at the next-to-next-to-next-to-leading order was computed in Ref. [68]. Except for the 3-loop non-logarithmic term of the perturbative QCD potential,[13] the energy levels of the $1S$ states were computed up to $\mathcal{O}(\alpha_{\rm s}^5 m)$ from this Hamiltonian [103]. The fine splittings have been calculated at NLO order $\mathcal{O}(\alpha_{\rm s}^5 m)$ in [104].

[9] There are estimates of higher-order corrections to the perturbative QCD potential in various methods [80–82].

[10] For similar work inside HQET see [86].

[11] This is true only in the range of r where the respective perturbative predictions are stable. All perturbative predictions become uncontrolled beyond certain distances, typically around $r \sim \Lambda_{\rm QCD}^{-1}$.

[12] Author: Yu. Sumino

[13] Estimates of the 3-loop correction to the QCD potential have been given in various methods [80–82].

In the meantime, the discovery of the renormalon cancellation in the quarkonium spectrum [83–85] led to a drastic improvement of the convergence of the perturbative expansion of the energy levels. (See Chapter 6 for precise determinations of the heavy quark masses, as important applications.) In Refs. [93, 95] the whole structure of the bottomonium spectrum up to $\mathcal{O}(\alpha_s^4 m)$ was predicted taking into account the cancellation of the $\mathcal{O}(\Lambda_{\rm QCD})$ renormalons, and a good agreement with the experimental data was found for the gross structure of the spectrum. (Only the states below the threshold for strong decays were considered.) The consistency of the perturbative predictions with the experimental data seems to indicate that, for bottomonium, the momentum scale of the system is larger than $\Lambda_{\rm QCD}$, i.e., $mv \gg \Lambda_{\rm QCD}$, up to some of the $n = 3$ states. This is, however, in apparent conflict with the fact that the leading nonperturbative effects scale as a power ≥ 4 of the principal quantum number (see *Nonperturbative effects* below) and, hence, are expected to be very important for any excited state.

Subsequently, in Refs. [96, 106] a specific formalism based on perturbative QCD was developed: using the static QCD potential computed in Ref. [78] and taking into account the cancellation of the $\mathcal{O}(\Lambda_{\rm QCD})$ renormalons, the Schrödinger equation was solved numerically to determine the zeroth-order quarkonium wave function; all the corrections up to $\mathcal{O}(\alpha_s^5 m)$ for the fine and hyperfine splittings have been included. Good agreements were found between the computed and the observed fine and hyperfine splittings of the bottomonium and charmonium spectra, in addition to the gross structure of the bottomonium spectrum[14].

In Table 3.2 particularly impressing is the result for the perturbative calculation of the B_c mass, that, with finite charm mass effects included, is equal to $6307 \pm 17\mathrm{GeV}$ and is in complete agreement, inside errors and with small errors, with lattice NRQCD unquenched result given in Eq. (4).

These analyses have shown that the perturbative predictions of the spectra agree with the corresponding experimental data within the estimated perturbative uncertainties, and that the size of nonperturbative contributions is compatible with the size of perturbative uncertainties.

Although uncertainties of the perturbative predictions for the individual energy levels grow rapidly for higher excited states, level spacings among them have smaller uncertainties, since the errors of the individual levels are correlated. In particular, uncertainties of the fine and hyperfine splittings are suppressed due to further cancellation of renormalons. These features enabled sensible comparisons of the level structures including the excited states.

In predicting the spectrum, pNRQCD is a useful tool not only for fully perturbative computations but also for factorizing short-distance contributions into matching coefficients (perturbatively computable) and nonperturbative contributions into matrix elements of operators [5, 48]. This will be discussed in *Nonperturbative effects* below.

The Renormalization group in heavy quarkonium spectroscopy [15]

In recent years, there has been a growing interest to perform renormalization group analysis in heavy quarkonium [6, 70, 101, 102, 107, 108, 110–117]. In many cases this interest has been driven by the lack of convergence and strong scale dependence one finds in the fixed (NNLO) analysis performed for sum rules and t–$\bar{t}$ production near threshold (see Chapter 6). This problem has turned out to be highly non-trivial. We will focus here on computations related with spectroscopy.

The heavy quarkonium spectrum is known with NNLL accuracy [101, 102]. These expressions have not yet been used for phenomenological analysis of single heavy quarkonium states either in bottomonium and charmonium systems. It would be very interesting to see their effects on the spectra.

The hyperfine splitting of the heavy quarkonium spectrum is known with LL [113, 114] and NLL accuracy for the bottomonium and charmonium spectrum [107] and also for the B_c spectrum [108]. For

[14] For technical reasons a linear extrapolation of the potential at $r > 4.5\ \mathrm{GeV}^{-1}$ was introduced in Ref. [96]. This artefact was eliminated in Ref. [106], in which it was also shown that effects caused by the linear extrapolation of the potential were minor.

[15] Author: A. Pineda

Table 3.2: Predicted masses of $b\bar{b}$, $c\bar{c}$ and $b\bar{c}$ states in perturbative QCD-based, renormalon-subtracted computations. BSV01 (and BV00) is the full perturbative computation up to $\mathcal{O}(\alpha_s^4 m)$ without non-zero charm-mass corrections; BSV02 is the full perturbative computation up to $\mathcal{O}(\alpha_s^4 m)$ including non-zero charm-mass corrections; RS03 is based on a specific scheme and specific reorganization of perturbative series, incorporates full corrections up to $\mathcal{O}(\alpha_s^4 m)$ in the individual levels and full corrections up to $\mathcal{O}(\alpha_s^5 m)$ in the fine splittings, includes non-zero charm-mass corrections. Errors shown in brackets represent $\sqrt{\delta_{\alpha_s}^2 + \delta_{\rm h.o.}^2}$ (BSV01,BV00) and $\sqrt{\delta_{\alpha_s}^2 + \delta_{\rm h.o.}^2 + \delta_{m_c}^2}$ (BSV02), respectively, where δ_{α_s} originates from the error of $\alpha_s(M_Z)$, $\delta_{\rm h.o.}$ is the error due to higher-order corrections, and δ_{m_c} is the error in the finite charm mass corrections. The errors do not include non-perturbative contributions estimates. Numbers without errors are those without explicit or reliable error estimates in the corresponding works.

State	expt	BSV01 [93]	BSV02 [95]	RS03 [96]	BV00 [97]
$b\bar{b}$ states					
1^3S_1	9460	9460	9460	9460	
1^3P_2	9913	9916(59)	10012(89)	9956	
1^3P_1	9893	9904(67)	10004(86)	9938	
1^3P_0	9860	9905(56)	9995(83)	9915	
2^3S_2	10023	9966(68)	10084(102)	10032	
2^3P_2	10269		10578(258)	10270	
2^3P_1	10255		10564(247)	10260	
2^3P_0	10232	10268	10548(239)	10246	
3^3S_1	10355	10327(208)	10645(298)	10315	
$c\bar{c}$ states					
1^3S_1	3097	3097			
1^1S_0	2980(2)	3056			
$b\bar{c}$ states					
1^1S_0	6400(400)	6324(22)	6307(17)		6326 (29)

Table 3.3: Predicted fine and hyperfine splittings (in MeV) of $b\bar{b}$ and $c\bar{c}$ states in perturbative QCD-based, renormalon-subtracted computations. ${}^3P_{\rm cog}$ denotes the centre of gravity of the triplet P-wave states. PT88 extracts the matrix elements of $\mathcal{O}(1/m^2)$ operators from the experimental values for the fine splittings, instead of computing them from perturbative QCD. BSV01 is the full perturbative computation up to $\mathcal{O}(\alpha_{\rm s}^4 m)$ without non-zero charm-mass corrections. BSV02 is the full perturbative computation up to $\mathcal{O}(\alpha_{\rm s}^4 m)$ including non-zero charm-mass corrections; RS03 and RS04 are based on specific schemes and specific reorganization of perturbative series, incorporate full corrections up to $\mathcal{O}(\alpha_{\rm s}^5 m)$ in the splittings, and include non-zero charm-mass corrections. KPPSS03 and PPSS04 are the full NNLL computation [up to order $\alpha_{\rm s}^5 m \times (\alpha_{\rm s} \ln \alpha_{\rm s})^n$)] without non-zero charm-mass corrections. Errors are shown in brackets when explicit and reliable estimates are given in the respective works. The errors do not include nonperturbative contributions estimates except in KPPSS03 and PPSS04 where they were roughly estimated using the multipole expansion.

Level splitting	expt	PT88 [105]	BSV01 [93]	BSV02 [95]	RS03 [96]	RS04 [106]	KPPSS03 [107]	PPSS04 [108]
				$b\bar{b}$ states				
$1^3P_2 - 1^3P_1$	20		12	8	18(10)			
$1^3P_1 - 1^3P_0$	33		-1	9	23(10)			
$2^3P_2 - 2^3P_1$	13			16	11(10)			
$2^3P_1 - 2^3P_0$	23			14	14(10)			
$1^3S_1 - 1^1S_0$						44(11)	$39(11)^{+9}_{-8}$	
$2^3S_1 - 2^1S_0$						21(8)		
$3^3S_1 - 3^1S_0$						12(9)		
$1^3P_{\rm cog} - 1^1P_1$		-0.5				$-0.4(0.2)$		
$2^3P_{\rm cog} - 2^1P_1$		-0.4				$-0.2(0.1)$		
				$c\bar{c}$ states				
$1^3P_2 - 1^3P_1$	46					43(24)		
$1^3P_1 - 1^3P_0$	95					56(34)		
$1^3S_1 - 1^1S_0$	118(1)					88(26)	104	
$2^3S_1 - 2^1S_0$	32(10)					38(36)		
$1^3P_{\rm cog} - 1^1P_1$	-0.9	-1.4				$-0.8(0.8)$		
				$b\bar{c}$ states				
$1^3S_1 - 1^1S_0$								$65(24)^{+19}_{-16}$

those observables a phenomenological analysis has been performed. The predictions can be found in Table 3.3. The general trend is that the introduction of these effects improves the agreement with experiment (when experimental data are available). In particular, the resummation of logarithms brings the perturbative prediction of the hyperfine splitting of charmonium significantly closer to the experimental figure if compared with a NLO computation. It is then possible to give predictions for the hyperfine splitting of the ground state of bottomonium, and in particular for the $\eta_b(1S)$ mass, as well as for the hyperfine splitting of the B_c ground state. In these computations a threshold mass was used (equivalent to the pole mass at this order). In any case, it should also be mentioned that the use of the $\overline{\rm MS}$ mass may give a NLO value for the charmonium hyperfine splitting in agreement with experiment [109].

As a final remark, for the bottomonium, charmonium and B_c spectrum, one should be careful, since the ultrasoft scale may run up to very low scales. On the other hand the general dependence on the renormalization scale appears to be the same no matter whether we talk of toponium, bottomonium or charmonium. This may point to the fact that the same physics holds for all of them.

Nonperturbative effects[16]

Given the Lagrangian in Eq. (3.9) it is possible to calculate the full quarkonium energy levels at order $m\alpha_{\rm s}^5$ [68, 69, 79]. At this order the energy E_n of the level n receives contributions both from standard quantum mechanics perturbation theory and from the singlet-octet interaction (retardation effect) through ultrasoft gluons. The latter reads

$$\delta E_n|_{us} = -i\frac{g^2}{3N_c}\int_0^\infty dt\, \langle n|\mathbf{r}e^{it(E_n^{(0)}-h_o)}\mathbf{r}|n\rangle\, \langle \mathbf{E}(t)\,\mathbf{E}(0)\rangle(\mu). \tag{3.10}$$

being $E_n^{(0)}$ and h_o the binding energy and the octet Hamiltonian respectively, at leading order. When we assume that the chromoelectric fields have a typical scale $\sim \Lambda_{\rm QCD}$, the expression (3.10) allows to discuss the nature of the leading nonperturbative contributions. Thus the integral in (3.10) is a convolution of two objects: the exponential with a typical scale mv^2 and the chromoelectric correlator with a typical scale $\Lambda_{\rm QCD}$. Depending on the relative size of the two scales three different situations occur:

- if $mv^2 \gg \Lambda_{\rm QCD}$, the correlator reduces to the local gluon condensate and one recovers the result of Refs. [119, 120], which is proportional to the sixth power of the principal quantum number. The NLO nonperturbative contribution has been evaluated in Ref. [122]. Note, however, that in this case the dominant contribution to the nonlocal chromoelectric correlator corresponds to fluctuations of order mv^2, which can be calculated perturbatively [69, 79].
- if $mv^2 \ll \Lambda_{\rm QCD}$, the exponential can be expanded and one obtains a quadratic short range nonperturbative potential [5, 123]. This potential absorbs the residual renormalons contained in the fully perturbative computations [5]. For a Coulombic system, its expectation value grows as the fourth power of the principal quantum number.
- if $mv^2 \sim \Lambda_{\rm QCD}$, no expansion can be performed and the nonlocal condensate has to be kept. Its expectation value grows as the fourth power of the principal quantum number [69].

Hence, both nonperturbative potentials and (non-potential) local condensates are obtained from pNRQCD in the weak coupling regime for different kinematical limits, see also [124].

2.3.2 *Strong coupling regime*[17]

When $k >\sim \Lambda_{\rm QCD} \gg E$, the pNRQCD Lagrangian consist of a singlet wave function field interacting with a potential and with pseudo-Goldstone bosons [5]. The dynamics of the singlet field S is described by the following Lagrangian (here, we do not specialize to the centre-of-mass system) [48, 125]

$$\mathcal{L}_{\rm pNRQCD} = {\rm Tr}\left\{ {\rm S}^\dagger \left(i\partial_0 - \frac{\mathbf{p}_1^2}{2m_1} - \frac{\mathbf{p}_2^2}{2m_2} - V(\mathbf{x}_1,\mathbf{x}_2,\mathbf{p}_1,\mathbf{p}_2)\right) {\rm S}\right\} \tag{3.11}$$

[16] Authors: N. Brambilla, J. Soto

[17] Authors: N. Brambilla, J. Soto

The dynamics of the pseudo-Goldstone boson is given by the Chiral Lagrangian [126]. The coupling of pseudo-Goldston bosons with the singlet field has not been worked out yet. If we ignore this coupling, we recover in Eq. (3.11) the structure of non-relativistic potential models [48, 125]. If we assume that V is analytical in $1/m$, the structure of the potential up to order $1/m^2$ is

$$V(\mathbf{x}_1,\mathbf{x}_2,\mathbf{p}_1,\mathbf{p}_2) = V^{(0)}(r) + \frac{V^{(1,0)}(r)}{m_1} + \frac{V^{(0,1)}(r)}{m_2} + \frac{V^{(2,0)}}{m_1^2} + \frac{V^{(0,2)}}{m_2^2} + \frac{V^{(1,1)}}{m_1 m_2}, \tag{3.12}$$

$$V^{(2,0)} = \frac{1}{2}\left\{\mathbf{p}_1^2, V^{(2,0)}_{\mathbf{p}^2}(r)\right\} + \frac{V^{(2,0)}_{\mathbf{L}^2}(r)}{r^2}\mathbf{L}_1^2 + V_r^{(2,0)}(r) + V_{LS}^{(2,0)}(r)\mathbf{L}_1\cdot\mathbf{S}_1, \tag{3.13}$$

$$V^{(0,2)} = \frac{1}{2}\left\{\mathbf{p}_2^2, V^{(0,2)}_{\mathbf{p}^2}(r)\right\} + \frac{V^{(0,2)}_{\mathbf{L}^2}(r)}{r^2}\mathbf{L}_2^2 + V_r^{(0,2)}(r) - V_{LS}^{(0,2)}(r)\mathbf{L}_2\cdot\mathbf{S}_2, \tag{3.14}$$

$$V^{(1,1)} = -\frac{1}{2}\left\{\mathbf{p}_1\cdot\mathbf{p}_2, V^{(1,1)}_{\mathbf{p}^2}(r)\right\} - \frac{V^{(1,1)}_{\mathbf{L}^2}(r)}{2r^2}(\mathbf{L}_1\cdot\mathbf{L}_2 + \mathbf{L}_2\cdot\mathbf{L}_1) + V_r^{(1,1)}(r)$$
$$+V^{(1,1)}_{L_1S_2}(r)\mathbf{L}_1\cdot\mathbf{S}_2 - V^{(1,1)}_{L_2S_1}(r)\mathbf{L}_2\cdot\mathbf{S}_1 + V^{(1,1)}_{S^2}(r)\mathbf{S}_1\cdot\mathbf{S}_2 + V^{(1,1)}_{S_{12}}(r)\mathbf{S}_{12}(\hat{\mathbf{r}}), \tag{3.15}$$

where $r=|\mathbf{r}|$, $\mathbf{r}=\mathbf{x}_1-\mathbf{x}_2$, $\mathbf{L}_j \equiv \mathbf{r}\times\mathbf{p}_j$ and $\mathbf{S}_{12}(\hat{\mathbf{r}}) \equiv 12\hat{\mathbf{r}}\cdot\mathbf{S}_1\,\hat{\mathbf{r}}\cdot\mathbf{S}_2 - 4\mathbf{S}_1\cdot\mathbf{S}_2$. The requisite of Poincaré invariance imposes well defined relations among the spin-dependent and velocity dependent potentials above [127–129]. If one further assumes that the matching to NRQCD can be done in the $1/m$ expansion, the explicit form of the potentials can be obtained in terms of Wilson loop operators [48, 128–133]. We display here some of them for illustration (for the form of all the potentials see [48]). For the static potential we have

$$V^{(0)}(r) = \lim_{T\to\infty}\frac{i}{T}\ln\langle W\rangle, \tag{3.16}$$

for the potential at order $1/m$

$$V_s^{(1,0)}(r) = \lim_{T\to\infty} -\frac{g^2}{4T}\int_{-T/2}^{T/2}dt\int_{-T/2}^{T/2}dt'|t-t'|\langle\!\langle \mathbf{E}(t)\cdot\mathbf{E}(t')\rangle\!\rangle_c. \tag{3.17}$$

At the order $1/m^2$ we display a potential contributing to the spin-dependent (precisely the spin–orbit) relativistic corrections

$$\begin{aligned} V_{LS}^{(2,0)}(r) &= \frac{c_F^{(1)}}{2r^2} i\mathbf{r}\cdot\lim_{T\to\infty}\frac{1}{T}\int_{-T/2}^{T/2}dt\int_{-T/2}^{T/2}dt''\,(t-t'')\,\langle\!\langle g\mathbf{B}(\mathbf{x}_1,t'')\times g\mathbf{E}(\mathbf{x}_1,t)\rangle\!\rangle \\ &\quad + \frac{c_S^{(1)}}{2r^2}\mathbf{r}\cdot(\boldsymbol{\nabla}_r V^{(0)}), \end{aligned} \tag{3.18}$$

and a potential contributing to the spin-independent velocity dependent relativistic corrections

$$V^{(2,0)}_{\mathbf{p}^2}(r) = \frac{i}{4}\hat{\mathbf{r}}^i\hat{\mathbf{r}}^j\lim_{T\to\infty}\frac{1}{T}\int_{-T/2}^{T/2}dt\int_{-T/2}^{T/2}dt''\,(t-t'')^2\,\langle\!\langle g\mathbf{E}^i(\mathbf{x}_1,t'')\,g\mathbf{E}^j(\mathbf{x}_1,t)\rangle\!\rangle_c. \tag{3.19}$$

The angular brackets $\langle\ldots\rangle$ stand for the average value over the Yang–Mills action, W for the rectangular static Wilson loop of extension $r\times T$ (the time runs from $-T/2$ to $T/2$, the space coordinate from $\mathbf{x}_1$ to $\mathbf{x}_2$):

$$W \equiv \mathrm{P}\exp\left\{-ig\oint_{r\times T}dz^\mu A_\mu(z)\right\}, \qquad dz^\mu A_\mu \equiv dz^0 A_0 - d\mathbf{z}\cdot\mathbf{A}, \tag{3.20}$$

and $\langle\!\langle\ldots\rangle\!\rangle \equiv \langle\ldots W\rangle/\langle W\rangle$; P is the path-ordering operator. Moreover, we define the connected Wilson loop with $O_1(t_1)$, $O_2(t_2)$ and $O_3(t_3)$ operator insertions by:

$$\langle\!\langle O_1(t_1)O_2(t_2)\rangle\!\rangle_c = \langle\!\langle O_1(t_1)O_2(t_2)\rangle\!\rangle - \langle\!\langle O_1(t_1)\rangle\!\rangle\langle\!\langle O_2(t_2)\rangle\!\rangle. \tag{3.21}$$

The operators $\mathbf{E}^i = F_{0i}$ and $\mathbf{B}^i = \epsilon^{ijk} F^{jk}/2$ ($F_{\mu\nu} = \partial_\mu A_\nu - \partial_\nu A_\mu + ig[A_\mu, A_\nu]$) are the chromoelectric and chromomagnetic field respectively.

Notice that the final result for the potentials (static and relativistic corrections) appears factorized in a part containing the high energy dynamics (and calculable in perturbation theory) which is inherited from the NRQCD matching coefficients (the c_j, d_j, cf. Section 2.1 on NRQCD in Chapter 1), and a part containing the low energy dynamics given in terms of Wilson loops and chromo-electric and chromo-magnetic insertions in the Wilson loop [48]. The inclusion of NRQCD matching coefficients solved the inconsistency between perturbative one-loop calculations and the Wilson loop approach which arose in the past [132, 134]. The low energy contributions can be calculated on the lattice [135, 136] or estimated in QCD vacuum models [134, 137].

Almost all the potentials given in Eq. (3.15) were evaluated on the lattice in Refs. [135, 136], but this is not so for the potentials of order $1/m$, $V^{(1,0)}, V^{(0,1)}$. It would be very interesting to have such an evaluation (the perturbative one exist at two loops [67]) since, phenomenologically, they have not been considered up to now. In general, it would be very interesting to have updated and more precise lattice calculations of all the potentials. We recall that these lattice calculations have also a definite impact on the study of the properties of the QCD vacuum in presence of heavy sources. So far the lattice data for the spin-dependent and spin-independent potentials are consistent with a flux-tube picture, while it is only for the spin-dependent terms that the so called scalar confinement is consistent with the lattice data [48, 134, 138].

It has recently been shown [139] that the assumption that V is analytic in $1/m$ is not correct. New non-analytic terms arise due to the three-momentum scale $\sqrt{m\Lambda_{\rm QCD}}$. These terms can be incorporated into local potentials ($\delta^3(\mathbf{r})$ and derivatives of it) and scale as half-integer powers of $1/m$. Moreover, it is possible to factorize these effects in a model independent way and compute them within a systematic expansion in some small parameters. In any case, the corrections to the spectrum coming from these non-analytical terms are subleading with respect to the terms given in Eq. (3.12).

We emphasize that, in this regime, non-relativistic potential models, as the ones discussed in Section 3 are demonstrated to be EFTs of QCD, provided that the potentials used there are compatible with the ones extracted from QCD (and the interaction with pseudo-Goldstone bosons neglected). It is a matter of debate, however, which states in bottomonium and charmonium should be considered as belonging to this regime. On one hand the mass should be sufficiently lower than the heavy-light meson pair threshold to justify the omission of higher Fock state effects. On the other hand if the states are too low in mass then the perturbative matching regime of Section 2.3.1 will apply and the problem can be further simplified.

Since the potentials are defined in an effective field theory framework they are not plagued by the inconsistency typically emerging in higher order calculations in potential models. It is well known that at second order in quantum mechanical perturbation theory the spin dependent terms result in a contribution which is as large as the leading order one. This is due to the fact that the resulting expression becomes ill-defined. Regulating it requires to introduce a cut-off (or dimensional regularization). A large cut-off gives rise to a linear and to a logarithmic divergence. These divergences can be renormalized by redefining the coupling constant of a delta potential [140]. This is a mere reflection of the fact that when one matches QCD to NRQCD, one expands the energy and three momentum. This induces infrared divergences in the matching coefficients. For quarkonium this happens in the calculation of a matching coefficient of a four Fermion operator at two loops. If one uses a consistent regularization scheme both for the QCD-NRQCD matching calculation and the quantum mechanical calculation in pNRQCD, the divergences exactly cancel and, at the end of the day, a totally consistent scale independent result is obtained (for a QED example see Refs. [141, 142]). Notice that an EFT framework is crucial to understand this second order calculation and to render the result meaningful.

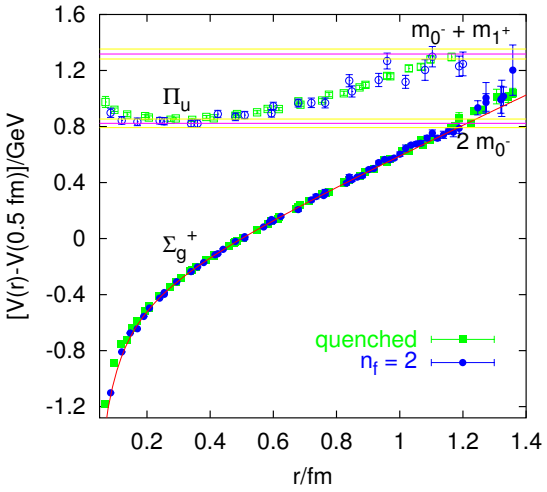

Fig. 3.6: The singlet static energy (quenched and unquenched data) from Ref. [51], see also [143]

2.3.3 The QCD static spectrum and mechanism of confinement [18]

The spectrum of gluons in the presence of a static quark–antiquark pair has been extensively studied with high precision using lattice simulations. Such studies involve the calculation of large sets of Wilson loops with a variety of different spatial paths. Projections onto states of definite symmetries are done, and the resulting energies are related to the static quark–antiquark potential and the static hybrids potentials. With accurate results, such calculations provide an ideal testing ground for models of the QCD confinement mechanism.

The singlet static energy

The singlet static energy is the singlet static potential $V_s^{(0)}$.

In the plot3.6, we report simulation results both with and without light quark–antiquark pair creation. Such pair creation only slightly modifies the energies for separations below 1 fm, but dramatically affects the results around 1.2 fm, at a distance which is too large with respect to the typical heavy quarkonium radius to be relevant for heavy quarkonium spectroscopy. At finite temperature, the so-called string breaking occurs at a smaller distance (cf. corresponding Section in Chapter 7, *Media*).

One can study possible nonperturbative effects in the static potential at short distances. As it has already been mentioned in the "static QCD potential" subsection, the proper treatment of the renormalon effects has made possible the agreement of perturbation theory with lattice simulations (and potential models) [78, 88–92]. Here we would like to quantify this agreement assigning errors to this comparison. In particular, we would like to discern whether a linear potential with the usual slope could be added to perturbation theory. In order to do so we follow here the analysis of Ref. [90, 144], where the potential is computed within perturbation theory in the Renormalon Subtracted scheme defined in Ref. [81]. The comparison with lattice simulations [145] in Fig. 3.7 shows that nonperturbative effects should be small and compatible with zero, since perturbation theory is able to explain lattice data within errors. The systematic and statistical errors of the lattice points are very small (smaller than the size of the points). Therefore, the main sources of uncertainty of our (perturbative) evaluation come from the uncertainty in the value of $\Lambda_{\overline{\rm MS}}$ ($\pm 0.48\, r_0^{-1}$) obtained from the lattice [146] and from the uncertainty in higher orders in perturbation theory. We show our results in Fig. 3.7. The inner band reflects the uncertainty in $\Lambda_{\overline{\rm MS}}$ whereas the outer band is meant to estimate the uncertainty due to higher orders in perturbation theory. We estimate the error due to perturbation theory by the difference between the NNLO and NNNLO evaluation. The usual confining potential, $\delta V = \sigma r$, goes with a slope $\sigma = 0.21 \mathrm{GeV}^2$. In lattice units

[18] Authors: N. Brambilla, C. Morningstar, A. Pineda

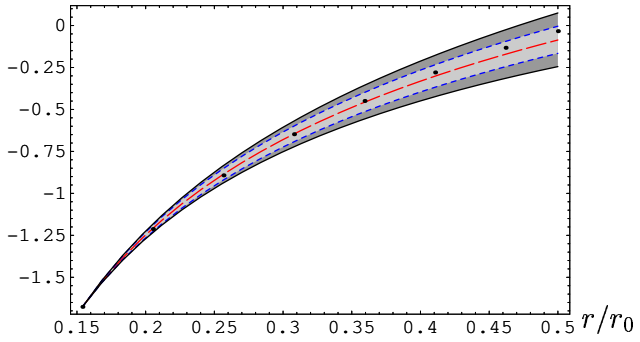

Fig. 3.7: Plot of $r_0(V_{\rm RS}(r) - V_{\rm RS}(r') + E_{latt.}(r'))$ versus r at three loops (estimate) plus the leading single ultrasoft log (dashed line) compared with the lattice simulations [145] $E_{latt.}(r)$. For the scale of $\alpha_{\rm s}(\nu)$, we set $\nu = 1/0.15399\, r_0^{-1}$. $\nu_{us} = 2.5\, r_0^{-1}$ and $r' = 0.15399\, r_0$. The inner and outer band are meant to estimate the errors in $\Lambda_{\overline{\rm MS}}$ and perturbative. For further details see the main text.

we take: $\sigma = 1.35\, r_0^{-2}$. The introduction of a linear potential at short distances with such slope is not consistent with lattice simulations. This is even so after the errors considered in Fig. 3.7 have been included.

At larger distances, $r \gg \Lambda_{\rm QCD}$, $V_s^{(0)}$ grows linearly, with the string tension $\sigma = 0.21{\rm GeV}^2$. Such a linear growth of the energy is often taken as evidence that the gluon field forms a flux tube whose dynamics can be described by an effective string theory. However, it should be pointed out that a linearly growing potential does not necessarily imply string formation; for example, the spherical bag model also predicts a linearly rising potential for moderate r. It has been shown [147] that the formation of a string-like flux tube implies a characteristic and universal $-\frac{\pi}{12r}$ correction to the ground-state energy, deriving from the zero-point energy of the transverse string vibration. Recent high precision simulations [148] (cf. also [149]) show that the coefficient of the $1/r$ correction differs from $-\pi/12$ by 12%. The authors of Ref. [148] introduce an *ad hoc* end-effect term with a fit parameter b to the effective string action to explain this significant difference. However, in a more recent paper [150], these authors show that an open-closed string duality relation requires $b = 0$. Furthermore, a simple resonance model was used in Refs. [151, 152] to show that the Casimir energy expected from a string description could be reproduced in a model in which string formation was not a good description, concluding that no firm theoretical foundation for discovering string formation from high precision ground state properties below the 1 fm scale currently exists.

Excitations of the static energy

The spectrum of gluons in the presence of a static quark–antiquark pair provides valuable clues about the nonperturbative dynamics of QCD. Adopting the viewpoint that the nature of the confining gluon field is best revealed in its excitation spectrum, in Ref. [47], recent advances in lattice simulation technology, including anisotropic lattices, improved gauge actions, and large sets of creation operators,were employed to investigate the static energies of gluonic excitations between static quarks (hybrid static energies).

In NRQCD (as in QCD) the gluonic excitations between static quarks have the same symmetries of a diatomic molecule plus charge conjugation. In the centre-of-mass system these correspond to the symmetry group $D_{\infty h}$ (substituting the parity generator by CP). The mass eigenstates are classified in terms of the angular momentum along the quark–antiquark axes ($|L_z| = 0, 1, 2, \ldots$ which traditionally are labelled as $\Sigma, \Pi, \Delta, \ldots$), CP (even, g, or odd, u), and the reflection properties with respect to a plane passing through the quark–antiquark axes (even, $+$, or odd, $-$). Only the Σ states are not degenerate with respect to the reflection symmetry, see also Section 2.2.2. In Fig. 3.8 we display lattice results of

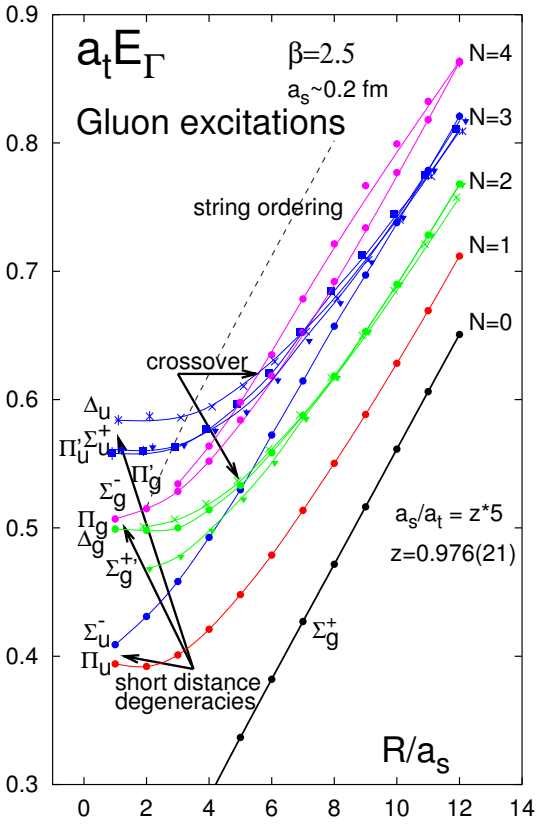

Fig. 3.8: The spectrum of gluonic excitations in the presence of a static quark–antiquark pair separated by a distance R in 4-dimensional $SU(3)$ gauge theory (from Ref. [47]). Results are from one simulation for lattice spacing $a_s \sim 0.2$ fm using an improved action on a $(10^2 \times 30) \times 60$ anisotropic lattice with coupling $\beta = 2.5$ and bare aspect ratio $\xi = 5$. At large distances, *all* levels without exception are consistent with the expectations from an effective string theory description. A dramatic level rearrangement is observed in the crossover region between $0.5 - 2.0$ fm. The dashed line marks a lower bound for the onset of mixing effects with glueball states.

the hybrid static energies V_H obtained from Wilson loops with operators of the appropriate symmetry inserted at the end points.

$D_{\infty h}$ is a subgroup of the rotational symmetry group $O(3)$ times charge conjugation. In the short-range limit, $r \ll \Lambda_{\rm QCD}$, the hybrid energies approach so-called gluelump levels that can be classified according to the usual $O(3)$ J^{PC}. The corresponding operators can be explicitly constructed using pNRQCD in the static limit [5]. In the case of pure gluodynamics, the spectrum then consists of static energies which depend on **r**. The energy units are provided by the only other scale in the problem, $\Lambda_{\rm QCD}$. The gluelumps operators are of the type $\mathrm{Tr}\{\mathrm{O}H\}$, where $\mathrm{O} = O^aT^a$ corresponds to a quark–antiquark state in the adjoint representation (the octet) and $H = H^aT^a$ is a gluonic operator. By matching the QCD static hybrid operators into pNRQCD, we get the static energies (also called hybrids static potentials) V_H of the gluelumps. At leading order in the multipole expansion, they read [5]

$$V_H(r) = V_o(r) + \frac{1}{T_g^H}, \tag{3.22}$$

being T_g^H the correlation time of the corresponding gluelump correlator $\langle H^a(t)\phi(t,0)^{\rm adj}_{ab}H^b(0)\rangle^{\rm non-pert.} \simeq h\, e^{-it/T_g^H}$. The lattice data confirm that (in the region in which decay into glueball channels is not yet possible) all the V_H behave like $V_o^{(0)} = \frac{\alpha_s}{6r}$ for $r \to 0$ cf. Fig. 3.8 and Ref. [65]. The constant T_g^H depends on the gluelump operator H, its inverse corresponds to the mass of the gluelump H. Note that

T_g^H are scheme and scale dependent. pNRQCD, in which r is integrated out, predicts the short-range degeneracies,

$$\Sigma_g^{+\prime} \sim \Pi_g \; ; \qquad \Sigma_g^- \sim \Pi_g' \sim \Delta_g \; ; \quad \Sigma_u^- \sim \Pi_u \; ; \qquad \Sigma_u^+ \sim \Pi_u' \sim \Delta_u \, . \tag{3.23}$$

This is confirmed by the lattice data, cf. Fig. 3.8. Similar observations have also been previously made in the lattice theory in Ref. [153]. It is interesting to notice that the hierarchy of the states, as displayed in Fig. 3.8, is reflected in the dimensionality of the operators of pNRQCD [5, 65].

By using only $\mathbf{E}$ and $\mathbf{B}$ fields and keeping only the lowest-dimensional representation we may identify the operator H for the short-range hybrids called $\Sigma_g^{+\prime}$ (and Π_g) with $\mathbf{r} \cdot \mathbf{E}$ (and $\mathbf{r} \times \mathbf{E}$) and the operator H for the short-range hybrids called Σ_u^- (and Π_u) with $\mathbf{r} \cdot \mathbf{B}$ (and $\mathbf{r} \times \mathbf{B}$). Hence, the corresponding static energies for small r are

$$V_{\Sigma_g^{+\prime},\Pi_g}(r) = V_o(r) + \frac{1}{T_g^E}, \qquad\qquad V_{\Sigma_u^-,\Pi_u}(r) = V_o(r) + \frac{1}{T_g^B}.$$

The lattice results of Ref. [47] show that, in the short range, $V_{\Sigma_g^{+\prime},\Pi_g}(r) > V_{\Sigma_u^-,\Pi_u}(r)$. This supports the sum-rule prediction [154] that the pseudovector hybrid lies lower than the vector one, i.e., $T_g^E < T_g^B$ and the lattice evaluations of Refs. [65, 153]. In this way, in the short-distance limit, we can relate the behavior of the energies for the gluonic excitations between static quarks with the large time behavior of gluonic correlators. We can extract results for gauge invariant two-point gluon field strength correlators (which are also the relevant nonperturbative objects in the stochastic vacuum model [137]) $\langle 0|F_{\mu\nu}^a(t)\phi(t,0)_{ab}^{\rm adj}F_{\mu\nu}^b(0)|0\rangle$, ϕ being the adjoint string. One can parameterize these correlators in terms of two scalar functions: $\langle 0|\mathbf{E}^a(t)\phi(t,0)_{ab}^{\rm adj}\mathbf{E}^b(0)|0\rangle$ and $\langle 0|\mathbf{B}^a(t)\phi(t,0)_{ab}^{\rm adj}\mathbf{B}^b(0)|0\rangle$ with correlations lengths: $T^E = 1/\Lambda_E$ and $T^B = 1/\Lambda_B$, respectively. Note that while differences between gluelump masses Λ_H are universal the absolute normalization is scheme- and scale-dependent [65].

The matching of pNRQCD to ($n_f = 0$) QCD has been performed in the static limit to $\mathcal{O}(\alpha_{\rm s}^3)$ in the lattice scheme and the (scheme- and scale-dependent) gluelump masses $\Lambda_H = 1/T_g^H$ have been determined both, in the continuum limit from short distance energy levels and at finite lattice spacing from the gluelump spectrum [65]. Perfect agreement between these two determinations was found. It would be highly desirable to have lattice determinations at even shorter distances to further increase the precision of such determinations, however, such calculations are rather challenging due to the need to properly treat lower-lying glueball scattering states.

The behaviour of the hybrid static energies for large r provides further valuable information on the mechanism of confinement. The linearly rising ground-state energy is *not* conclusive evidence of string formation [138]. Computations of the gluon action density surrounding a static quark–antiquark pair in $SU(2)$ gauge theory also hint at flux tube formation [155]. Complementary information come from the study of the static energies of the gluonic excitations between static quarks. A treatment of the gluon field in terms of the collective degrees of freedom associated with the position of the long flux might then be sufficient for reproducing the long-wavelength physics. If true, one then hopes that the oscillating flux can be well described in terms of an effective string theory [66]. In such a case, the lowest-lying excitations are expected to be the Goldstone modes associated with the spontaneously broken transverse translational symmetry. These modes are a universal feature of any low-energy description of the effective QCD string and have energy separations above the ground state given by multiples of π/R. A well-defined pattern of degeneracies and level orderings among the different symmetry channels form a very distinctive signature of the onset of the Goldstone modes for the effective QCD string.

The spectrum of more than a dozen levels shown in Fig. 3.8 provides strong evidence that the gluon field can be well approximated by an effective string theory for large separations R. For separations above 2 fm, the levels agree *without exception* with the ordering and degeneracies expected from an effective string theory. The gaps agree well with $N\pi/R$, but a fine structure remains, offering the possibility

to obtain details of the effective QCD string action in future higher precision simulations. For small $R < 2$ fm, the level orderings and degeneracies are not consistent with the expectations from an effective string description, and the gaps differ appreciably from $N\pi/R$ with $N = 1, 2, 3, \ldots$. Such deviations, as large as 50% or more, cannot be considered mere corrections, making the applicability of an effective string description problematical. Between 0.5 to 2 fm, a dramatic level rearrangement occurs.

Non-universal details of the underlying string description for large separations, such as higher order interactions and their couplings, are encoded in the fine structure of the spectrum at large separations. It is hoped that near future simulations will have sufficient precision to be able to differentiate between such corrections. In the meantime, the excitation spectrum in other space–time dimensions and other gauge theories, such as $SU(2)$ and $Z(2)$, are being explored [149, 156].

2.3.4 pNRQCD for QQQ and QQq baryons[19]

In the case of a bound state formed by three heavy quarks, still a hierarchy of physical scales similar to the quarkonium case exists. Consequently, starting from a NRQCD description for each heavy quark, it is possible to integrate out the scale of the momentum transfer $\simeq mv$ and write the pNRQCD Lagrangian for heavy baryons [157, 158]. Similarly to before two different dynamical situations may occur: the momentum transfer is much larger than $\Lambda_{\rm QCD}$, or it is of order $\Lambda_{\rm QCD}$. In the first case the matching is perturbative and the Lagrangian is similar to Eq. (3.9) with more degrees of freedom for the quark part: two octets, one singlet and one decuplet (as it comes from the colour decomposition of $3 \times 3 \times 3$) [157]. In the second case the matching is nonperturbative and the Lagrangian is similar to Eq.(3.11) with only the three quark singlet as degree of freedom. The (matching) potentials are nonperturbative objects and their precise expression in terms of static Wilson loop and (chromo)electric and (chromo)magnetic insertions in static Wilson loops can be calculated [157]. Experimental data for baryons composed by three quarks are not existing at the moment, however lattice calculation of the three quark potential exist [53–55].

Baryons made by two heavy quarks and a light quark QQq combine the slow motion of the heavy quark with the fast motion of the light quark. Thus a treatment combining in two steps an effective field theory for the QQ interaction and an effective field theory for the QQ degrees of freedom with the light quark is the most appropriate one. The interest of these states is also related to the fact that the SELEX experiment recently announced the discovery of four doubly charmed baryon states. This will be discussed in more detail in Section 3.4.2. The non relativistic motion of the two heavy quarks is similar to quarkonium while the light quark is moving relativistically around the slowly moving QQ. Since the QQ is in a colour antitriplet state, in the heavy quark limit the system is similar to a $\bar{Q}q$ system. However, the situation is much more interesting because if one constructs first the EFT for the two heavy quarks more degrees of freedom enter and depending on the dynamical situation of the physical system, these degrees of freedom may or may not have a role. In particular if we work under the condition that the momentum transfer between the two heavy quarks is smaller than $\Lambda_{\rm QCD}$, then we can construct a pNRQCD Lagrangian of the type Eq. (3.9) with a triplet and a sextet as QQ degrees of freedom [157]. Such degrees of freedom, would also be relevant for the study of double charmonia production [159].

2.4 Thresholds effects (EFT)[20]

For states for which $k \sim E \sim \Lambda_{\rm QCD}$, namely close or beyond threshold, one has to stay at the NRQCD level. It is still an open question whether one can build a suitable EFT to study mixing and threshold effects.

For a confining potential (e.g., harmonic oscillator), however, the typical momentum transfer k decreases with the principal quantum number whereas both the typical relative three-momentum p and the binding energies increase. For some principal quantum number n, the binding energy will become com-

[19] Author: N. Brambilla

[20] Authors: N. Brambilla, J. Soto

parable to the momentum transfer and hence $k \geq E$ will not hold anymore. For these states pNRQCD is not a good effective theory anymore (it may still remain a successful model). This is expected to happen for states close to or higher than the heavy-light meson pair threshold. There is no EFT beyond NRQCD available for this regime at the moment. Notice also that for some n the typical three momentum will become comparable to m and hence relativistic effects will not be small and NRQCD will not be a good EFT anymore. This is expected to happen for states much higher than the heavy-light meson pair threshold. Relativistic quark models like the ones discussed in Section 3 are probably unavoidable for this situation although it is not known at the moment how to link them to QCD.

3 PHENOMENOLOGICAL APPROACH[21]

From the discovery of charmonium states [160–162], QCD motivated potential models have played an important role in understanding quarkonium spectroscopy [163–166]. The initial models describing charmonium spectroscopy, using a QCD motivated Coulomb plus linear confining potential with colour magnetic spin dependent interactions, have held up quite well. This approach also provides a useful framework for refining our understanding of QCD and guidance towards progress in quarkonium physics. The discovery of the Υ family of meson [167] was quickly recognized as a $b\bar{b}$ bound state whose spectroscopy was well described by the potential model picture used to describe the charmonium system.

In this section we give an overview of potential models of quarkonium spectroscopy [168]. Most models [169–180] have common ingredients. Almost all such models are based on some variant of the Coulomb plus linear potential confining potential expected from QCD. Quark potential models typically include one-gluon exchange and most models also include the running constant of QCD, $\alpha_{\rm s}(Q^2)$. Finally, relativistic effects are often included at some level [169–183]. At the minimum, all models we consider include the spin-dependent effects that one would expect from one-gluon-exchange, analogous to the Breit–Fermi interaction in QED, plus a relativistic spin–orbit Thomas precession term expected of an object with spin (the quark or antiquark) moving in a central potential. Potential models have been reasonably successful in describing most known mesons. Although cracks have recently appeared [187, 188] these point to the need for including physics effects that have hitherto been neglected such as coupled channel effects [188].

In the next section we will give a brief introduction to quark potential models and attempt to describe the differences between models. The subject is roughly thirty years old and a large literature on the subject exists. It is impossible to cover all variants and we will almost totally neglect the considerable work that brought us to where we are today. We apologise to all those whose work we do not properly cite and hope they understand. In the next sections we compare the predictions of some models with experiment for the $c\bar{c}$, $b\bar{b}$ and $c\bar{b}$ mesons and point out variations in predictions and how they arise from the underlying model.

3.1 Potential models[22]

Quarkonium potential models typically take the form of a Schrödinger like equation:

$$[T + V]\Psi = E\Psi \tag{3.24}$$

where T represents the kinetic energy term and V the potential energy term. We lump into these approaches the Bethe–Salpeter equation (e.g., Ref. [182, 184]) and quasi-potential approaches (e.g., Ref. [173]).

[21] Author: S. Godfrey
[22] Author: S. Godfrey

Different approaches have been used for the kinetic energy term ranging from the non-relativistic Schrödinger equation to relativistic kinetic energy [171, 179, 189]

$$T = \sqrt{p^2 + m_Q^2} + \sqrt{p^2 + m_{\bar{Q}}^2} \tag{3.25}$$

in the spinless Salpeter equation.

3.1.1 The potential

The quark–antiquark potential is typically motivated by the properties expected from QCD [48, 128–134] and while there are differences, most recent potentials show strong similarities. It is worth pointing out that in the early days of quarkonium spectroscopy this was not obvious and much effort was expended in fitting different functional forms of the potential to the observed quarkonium masses. In the end, the shape of the potentials converged to a form that one might expect from the asymptotic limits of QCD and which has been qualitatively verified by Lattice QCD calculations [135] of the expression of the potentials obtained in the Wilson loop [128–134] and in the EFT [48] approach. This is a great success of quarkonium phenomenology.

To derive the quarkonium potential we start with QCD where the gluons couple to quarks and to each other. The quark–gluon interaction is similar to the electron–photon interaction in quantum electrodynamics with the Born term for the qq or $q\bar{q}$ interaction at short distance being the familiar $1/r$ form. In contrast with QED the gluon self-coupling results in a slow decrease of the effective coupling strength at short distance. In terms of the Fourier conjugate momentum the lowest order QCD corrections to $\alpha_{\rm s} = g_s^2/4\pi$ can be parametrized as

$$\alpha_{\rm s}(Q^2) = \frac{12\pi}{(33 - 2n_f)\ln(Q^2/\Lambda^2)} \tag{3.26}$$

where n_f is the number of Fermion flavours with mass below Q, and $\Lambda \sim \Lambda_{\rm QCD}$ is the characteristic scale of QCD measured to be ~ 200 MeV. At short distances one-gluon-exchange leads to the Coulomb like potential

$$V(r) = -\frac{4}{3}\frac{\alpha_{\rm s}(r)}{r} \tag{3.27}$$

for a $q\bar{q}$ pair bound in a colour singlet where the factor of $4/3$ arises from the SU(3) colour factors. At short distances one-gluon-exchange becomes weaker than a simple Coulomb interaction.

At momentum scales smaller than $\Lambda_{\rm QCD}$ which corresponds to a distance of roughly 1 fm, $\alpha_{\rm s}$ blows up and one-gluon-exchange is no longer a good representation of the $q\bar{q}$ potential. The qualitative picture is that the chromoelectric lines of force bunch together into a *flux tube* which leads to a distance-independent force or a potential

$$V(r) = \sigma r. \tag{3.28}$$

This has been validated by Lattice QCD calculations. Phenomenologically, every recent model which we will consider has found $\sigma \sim 0.18$ GeV^2.

Numerous variations of the resulting Coulomb plus linear potential exist in the literature. Some of the better known ones are the Cornell potential [170], Richardson's potential [190], and the Buchmüller Tye potential [191]. Overall, the spin-independent features of quarkonium spectroscopy are well described by the potentials just described.

Let us also mention that heavy quark mass corrections to the (static) central (spin and velocity independent) potential exist, although they have not yet been taken into account in potential models applications so far. They correspond to $V_r^{(1,0)}$, $V_r^{(2,0)}$ and $V_r^{(1,1)}$ in Section 2.3.2. Their expressions in perturbation theory are known [48, 68]. Part of $V_r^{(2,0)}$ and $V_r^{(1,1)}$ was included in the phenomenological application to the spectrum in Refs. [128, 129, 135, 185].

3.1.2 Spin-dependent potentials

Spin dependent multiplet splittings are an important test of the details of quarkonium models. In particular, the nature of spin dependent potentials are decided by the Lorentz nature of the confining potentials [129, 131, 138, 186]. While there is general consensus that the short distance one-gluon-exchange piece is Lorentz vector and the linear confining piece is Lorentz scalar this is by no means universal and other possibilities are vigorously advocated. Gromes described how to obtain the spin-dependent potentials given the Lorentz structure of the interaction [129] and one can also use the prescription given in Berestetskij, Lifschitz and Pitaevskij [192]. Simply put, one can obtain the form of the spin dependent interaction by Fourier transforming the on-shell $q\bar{q}$ scattering amplitude:

$$M = [\bar{u}(p'_f)\Gamma u(p'_i)]\; V(Q^2)\; [\bar{u}(p_f)\Gamma u(p_i)] \tag{3.29}$$

where the Γ matrices give the Lorentz structure of the interaction and $V(Q^2)$ is the Fourier transform of the spin-independent potential. For example, for a Lorentz-vector interaction $\Gamma = \gamma^\mu$ and for a Lorentz-scalar interaction $\Gamma = \mathrm{I}$. In principle other forms are possible with each giving rise to characteristic spin-dependent interactions. These can be found by expanding the scattering amplitude to order $(v/c)^2$ which corresponds to an expansion in inverse powers of quark masses. In the early years of quarkonium phenomenology they were all tried and it was found that the Lorentz-vector one-gluon-exchange plus Lorentz scalar linear confining potential gave the best agreement with experiment [23]. Note that the form of the full QCD potential at order $1/m^2$ [48, 128, 130–133] has now been obtained in the EFT (cf. Section 2.3.2), and while the spin-dependent nonperturbative potential may correspond to a scalar interaction in the language used above, the velocity-dependent potentials do not fit such a picture. The effective kernel is thus not a simple scalar, precisely the dependence both on the momentum and on the Lorentz structure is more involved than a pure convolution (i.e., only depending on the momentum transfer) scalar structure [48, 134, 138, 186]. However, the spin dependency is well approximated by a scalar interaction for phenomenological applications. The QCD spin-dependent potentials are explicitly given in Section 2.3.2. A complete calculation of the spin structure of the spectrum using the full expression given in Section 2.3.2 does not yet exist.

To lowest order in $(v/c)^2$ the Lorentz-vector one-gluon-exchange gives rise to terms familiar from one-photon exchange in atomic physics. The colour contact interaction, which in the language of Section 2.3.2 corresponds to taking $V_{S^2}^{(1,1)}(r)$ at leading order in perturbation theory,

$$H_{q\bar{q}}^{cont} = \frac{32\pi}{9}\frac{\alpha_{\mathrm{s}}(r)}{m_q m_{\bar{q}}}\mathbf{S}_q \cdot \mathbf{S}_{\bar{q}}\, \delta^3(\mathbf{r}) \tag{3.30}$$

gives rise to, for example the $J/\psi - \eta_c$ splitting. The colour tensor interaction, which in the language of Section 2.3.2 corresponds to taking $V_{\mathbf{S}_{12}}^{(1,1)}(r)$ at leading order in perturbation theory,

$$H_{q\bar{q}}^{ten} = \frac{4}{3}\frac{\alpha_{\mathrm{s}}(r)}{m_q m_{\bar{q}}}\frac{1}{r^3}\left[\frac{3\,\mathbf{S}_q \cdot \mathbf{r}\;\mathbf{S}_{\bar{q}} \cdot \mathbf{r}}{r^2} - \mathbf{S}_q \cdot \mathbf{S}_{\bar{q}}\right] \tag{3.31}$$

contributes to splitting of $L \neq 0$ spin triplet multiplets like the χ_{cJ} and χ_{bJ} multiplets. The final spin dependent term is the spin orbit interaction which has two contributions. The first piece arises from the colour-magnetic one-gluon-exchange while the second piece is the Thomas precession term which is a relativistic effect for an object with spin moving in a central potential

$$H_{q\bar{q}}^{s.o.} = H_{q\bar{q}}^{s.o.(cm)} + H_{q\bar{q}}^{s.o.(tp)}. \tag{3.32}$$

The colour magnetic piece arising from one-gluon exchange is given by:

$$H_{q\bar{q}}^{s.o.(cm)} = \frac{4}{3}\frac{\alpha_{\mathrm{s}}(r)}{r^3}\left(\frac{\mathbf{S}_q}{m_q m_{\bar{q}}} + \frac{\mathbf{S}_{\bar{q}}}{m_q m_{\bar{q}}} + \frac{\mathbf{S}_q}{m_q^2} + \frac{\mathbf{S}_{\bar{q}}}{m_{\bar{q}}^2}\right) \cdot \mathbf{L} \tag{3.33}$$

[23] Although other forms are still advocated. See Ebert *et al.* [173, 193].

and the Thomas precession term is given by

$$H_{q\bar{q}}^{s.o.(tp)} = -\frac{1}{2r}\frac{\partial H_{q\bar{q}}^{conf}}{\partial r}\left(\frac{\mathbf{S}_q}{m_q^2} + \frac{\mathbf{S}_{\bar{q}}}{m_{\bar{q}}^2}\right)\cdot\mathbf{L} \tag{3.34}$$

which includes a contribution from both the short distance $1/r$ piece and the linear Lorentz-scalar confining potential. In the language of Section 2.3.2, both terms in (3.32) are obtained by taking $V_{LS}^{(1,1)}$ at leading order in perturbation theory and using the Gromes relation for $V_{LS}^{(2,0)}$. In these formulae $\alpha_{\rm s}(r)$ is the running coupling constant of QCD.

For mesons consisting of quarks with different flavours such as the B_c meson, charge conjugation is no longer a good quantum number so states with different total spins but with the same total angular momentum, like the ${}^3P_1$ – ${}^1P_1$ and ${}^3D_2$ – ${}^1D_2$ pairs (i. e. $J = L$ for $L \geq 1$) can mix via the spin–orbit interaction or some other mechanism. Equations (3.33) and (3.34) can be rewritten to explicitly give the antisymmetric spin–orbit mixing term:

$$H_{s.o.}^{-} = +\frac{1}{4}\left(\frac{4}{3}\frac{\alpha_{\rm s}}{r^3} - \frac{k}{r}\right)\left(\frac{1}{m_Q^2} - \frac{1}{m_{\bar{Q}}^2}\right)\,\mathbf{S}_-\cdot\mathbf{L} \tag{3.35}$$

where $\mathbf{S}_- = \mathbf{S}_Q - \mathbf{S}_{\bar{Q}}$. Consequently, the physical the physical $J = L$ ($J \geq 1$) states are linear combinations of ${}^3L_J$ and ${}^1L_J$ states which we describe by the following mixing:

$$\begin{aligned} L' &= {}^1L_J\cos\theta_{nL} + {}^3L_J\sin\theta_{nL} \\ L &= -{}^1L_J\sin\theta_{nL} + {}^3L_J\cos\theta_{nL} \end{aligned} \tag{3.36}$$

where L designates the relative angular momentum of the $Q\bar{Q}$ pair and the subscript is the total angular momentum of the $Q\bar{Q}$ which is equal to L. Our notation implicitly implies $L-S$ coupling between the quark spins and the relative angular momentum. In the limit in which only one quark mass is heavy, $m_Q \to \infty$, and the other one is light the states can be described by the total angular momentum of the light quark which is subsequently coupled to the spin of the heavy quark. This limit gives rise to two doublets, one with $j = 1/2$ and the other $j = 3/2$ and corresponds to two physically independent mixing angles $\theta = -\tan^{-1}(\sqrt{2}) \simeq -54.7^\circ$ and $\theta = \tan^{-1}(1/\sqrt{2}) \simeq 35.3^\circ$ [194, 195]. Some authors prefer to use the $j-j$ basis [196] but we will follow the $L-S$ eigenstates convention implied in the spin–orbit terms given above and include the LS mixing as a perturbation. It is straightforward to transform between the $L-S$ basis and the $j-j$ basis. We note that radiative transitions are particularly sensitive to the ${}^3L_L$ – ${}^1L_L$ mixing angle with the predictions from the different models giving radically different results. We also note that the definition of the mixing angles are fraught with ambiguities. For example, charge conjugating $c\bar{b}$ into $b\bar{c}$ flips the sign of the angle and the phase convention depends on the order of coupling $\mathbf{L}$, $\mathbf{S}_Q$ and $\mathbf{S}_{\bar{Q}}$ [195].

3.1.3 Relativistic corrections

The Hamiltonian with the spin-dependent terms as written above is actually inconsistent as it stands as the terms more singular than r^{-2} are illegal operators in the Schrödinger equation. This is resolved by returning to the full scattering amplitude which has the effect of smearing the coordinate $\mathbf{r}$ out over distances of the order of the inverse quark mass and the strengths of the various potentials become dependent on the momentum of the interacting quarks. The smearing of the potentials has the consequence of taming the singularities. Alternatively, if one regards this Hamiltonian in the spirit of effective field theories, these singular operators are subleading in any reasonable power counting, and hence they must be treated as a perturbation. They may need regularization (smearing) at higher orders of perturbation theory, which introduces a scale dependence. This scale dependence cancels against the one of higher order NRQCD matching coefficients, see Section 2.3.2,

From this starting point different authors [169–180] diverge in how they incorporate further relativistic corrections. For example, Godfrey and Isgur (GI) [171] use the full relativistic scattering amplitude as the starting point but do not take it literally and instead parameterize the various relativistic effects. The relativistic smearing is described by a quark form factor and momentum dependent corrections are parametrized in a form that is in keeping with the generalities, if not the details, of the $q\bar{q}$ scattering amplitude. The reasoning is that the scattering amplitudes are for free Dirac Fermions while quarks inside a hadron are strongly interacting and will have off-mass-shell behavior. In addition, in field theory the Schrödinger equation arises in the $q\bar{q}$ sector of Fock space by integrating over more complex components of Fock space such as $|q\bar{q}g\rangle$. This integration will introduce additional momentum dependence in the $q\bar{q}$ potential not reflected in eq. (3.29). There are other deficiencies that arise from taking eq. (3.29) literally. Thus, GI use the full scattering amplitude as a framework on which to build a semiquantitative model of relativistic effects. While they acknowledge that this procedure is not entirely satisfactory they argue that it enables them to successfully describe all mesons, from the lightest to the heaviest, in a unified framework.

In contrast, the more recent work by Ebert, Faustov and Galkin performs an expansion in powers of velocity, including all relativistic corrections of order v^2/c^2, including retardation effects and one-loop radiative corrections [173, 193]. Ebert *et al* use a quasipotential approach in which the quasipotential operator of the quark–antiquark interaction is constructed with the help of the off-mass-shell scattering amplitude. The expression they derived to describe the spin-independent and spin-dependent corrections are rather lengthy and we refer the reader to their papers [173, 193, 197]. They found that relativistic effects are important, particularly in radiative transitions (which are outside the scope of this section).

While the GI calculation [171] assumed a short distance Lorentz-vector interaction and a Lorentz-scalar confining potential Ebert *et al* [173, 193] employ a mixture of long-range vector and scalar linear confining potentials. The effective long-range vector vertex includes an anomalous chromomagnetic moment of the quark, κ. The fitted value for κ results in the vanishing of the long-range magnetic contribution to the potential so that the long range confining potential is effectively Lorentz scalar.

In both cases taking the non-relativistic limit recovers eqns. (3.30–3.34). Despite differences in the details of the various approaches most recent calculations are in fairly good agreement.

3.1.4 Charm mass corrections to the bottomonium mass spectrum[24]

For the calculation of the bottomonium mass spectrum it is necessary to take into account additional corrections due to the non-zero mass of the charm quark [75, 95, 198, 199]. The one-loop correction to the one-gluon exchange part of the static $Q\bar{Q}$ potential in QCD due to the finite c quark mass is given by [75, 200]

$$\Delta V_{m_c}(r) = -\frac{4}{9}\frac{\alpha_{\rm s}^2(\mu)}{\pi r}\left[\ln(\sqrt{a_0}m_c r) + \gamma_E + E_1(\sqrt{a_0}m_c r)\right], \qquad E_1(x) = \int_x^\infty e^{-t}\,\frac{dt}{t} \tag{3.37}$$

where $\gamma_E \cong 0.5772$ is the Euler constant and $a_0 \cong 5.2$. Averaging of $\Delta V_{m_c}(r)$ over solutions of the relativistic wave equation with the Cornell and Coulomb potentials yields the bottomonium mass shifts presented in Table 3.4.

The Table 3.4 shows that for a fixed value of $\alpha_{\rm s}$ the averaging with and without confining potential substantially differ especially for the excited states. For growing $n = n_r + L + 1$ the values of $\langle \Delta V_{m_c} \rangle$ slowly decrease for Cornell potential whereas for the Coulomb potential with a fixed value of $\alpha_{\rm s}$ they fall rapidly. The bottomonium mass spectrum with the account of the finite charm mass corrections was obtained in Refs. [95, 173]

[24] Author: R. Faustov

Table 3.4: Charm mass corrections to the bottomonium masses (in MeV).

State	$1S$	$1P$	$2S$	$1D$	$2P$	$3S$
$\langle\Delta V_{m_c}\rangle^{\alpha_s=0.22}_{\rm Cornell}$ [200]	-12	-9.3	-8.7	-7.6	-7.5	-7.2
$\langle\Delta V_{m_c}\rangle^{\alpha_s=0.22}_{\rm Coul}$	-9.5	-4.2	-3.8	-2.3	-2.2	-2.1
$\langle\Delta V_{m_c}\rangle^{\alpha_s=0.3}_{\rm Coul}$	-20.7	-9.7	-8.8	-5.5	-5.2	-4.9
$\langle\Delta V_{m_c}\rangle_{\rm Coul}$ [95]	-14.3	-22.1	-21.9		-49	-40.5
$\alpha_s(\mu)$	0.277	0.437	0.452		0.733	0.698

3.1.5 Coupled-channel effects

An important ingredient that has not received the attention it deserves but which has been brought to the forefront by some spectacular recent failures of quark models are coupled channel effects. As the mass of a quarkonium state approaches the threshold for decay to pairs of flavoured mesons, contributions from virtual loops of the flavoured meson channels are expected to make important contributions to masses and other meson properties [169, 170, 201]. These coupled channel effects are expected to shift masses from naive quark model predictions and to alter decay and production properties due to higher order Fock-space components present in the wavefunctions. These may account for the discrepancies between quark model predictions and those of the recently discovered and $X(3872)$ properties [187, 188]. There has been very little work on this important subject since the original Cornell model [169, 170] and it is an important topic that needs to be addressed [188]. For the charmonium example the present situation is discussed in Section 3.3.

3.2 Comparison of models with experiment[25]

3.2.1 Bottomonium

We start with the $b\bar{b}$ system as it has the most states observed of any of the heavy quarkonium systems (see Table 3.5). This is due to the fact that threshold for the Zweig allowed decay to $B\overline{B}$ lies above the $3S$ state. The $J^{PC} = 1^{--}$ n^3S_1 states are copiously produced in e^+e^- annihilation and can decay via $E1$ transitions to the 1^3P_J and 2^3P_J multiplets. The masses of the χ_b states provide valuable tests of the spin-dependence of the various models. In particular, the splittings of the ^3P_J masses are determined by the spin–orbit and tensor terms which are sensitive to the presence of vector and scalar interactions. The Lorentz vector one-gluon-exchange plus Lorentz scalar linear confinement gives a good description of the data (as long as no velocity dependent corrections are included [185, 202].

A test of potential models is their ability to predict as yet unseen properties correctly. Most potential models predict that the lowest D-wave centre of gravity is around 10.16 GeV. Although details of the multiplet splittings differ most models predict that the splittings are smaller than in the P-wave states. Thus, the observation of these states represents an important test of potential models.

Recently the CLEO collaboration has observed the first D-wave $b\bar{b}$ state in the cascade $\Upsilon(3S)\to\chi_b'\gamma\to{}^3D_J\gamma\gamma\to\chi_b\gamma\gamma\gamma\to\Upsilon(1S)\gamma\gamma\gamma\gamma$ [203]. Due to expected transition probabilities (essentially reliable Clebsch factors) it is believed that the observed state is the $J = 2$, 1^3D_2 state. This is an important observation as it is able to distinguish among the various models [204]. Unfortunately this programme at CLEO is completed and it is not clear when there will be another opportunity to search for more of the missing states.

So far no spin singlet $b\bar{b}$ state has been observed. The mass splittings between the singlet and triplet states is a key test of the applicability of perturbative quantum chromodynamics to the $b\bar{b}$ system and is a useful check of lattice QCD results. The η_b (n^1S_0) states can be produced via M1 radiative

[25] Authors:S. Godfrey

Table 3.5: Predicted and observed masses of $b\bar{b}$ states.

State	expt	GI85 [171]	FU91 [175]	EQ94 [196]	GJ96 [179]	EFG03 [173]	ZVR95 [180]
1^3S_1	9460	9465	9459	9464	9460	9460	9460
1^1S_0		9402	9413	9377	9408	9400	9410
1^3P_2	9913	9897	9911	9886	9914	9913	9890
1^3P_1	9893	9876	9893	9864	9893	9892	9870
1^3P_0	9860	9847	9865	9834	9862	9863	9850
1^1P_1		9882	9900	9873	9901	9901	9880
2^3S_1	10023	10003	10015	10007	10016	10023	10020
2^1S_0		9976	9992	9963	9991	9993	10000
1^3D_3		10155	10172	10130		10162	10150
1^3D_2	10162	10147	10166	10126		10158	10150
1^3D_1		10138	10158	10120		10153	10140
1^1D_2		10148	10167	10127		10158	10150
2^3P_2	10269	10261	10269	10242	10270	10268	10280
2^3P_1	10255	10246	10256	10224	10254	10255	10260
2^3P_0	10232	10226	10234	10199	10229	10234	10240
2^1P_1		10250	10261	10231	10259	10261	10270
3^3S_1	10355	10354	10356	10339	10358	10355	10390
3^1S_0		10336	10338	10298	10338	10328	10370

transitions from the Υ (n^3S_1) states, either unhindered or hindered, and via E1 radiative transitions from the n^1P_1 states [205]. In the latter case, the decay chain would be $\Upsilon(3S)\to h_b(^1P_1)\pi\pi$ followed by $h_b\to\eta_b\gamma$. The decay chain $\Upsilon(3S)\to h_b + \pi^0\to\eta_b + \pi^0 + \gamma$ is also possible [206]. We note that there does not appear to be a consensus in the literature on the relative importance of the two $\Upsilon\to h_b$ hadronic transitions. The decay chains proceeding via an intermediate h_b would also be a means of observing the h_b state. A recent run by CLEO did not lead to reports of the observation of the η_b state although the limits straddles the range of predictions. There is also the possibility that the η_b can be observed by the Tevatron and LHC experiments.

3.2.2 Charmonium

The discovery of the J/ψ and ψ' states revolutionized our understanding of hadron spectrocopy by demonstrating that they could be well described by potential models with the qualitative features expected from QCD (see Table 3.6).

The spin triplet $^3S_1$ states are produced copiously in e^+e^- annihilation and the ^3P_J states are produced via $E1$ radiative transitions. The χ_0 ($^3P_0$), χ_1 ($^3P_1$) and χ_2 ($^3P_2$) $c\bar{c}$ states were first discovered in radiative decays from the 2^3S_1 level (the $\psi(3685)$). The χ states themselves undergo radiative transitions to the J/ψ with measured partial widths in reasonable agreement with theoretical predictions once relativistic effects are taken into account.

The singlet states have been far more elusive. The 1^1S_0 state has been known for some time, seen in magnetic dipole ($M1$) transitions from both the J/ψ and ψ'. In contrast, a strong claim for observation of the 2^1S_0 state has only occurred recently, first with its observation in the decay $B\to K\eta_c'$, $\eta_c'\to K_sK^+\pi^-$ by the Belle Collaboration [207] and its subsequent observation by Belle in the mass

spectrum recoiling against J/ψ in e^+e^- annihilation [208] and by CLEO [209] and Babar [210] in $\gamma\gamma$ collisions. While the mass measurement by Belle was higher than expected by most quark potential models, the current world average [245] is in reasonable agreement with theory.

One place the models disagree is in the mass of the 1^1P_1 state relative to the 1^3P_J cog [206]. However, the $^1P_1$ state has yet to be confirmed. The $1^3P_{cog} - 1^1P_1$ splitting is dependent on the Lorentz structure of the interquark potentials and relativistic corrections so that the h_c mass measurement is an important test of perturbative QCD and more phenomenological quark potential models which have a large variation of predictions. The decay chain $\psi' \to h_c + \pi^0 \to \eta_c + \pi^0 + \gamma$ has been discussed as a possible mode of discovery of the h_c [206]. Optimistically, one might hope that the current CLEO run will see evidence for the h_c in this cascade.

The charmonium D-wave states are predicted to lie above $D\overline{D}$ threshold. The $\psi(3770)$ is associated with the 1^3D_1 state. It's leptonic width is larger than expected for a pure D state which is probably due to mixing with the 2^3S_1 state induced by tensor mixing or coupled channel effects. The 1^3D_3, 1^3D_2, and 1^1D_2 are predicted to lie close in mass to the $\psi(3770)$. A $J^P = 2^-$ state cannot decay to two 0^- particles so the 1^3D_2 and $^1D_2$ cannot decay to $D\overline{D}$ and are expected to lie below the $D^*\overline{D}$ threshold. They are therefore expected to be narrow with prominent transitions to lower $c\bar{c}$ states. While there is no such conservation law for the 1^3D_3 state, recent calculations indicate that it should also be relatively narrow, $\mathcal{O}$(MeV), due to the angular momentum barrier [187, 188]. It is therefore possible that all $c\bar{c}$ D-wave states will be observed. A $c\bar{c}$ state has recently been observed in B decay, the $X(3872)$ [211]. It's mass is higher than expected by quark models which has led to considerable speculation about whether it is a conventional $c\bar{c}$ state or a $D\bar{D}^*$ molecule [212]. A number of tests have been proposed to sort this out [187, 188] and experimental analysis is in progress. Observation of the η_{c2} and $\psi_{(2,3)}$ states would constrain spin-dependent interactions and provide insights into the importance of coupled channel effects in the charm threshold region.

Table 3.6: Predicted and observed masses of $c\bar{c}$ states (in MeV).

State	Expt	GI85 [171]	EQ94 [196]	FU91 [175]	GJ96 [179]	EFG03 [173]	ZVR95 [180]
1^3S_1	3096.87 ± 0.04	3098	3097	3104	3097	3096	3100
1^1S_0	2979.8 ± 1.8	2975	2980	2987	2979	2979	3000
1^3P_2	3556.18 ± 0.13	3550	3507	3557	3557	3556	3540
1^3P_1	3510.51 ± 0.12	3510	3486	3513	3511	3510	3500
1^3P_0	3415.0 ± 0.8	3445	3436	3404	3415	3424	3440
1^1P_1		3517	3493	3529	3526	3526	3510
2^3S_1	3685.96 ± 0.09	3676	3686	3670	3686	3686	3730
2^1S_0	3654 ± 10	3623	3608	3584	3618	3588	3670
1^3D_3		3849		3884		3815	3830
1^3D_2		3838		3871		3813	3820
1^3D_1	3769.9 ± 2.5	3819		3840		3798	3800
1^1D_2		3837		3872		3811	3820
2^3P_2		3979				3972	4020
2^3P_1		3953				3929	3990
2^3P_0		3916				3854	3940
2^1P_1		3956				3945	3990
3^3S_1		4100				4088	4180
3^1S_0		4064				3991	4130

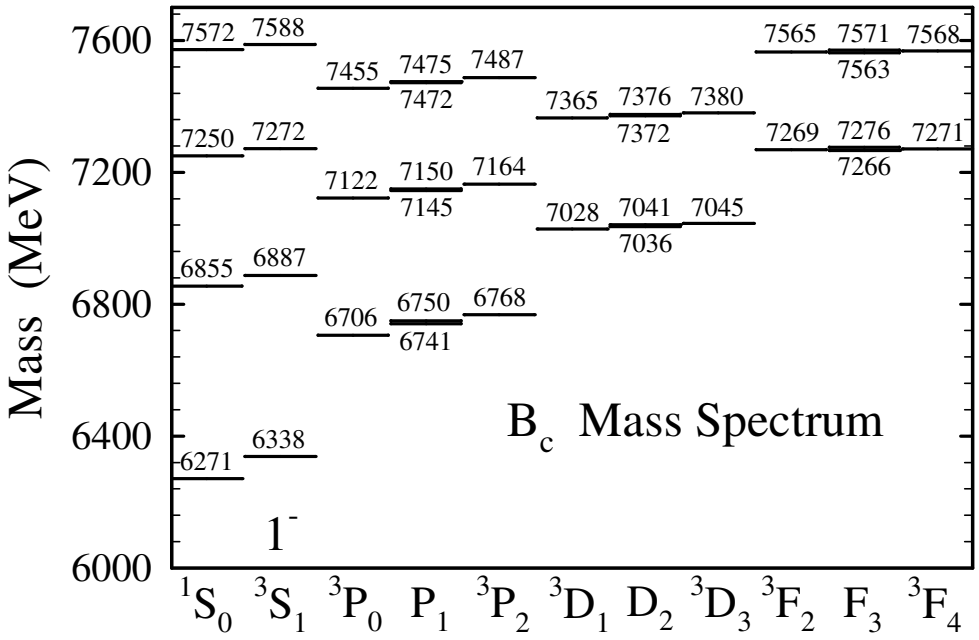

Fig. 3.9: B_c spectrum.

3.2.3 B_c mesons

The B_c mesons provide a unique window into heavy quark dynamics. Although they are intermediate to the charmonium and bottomonium systems the properties of B_c mesons are a special case in quarkonium spectroscopy as they are the only quarkonia consisting of heavy quarks with different flavours. Because they carry flavour they cannot annihilate into gluons so are more stable and excited B_c states lying below BD (and BD^* or B^*D) threshold can only undergo radiative or hadronic transitions to the ground state pseudoscalar which then decays weakly. This results in a rich spectroscopy of narrow radial and orbital excitations (Fig. 3.9 and Table 3.7) [171, 173, 174, 176, 179, 180, 182, 196, 213–216]. which are more stable than their charmonium and bottomonium analogues. The hadronic transitions emitting two charged pions should offer a good opportunity to reconstruct the excited B_c state.

The discovery of the B_c meson by the Collider Detector at Fermilab (CDF) Collaboration [217] in $p\bar{p}$ collisions at $\sqrt{s} = 1.8$ TeV has demonstrated the possibility of the experimental study of this system and has stimulated considerable interest in B_c spectroscopy. Calculations of B_c cross-sections at hadron colliders predict that large samples of B_c states should be produced at the Tevatron and at the LHC opening up this new spectroscopy. It should therefore be possible to start exploring $c\bar{b}$ spectroscopy at the Tevatron, producing $1P$ and $2S$ states and possibly even the D-wave states in sufficient numbers to be observed. At the LHC, with its higher luminosity, the D-wave $c\bar{b}$ states should be produced in a sizable number so that the LHC should allow the study of the spectroscopy and decay of B_c mesons.

3.3 Coupling to open-charm channels[26]

3.3.1 Theoretical models

Near the threshold for open heavy flavour pair production, there are significant nonperturbative contributions from light quark pairs to the masses, wavefunctions and decay properties of physical $Q\bar{Q}$ states. QCD sum rules [218, 219] have been used to obtain some results [220–222] and lattice QCD calculations extended into the flavour-threshold region [223] should eventually give a firm basis for predictions.

[26] Authors: E. Eichten

Table 3.7: Predicted B_c masses and spin–orbit mixing angles (in MeV).

State	GI85 [171]	EFG03 [173]	FU99 [176]	GKLT94 [174]	EQ94 [196]	GJ96 [179]	ZVR95 [180]	Lattice
1^3S_1	6338	6332	6341	6317	6337	6308	6340	6321 ± 30
1^1S_0	6271	6270	6286	6253	6264	6247	6260	$6280 \pm 30 \pm 190$
1^3P_2	6768	6762	6772	6743	6747	6773	6760	6783 ± 30
$1P_1'$	6750	6749	6760	6729	6730	6757	6740	6765 ± 30
$1P_1$	6741	6734	6737	6717	6736	6738	6730	6743 ± 30
1^3P_0	6706	6699	6701	6683	6700	6689	6680	6727 ± 30
θ_{1P}	22.4°	20.4°	28.5°	17.1°	$\sim 2°$	25.6°		$33.4 \pm 1.5°$
2^3S_1	6887	6881	6914	6902	6899	6886	6900	6990 ± 80
2^1S_0	6855	6835	6882	6867	6856	6853	6850	6960 ± 80
2^3P_2	7164	7156		7134	7153		7160	
$2P_1'$	7150	7145		7124	7135		7150	
$2P_1$	7145	7126		7113	7142		7140	
2^3P_0	7122	7091		7088	7108		7100	
θ_{2P}	18.9°	23.0°		21.8°	17°			
3^3S_1	7272	7235			7280		7280	
3^1S_0	7250	7193			7244		7240	
1^3D_3	7045	7081	7032	7007	7005		7040	
$1D_2'$	7036	7079	7028	7016	7012		7030	
$1D_2$	7041	7077	7028	7001	7009		7020	
1^3D_1	7028	7072	7019	7008	7012		7010	
θ_{1D}	44.5°	-35.9°			34.4°			
1^3F_4	7271						7250	
$1F_3'$	7266						7250	
$1F_3$	7276						7240	
1^3F_2	7269						7240	
θ_{1F}	41.4°							

However, at present a more phenomenological approach is required to provide a detailed description of these effects.

The effects of light quark pairs near open heavy flavour threshold can be described by coupling the potential model $Q\bar{Q}$ states to nearby physical multibody states. In this threshold picture, the strong interactions are broken into sectors defined by the number of valence quarks. This separation is reminiscent of the Tamm–Dancoff approximation [224]. The dynamics of the $Q\bar{Q}$ states (with no valence light quarks, q) is described by the interaction $\mathcal{H}_0$. Nonrelativistic potential models are normally used to determine the properties of the resulting bound states in this sector. In this framework excitations of the gluonic degrees of freedom would also be contained the spectrum of $\mathcal{H}_0$.

The two meson sector $Q\bar{q} + q\bar{Q}$ are described by the Hamiltonian $\mathcal{H}_2$. In the simplest picture, $\mathcal{H}_2$ is assumed to be described the low-lying spectrum of two free heavy-light mesons. The physical situation is more complex. At large separation between two mesons the interactions are dominated t-channel pion exchanges. For states very near threshold such as the X(3872) charmonium state such pion exchange in attractive channels might have significant effects on properties of the physical states [225]. At somewhat shorter distances, more complicated interactions exist and new bound states might arise, e.g., molecular states [226, 227].

Our command of quantum chromodynamics is inadequate to derive a realistic description of the interactions, $\mathcal{H}_I$, that communicate between the $Q\bar{Q}$ and $Q\bar{q}+q\bar{Q}$ sectors. Two simple phenomenological models have been used to describe this coupling: the Cornell coupled-channel model (CCC) and the vacuum quark pair creation model (QPC).

The Cornell coupled-channel model for light quark pair creation [169] generalizes the Cornell $Q\bar{Q}$ model [170] without introducing new parameters, writing the interaction Hamiltonian as

$$\mathcal{H}_I = \frac{3}{8}\sum_a \int : \rho_a(\mathbf{r}) V(\mathbf{r}-\mathbf{r}') \rho_a(\mathbf{r}') : d^3r\, d^3r' \,, \tag{3.38}$$

where V is the quarkonium potential and $\rho_a(\mathbf{r}) = \frac{1}{2}\psi^\dagger(\mathbf{r})\lambda_a\psi(\mathbf{r})$ is the colour current density, with ψ the quark field operator and λ_a the octet of SU(3) matrices. To generate the relevant interactions, ψ is expanded in creation and annihilation operators (for up, down, strange and heavy quarks), but transitions from two mesons to three mesons and all transitions that violate the Zweig rule are omitted. It is a good approximation to neglect all effects of the Coulomb piece of the potential in Eq. (3.38). It was shown that this simple model coupling charmonium to charmed-meson decay channels gives a qualitative understanding of the structures observed above threshold while maintaining the successes of the single-channel $c\bar{c}$ analysis below threshold [170].

The characteristic of the CCC model is the use of the time component of a long-range vector interaction between the heavy quarks colour densities rather than the Lorentz scalar confining interaction.

The vacuum quark pair creation model (QPC). This model was developed by Le Yaouanc *et. al.* [228–230] based on an earlier idea of Micu [231] that the light quark pair is produced from the vacuum with vacuum quantum numbers $\mathrm{J^{PC}} = 0^{++}$. The model is also referred to as the $^3\mathrm{P}_0$ model. The form of the interaction Hamiltonian is

$$\mathcal{H}_I = \gamma \int \bar{\psi}\psi(\mathbf{r}) d^3r \tag{3.39}$$

The constant γ is a free parameter of the model. This model has been applied to the light meson states [232, 233]. It was first applied above charm threshold by the Orsay group [234].

The main theoretical weakness of the QPC model is its failure to reproduce the vanishing of the pair production amplitudes for a static $Q\bar{Q}$ source at zero spatial separation. The flux tube breaking model [235, 236] somewhat addresses this weakness. It has the same basic interaction as the QPC model (Eq. 3.39) but the integration is only over a region near a "string" between the Q and $\bar{Q}$ positions. This region is defined by a upper bound on the shortest distance between the pair creation point and the string. Detailed applications of QPC models to the quarkonium systems are presently under investigation [237].

There have been attempts to compare the various models for quark pair creation [185, 238, 239]. At present the most studied system is the open charm threshold region and we will focus on that system below. However, the same threshold effects are present in the $b\bar{b}$ states near $B\overline{B}$ threshold and $c\bar{b}$ states near $D\overline{B}$ threshold. A detailed comparison of the scaling behaviour between different heavy quark systems would provide valuable insight into the correct form for the coupling to light-quark pairs.

3.3.2 Mass shifts

The mass ω of the quarkonium state ψ in the presence of coupling to decay channels is given by:

$$[\mathcal{H}_0 + \mathcal{H}_2 + \mathcal{H}_I]\psi = \omega\psi. \tag{3.40}$$

Above threshold ω has both a real (mass) and imaginary part (width).

The basic coupled-channel interaction $\mathcal{H}_I$ (Eq. (3.38) or Eq. (3.39)) appearing in Eq. (3.40) is independent of the heavy quarks spin, but the hyperfine splittings of D and D^*, D_s and D_s^*, induce

Table 3.8: Charmonium spectrum, including the influence of open-charm channels. All masses are in MeV. The penultimate column holds an estimate of the spin splitting due to tensor and spin–orbit forces in a single-channel potential model. The last column gives the spin splitting induced by communication with open-charm states, for an initially unsplit multiplet. From [188].

State	Mass	Centroid	Splitting (Potential)	Splitting (Induced)
1^1S_0	2 979.9	3 067.6	-90.5	$+2.8$
1^3S_1	3 096.9		$+30.2$	-0.9
1^3P_0	3 415.3	3 525.3	-114.9	$+5.9$
1^3P_1	3 510.5		-11.6	-2.0
1^1P_1	3 525.3		$+1.5$	$+0.5$
1^3P_2	3 556.2		$+31.9$	-0.3
2^1S_0	3 637.7	3 673.9	-50.4	$+15.7$
2^3S_1	3 686.0		$+16.8$	-5.2
1^3D_1	3 769.9	(3 815)	-40	-39.9
1^3D_2	3 830.6		0	-2.7
1^1D_2	3 838.0		0	$+4.2$
1^3D_3	3 868.3		$+20$	$+19.0$
2^3P_0	3 931.9	3 968	-90	$+10$
2^3P_1	4 007.5		-8	$+28.4$
2^1P_1	3 968.0		0	-11.9
2^3P_2	3 966.5		$+25$	-33.1

spin-dependent forces that affect the charmonium states. These spin-dependent forces give rise to S–D mixing that contributes to the $\psi(3770)$ electronic width, for example, and are a source of additional spin splitting.

The masses resulting from a full coupled channel analysis [188] in the CCC model are shown in the second column of Table 3.8. The parameters of the potential model sector, $\mathcal{H}_0$, must be readjusted to fit the physical masses, ω, to the observed experimental values. To compute the induced splittings, the bare centroid of the spin-triplet states is adjusted so that the physical centroid, after inclusion of coupled-channel effects, matches the value in the middle column of Table 3.8. The centroid for the 1D masses is determined by pegging the observed mass of the 1^3D_1 $\psi(3770)$. For the 2P levels, the bare centroid is adjusted so that the 2^1P_1 level lies at the centroid of a potential-model calculation. The assumed spin splittings in the single-channel potential model are shown in the penultimate column and the induced coupled channel spin splittings for initially unsplit multiplets are presented in the rightmost column of Table 3.8. The shifts induced in the low-lying 1S and 1P levels are small. For the other known states in the 2S and 1D families, coupled-channel effects are noticeable and interesting.

In a simple potential picture, the $\eta_c(2S)$ level lies below the $\psi(2S)$ by the hyperfine splitting given by

$$M(\psi(2S)) - M(\eta_c(2S)) = \frac{|\psi(2S)(0)|^2}{|\psi(0)|^2}[M(\psi) - M(\eta_c)] \ . \tag{3.41}$$

Using the observed 1S hyperfine splitting, $M(\psi) - M(\eta_c) = 117$ MeV, one would find $M(\psi(2S)) - M(\eta_c(2S)) = 67$ MeV, which is larger than the observed 48.3 ± 4.4 MeV, as is typical for potential-model calculations.

One important result of coupling the open-charm threshold is that the $\psi\,'$ receives a downward shift of the nearby $D\overline{D}$, that the η_c' does not get, as this state does not couple to $D\overline{D}$. This is implicitly present in the early Cornell papers [170], but the shift of spin singlets states was not explicitly calculated. The effect was first mentioned by Martin and Richard [240, 241], who calculated the size of the effect. Recent papers using the CCC model interaction [188, 242] have confirmed this behaviour. In fact, the 2S induced shifts in Table 3.8 draw ψ' and η_c' closer by 20.9 MeV, substantially improving the agreement between theory and experiment. This suggests that the ψ'–η_c' splitting reflects the influence of virtual decay channels.

If the observed $X(3872)$ is a charmonium state, it is most naturally interpreted as the $1^3\mathrm{D}_2$ or $1^3\mathrm{D}_3$ level [187, 188]; if not, both these states remain to be observed and the dynamics of $\mathcal{H}_2$ is significantly richer. As shown in Table 3.8, the coupling to open-charm channels increases the $1^3\mathrm{D}_2$–$1^3\mathrm{D}_1$ splitting by about 20 MeV, but does not fully account for the observed 102 MeV separation between $X(3872)$ and $\psi(3770)$. However the position of the 3^{--} $1^3\mathrm{D}_3$ level turns out to be very close to 3872 MeV.

3.3.3 Mixing and physical state properties

The physical states are not pure potential-model eigenstates but include components with two virtual (real above threshold) open flavour meson states. Separating the physical state (ψ) into $Q\bar{Q}$ (ψ_0) and two meson components (ψ_2), the resulting separation $\mathcal{H}$ by sector leads to an effective Hamiltonian for the ψ_0 sector given by:

$$\left[\mathcal{H}_0 + \mathcal{H}_I^\dagger \frac{1}{\omega - \mathcal{H}_2 + i\epsilon}\mathcal{H}_I\right]\psi_0 = \omega\psi_0 \tag{3.42}$$

Table 3.9: Charmonium content of states near flavour threshold. The wave function ψ takes account of mixing induced through open charm–anticharm channels. Unmixed potential-model eigenstates are denoted by $|n^{2s+1}L_J\rangle$. The coefficient of the dominant eigenstate is chosen real and positive. The 1S, 1P, 2S, and $1^3\mathrm{D}_1$ states are evaluated at their physical masses. The remaining 1D states are considered at the masses in Table 3.8. $\mathcal{Z}_{cc}$ represents the $(c\bar{c})$ probability fraction of each state.

State	Major Components	$\mathcal{Z}_{c\bar{c}}$
$\psi(1^1\mathrm{S}_0)$	$0.986\|1^1\mathrm{S}_0\rangle - 0.042\|2^1\mathrm{S}_0\rangle - 0.008\|3^1\mathrm{S}_0\rangle$	0.974
$\psi(1^3\mathrm{S}_1)$	$0.983\|1^3\mathrm{S}_1\rangle - 0.050\|2^3\mathrm{S}_1\rangle - 0.009\|3^3\mathrm{S}_1\rangle$	0.968
$\psi(1^3\mathrm{P}_0)$	$0.919\|1^3\mathrm{P}_0\rangle - 0.067\|2^3\mathrm{P}_0\rangle - 0.014\|3^3\mathrm{P}_0\rangle$	0.850
$\psi(1^3\mathrm{P}_1)$	$0.914\|1^3\mathrm{P}_1\rangle - 0.075\|2^3\mathrm{P}_1\rangle - 0.015\|3^3\mathrm{P}_1\rangle$	0.841
$\psi(1^1\mathrm{P}_1)$	$0.918\|1^1\mathrm{P}_1\rangle - 0.077\|2^1\mathrm{P}_1\rangle - 0.015\|3^1\mathrm{P}_1\rangle$	0.845
$\psi(1^3\mathrm{P}_2)$	$0.920\|1^3\mathrm{P}_2\rangle - 0.080\|2^3\mathrm{P}_2\rangle - 0.015\|3^3\mathrm{P}_2\rangle - 0.002\|1^3\mathrm{F}_2\rangle$	0.854
$\psi(2^1\mathrm{S}_0)$	$0.087\|1^1\mathrm{S}_0\rangle + 0.883\|2^1\mathrm{S}_0\rangle - 0.060\|3^1\mathrm{S}_0\rangle - 0.016\|4^1\mathrm{S}_0\rangle$	0.791
$\psi(2^3\mathrm{S}_1)$	$0.103\|1^3\mathrm{S}_1\rangle + 0.838\|2^3\mathrm{S}_1\rangle - 0.085\|3^3\mathrm{S}_1\rangle - 0.017\|4^3\mathrm{S}_1\rangle$ $+0.040\|1^3\mathrm{D}_1\rangle - 0.008\|2^3\mathrm{D}_1\rangle$	0.723
$\psi(1^3\mathrm{D}_1)$	$0.694\|1^3\mathrm{D}_1\rangle + 0.097\,e^{0.935i\pi}\|2^3\mathrm{D}_1\rangle + 0.008\,e^{-0.668i\pi}\|3^3\mathrm{D}_1\rangle$ $+0.013\,e^{0.742i\pi}\|1^3\mathrm{S}_1\rangle + 0.168\,e^{0.805i\pi}\|2^3\mathrm{S}_1\rangle + 0.014\,e^{0.866i\pi}\|3^3\mathrm{S}_1\rangle$ $+0.012\,e^{-0.229i\pi}\|4^3\mathrm{S}_1\rangle$	0.520
$\psi(1^3\mathrm{D}_2)$	$0.754\|1^3\mathrm{D}_2\rangle - 0.084\|2^3\mathrm{D}_2\rangle - 0.011\|3^3\mathrm{D}_2\rangle$	0.576
$\psi(1^1\mathrm{D}_2)$	$0.770\|1^1\mathrm{D}_2\rangle - 0.083\|2^1\mathrm{D}_2\rangle - 0.012\|3^1\mathrm{D}_2\rangle$	0.600
$\psi(1^3\mathrm{D}_3)$	$0.812\|1^3\mathrm{D}_3\rangle + 0.086\,e^{0.990i\pi}\|2^3\mathrm{D}_3\rangle + 0.013\,e^{-0.969i\pi}\|3^3\mathrm{D}_3\rangle$ $+0.007\,e^{0.980i\pi}\|4^3\mathrm{D}_3\rangle + 0.016\,e^{0.848i\pi}\|1^3\mathrm{G}_3\rangle$	0.667

Solving Eq. (3.42) in the $Q\bar{Q}$ sector determines the mixing between the potential model states and

coupling to decay channels. This approach has been described in detail [170] for the CCC model with $\mathcal{H}_I$ (Eq. 3.38). An effective Hamiltonian approach has also been considered in the QPC model [201].

The results for the low-lying $c\bar{c}$ states is shown in Table 3.9 for the CCC model. The overall probability for the physical state to be in the $c\bar{c}$ sector, denoted $\mathcal{Z}_{c\bar{c}}$, decreases as open charm threshold is approached. For states above threshold the mixing coefficients become complex. These mixing effects contribute to observed S–D mixing as well as modifying radiative transition rates [243, 244]. A more detailed discussion of these effects appear in the Decay section.

3.3.4 Zweig-allowed strong decays

Once the mass of a resonance is given, the coupled-channel formalism yields reasonable predictions for the other resonance properties. Eichten, Lane and Quigg [188] have estimated the strong decay rates within the CCC model for all the charmonium levels that populate the threshold region between $2M_D$ and $2M_{D^*}$. For $1^3\mathrm{D}_1$ state $\psi''(3770)$, which lies some 40Mev above charm threshold, they obtain $\Gamma(\psi''(3770) \to D\overline{D}) = 20.1$ MeV, to be compared with the PDG's fitted value of 23.6 ± 2.7 MeV [245]. The natural-parity $1^3\mathrm{D}_3$ state can decay into $D\overline{D}$, but its F-wave decay is suppressed by the centrifugal barrier factor. The partial width is only 0.77 MeV at a mass of 3868 MeV and the $1^3\mathrm{D}_3$ may be discovered as a narrow $D\overline{D}$ resonance up to a mass of about 4000 MeV.

Barnes and Godfrey [187] have estimated the decays of several of the charmonium states into open charm, using the $^3\mathrm{P}_0$ model. Their estimates of open-charm partial decay widths into $D\overline{D}$ are 42.8 MeV for the $1^3\mathrm{D}_1$ state and 3.6 MeV for a $1^3\mathrm{D}_3$ state at a mass of 3868 MeV. They did not carry out a coupled-channel analysis which makes a direct comparison of models more difficult. Detailed comparisons (e.g., Ackleh, Barnes and Swanson [238]) between various light quark pair creation models are highly desirable.

Estimates for decay widths of the 1^{--} charmonium states above open-charm threshold in the $^3\mathrm{P}_0$ model have recently been reported by Barnes [237]. The comparison with experimentally extracted values is shown in Table 3.10. Along with the current PDG values for the total widths of $c\bar{c}$ resonances, a reanalysis by Seth [246] of the existing experimental data is also shown in Table 3.10.

The resonance decay widths are determined from fitting measurements of ΔR in e^+e^- annihilation to a model for each resonance including radiative corrections. This whole procedure is complicated by its dependence on the resonance shape, i.e., the expected non Breit–Wigner nature of the partial widths for radially excited resonances. It may be more useful for theorists to produce a model of ΔR for direct comparison with data. Greater resolving power between models is possible if the contribution from each individual open heavy flavour final state is separately reported.

For the CCC model, the structure of $\Delta R(b\bar{b})$ in the threshold region was studied in the original Cornell group works [169, 170] and later extended to the $\Delta R(b\bar{b})$ in the threshold region [247]. The structure of $\Delta R(c\bar{c})$ and $\Delta R(b\bar{b})$ has also been studied in QPC models [248]. There are also some attempts to compare the different models [249, 250].

Experiments can also search for additional narrow charmonium states in neutral combinations of charmed mesons and anticharmed mesons. The most likely candidates correspond to the $1^3\mathrm{D}_3$, $2^3\mathrm{P}_2$, and $1^3\mathrm{F}_4$ levels [188, 242, 251]. These detailed analyses of the $c\bar{c}$ system can be extended to the $b\bar{b}$ system, where it may be possible to see discrete threshold-region states in direct hadronic production.

3.4 QQq states and molecules[27]

3.4.1 Doubly charmed baryons

The earliest studies on QQq baryons were based on the flavour group $\mathrm{SU(4)_F}$, as an extension of $\mathrm{SU(3))_F}$. After the discovery of hidden and naked charm, some classic papers were written on hadrons with charm, including a section on (ccq) states [252, 253].

[27] Author: J. M. Richard

Table 3.10: Open-charm strong decay modes of the 1^{--} states. Experimental widths from the PDG [245] and a recent analysis of Seth [246]. The theoretical widths using the QPC model [237] and the CCC model [188] are shown. For the $\psi(4159)$ some S wave plus P wave charmed meson two body channels are also open.

State	Mode	$\Gamma_{\rm EXP}$ (MeV)		$\Gamma_{\rm THEORY}$ (MeV)	
		PDG	Seth	QPC Model	CCC model
$\psi(3770)$ (^{3}D$_1$)	DD			42.8	20.1
	total	23.6 ± 2.7		42.8	20.1
$\psi(4040)$ ($3\,^3$S$_1$)	DD			0.1	
	DD*			33.	
	D$_s$D$_s$			8.	
	D*D*			33.	
	total	52 ± 10	88 ± 5	74.	
$\psi(4159)$ ($2\,^3$D$_1$)	DD			16.	
	DD*			0.4	
	D*D*			35.	
	D$_s$D$_s$			8.	
	total	78 ± 20	107 ± 8	73.	
$\psi(4415)$ ($4\,^3$S$_1$)	DD			0.4	
	DD*			2.3	
	D*D*			16.	
	D$_s$D$_s$			1.3	
	D$_s$D$_s^*$			2.6	
	D$_s^*$D$_s^*$			0.7	
	total	43 ± 15	119 ± 15		

Now, our ideas on flavour symmetry have evolved. The conventional SU$(n)_{\rm F}$ approach, with elegant mass formulae, is replaced by *flavour independence*. The potential between two quarks is generated by their colour, and flavour enters only in recoil corrections through the quark mass, mainly for describing the fine and hyperfine structure.

Flavour independence was the main guide line of the detailed studies of (QQq) baryons made in the 80's and later [254, 255, 258–263]: the dynamics tuned for mesons, light baryons and single-charm baryons was tentatively extrapolated to the (QQq) sector. More papers came after the recent findings at SELEX (cf. the experimental part of this chapter), for instance Ref. [264], where a link is made with double-charm exotics, to be discussed shortly.

To study confinement, (QQq) baryons are perhaps the most interesting of ordinary hadrons, as they combine two extreme regimes in a single bag:

1. the slow relative motion of two heavy quarks, as in charmonium,
2. the fast motion of a light quark. Remember that the electron moves faster in hydrogen than in positronium. Similarly, a light quark is likely more relativistic in heavy-light hadrons than in light mesons.

In the (QQq) wave function, the average QQ separation is smaller than the Qq one. This leads to envisage approximations. One of them consists of replacing the full three-body calculation by a two-step procedure where one first calculates the QQ mass, by solving a two-body problem, and then estimates the $QQ - q$ mass by solving another two-body problem. The second step is rather safe. The finite-size corrections are small. For instance, they cancel out exactly for the harmonic oscillator. As for the first step, one should be aware that the QQ potential is *effective*, since it contains both the direct QQ

interaction and a contribution from the light quark. For instance, in the harmonic oscillator model, 1/3 of the QQ interaction comes from the light quark, and neglecting this term results into an underestimation of energies and spacings by a factor $\sqrt{3/2}$. Another limitation to the quark–diquark picture, is that the diquark is not frozen. The first excitations of QQq occur inside the diquark. So one should recalculate the properties of the diquark for each level.

Another way to take advantage of the large mass ratio M/m is to use the Born–Oppenheimer approximation, as done, e.g., by Fleck and Richard [254]. For a given QQ separation r_{12}, the two-centre problem is solved for the light quark, with proper reduced mass. The ground-state energy $E_0(r_{12})$, supplemented by the direct QQ interaction, provides the adiabatic potential V_{QQ}. Solving the 2-body problem with this potential gives the first levels. The adiabatic potential built out of the second "electronic" energy $E_1(r_{12})$ leads to a second series of levels. This is very similar to the spectroscopy of H_2^+ in atomic physics.

Within explicit potential models, the Born–Oppenheimer approximation can be checked against an accurate solution of the 3-body problem, using for instance a systematic hyperspherical expansion. The approximation is excellent for (bbq) and (ccq), with $q = u$, d or s, or even for (ssu) or (ssd) [254, 265].

In Ref. [254], (ccq) masses were estimated from a specific variant of the bag model, already used for charmed mesons. The results turn out to be rather sensitive to details such as centre-of-mass corrections, value of the bag constant, etc. Other bag-model calculations have been performed [266].

Potential models, on the other hand, tend to give very stable results, when the parameters are varied while maintaining a reasonable fit of lighter hadrons. One typically obtains:

- a ground-state near or slightly above 3.6 GeV for the (ccu) or (ccd) ground state,
- a hyperfine splitting of about 80 MeV between the spin 3/2 and spin 1/2 states,
- the first orbital excitation about 300 MeV above the ground-state,
- the first (ccs) state near 3.7 GeV

Note that models tuned to (cqq) or lighter baryons might underestimate the short-range QQ attraction. If models are adjusted to $(c\bar{c})$ spectroscopy, there is an ambiguity on how to translate it to cc. The usual recipe stating that

$$V_{QQ} = \frac{1}{2} V_{Q\bar{Q}} \,, \tag{3.43}$$

implies pairwise forces mediated by colour-octet exchanges. Small, non-confining, colour-singlet exchanges, as well as three-body forces might complicate the issue.

Most existing calculations are of rather exploratory nature, since made when double charm was considered as science fiction, or far future. Meanwhile, the art of QCD has made significant progress. One could retain from simple potential models that the Born–Oppenheimer approximation provides an adequate framework. The effective QQ potential could be estimated from relativistic models or from lattice calculations, similar to those of the $Q\bar{Q}$ potential or the effective QQ potential in exotic $(QQ\bar{q}\bar{q})$ mesons, to be discussed shortly. It is hoped that the new experimental results will stimulate such calculations.

The literature already contains approaches somewhat more ambitious than simple bag or non-relativistic potential models: relativistic models [267], QCD sum rules [258], string picture [261], etc. The lattice QCD approach is presented in Section 2.2.3 and the EFT one is presented in Section 2.4

The appearance of the $D^*_{s,J}$ state not very far above the ground state D_s of meson with flavour content $(c\bar{s})$ has stimulated several studies on the dynamics of light quarks in a static colour field. In Ref. [268], it is suggested that the same phenomenon will occur for double-charm baryons. On this respect the doubling of states in the preliminary data by SELEX is of particular interest.

3.4.2 Exotic mesons with double charm

The physics of multiquarks, though it benefits from a dramatic revival since the tentative discovery of a light pentaquark, remains penalized by the confusion about baryonium states in the late 70's and early 80's. This is actually a difficult field, where speculations about confinement mechanisms should be combined with delicate few-body calculations.

The H dibaryon [269], and the heavy pentaquark P proposed independently by Lipkin [270] and the Grenoble group [271], owe their tentative stability to chromomagnetic forces, schematically [253]

$$H_{\rm cm} = -C \sum_{i<j} \frac{\boldsymbol{\sigma}_i \cdot \boldsymbol{\sigma}_j \, \tilde{\lambda}_i \cdot \tilde{\lambda}_j}{m_i m_j} \delta^{(3)}(\mathbf{r}_{ij}) \; , \tag{3.44}$$

or its bag model analogue [272], that describes the observed hyperfine splittings such as $\Delta - N$ or $J/\Psi - \eta_c$. The astute observation by Jaffe [269] is that this operator provides a binding $(ssuudd) - 2(sud) \sim -150\,\mathrm{MeV}$ to the $H = (ssuudd)$ dibaryon with spin and isospin $J = I = 0$. This estimate, however, relies on $\mathrm{SU(3)_F}$ flavour symmetry and $\langle \delta^{(3)}(\mathbf{r}_{ij}) \rangle$ being independent of (i,j) pair and borrowed from the wave function of ordinary baryons. Relaxing these hypotheses, and introducing kinetic energy and spin-independent forces in the 6-body Hamiltonian, and a realistic estimate of short-range correlations, usually spoils the stability of H [273–275]. The existence of H is nowadays controversial. It has been searched in many experiments, without success so far. For instance, the doubly-strange hypernucleus ${}^{\;\;6}_{\Lambda\Lambda}\mathrm{He}$ is not observed to decay into $H + \alpha$ [276].

If the calculation made for the H is repeated in the limit where $m(Q) \to \infty$, the same binding $(\bar{Q}qqqq) - (\bar{Q}q) - (qqq) \sim -150\,\mathrm{MeV}$ is obtained for the pentaquark $(\bar{Q}qqqq)$, $qqqq$ being in a $\mathrm{SU(3)_F}$ triplet [270, 271]. All corrections, again, tend to weaken this binding [275, 277] so it is not completely sure that the actual pentaquark is stable. See, also, [278].

After the tentative discovery of a light pentaquark state at about 1.53 GeV, with flavour content $(uudd\bar{s})$, and possible partners with strangeness $S = -2$, many authors have revisited the possibility of stable or metastable pentaquarks with heavy antiflavour. See, for instance Refs. [279–284]. In the light pentaquark, the binding is achieved by the chiral dynamics of light quarks. A forerunner in this field was Stancu [285], who proposed positive-parity pentaquarks with a heavy antiquark in a simple potential model where the chromomagnetic interaction is replaced by a short-range spin-flavour interaction which looks like the exchange of Goldstone bosons between quarks.

In short, there are still many open issues for the H dibaryon, the pentaquarks, as well as for possible light scalar mesons made out of two quarks and two antiquarks. This is, however, more of the domain of light-quark spectroscopy.

More than twenty years ago, another mechanism for multiquark binding was proposed. It was pointed out that current confining potentials applied to a $(QQ\bar{q}\bar{q})$ system put its mass below the dissociation threshold into $(Q\bar{q}) + (Q\bar{q})$, provided the mass ratio $m(Q)/m(q)$ is large enough [286]. This *chromoelectric* binding was studied by several authors, in the context of flavour-independent potentials [264, 287–295] [296, 297] (see, also, [298, 299]), with a remarkable convergence towards the same conclusion. This somewhat contrasts with the confusion in other sectors of multiquark spectroscopy.

Let us consider, indeed, the limit of a purely flavour-independent potential V for $(QQ\bar{q}\bar{q})$. The situation becomes similar to that of exotic four-body molecules (M^+, M^+, m^-, m^-), all of them using the very same Coulomb potential when M and m are varied. The hydrogen molecule with $M \gg m$ is much more stable than the positronium molecule Ps_2 with $M = m$. If one decomposes the 4-body Hamiltonian as

$$\mathcal{H}_4 = \left[\frac{M^{-1} + m^{-1}}{4} \left(\mathbf{p}_1^2 + \mathbf{p}_2^2 + \mathbf{p}_3^2 + \mathbf{p}_4^2 \right) + V \right] + \frac{M^{-1} - m^{-1}}{4} \left(\mathbf{p}_1^2 + \mathbf{p}_2^2 - \mathbf{p}_3^2 - \mathbf{p}_4^2 \right) \; , \tag{3.45}$$

the first term, even under charge conjugation, corresponds to a rescaled equal-mass system with *the same threshold* as $\mathcal{H}_4$. The second term, which breaks charge conjugation, improves the energy of $\mathcal{H}_4$ (one

can applies the variational principle to $\mathcal{H}_4$ using the symmetric ground state of the first term as a trial wave function). In the molecular case, the second term changes the marginally bound Ps_2 (or rescaled copy) into the deeply bound H_2. In quark models, an unbound $(qq\bar{q}\bar{q})$ becomes a stable $(QQ\bar{q}\bar{q})$.

The effective QQ potential has been estimated by Rosina et al. [294] in the framework of empirical potential models, and by Mihaly et al. [296] and Michael et al. (UKQCD) [297], who used lattice simulations of QCD. The question is obviously: is the c quark heavy enough to make $(cc\bar{q}\bar{q})$ bound when $q = u$ or d? At this point, the answer is usually negative, most authors stating that b is required to bind $(QQ\bar{q}\bar{q})$ below its $(Q\bar{q}) + (Q\bar{q})$ threshold.

There is, however, another mechanism: pion-exchange or, more generally, nuclear-like forces between hadrons containing light quarks or antiquarks. This effect was studied by several authors, in particular Törnqvist [300, 301], Manohar and Wise [302], and Ericson and Karl [303]. In particular a D and D^* can exchange a pion, this inducing an attractive potential. It is weaker than in the nucleon–nucleon case, but what matters for a potential $gV(r)$ to bind, is the product gm of the strength g and reduced mass m. It is found that (DD^*) is close to be bound, while binding is better established for (BB^*). The result depends on how sharply the long-range potential is empirically regularised at short distances.

A lattice calculation such as those of Refs. [296, 297] contains in principle all effects. In practice, the pion is unphysically heavy such that long-range forces are perhaps not entirely included. Explicit quark models such as [294] make specific assumptions about interquark forces, but do not account for pion exchange. In our opinion, a proper combination of long- and short-range forces should lead to bind (DD^*), since each component is almost sufficient by itself. This is presently under active study.

There is a further possibility to build exotic, multicharmed systems. If the interaction between two charmed mesons is slightly too weak to lead to a bound state (this is presumably the case for (DD), since pion exchange does not contribute here), it is likely that the very same meson–meson interaction binds three or more mesons. This is known as the phenomenon of "Boromean" binding.

For instance, in atomic physics, neither two ^{3}He atoms nor a ^{3}He atom and a ^{4}He atom can form a binary molecule, even at vanishing temperature, but it is found that ^{3}He^{3}He^{4}He is bound [304]. Similarly, in nuclear physics, the isotope ^{6}He is stable against evaporating two neutrons, or any other dissociation process, while ^{5}He is unstable. In a 3-body picture, this means that (α, n, n) is stable, while neither (α, n) nor (n, n) have a stable bound state. In short, binding three constituents is easier than two.

3.5 Quarkonium hybrids[28]

The existence of gluonic excitations in the hadron spectrum is one of the most important unanswered questions in hadron physics. Hybrid mesons form one such class which consists of a $q\bar{q}$ with an excited gluonic degree of freedom. Their spectroscopy are discussed extensively in this Chapter. Recent observations of charmonium states in exclusive B-meson decays [207, 305–309] suggest that charmonium hybrid mesons (ψ_g) [310] with mass ∼4 GeV may be produced in B-decay via $c\bar{c}$ colour octet operators [311, 312]. Some of these states are likely to be narrow with clean signatures to $J/\psi\pi^+\pi^-$ and $J/\psi\gamma$ final states. The unambiguous discovery of such a state would herald an important breakthrough in hadronic physics, and indeed, in our understanding of Quantum Chromodynamics, the theory of the strong interactions. In this section we give a brief overview of charmonium hybrid properties and and suggest search strategies for charmonium hybrids at existing B-factories [313].

3.5.1 Spectroscopy

Lattice gauge theory and hadron models predict a rich spectroscopy of charmonium hybrid mesons [12, 23, 235, 310, 314–319]. For example, the flux tube model predicts 8 low lying hybrid states in the 4 to

[28] Author: S. Godfrey

4.2 GeV mass region with $J^{PC} = 0^{\pm\mp}$, $1^{\pm\mp}$, $2^{\pm\mp}$, and $1^{\pm\pm}$. Of these states the 0^{+-}, 1^{-+}, and 2^{+-} have exotic quantum numbers; quantum numbers not consistent with the constituent quark model. The flux-tube model predicts $M(\psi_g) \simeq 4 - 4.2$ GeV [314,315]; lattice QCD predictions for the $J^{PC} = 1^{-+}$ state range from 4.04 GeV to 4.4 GeV [23, 317] with a recent quenched lattice QCD calculation [12] finding $M(1^{-+}) = 4.428 \pm 0.041$ GeV. These results have the 1^{-+} lying in the vicinity of the $D^{**}D$ threshold of 4.287 GeV. There is the tantalising possibility that the 1^{-+} could lie below $D^{**}D$ threshold and therefore be relatively narrow.

3.5.2 Decays

There are three important decay modes for charmonium hybrids: (i) the Zweig allowed fall-apart mode $\psi_g \to D^{(*,**)}\bar{D}^{(*,**)}$ [320–322]; (ii) the cascade to conventional $c\bar{c}$ states, of the type $\psi_g \to (c\bar{c})(gg) \to (c\bar{c})$ + (light hadrons) and $\psi_g \to (c\bar{c}) + \gamma$ [323]; (iii) decays to light hadrons via intermediate gluons, $\psi_g \to (ng)$ $\to$ light hadrons, analogous to $J/\psi \to$ light hadrons and $\eta_c \to$ light hadrons. Each mode plays a unique role. ψ_g hybrids with exotic J^{PC} quantum numbers offer the most unambiguous signal since they do not mix with conventional quarkonia.

3.5.2.1 (i) Decays to $D^{(*)}D^{(*)}$: In addition to J^{PC} selection rules (for example, 2^{-+} and 2^{--} decay to $D\bar{D}$ are forbidden by parity and the exotic hybrid $\psi_g(0^{+-})$ decays to $D^{(*)}D^{(*)}$ final states are forbidden by P and/or C conservation) a general feature of most models of hybrid meson decay is that decays to two mesons with the same spatial wave function are suppressed [324]. The dominant coupling of charmonium hybrids is to excited states, in particular $D^{(*)}(L = 0) + D^{**}(L = 1)$ states for which the threshold is ~ 4.3 GeV. This is at the kinematic limit for most mass predictions so that decays into the preferred $D^{(*)}D^{**}$ states are expected to be significantly suppressed if not outright kinematically forbidden. A refined version of the Isgur Kokoski Paton flux model [320] predicts partial widths of 0.3–1.5 MeV depending on the J^{PC} of the hybrid [322]. These widths are quite narrow for charmonia of such high mass. If the hybrid masses are above D^{**} threshold then the total widths increase to 4–40 MeV for 4.4 GeV charmonium hybrids which are still relatively narrow for hadron states of such high mass. The challenge is to identify decay modes that can be reconstructed by experiment.

3.5.2.2 (ii) Decays to $(c\bar{c})$ + (light hadrons): The $\psi_g \to (c\bar{c})$ + (light hadrons) mode offers the cleanest signature for ψ_g observation if its branching ratio is large enough. In addition, a small total width also offers the possibility that the radiative branching ratios into J/ψ, η_c, χ_{cJ}, and h_c could be significant and offer a clean signal for the detection of these states.

For masses below DD^{**} threshold the cascade decays $\psi_g \to (\psi,\ \eta_c, \ldots) + (gg)$ and annihilation decays $\psi_g(C = +) \to (gg) \to$ light hadrons will dominate. If the masses of exotic J^{PC} states are above DD^{**} threshold their widths are also expected to be relatively narrow for states of such high mass, in which case cascades to conventional $c\bar{c}$ states transitions of the type $\psi_g \to (\psi,\ \psi') +$ (light hadrons) should have significant branching ratios [323] making them important signals to look for in ψ_g searches. In the Kuang–Yan formalism [325] the matrix elements for hadronic transitions between conventional quarkonia are related to hybrid-conventional quarkonium hadronic transitions. A not unreasonable assumption is that the partial widths for the decays $\psi_g(1^{-+}) \to \eta_c + (\pi\pi, \eta, \eta')$ and $\psi_g(0^{+-}, 2^{+-}) \to J/\psi + (\pi\pi, \eta, \eta')$ will be similar in magnitude to $(c\bar{c}) \to \pi\pi J/\psi$ and $(c\bar{c}) \to \eta J/\psi$, of $\mathcal{O}(10 - 100)$ keV.

Estimates of radiative transitions involving hybrids with light quarks [326, 327] found that the $E1$ transitions between hybrid and conventional states to be comparable in magnitude to transitions between conventional mesons. While neither calculation can be applied directly to $c\bar{c}$ one might take this to suggest that the partial widths for $\psi_g(1^{-+}) \to \gamma + (J/\psi, h_c)$ and $\psi_g(0^{+-}, 2^{+-}) \to \gamma + (\eta_c, \chi_{cJ})$ are the same order of magnitude as transitions between conventional charmonium states. However, a recent flux-tube model calculations by Close and Dudek [327] found that the $\Delta S = 0$ E1 transitions to hybrids

only occur for charged particles, and hence would vanish for $c\bar{c}$. The $\Delta S = 1$ M1 transitions can occur, but are non-leading and less well defined. Estimates [327] for their widths are $\mathcal{O}(1-100)$ keV. Clearly, given our general lack of understanding of radiative transitions involving hybrids, the measurement of these transitions, $\psi_g \to (c\bar{c})\gamma$, has important implications for model builders.

3.5.2.3 (iii) Decays to light hadrons: Decays of the type $\psi_g \to$light hadrons offer the interesting possibility of producing light exotic mesons. Estimates of annihilation widths to light hadrons will be order of magnitude guesses at best due to uncertainties in wavefunction effects and QCD corrections. We estimate the annihilation widths $\Gamma[\psi_g(C=-) \to$ light hadrons$]$ and $\Gamma[c\bar{c}(C=+) \to$ light hadrons$]$ by comparing them to $\Gamma(\psi' \to$ light hadrons$)$ and $\Gamma(\eta_c' \to$ light hadrons$)$. The light hadron production rate from $\psi_g(C=-)$ decays is suppressed by one power of $\alpha_{\rm s}$ with respect to $\psi_g(C=+)$ decays. This very naive assumption gives $\Gamma[\psi_g(C=-) \to$ light hadrons$] \sim \mathcal{O}(100)$ keV and $\Gamma[c\bar{c}(C=+) \to$ light hadrons$] \sim \mathcal{O}(10)$ MeV [328]. These widths could be smaller because the $q\bar{q}$ pair in hybrids is expected to be separated by a distance of order $1/\Lambda_{QCD}$ resulting in a smaller annihilation rate than the S-wave ψ' and η_c' states.

3.5.3 Hybrid production

Recent developments in both theory and experiment lead us to expect that charmonium hybrids will be produced in B decays. The partial widths for $B \to c\bar{c} + X$, with $c\bar{c}$ representing specific final states such as $J/\psi, \psi', \chi_{c0}, \chi_{c1}, \chi_{c2}, {}^3D_2, {}^1D_2$ etc., have been calculated in the NRQCD formalism [3,329–333] which factorizes the decay mechanism into short (hard) and nonperturbative (soft) contributions. The hard contributions are fairly well understood but the soft contributions, included as colour singlet and colour octet matrix elements, have model dependent uncertainties. Insofar as hybrid $c\bar{c}$ wavefunctions have a non-trivial colour representation they can be produced via a colour octet intermediate state. Chiladze *et al.* [312] estimated the branching ratio $\mathcal{B}[B \to \psi_g(0^{+-}) + X] \sim 10^{-3}$ for $M \sim 4$ GeV (though recent quenched lattice calculations suggest $M(0^{+-}) = 4.70 \pm 0.17$ GeV, and hence will be inaccessible). Close *et al.* [311] estimate a similar branching ratio to 1^{-+} and argued that if $M_g < 4.7$ GeV, the total branching ratio to ψ_g for all J^{PC} could be $\mathcal{B}[\psi_g(\text{all } J^{PC}) + X] \sim \mathcal{O}(1\%)$. Thus, using two different approaches for estimating $\mathcal{B}[B \to \psi_g + X]$ both Chiladze *et al.* [312] and Close *et al.* [311] obtain similar results. Both calculations estimate $\mathcal{B}$'s of $\mathcal{O}(0.1-1\%)$ which are comparable to the $\mathcal{B}$'s for conventional $c\bar{c}$ states.

3.5.4 Experimental signatures

The decays discussed above lead to a number of possible signals: $\psi_g \to D^{(*)}D^{(*,**)}$, $\psi_g(0^{+-}, 2^{+-}) \to J/\psi + (\pi^+\pi^-, \eta, \eta')$, $\psi_g(1^{-+}) \to \eta_c + (\pi^+\pi^-, \eta, \eta')$, $\psi_g \to (c\bar{c})\gamma$, and $\psi_g \to$light hadrons. Of the possible decay modes, $\psi_g \to J/\psi\pi^+\pi^-$, $\psi_g \to J/\psi\eta$, and $\psi_g \to (c\bar{c})\gamma$ give distinctive and easily reconstructed signals. In the former case, the subsequent decay, $J/\psi \to e^+e^-$ and $\mu^+\mu^-$ offers a clean tag for the event so that searches for peaks in the invariant mass distributions $M(e^+e^-\pi^-\pi^+) - M(e^+e^-)$ is a promising search strategy for hybrids. Both the 0^{+-} and 2^{+-} should decay via the $\psi_g \to J/\psi\pi\pi$ cascade. For the ψ_g lying below DD^{**} threshold combining estimates of $\mathcal{B}(B \to \psi_g + X) \simeq 10^{-3}$ and $\mathcal{B}[\psi_g(2^{+-}) \to J/\psi\pi^+\pi^-] \simeq 0.2$ with the PDG value of $\mathcal{B}(\psi \to \ell^+\ell^-) = 11.81\%$ and the Babar detection efficiency we estimate that for 100 fb^{-1} of integrated luminosity each experiment should observe roughly 50 events. If the 2^{+-} lies above the DD^{**} threshold the $\mathcal{B}$ for $2^{+-} \to J/\psi\pi\pi$ decreases significantly to 2.6×10^{-2} lowering the expected number to about 6 events. Similarly, for the 0^{+-} hybrid we estimate roughly 1200 events if it lies below threshold but only 5 events once the DD^{**} decay modes open up.

The 1^{-+} state is expected to be the lightest exotic $c\bar{c}$ hybrid [12, 23] and therefore the most likely to lie below DD^{**} threshold. However, in this case the cascade goes to $\eta_c\pi\pi$, a more difficult final state to reconstruct. Estimates of the relevant partial widths are $\mathcal{B}(B \to \psi_g + X) \simeq 10^{-3}$ and

$\mathcal{B}(\psi_g(1^{-+}\to\eta_c\pi^+\pi^-) \simeq 9\times10^{-3}$. The Babar collaboration studied the decay $B\to\eta_c K$ by observing the η_c in $KK\pi$ and $KKKK$ final states. Combining the PDG values for the $\mathcal{B}$'s to these final states with the Babar detection efficiencies of roughly 15% and 11% respectively we estimate that for 100 fb^{-1} each experiment should observe roughly 10 events. If the 1^{-+} lies above the DD^{**} threshold, the $\mathcal{B}$ for $1^{-+}\to\pi\pi\eta_c$ decreases to 3×10^{-3} lowering the expected number to about 3 events.

The radiative transition, $\psi_g(1^{-+})\to\gamma J/\psi$, also has a distinct signal if it has a significant branching ratio. The conservative value of $\Gamma(\psi_g(1^{-+})\to\gamma J/\psi) \simeq 1$ keV, yields a rather small $\mathcal{B}$ for this transition. On the other hand, a monochramatic photon offers a clean tag with a high efficiency. One could look for peaks in $M(\mu^+\mu^-\gamma) - M(\mu^+\mu^-)$. Babar observed χ_{c1} and χ_{c2} this way [307] obtaining $\simeq 394$ χ_{c1}'s and $\simeq 1100$ χ_{c2}'s with a 20.3 fb^{-1} data sample and an efficiency of about 20 % for the $J/\psi\gamma$ final state [307]. So although the rate may be too small to observe, given the potential payoff, it is probably worth the effort to perform this search.

Experiments might also look for charmonium hybrids in invariant mass distributions of light hadrons. For example, Belle observed the χ_{c0} by looking at the invariant mass distributions from the decays $\chi_{c0}\to\pi^+\pi^-$ and $\chi_{c0}\to K^+K^-$ [306]. They found efficiencies of 21% for $\chi_{c0}\to\pi^+\pi^-$ and 12.9% for $\chi_{c0}\to K^+K^-$, obtaining ~ 16 events in the former case and ~ 9 in the latter.

The decay to charmed mesons also needs to be studied. Because there are more particles in the final state it will be more difficult to reconstruct the charmonium hybrid. On the other hand, with sufficient statistics these channels will be important for measuring the ψ_g quantum numbers and distinguishing their properties from conventional $c\bar{c}$ states.

3.5.5 Summary and future opportunities

The fundamental problem with all the estimates given above is that they are based on models that have not been tested against experiment. Observing a charmonium hybrid and measuring its properties is necessary to test these calculations. It may be that the models are correct but it is also possible that they have totally missed the mark.

Establishing the existence of mesons with explicit gluonic degrees of freedom is one of the most important challenges in strong interaction physics. As demonstrated by the discovery of the $\eta_c(2S)$ in B decay, B decays offer a promising approach to discovering charmonium hybrid mesons. We have focused on how to search for these states in B-decay. Other possibilities are 1^{--} hybrids produced in e^+e^- annihilation. These would likely mix with conventional vector quarkonium states so that it would be very difficult to distinguish them from conventional states. And recently the Belle collaboration observed the η_c' in double charm production in e^+e^- collisions. Part of the GSI upgrade is to study and search for charmonium states in $p\bar{p}$ annihilation. It is quite possible that hybrids can be studied once the PANDA project comes to fruition. While there is no question that the estimates for the various partial widths are crude, the essential point is that these states are expected to be relatively narrow and that distinctive final states are likely to have observable branching ratios. Given how much we can learn by finding these states we strongly advocate that some effort be devoted to their searches. In the long term, with the various facilities mentioned above, we should be able to open up and study an exciting new spectroscopy.

4 INTRODUCTION TO EXPERIMENTAL SPECTROSCOPY[29]

The experimental spectroscopy review is made of four Sections on charmonia and bottomonia, followed by a Section on B_c, and one on the ccq systems. The paragraphs follow a hyerarchical structure, based on the precision reached in the knowledge of the parameters of these states. Therefore we start from the vector states (ψ's and Υ's), which were first discovered, have the narrowest widths, and are easiest to produce and detect. At present, with the resonant depolarization technique, it is possible to know these

[29] Author: R. Mussa

masses with absolute precision between 10 and 100 keV, and these states are widely used as calibration tools for HEP detectors.

Section 6 scans through triplet P-wave states (known as χ_c's and χ_b's), which were discovered from radiative transitions of upper vector excitations. χ_c's could not be precisely studied before the 90's, when direct access to the formation of these states in $\bar{p}p$ annihilations allowed to reach 100–200 keV precisions on their masses, and $\approx 10\%$ resolution of their total widths. The first two Sections allow to realize that the S and P wave states of both ortho-charmonium and -bottomonium constitute a very solid, well established system of resonant states. These narrow resonances can be detected with very small or negligible experimental background and have reached the mature stage, from a barely spectroscopical point of view.

In contrast, all S=0 states are a very active field of research for spectroscopy. The best known among those, $\eta_c(1S)$ (described in Section 7.1) despite being produced with a wide variety of techniques, has still an uncertainty above 1 MeV on the measured mass, and a rapid progress is expected to happen in the next few years. Same can be said of the recently re-discovered $\eta_c(2S)$, described in Section 7.1 which greatly benefits from the advent of the new generation of B-factories. The hyperfine splitting on charmonium S states is then approaching maturity. On the other side, the large amount of data taken by CLEO at $\Upsilon(1,2,3S)$ energies did not yield so far to the discovery of η_b states. A comprehensive review of these searches, also performed at LEP experiments and CDF, is then given in Section 7.2. The elusive singlet P state of charmonium, named h_c, has been extensively searched by the $p\bar{p}$ experiments, resulting in inconclusive evidences; its saga is described in Section 7.3. With the advent of B-factories, its search has regained interest.

Being right across the first open charm threshold, charmonium D-wave multiplets still lack a complete understanding, while the first evidence of bottomonium D state comes from the recent CLEO III run at $\Upsilon(3S)$, described in Section 6.3. The phenomenology of all the other vector orbital excitations is still quite unclear as the different thresholds open up: R scans between 3.7 and 4.7 GeV are reviewed in Section 8.1. Further studies on these states have regained priority after the discovery of the narrow state X(3872), seen by Belle, and confirmed by BaBar, CDF and D0. An overview on the experimental evidences of this resonance, as well as the current experimental attempts to clarify its nature and its quantum numbers, is given separately in Section 8.2. Despite its most likely interpretation as one of the two above mentioned D states, other possible assignments of this resonance, extensively described in the theory chapter, span from orbital excitations of P wave states to molecular charmonia, opening a wide number of possible searches in this energy region.

Another field of research which can bloom in the next years, mostly thanks to large samples of B states taken at the Tevatron as well as HERA-B, is the study of the B_c. Despite the weak decay of its ground state may accomunate this object to the heavy light mesons, the mass of its two components suggests that the spectrum of its excited states can be quite similar to the one of charmonium and bottomonium. The experimental evidence of the ground state of such system and the searches for its excitations are described in Section 9.

The last Section is devoted to another class of bound states which share a set of similarities with the heavy quarkonia. The evidence of the doubly charmed baryons claimed by Fermilab experiment E781 is still rather weak and is described in Section 10; further searches, possibly by the B-factories, are needed before speculating on their phenomenology.

5 HIGH PRECISION MEASUREMENTS OF VECTOR STATE MASSES AND WIDTHS

5.1 Charmonia[30]

The first precise measurement of the $J/\psi(1S)$ and $\psi(2S)$ meson masses [334] set the mass scale in the range around 3 GeV which provided a base for the accurate determination of the charmonium state

[30] Author:S. Eidelman

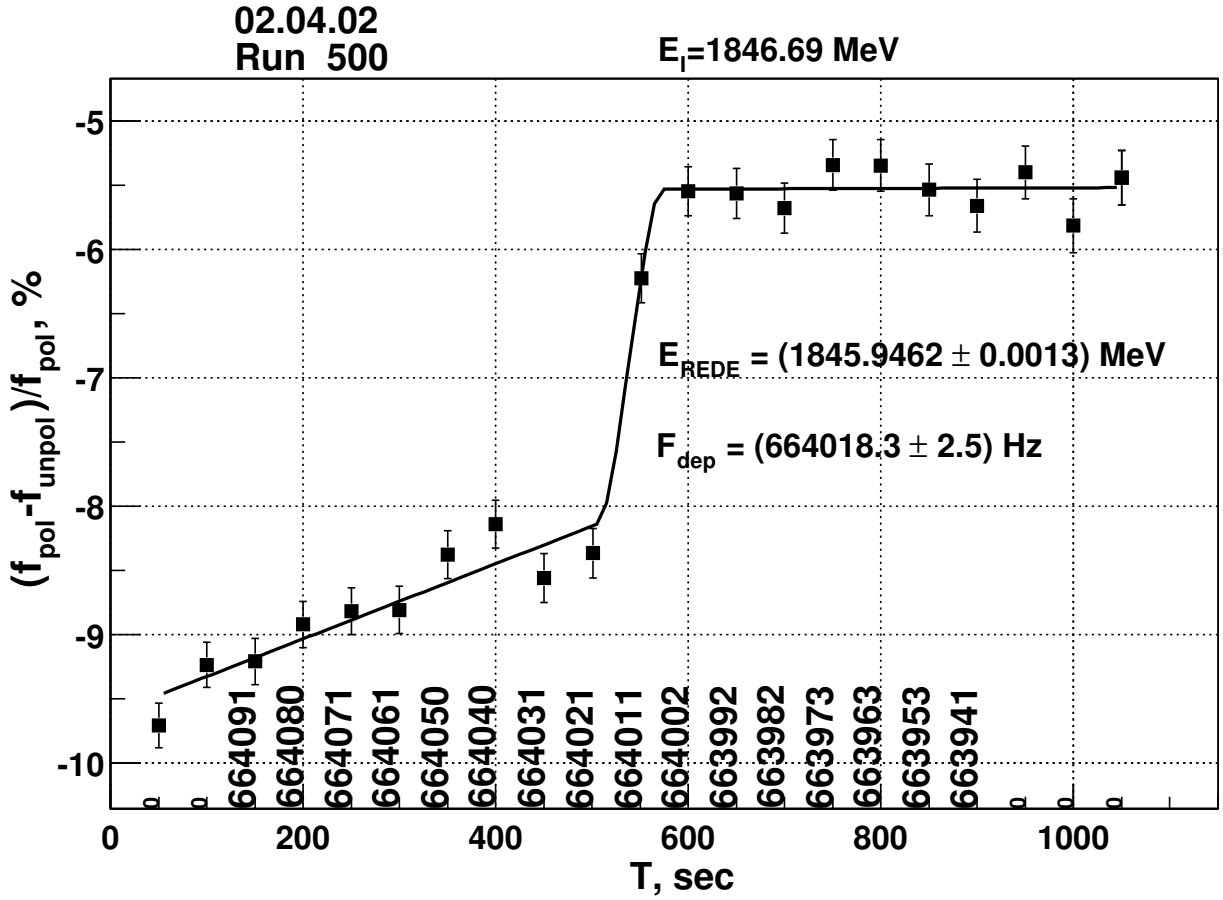

Fig. 3.10: The variation of the coincidence rate ratio for the polarized and unpolarized beams.

location. The method of resonant depolarization, described in Appendix 8.1 of Chapter 2, has been developed in Novosibirsk and first applied to the ϕ meson mass measurement at the VEPP-2M storage ring [339]. Later it was successfully used to measure masses of the ψ- [334] and Υ-meson family [340, 342, 343], see also Ref. [344], in which the values of the masses were rescaled to take into account the change of the electron mass value. The accuracy of the $J/\psi(1S)$ meson mass measurement was later improved in the Fermilab $p\bar{p}$-experiment E760 [347] to $1.2 \cdot 10^{-5}$ using the $\psi(2S)$ mass value from Ref. [334]. The new high precision measurement [337] of the J/ψ and ψ' meson masses has been performed at the collider VEPP-4M using the KEDR detector [352]. The polarimeter unit was installed in the technical straight section of VEPP-4M and consisted of the polarimeter — two scintillation counters detecting electron pairs of the intrabeam scattering whose rate is spin-dependent (Touschek effect [350]) and the TEM wave-based depolarizer [351]. The characteristic jump in the relative rate of scattered electrons at the moment of resonant depolarization is $3 \div 3.5\%$ with the statistical error of 0.3–0.4% for the beam polarization degree higher than 50%. Typical behavior of the rate ratio is shown in Fig. 3.10.

The characteristic uncertainty of the beam energy calibration due to the depolarization procedure is 1.5 keV.

The first part of the experiment consisted of three scans of the $J/\psi(1S)$ region (the integrated luminosity $\approx$ 40 nb^{-1}, the beam energy spread $\sigma_E \approx 0.6$ MeV) and three scans of the $\psi(2S)$ region (the integrated luminosity $\approx$ 76 nb^{-1}, $\sigma_E \approx 0.9$ MeV). Then the betatron and synchrotron dumping decrements of VEPP-4M were rearranged to reduce the energy spread down to 0.45 MeV and the fourth scan of $J/\psi(1S)$ was performed (the integrated luminosity is $\approx$ 10 nb^{-1}). The goal of this was the verification of systematic errors connected with the collider operating mode and the beam energy spread.

The beam polarization time in the VEPP-4M ring is about 100 hours at the $J/\psi(1S)$-energy. For the energy calibration runs, the beam spent the time sufficient for the polarization in the booster ring VEPP-3 (2.5 hours at $J/\psi(1S)$ and about 1 hour at $\psi(2S)$) and was injected to VEPP-4M without essential loss of the polarization degree.

During the scan the data were acquired at seven energies around the resonance peak. Before data acquisition, the beam energy calibration was made at point 1 to fix the current energy scale. At points 2–6 the calibrations before and after data taking were performed with the opposite direction of the depolarizer frequency scan. The point 7 requires no energy calibration.

On completion of the scan the VEPP-4M magnetization cycle was performed and the whole procedure was repeated. The energy dependence of the resonance cross-section was fitted taking into account the interference with continuum and radiative corrections. The results obtained can be presented in the form

$$M_{J/\psi(1S)} - M^{PDG}_{J/\psi(1S)} = \ 47 \pm 10 \pm 7 \,\mathrm{keV},$$

$$M_{\psi(2S)} \ - \ M^{PDG}_{\psi(2S)} = 151 \pm 25 \pm 9 \,\mathrm{keV},$$

demonstrating the agreement with the world average values taking into account their uncertainties of ± 40 keV and ± 90 keV, respectively [245]. The following mass values have been obtained:

$$M_{J/\psi(1S)} = 3096.917 \pm 0.010 \pm 0.007 \ \mathrm{MeV},$$

$$M_{\psi(2S)} = 3686.111 \pm 0.025 \pm 0.009 \ \mathrm{MeV}.$$

The relative measurement accuracy reached $4 \cdot 10^{-6}$ for the $J/\psi(1S)$, $7 \cdot 10^{-6}$ for the $\psi(2S)$ and is approximately 3 times better than that of the previous precise experiments in [334] and [347].

The new result for the mass difference is

$$M_{\psi(2S)} - M_{J/\psi(1S)} = 589.194 \pm 0.027 \pm 0.011 \ \mathrm{MeV}.$$

Substantial improvement in the beam energy accuracy obtained by the presented experiment sets a new standard of the mass scale in the charmonium range.

5.2 Bottomonia[31]

Development of the resonant depolarization method suggested and first realized in Novosibirsk [339,353] also allowed high precision measurements of the resonance masses in the Υ family. The MD-1 group in Novosibirsk carried out three independent measurements of the $\Upsilon(1S)$ mass [340, 342, 343, 354]. The $\Upsilon(1S)$ mass was also measured by the CUSB collaboration in Cornell [345]. Their result was by 0.63 ± 0.17 MeV or 3.8σ lower than that of MD-1. The reasons of this discrepancy are not clear, however, when the MD-1 group performed a fit of the CUSB results using the Novosibirsk procedure (in particular, it included a new method or calculating radiative corrections according to [355] instead of the older approach of Ref. [356]), the difference between the two results decreased to 0.32 ± 0.17 MeV or 1.9σ only.

The mass of the $\Upsilon(2S)$ meson was measured by the MD-1 group in Novosibirsk [342, 354] and two groups in DESY — ARGUS and Crystal Ball [346]. Both groups in DESY obtained the mass value consistent with that in Novosibirsk, the average being 0.5 ± 0.8 MeV lower than that of MD-1.

The mass of the $\Upsilon(3S)$ meson was measured by the MD-1 group only [342, 354]. As in the case of the $\Upsilon(2S)$ meson, a systematic error of the measurement was less than 0.2 MeV, much smaller than the statistical one.

[31] Author: S. Eidelman

Finally, in 2000 all the results on the mass of the ψ [334,357] and Υ [340,342,343,354,354] family resonances were updated [344] to take into account a more precise value of the electron mass [358, 359] (for the ψ family an additional correction has been made to take into account the new way of calculating radiative corrections [355]). In Table 3.11 we summarize the information on these experiments presenting for each detector the number of energy points and the energy range studied, the integrated luminosity and the final value of the mass. The results after the update mentioned above are shown in parentheses.

Table 3.11: Mass Measurements in the Υ Meson Family

Resonance	Collider	N of Points $\sqrt{s}$, MeV	Detector Reference	$\int$ Ldt, pb^{-1}	Mass, MeV
$\Upsilon(1S)$	VEPP-4	43 9420–9490	MD-1 [343] ([344])	2.0	$9460.59 \pm 0.09 \pm 0.05$ $(9460.51 \pm 0.09 \pm 0.05)$
	CESR	13 9446–9472	CUSB [345]	0.285	$9459.97 \pm 0.11 \pm 0.07$
$\Upsilon(2S)$	VEPP-4	37 9980–10075	MD-1 [354] ([344])	0.6	10023.6 ± 0.5 (10023.5 ± 0.5)
	DORIS	13 9960–10040	ARGUS [346] Cr. Ball [346] Average [346]	2.0 2.0	10023.43 ± 0.45 10022.8 ± 0.5 $10023.1 \pm 0.4 \pm 0.5$
$\Upsilon(3S)$	VEPP-4	35 10310–10410	MD-1 [354] ([344])	1.25	10355.3 ± 0.5 (10355.2 ± 0.5)

6 SPIN AVERAGED AND FINE SPLITTINGS

6.1 Charmonium P states: COG and fine splittings[32]

The most precise determinations of mass and width come from the study of charmonium spectroscopy by direct formation of $\bar{c}c$ states in $\bar{p}p$ annihilation at the Fermilab Antiproton Source (experiments E760 and E835). The E760 collaboration measured the resonance parameters of the χ_{c1} and χ_{c2} [360].

For both E760 and E835-I, the transition energy of the Antiproton Accumulator was close enough to the χ_{c0} mass to prevent stable running with large stacks in this energy region. Nevertheless, a few stacks were decelerated to the χ_{c0} region at the end of Run I, yielding an unexpectedly high rate of $J/\psi\gamma$ events. The Accumulator underwent a major upgrade between 1997 and 2000, shifting the transition energy [362] and allowing a smooth running at the χ_{c0}, with substantial increase in statistics [361], and a better control of systematics.

A new measurement of the χ_{c1} parameters was made in year 2000, with roughly 15 times more statistics than the predecessor experiment E760. The χ_{c2} parameters were also remeasured with statistics comparable to those of experiment E760. This report includes the new results, in publication, not yet included in the PDG.

The effect of scanning a narrow resonance with a beam of comparable width is show in Fig. 3.11, where the excitation curve for one scan at the χ_{c1} is compared with the deconvoluted Breit Wigner shape and the measured beam energy profiles for each point.

In mass and width measurements, the systematic error comes from uncertainties on auxiliary variables measured concurrently to data taking (changes in beam orbit length, efficiency and luminosity at each energy point), as well as the absolute calibration of the beam energy. The absolute calibration of the beam energy is deduced from the absolute calibration of the orbit length, done using $\psi(2S)$ scans, and

[32] Authors: R. Mussa, G. Stancari

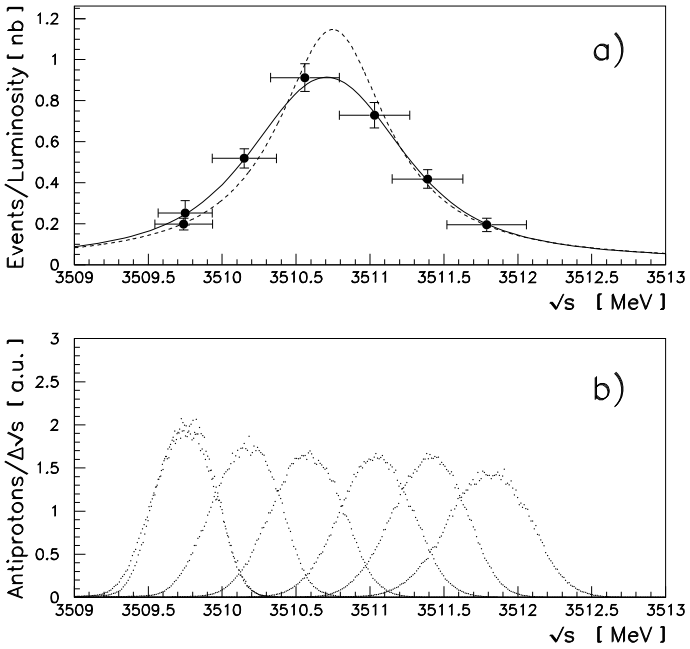

Fig. 3.11: Measured cross-section at each data point, excitation curve (full line) and deconvoluted resonance curve (dotted line) for one scan at the χ_{c1} ; plotted in the lower part of the figure are the beam energy profiles corresponding to each data point

assuming 3686.000 for the mass of this state. The more precise determination recently done at VEPP-4, documented in the previous section, implies a systematic shift (up) of 70, 83, 89 keV of the $\chi_{c0,1,2}$ measurements respectively. The systematic error on χ_c masses from $\psi(2S)$ mass determination reduces then to 16,19,20 keV respectively, and is now negligible if compared to the other sources, which are uncorrelated when we merge different scans. The impact of radiative corrections to account for proton bremsstrahlung is still well below other systematic errors; it was estimated using the expression:

$$\sigma_{BW}^{rad}(\beta, s) = \beta \int_0^{\frac{\sqrt{s}}{2}} \frac{dk}{k} \left(\frac{2k}{\sqrt{s}}\right)^{\beta} \sigma_{BW}(s - 2k\sqrt{s})$$

with

$$\begin{aligned} \beta &= \frac{2\alpha}{\pi} \times \left(\frac{s - 2m_p^2}{\sqrt{s(s-4m_p^2)}} \times \ln \frac{s + \sqrt{s(s-4m_p^2)}}{s - \sqrt{s(s-4m_p^2)}} - 1 \right) \\ &= 6.7 \times 10^{-3} (\chi_{c0}), \quad 7.0 \times 10^{-3} (\chi_{c1}), \quad 7.2 \times 10^{-3} (\chi_{c2}). \end{aligned}$$

Systematic shifts on masses are $\Delta m(\chi_{c0,1,2}) = -0.06, -0.01, -0.02\,\mathrm{MeV}/c^2$; the shifts on total widths are $\Delta\Gamma/\Gamma \approx -1\%$ for all χ_c states.

E835 could also measure the χ_{c0} excitation curve in the $p\bar{p}\to\pi^0\pi^0$ channel, exploting the amplification due to interference with continuum. The measurement is compatible with result obtained in $\psi\gamma$ and of course has correlated systematic errors.

A measurement of mass [365] and width [366] with accuracy almost comparable to the one obtained in $p\bar{p}$ annihilations was made by BES on the χ_{c0}, exploiting the sample of 3.8M ψ' decays to various decay channels. There are not yet mass and width measurements of χ_c states from the 14M ψ' sample. Table 3.12 summarizes the most accurate results on masses and widths at present. Statistical

Table 3.12: Parameters of χ_c states from E760, E835, and BES

R	Expt.	Mass(MeV/c^2)	Γ(MeV)	Ref.
χ_{c0}				
	BES	3414.1±0.6±0.8	14.3±2.0±3.0	[365]
	E835	3415.4±0.4±0.2	9.9±1.0±0.1	[361]
	E835	3414.7±0.7±0.2	8.6±1.7±0.1	[363]
	PDG 2004	3415.19±0.34	10.1±0.8	[245]
χ_{c1}				
	E760	3510.61±0.10±0.02	0.88±0.11±0.08	[360]
	PDG 2004	3510.59±0.10	0.91±0.13	[245]
	E835	3510.725±0.065±0.018	0.88±0.06±0.09	[364]
χ_{c2}				
	E760	3556.24±0.07±0.12	1.98±0.17±0.07	[360]
	PDG 2004	3556.26±0.11	2.11±0.16	[245]
	E835	3556.10±0.09±0.17	1.93±0.19±0.09	[364]

errors on $\chi_{c1,2}$ masses are obtained from gaussian sums of errors from event statistics and errors from orbit length measurements; the latter are dominant, therefore future improvements will require to push fractional errors on orbit lengths below 10^{-6}. In the case of χ_{c0} there is still room for improvement: ten times more statistics at the χ_{c0} in a $p\bar{p}$ annihilation experiment could take errors on masses down to 200 keV, and on widths down to 3%. To reach a comparable level on narrow χ_b states is very challenging, and will require new ideas.

It is finally possible to present the results on P states by calculating the spin independent (M_{COG}), spin–orbit (h_{LS}) and tensor (h_T) terms of the $c\bar{c}$ Hamiltonian. All values are summarized in Table 3.13.

Table 3.13: Fine splittings between χ_c states

	$c\bar{c}(n=1)$
M_{COG} (in MeV)	
$\Delta M_{21} = M(\chi_{c2}) - M(\chi_{c1})$ (in MeV)	45.6±0.2
$\Delta M_{10} = M(\chi_{c1}) - M(\chi_{c0})$ (in MeV)	95.3±0.4
$\rho(\chi) = \Delta M_{21}/\Delta M_{10}$	0.470±0.003
h_T (in MeV)	10.06±0.06
h_{LS} (in MeV)	34.80±0.09

6.2 Bottomonium P states: COG and Fine splittings[33]

After discovery of the $\Upsilon(1S)$, $\Upsilon(2S)$ and $\Upsilon(3S)$ resonances at the fixed target pN experiment at Fermilab in 1997 [367] the first two were observed a year later at the e^+e^- storage ring DORIS at DESY [368]. Since DORIS energy reach was stretched well beyond its design, the $\Upsilon(3S)$ could not be reached. The

[33] Author: T. Skwarnicki

limited statistics and limited photon detection capabilities of the detectors prevented observation of the $\chi_{bJ}(1P)$ states via E1 photon transitions from $\Upsilon(2S)$ at that time. Energy range of another e^+e^- storage ring, CESR at Cornell University, was extended high enough to reach the $\Upsilon(3S)$ in 1982. The CUSB detector at CESR had sufficient photon detection resolution in NaI(Tl)/Lead-glass calorimeter to discover the three $\chi_{bJ}(2P)$ states in inclusive photon spectrum in $\Upsilon(3S)$ decays [369]. The $J = 1$ and $J = 2$ states were also observed in two-photon cascade, $\Upsilon(3S) \to \gamma\chi_{bJ}(2P)$, $\chi_{bJ}(2P)\to\gamma\Upsilon(nS)$ $(n = 1, 2)$, followed by $\Upsilon(nS)\to l^+l^-$, where l^+l^- stands for e^+e^- or $\mu^+\mu^-$ [370]. The latter "exclusive" approach eliminates all photon backgrounds from π^0s copiously produced in hadronic decays of $b\bar{b}$ states, but results in low signal statistics. In fact, the $J = 0$ is very difficult to observe this way since it has larger gluonic annihilation width, which suppresses branching ratios for radiative transitions. A year later the CUSB experiment produced similar evidence for $\chi_{bJ}(1P)$ states in the $\Upsilon(2S)$ data [371]. The $J = 2$ and $J = 1$ states were also observed by the CLEO experiment in inclusive photon spectrum, with photons reconstructed in the tracking system after conversion to e^+e^- pairs at the beam-pipe [372].

Meanwhile DORIS accumulated more data at the $\Upsilon(2S)$ resonance with two new detectors: magnetic spectrometer ARGUS, and NaI(Tl)-calorimeter Crystal Ball, which previously explored photon spectroscopy in charmonium at SPEAR. The Crystal Ball confirmed the CUSB results on the $\chi_{bJ}(1P)$ states [373], though the $J = 0$ photon line was observed at a different energy, soon confirmed by ARGUS via photon conversion technique [374]. Analysis of angular correlation in $\gamma\gamma l^+l^-$ by Crystal Ball established spin assignment to the observed $\chi_{b2}(1P)$ and $\chi_{b1}(1P)$ states [375]. Next round of improvements in experimental results came about a decade later from the CESR upgraded to higher luminosity and upgraded CUSB and CLEO experiments. The CUSB-II detector was equipped with compact BGO calorimeter. The CLEO II collaboration built large CsI(Tl) calorimeter which was put inside the superconductive magnet. Both experiments improved the results on $\chi_{bJ}(2P)$ states, with the increased $\Upsilon(3S)$ data size [376].

A few years later the CLEO II experiments took a short $\Upsilon(2S)$ run. Even though the number of $\Upsilon(2S)$ resonance decays was not much larger than in the previous measurements, the results on $\chi_{bJ}(1P)$ states were substantially improved [377] thanks to much larger photon detection efficiency of well-segmented CLEO II calorimeter.

CESR continued to improve its luminosity via the storage ring upgrades. Its running time was exclusively devoted to B-meson physics with data taken at the $\Upsilon(4S)$ resonance. The CLEO tracking and particle identification systems were replaced, while the CsI(Tl) calorimeter was preserved. After the B physics program at CESR had ended, the CLEO III detector accumulated large samples at the narrow $\Upsilon(nS)$ resonances. Number of collected $\Upsilon(2S)$ and $\Upsilon(3S)$ resonant decays was increased by an order of magnitude. Analysis of inclusive photon spectra has been recently completed [378]. Photon lines due to $\Upsilon(2S)\to\gamma\chi_{bJ}(1P)$ and $\Upsilon(3S)\to\gamma\chi_{bJ}(2P)$ observed in inclusive photon spectrum are shown in Fig. 3.12 and Fig. 3.13 respectively. Determination of energies of these photon lines is limited by the systematic error in calibration of the calorimeter. The latter was improved in CLEO III by analysis of the $\psi(2S)$ photon spectrum obtained with the same detector [379]. Since the photon energies in $\psi(2S)\to\gamma\chi_{cJ}(1P)$ transitions are precisely know from the scans of the resonant cross-sections in e^+e^- ($\psi(2S)$) or $\bar{p}p$ (χ_{cJ}) collisions, the $\psi(2S)$ photon lines were turned into the calibration points.

Comparisons of the photon energies for $\Upsilon(2S)\to\gamma\chi_{bJ}(1P)$ and $\Upsilon(3S)\to\gamma\chi_{bJ}(2P)$ determined in various experiments, together with the world average values, are shown in Fig. 3.14 and Fig. 3.15 respectively. The masses of the $\chi_{bJ}(1P)$ ($\chi_{bJ}(2P)$) states can be calculated from these photon energies and the masses of $\Upsilon(2S)$ ($\Upsilon(3S)$). The errors on the latter are significant, thus the errors on the masses of the $\chi_{bJ}(nP)$ states are strongly correlated between different values of J. These need to be properly taken into account when calculating the centre-of-gravity mass and fine-splitting parameters. The results are tabulated in Table 3.14.

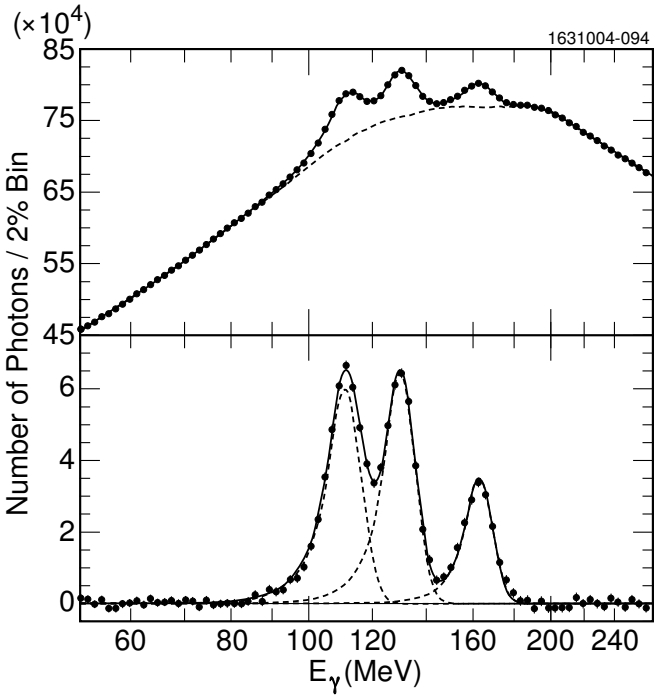

Fig. 3.12: Fit to the $\Upsilon(2S)\to\gamma\chi_{bJ}(1P)$ ($J = 2, 1, 0$) photon lines in the CLEO III data. The points represent the data (top plot). Statistical errors on the data are smaller than the point size. The solid line represents the fit. The dashed line represents total fitted background. The background subtracted data (points with error bars) are shown at the bottom. The solid line represents the fitted photon lines together. The dashed lines show individual photon lines.

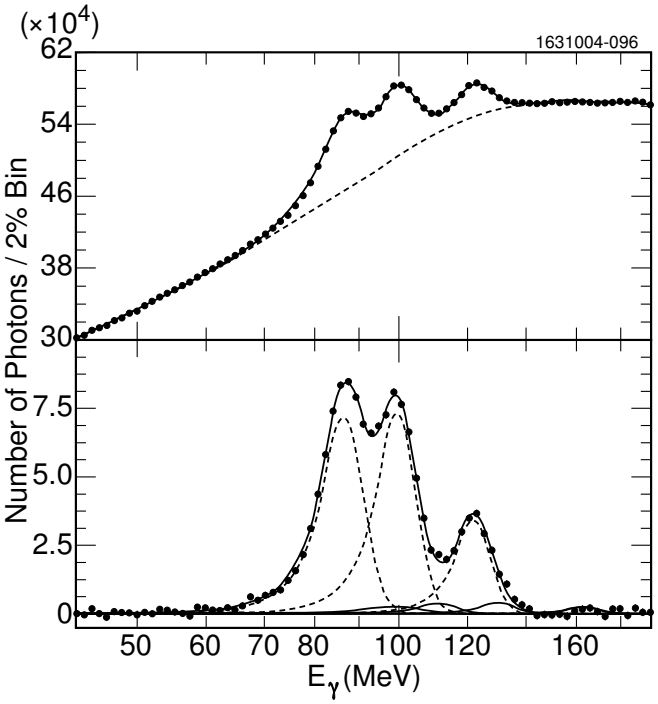

Fig. 3.13: Fit to the $\Upsilon(3S)\to\gamma\chi_{bJ}(2P)$ ($J = 2, 1, 0$) photon lines in the CLEO III data. See caption of Fig. 3.12 for the description. Small solid-line peaks in the bottom plot show the $\chi_{bJ}(2P)\to\gamma\Upsilon(1D)$ and $\Upsilon(2S)\to\gamma\chi_{bJ}(1P)$ contributions.

Average: (110.4 ± 0.3) MeV

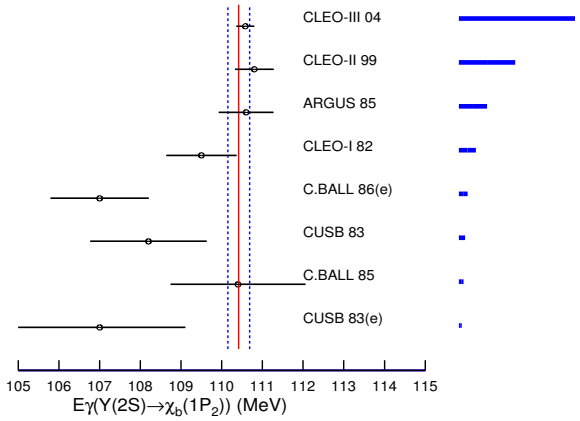

Average: (129.6 ± 0.3) MeV

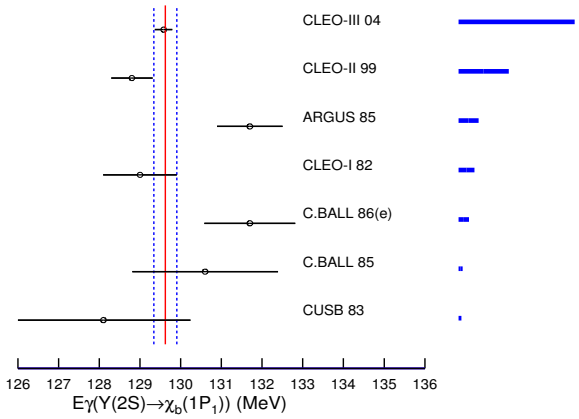

Average: (162.4 ± 0.4) MeV

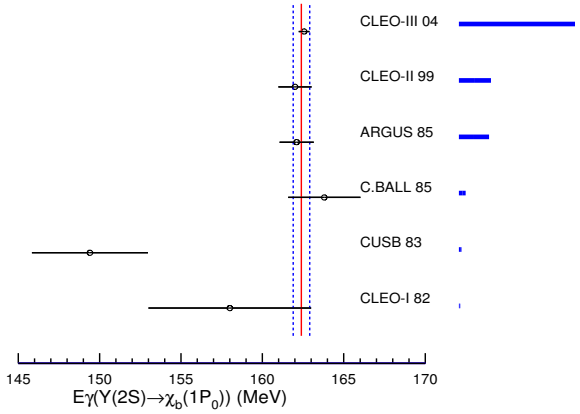

Fig. 3.14: Measurements of the photon energies in $\Upsilon(2S) \to \gamma\chi_{bJ}(1P)$. The vertical bars indicate the world average value (solid) and its error (dashed). These are also listed on top. The thick horizontal bars to the right of the name of the experiment give the relative weight of each experiment into the average value. Photon energy measurements from analyses of exclusive $\gamma\gamma l^+ l^-$ events are indicated with an "(e)" after the date of the publication.

Average: (86.1 ± 0.2) MeV

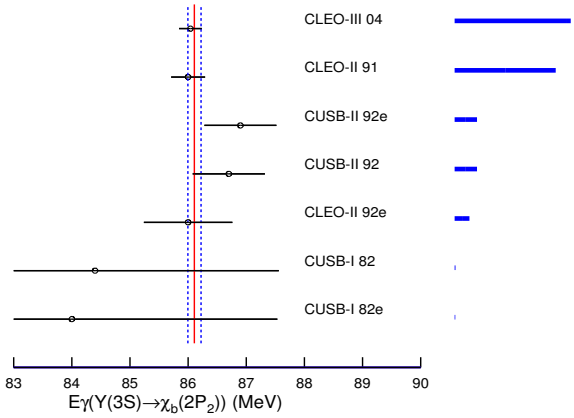

Average: (99.3 ± 0.2) MeV

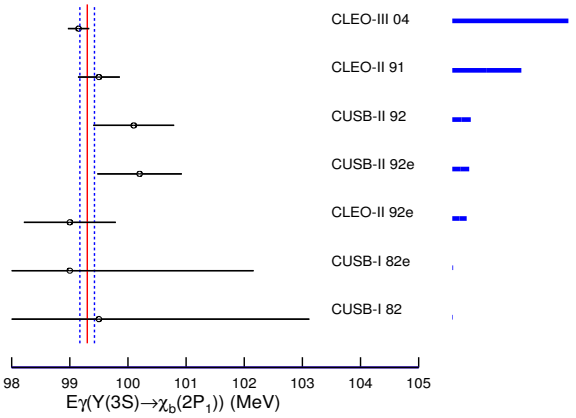

Average: (121.9 ± 0.4) MeV

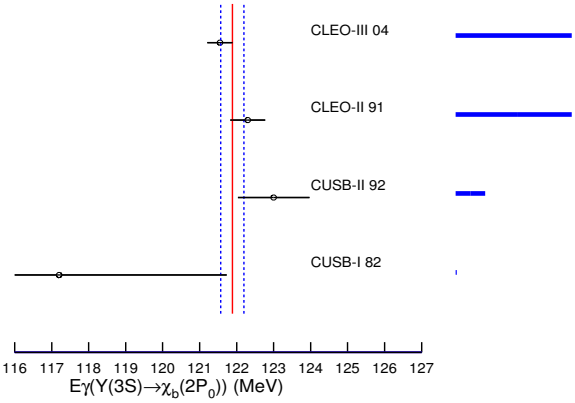

Fig. 3.15: Measurements of the photon energies in $\Upsilon(3S) \to \gamma\chi_{bJ}(2P)$. The vertical bars indicate the world average value (solid) and its error (dashed). These are also listed on top. The thick horizontal bars to the right of the name of the experiment give the relative weight of each experiment into the average value. Photon energy measurements from analyses of exclusive $\gamma\gamma l^+ l^-$ events are indicated with an "(e)" after the date of the publication.

Table 3.14: Masses and fine splittings for the $\chi_b(nP)$ states obtained from the world average values. The values of ρ given in brackets come from the CLEO III measurements [378] and have smaller errors than the world average values since cancellations in the systematic errors of photon energies for different J values are properly considered.

	$b\bar{b}(n=1)$
$M(\chi_{b2})$	9912.2±0.4 (in MeV)
$M(\chi_{b1})$	9892.8±0.4 (in MeV)
$M(\chi_{b0})$	9859.5±0.5 (in MeV)
M_{COG}	9899.9±0.4 (in MeV)
$\Delta M_{21} = M(\chi_{b2}) - M(\chi_{b1})$ (in MeV)	19.4±0.4
$\Delta M_{10} = M(\chi_{b1}) - M(\chi_{b0})$ (in MeV)	33.3±0.5
$\rho(\chi) = \Delta M_{21}/\Delta M_{10}$	0.584±0.016 (0.574±0.012)
h_T (in MeV)	3.27±0.08
h_{LS} (in MeV)	13.64±0.14
	$b\bar{b}(n=2)$
$M(\chi_{b2})$	10268.7±0.5 (in MeV)
$M(\chi_{b1})$	10255.4±0.5 (in MeV)
$M(\chi_{b0})$	10232.6±0.6 (in MeV)
M_{COG}	10260.3±0.5 (in MeV)
$\Delta M_{21} = M(\chi_{b2}) - M(\chi_{b1})$ (in MeV)	13.3±0.3
$\Delta M_{10} = M(\chi_{b1}) - M(\chi_{b0})$ (in MeV)	22.8±0.4
$\rho(\chi) = \Delta M_{21}/\Delta M_{10}$	0.583±0.020 (0.584±0.014)
h_T (in MeV)	2.25±0.07
h_{LS} (in MeV)	9.35±0.12

6.3 Bottomonium D states[34]

The lowest radial excitations of the D states in charmonium have masses above the the $D\bar{D}$ meson threshold. The lightest member of the spin-triplet is a vector state. It is identified with the $\psi(3770)$ state, which is a third $c\bar{c}$ resonance observed in the e^+e^- cross-section. Unlike the $J/\psi(1S)$ and the $\psi(2S)$ resonances, the $\psi(3770)$ is broad because it decays to $D\bar{D}$ meson pairs. Since, the coupling of the D state to e^+e^- is expected to be small, its large e^+e^- cross-section is attributed to a significant mixing between the $2S$ and $1D$ $J^{PC} = 1^{--}$ states. Whether the narrow $X(3872)$ state is one of the other members of the $1D$ family is a subject of intense disputes. The $J=2$ states (the spin triplet and the spin singlet) are narrow below the $D\bar{D}^*$ threshold, since they can't decay to $D\bar{D}$. The $J=3$ state can decay to $D\bar{D}$ but, perhaps, its width is sufficiently suppressed by the angular momentum barrier [187]. In all scenarios, masses of all $1D$ states must be strongly affected by the proximity of open-flavour thresholds via coupled channel effects.

In contrast, the $1D$ states of bottomonium are well below the open-flavour threshold, thus their masses are easier to predict theoretically. Unfortunately, the mixing of the $2S$ and $1D$ $J^{PC} = 1^{--}$ states is expected to be small for bottomonium. Not surprisingly, the $J=1$ $1D$ $b\bar{b}$ state has not been observed in e^+e^- collisions. The spin-triplet states are accessible from the $\Upsilon(3S)$ resonance by two subsequent E1 photon transitions via intermediate $\chi_{bJ}(2P)$ states. Energies of photons in the $\chi_{bJ}(2P)\to\gamma\Upsilon(1D)$ transitions fall in the same range as the dominant $\Upsilon(3S)\to\gamma\chi_{bJ}(2P)$ photon lines. Therefore, they cannot be resolved in the inclusive photon spectrum. Two-photon coincidence is of not much help, since the photon background from π^0 decays is very large in $\Upsilon(3S)$ decays. Nevertheless, the $\Upsilon(1D)$ states have been discovered by CLEO III in the $\Upsilon(3S)$ decays [380]. The photon backgrounds are removed

[34] Author:T. Skwarnicki

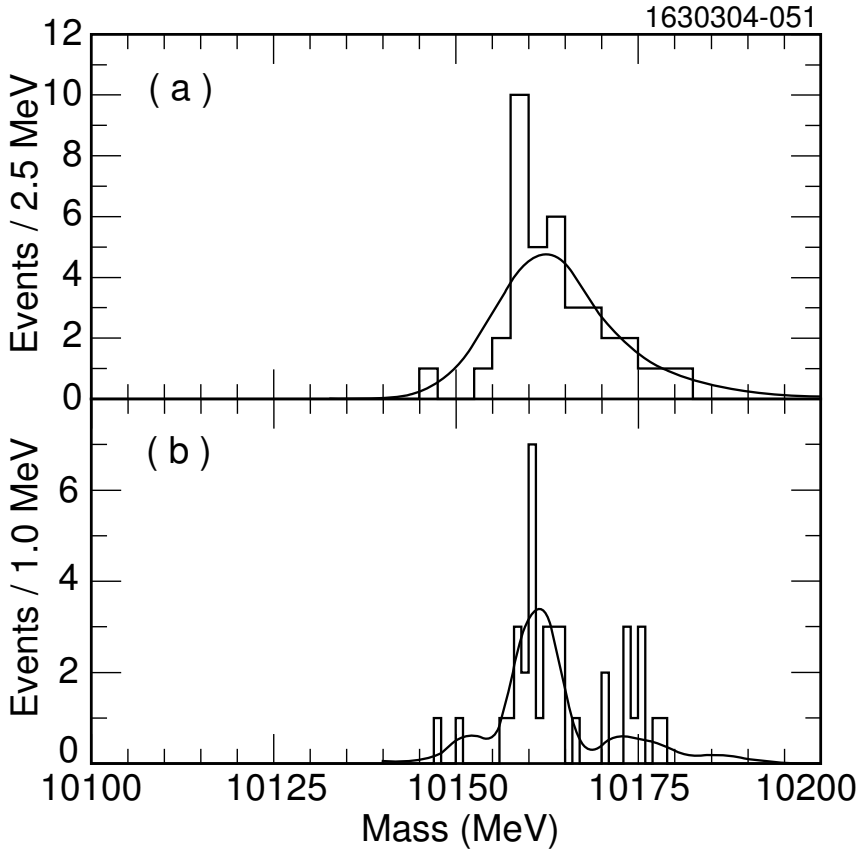

Fig. 3.16: Distributions of the measured $\Upsilon(1D)$ mass in the CLEO III data [380] using (a) the recoil mass against the two lowest energy photons, (b) the fit implementing the $\chi_{bJ'}(2P)$, $\chi_{bJ}(1P)$, $\Upsilon(1S)$ mass constraints. The results of fits for a single $\Upsilon(1D)$ state are superimposed. The mass-constraint method produces satellite peaks because of ambiguities in J' and J values.

by using the "exclusive" approach (see the previous section), in which the three additional decays are required, $\Upsilon(1D)\to\gamma\chi_{bJ}(1P)$, $\chi_{bJ}(1P)\to\gamma\Upsilon(1S)$, $\Upsilon(1S)\to l^+l^-$. Since the product branching ratio for these five subsequent decays is rather small [204, 381], the large CLEO III sample of the $\Upsilon(3S)$ resonances was essential for this measurement. After suppression of the $\Upsilon(3S)\to\pi^0\pi^0\Upsilon(1S)$ and 4-photon cascades via the $\chi_{bJ}(2P)$, $\Upsilon(2S)$, $\chi_{bJ}(1P)$ states 38 $1D$ candidates are observed in the CLEO III data. The mass of the $1D$ state is estimated by two different techniques, as shown in Fig. 3.16. In both cases, the mass distribution appears to be dominated by production of just one state. The theoretical and experimental clues point to the $J = 2$ assignment. The mass of the $\Upsilon_2(1D)$ state is measured by CLEO III to be: $(10161.1 \pm 0.6 \pm 1.6)$ MeV.

Masses of the other bottomonium $1D$ states remain unknown. However, the fine structure of the $1D$ spin-triplet is predicted to be small. All potential model calculations predict the $\Upsilon_2(1D)$ mass to be between 0.5 and 1.0 MeV lower than the centre-of-gravity (c.o.g.) mass for this triplet [204]. Adding this theoretical input, CLEO obtains (10162 ± 2) MeV for the c.o.g. mass, where they assigned an additional uncertainty of 1 MeV to the correction for the 1^3D_2-c.o.g. mass difference.

The CLEO III also looked for $\Upsilon(1D)\to\pi^+\pi^-\Upsilon(1S)$ and $\Upsilon(1D)\to\eta\Upsilon(1S)$ transitions. No evidence for such decays was found and upper limited were set [380]. The upper limit on $\Upsilon(1D) \to \pi^+\pi^-\Upsilon(1S)$ rules out rather large width for this transition predicted by the Kuang–Yan model [325, 382].

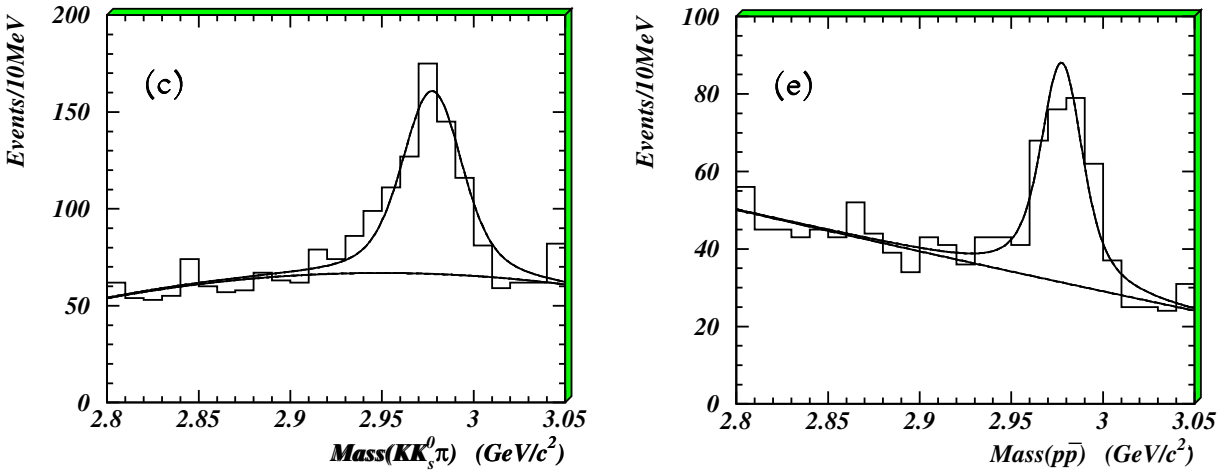

Fig. 3.17: Invariant mass distributions for $K^0_S K^{\pm}\pi^{\mp}$(left) and $p\bar{p}$(right) events from BES

7 HYPERFINE SPLITTINGS

7.1 $\eta_c(1,2S)$: comparison of all measurements[35]

Despite the large variety of available data on the $\eta_c(1S)$, the precise determination of its mass and width is still an open problem. It is likely that unexpected systematic errors be present in some of these measurements. It is worth to compare the subsets of measurements of masses and widths of the η_c done with the same reaction, before comparing the large variety of techniques which allowed to measure this state, each one with its own dominant systematic error. The two states share most of the decay channels, therefore the same analysis is usually applied to extract their signal.

7.1.1 η_c(1S) in J/ψ and ψ' decays

The η_c parameters have been extracted from the radiative transitions of J/ψ and ψ' by a large number of experiments: while Crystal Ball (and more recently CLEO-c) studied the inclusive photon spectrum, Mark II and III, DM2, BES studied the invariant mass distributions of decay products in reactions with 2 or 4 charged tracks and 0 to 2 neutral pions. The samples taken in the 80's and early 90's were recently overwhelmed by the 58 M BES sample. Table 3.15 summarizes the mass and width measurements done in the past 20 years. The η_c peak is observed in the invariant mass of the following decay modes: $K^0_S K^{\pm}\pi^{\mp}$, $\pi^+\pi^-\pi^+\pi^-$, $\pi^+\pi^- K^+K^-$, $K^+K^-K^+K^-$, $p\bar{p}$. Figure 3.17 shows two of these distributions.

Table 3.15: The world largest samples of J/ψ and ψ' used for the determination of the η_c mass and width.

Expt.	MarkIII	DM2	BES I	BES II
year	1986	1991	2000	2003
Mass(MeV/c^2)	2980.2±1.6	2974.4±1.9	2976.3±2.3±1.2	2977.5±1.0±1.2
Width(MeV)	$10.1^{+33.0}_{-8.2}$	–	11.0±8.1±4.1	17.0±3.7±7.4
Sample	2.7MJ/ψ	8.6MJ/ψ	3.8Mψ' +7.8MJ/ψ	58MJ/ψ

[35] Authors: R. Galik, R. Mussa, S. Ricciardi

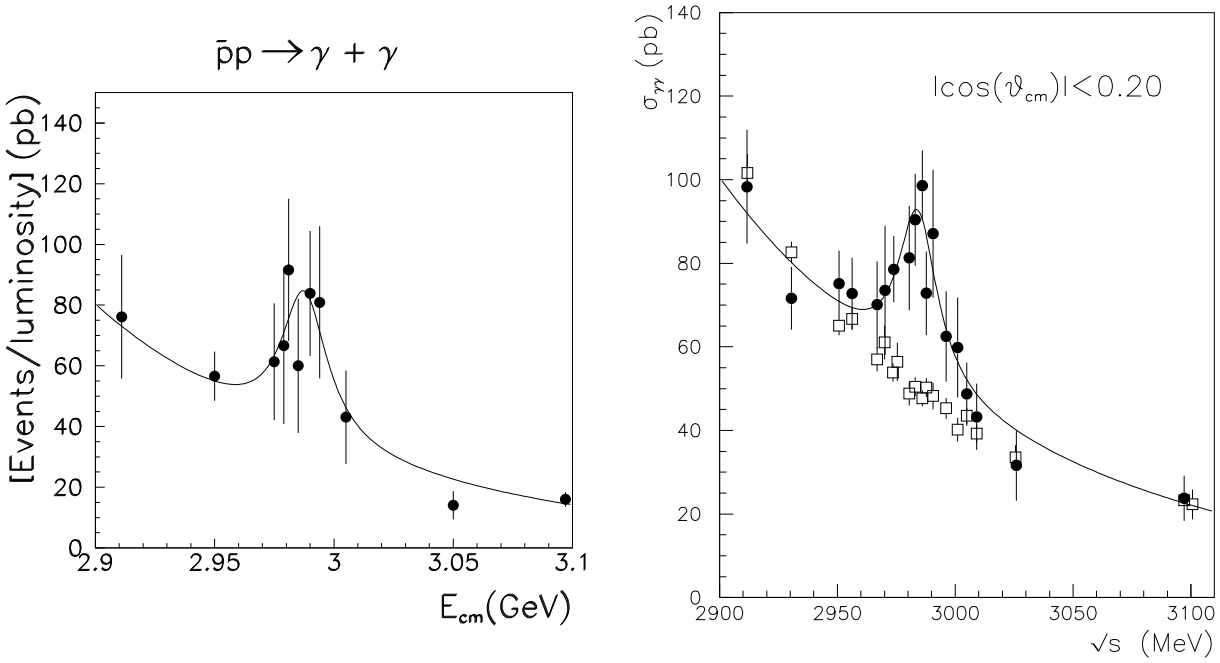

Fig. 3.18: Cross-section (black dots) observed by E760 (left) and E835(right) for the reaction $p\bar{p}\to\gamma\gamma$ in the region with cosθ_{CM} <0.25(E760), 0.2(E835). The blank squares show the expected feed-down from $\pi^0\pi^0$, $\pi^0\gamma$.

A cut on the kinematic fit to the exclusive hypothesis (referred as J/ψ veto) is applied, to reject direct J/ψ decays to the same channels, or feed-down from other decay channels, such as $(\omega,\phi)\pi\pi$, ωK^+K^-, $\gamma K^0_S K^0_S$. The systematic errors on mass determination come mostly from the mass scale calibration (0.8 MeV/c^2, calculated by comparing K^0_S, ϕ and even χ_c masses with PDG values) and from the J/ψ veto. The J/ψ veto is also the dominant source of systematics on the total width determination: 5.6 out of 7.4 MeV/c^2.

7.1.2 η_c(1S) in $p\bar{p}$ annihilations

The η_c was investigated in $p\bar{p}$ annihilation only in the $\gamma\gamma$ channel, which is affected by a substantial feeddown from the continuum reactions $\pi^0\pi^0$ and $\pi^0\gamma$: both reactions are sharply forward-backward peaked. The number of 'signal' events is 12 in R704, 45 in E760 and 190 in E835, which respectively took 0.7,3.6,17.7 pb^{-1} of data in the η_c mass region. It is worth to stress the fact that an increasing amount of integrated luminosity was taken away from the peak , in order to better understand the size and nature of the non resonant background. The experiment E835 can discriminate a π^0 from a single photon with 96.8% efficiency: this reduces the feed-down to $0.1\%\sigma_{\pi^0\pi^0}$+ 3.2% $\sigma_{\pi^0\gamma}$ at $\sqrt{s} = 2984$ MeV/c^2.

The very small sample taken by R704 in the resonant region ends up with a remarkably small result on the η_c width: all this is based on the *ansatz* to have a small background. Such hypothesis was strongly disconfirmed by E760, therefore the R704 result is affected by a very large hidden systematic error. The statement is even stronger, if we take into account that the R704 fiducial region was extended up to $cos(\theta_{cm,\pi^0}) = 0.35$, where the feeddown dominates, and the detector did not have full azimuthal coverage (thus introducing an even larger feeddown).

E835 precisely measured the $\pi^0\gamma$ and $\pi^0\pi^0$ cross-section: the feeddown from these reactions can account for most of the background. E835 could not exclude the existence of a residual tiny $\gamma\gamma$ continuum, which can in principle interfere with the resonant reaction, but is not large enough to shift the mass peak beyond the statistical error. Figure 3.18, on the right, shows both signal and feed-down

cross-section observed in E835. A power law dependence on energy was assumed for the background, in the fits. The choice of background parametrization and of the fiducial region for the signal are the dominant sources of systematic error, which amounts to 1 MeV/c^2 on the mass and 2 MeV on the width. A comparative summary of $p\bar{p}$ measurements on $\eta_c(1S)$ parameters can be found in Table 3.16.

Table 3.16: Comparison of E760 and E835 results.

Expt.	E760	E835
Ldt (pb^{-1})	3.6	17.7
$m(\eta_c)$(MeV/c^2)	2988.3 $\pm$3.3	2984.1 $\pm$2.1 $\pm$1.0
$\Gamma(\eta_c)$ (MeV/c^2)	$23.9^{+12.6}_{-7.1}$	$20.4^{+7.7}_{-6.7}$ $\pm$ 2.0

E760 and E835 also searched for the $\eta_c(2S)$ state in the energy range $3575\,\mathrm{MeV}/c^2 < \sqrt{s} < 3660\,\mathrm{MeV}/c^2$, putting a 90% CL upper limit at $\simeq$ 0.4 eV on $\mathcal{B}(\eta_c(2S)\to p\bar{p}) \times \Gamma(\eta_c(2S)\to\gamma\gamma)$.

7.1.3 η_c(1,2S) in B decays

In the last years, the B-factories have exploited the B meson decays to charmonium as a new powerful tool for the measurement of the η_c mass [393], as well as for the discovery of $\eta_c(2S)$ and the measurement of its mass. Exclusive decays of both B^0 and B^+ mesons were detected with the η_c reconstructed in the $K^0_S K^\mp \pi^\pm$, $K^+K^-\pi^0$, $K^{*0}K^\mp\pi^\pm$, $\bar{p}p$ decay channels. Exploiting common decay modes, it was possible to measure the mass difference between J/ψ and η_c, Fig. 3.19 (left) shows the invariant mass distribution of decay products from $B \to K + X$ in the 2.75–3.2 GeV/c^2 region: J/ψ and η_c peaks are clearly visible. Fitting the distribution with a Breit–Wigner convoluted with a MonteCarlo generated resolution function, it was possible to extract a value of 2979.6$\pm$2.3$\pm$1.6 MeV/c^2 for the mass , and a total width of 29$\pm$8$\pm$6 MeV (from a sample of 182$\pm$25 events, out of 31.3 M $B\bar{B}$ pairs). The systematic errors include the effect of varying the bin size as well as the shape of background, and the difference between data and MC generated detector resolutions.

The $K^0_S K^\mp\pi^\pm$ final state is an ideal place to look for the $\eta_c(2S)$, a state which was awaiting confirmation since its first and only observation by Crystal Ball in the inclusive photon spectrum from $\psi\,'$ decays. In 2002, the Belle collaboration reported the evidence of $\eta_c(2S)$ production via the exclusive processes $B^+\to K^+\eta_c(2S)$ and $B^0\to K^0_S\eta_c(2S)$. Given the suppression of the $\psi\,'\to K_S K^\pm\pi^\mp$ decay, contamination from the process $B\to K\psi\,'$ is estimated to be negligible. The first evidence [207] of the $\eta_c(2S)$ came from a sample of 44.8M$B\bar{B}$ pairs, using the exclusive channel $B\to K(K^0_S K^-\pi^+)$. A likelihood function based on the angle between the B candidate and the e^+e^- axis, and on the transverse momenta of the other tracks with the respect to the B candidate thrust axis, was used to suppress any background from continuum processes. Given a good B candidate, the feeddown from $B\to D(D_s) + X$ was reduced by cutting at $|M_{K\pi} - M_D| > 10\,\mathrm{MeV}/c^2$ and $|M_{K_S K^+} - M_{D_s}| > 10\,\mathrm{MeV}/c^2$; the feeddown from $B\to K^* + X$ was reduced by cutting at $|M_{K\pi} - M_{K^*}| > 50\,\mathrm{MeV}/c^2$, as the $\eta_c(nS)\to KK^*$ component is expected to be suppressed by the angular momentum barrier. The mass for the $\eta_c(2S)$ was measured to be 3654$\pm$6$\pm$8 MeV/c^2, with systematic error coming mostly from the choice of binning. A 90%C.L. upper limit on the width at 55 MeV was given.

7.1.4 η_c(1S) in $\gamma\gamma$ fusion

The e^+e^- collider detectors collecting data in the $\Upsilon(4S)$ region (CLEO, BaBar, BELLE) have good "reach" to produce $C = +1$ charmonium states through two-photon fusion. These are states such as

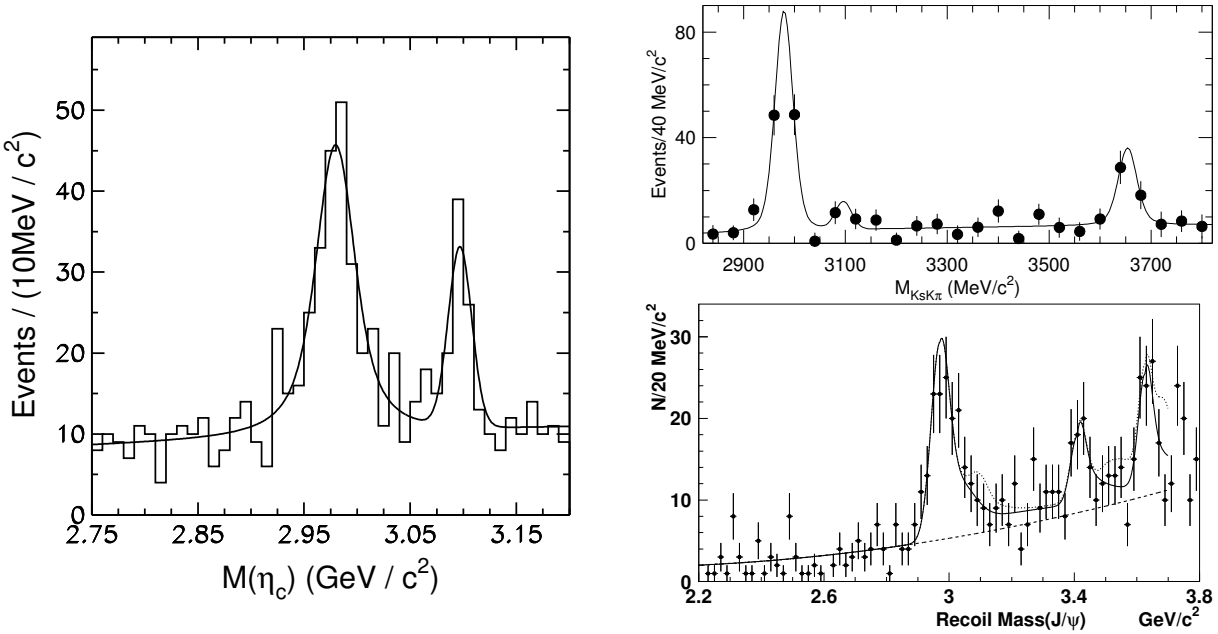

Fig. 3.19: On the left: distribution of reconstructed B decays to $\eta_c(1S)$ and J/ψ, in the common final state $K^0_S K^{\mp}\pi^{\pm}$, from refs. [393]. On the right: Belle observed the $\eta_c(2S)$ both in B decays (top, from ref. [207]) and in double $c\bar{c}$ (bottom, from ref. [394]).

the η_c and χ_c which are not produced directly in the e^+e^- annihilation process. Such $\gamma\gamma$ interactions strongly peak at low q^2 so that the scattered lepton are not detected ("untagged" events) and the photons are approximately real. For instance, in CLEO the active detector elements go to within 22° of the beam axis, or $|\cos\theta|<0.93$; this means that untagged events all have photons with Q^2 less than roughly 1 GeV^2, and usually *much* less.[36] Both CLEO and BaBar have thus recently studied the reactions:

$$\gamma\gamma\to(\eta_c/\eta_c')\to K^0_S K^{\pm}\pi^{\mp} \ .$$

The η_c is known to be coupled to two photons ($\mathcal{B}(\eta_c\to\gamma\gamma) \sim 5\cdot 10^{-4}$). An estimate of the two-photon production rate of $\eta_c(2S)$suggests that also the radial excitation could be identified in the current e^+e^- B-factory [395]. The regions of the detector acceptance occupied by such $\gamma\gamma$ fusion reactions and the competing initial state radiation (ISR for short, also called "radiative return") processes are quite dissimilar for a symmetric collider experiment such as CLEO and the asymmetric B-factories. Given this and the differing sources of systematic uncertainties, the BaBar and CLEO results are rather independent.

The CLEO analysis used ≈ 14 fb^{-1} and ≈ 13 fb^{-1} of data taken with the CLEO II and CLEO III detectors, respectively, mostly near the Υ(4S) resonance. The particle identification systems and tracking chambers in these two configurations are quite different, so these can be considered truly independent experiments. The preliminary results were first shown at the April 2003 APS meeting and submitted [387] to the EPS meeting of that summer; final results have recently been submitted for publication [388]. The BaBar collaboration has both preliminary [210] and final results [389], based on a sample of data corresponding to an integrated luminosity of about 90 fb^{-1}. In the CLEO analysis, these events are characterized by lots of missing energy and momentum, but very little transverse momentum (p_T) of the hadronic system and very little excess energy in the detectors. The selection criteria included that $p_{\rm T} < 0.6\,{\rm GeV}/c$, that there were no additional charged tracks, and that the unassociated energy in the electromagnetic calorimeter was less than 200 MeV (300 MeV) for CLEO II (CLEO III). The CLEO mass spectra are shown in Fig. 3.20(a,b) , clearly indicating evidence for both the η_c and η_c'. Fits to

[36] The one published *tagged* CLEO analysis started at $Q^2 = 1.5{\rm GeV}^2$.

these spectra (polynomial backgrounds, Breit–Wigner line shapes, double-Gaussian detector resolution functions) yielded the results shown in Table 3.18.

In the BaBar analysis, events are selected by requiring four charged particles with total transverse momentum $p_{\rm T} < 0.5\,{\rm GeV}/c$ and total energy in the laboratory frame $E_{tot} < 9$ GeV, in order to suppress $e^+e^- \to q\bar{q}$ events. One track is required to be identified as a kaon and pairs of oppositely charged tracks are used to reconstruct $K^0_S \to \pi^+\pi^-$ decays. The $K^0_S K^+\pi^-$ vertex is fitted, with the K^0_Smass constrained to the world average value.

Figure 3.20 (c) shows the resulting $K^0_S K^+\pi^-$ invariant mass spectrum. The presence of a peak at the J/ψ mass is due to ISR events, where a photon is emitted in the initial state, and a backward-going J/ψ is produced, its decay products falling into the detector acceptance because of the Lorentz boost of the centre of mass. A fit to this distribution with a sum of a smooth background shape, a Gaussian function for the J/ψ peak and the convolution of a non-relativistic Breit–Wigner shape with a Gaussian resolution function for the η_c peak, gives: $m(J/\psi) - m(\eta_c)$ = (114.4 $\pm$ 1.1) MeV/c^2, $m(J/\psi)$ = (3093.6 $\pm$ 0.8) MeV/c^2, $\Gamma(\eta_c)$ = (34.3 $\pm$ 2.3 MeV/c^2), $\sigma(J/\psi)$ = (7.6 $\pm$ 0.8) MeV/c^2. The numbers of η_c and J/ψ events are respectively 2547 $\pm$ 90 and 358 $\pm$ 33.

The results from B-factories can be compared in Table 3.19.

For CLEO, the three major sources of systematic uncertainty in the masses of these singlets are (i) comparisons of masses of the K^0_S (in $\pi^+\pi^-$), the D^0 (in $K^0_S\pi^+\pi^-$), and the D^+ (in $K^+\pi^+\pi^-$) between CLEO data and the Particle Data Group compilations, (ii) dependences on fitting shapes used for background and for signal, and (iii) the observed shifts between mass values used as input to the Monte Carlo simulations and the mass values reconstructed. In obtaining the widths of these mesons, the dominant source of possible bias is the shape assumed for the background.

In BaBar, the η_c mass resolution $\sigma(\eta_c)$ is constrained by the close J/ψ peak; the small difference (0.8 MeV/c^2) observed between $\sigma(J/\psi)$ and $\sigma(\eta_c)$ in the simulation is taken into account in the fit to data. The simulation is also used to check for possible bias in the fitted masses. The η_c and J/ψmass peaks are shifted by the same amount (1.1 MeV/c^2) in the simulation, therefore the bias does not affect the mass difference. The systematic error on the mass accounts for an uncertainty on $m(J/\psi) - m(\eta_c)$ due to the background subtraction, and for an uncertainty associated to the different angular distributions of the $J/\psi$and the η_c . The systematic error on the width is dominated by the uncertainty in the background-subtraction and in the mass resolution.

7.1.5 Overview on all results

Table 3.20 and Figs. 3.21 and 3.22 summarize the results of an attempt to fit the mass of the $\eta_c(1S)$ by using (a) all measurements quoted in this review, (b) only measurements published in the last 5 years, and results from (c) $\psi(1,2S)$ decays, (d) $p\bar{p}$ annihilation, (e) B-factories. The only *rationale* for dataset (b) is to exclude samples that were superseded by new data taken by the same experiment. A scale factor S was applied on the σ's whenever the confidence level of the χ^2 obtained from the fits was below 10%. The results are then compared with the values found in PDG 2004. The B-factories have been arbitrarily grouped together, despite they use different techniques.

Despite the substantial improvement in statistics, and the new ways to explore the $\eta_c(nS)$ states which came from the B-factories, a discrepancy between results obtained by different techniques remains. The increase in statistics has been surely beneficial in understanding systematic effects. Nonetheless , crosschecks between all different measurement techniques will be even more vital in the future, when statistic errors will be further reduced. Hopefully both asymmetric B-factories will be able to do internal crosschecks of the results from $\gamma\gamma$ fusion and from B-decays. CLEO-c will be able to crosscheck the $\gamma\gamma$ measurement by CLEO III with one from $\psi(1,2S)$ decays.

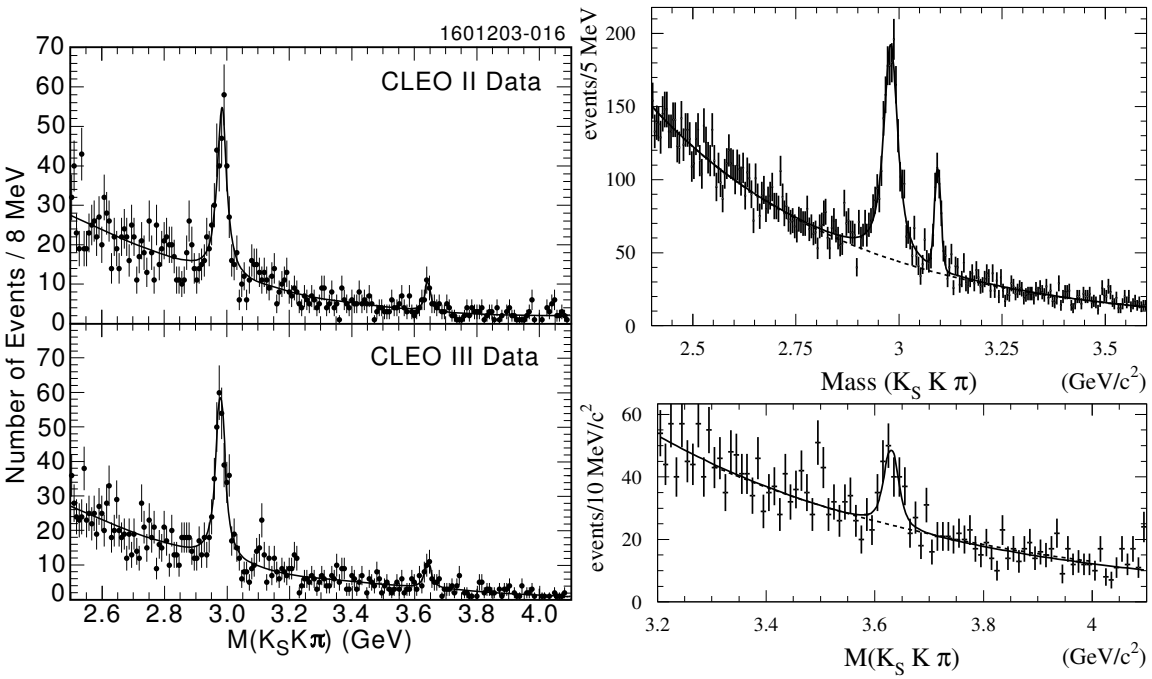

Fig. 3.20: Invariant mass distributions for $K^0_S K^{\pm}\pi^{\mp}$ events from (a) CLEO II, (b) CLEO III; from BaBarin the (c) η_c (and J/ψ) region and (d) $\eta_c(2S)$region. The results from the fit are superimposed.

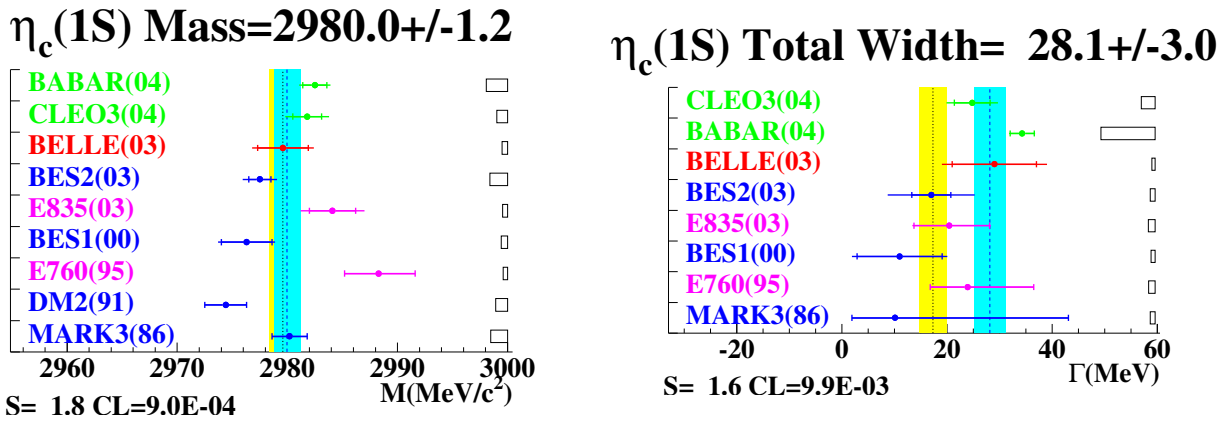

Fig. 3.21: Mass and width fits for $\eta_c(1S)$

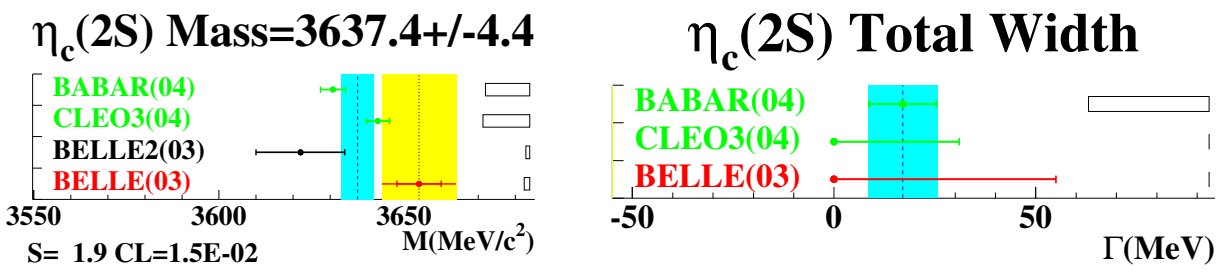

Fig. 3.22: Mass and width fits for $\eta_c(2S)$

Table 3.17: Various theoretical estimates for the mass splitting $\Delta m = m(\Upsilon) - m(\eta_b)$.

	Δm [MeV/c^2]	Ref
lattice NRQCD	19 – 100	[53, 406–410]
lattice potential	60 – 110	[411]
pQCD	36 – 55	[93, 412]
$1/m$ expansion	34 – 114	[413]
potential model	57 – 141	[414] [415–418]

Table 3.18: Summary of the results for η_c and η_c' for both CLEO II and CLEO III data sets. The errors shown are statistical only.

	CLEO II		CLEO III	
	η_c	η_c'	η_c	η_c'
Yield (events)	282±30	28^{+13}_{-10}	310 ±29	33^{+14}_{-11}
Mass (MeV)	2984.2±2.0	3642.4±4.4	2980.0±1.7	3643.4±4.3
Width (MeV)	24.7±5.1	3.9±18.0	24.8±4.5	8.4 ±17.1
significance	15.1σ	4.4σ	17.0σ	4.8σ
$R(\eta_c'/\eta_c)$	0.17±0.07		0.19±0.08	

Table 3.19: Comparison of CLEO, BaBar and Belle results.

Expt.	CLEO	BaBar	Belle
Ldt(fb^{-1})	13+14	90	29.1 [393], 31.3 [207]
$m(\eta_c)$(MeV/c^2)	2981.8 ±1.3 ±1.5	2982.5 ±1.1 ±0.9	2979.6 ±2.3 ±1.6 [393]
$\Gamma(\eta_c)$ (MeV)	24.8 ±3.4 ±3.5	34.3 ±2.3 ±0.9	29 ±8 ±6 [393]
$m(\eta_c(2S))$(MeV/c^2)	3642.9 ±3.1 ±1.5	3630.8 ±3.4 ±1.0	3654 ±6 ±8 [207]
$\Gamma(\eta_c(2S))$ (MeV)	<31 (90%CL)	17.0 ±8.3 ±2.5	<55 (90%CL) [207]

Table 3.20: Fits of all η_c mass measurements

Dataset	Mass(MeV/c^2)	S	C.L.
(a) ALL	2980.0 ±1.2	1.82	0.09%
(b) ALL after 1999	2980.4 ±1.2	1.44	6.6%
(c) $\psi(1,2S)$ decays	2977.5 ±0.9	1(1.38)	13%
(d) $p\bar{p}$	2984.5 ±1.6	1(1.05)	33%
(e) B-factories	2981.9 ±1.1	1(0.65)	65%
PDG 2004	2979.6 ±1.2	1.7	0.1%

7.2 η_b(nS) and h_b(nP): searches[37]

Over twenty-five years after the discovery of the $\Upsilon(1S)$, no pseudoscalar $b\overline{b}$ states have been conclusively uncovered. In recent years, the search has been conducted at CLEO, LEP, and CDF, using both inclusive and exclusive methods.

The inclusive CLEO search [399] identifies distinctive single photons with its high-resolution CsI electromagnetic calorimeter. These photons are signatures of Υ radiative decays, in this case $\Upsilon(3S) \to \eta_b\gamma$, $\Upsilon(2S) \to \eta_b\gamma$, $\Upsilon(3S) \to \eta_b'\gamma$, and $\Upsilon(3S) \to h_b\pi^0$ or $h_b\pi^+\pi^-$ followed by $h_b \to \eta_b\gamma$. Godfrey and Rosner have pointed out that these hindered M1 transitions could have observable branching ratios, in spite of their small associated matrix elements, because of their large phase space [204].

No evidence of a signal for any of the above modes has been seen in the total 2.4 fb^{-1} of data taken at the $\Upsilon(2S)$ and $\Upsilon(3S)$ resonances between 2001 and 2002, corresponding to roughly six million decays of each resonance. Figure 3.23 shows the resulting 90% C.L. upper limits on the branching fractions. Several of the theoretical predictions shown can be ruled out.

It has been shown that with the full data samples of LEP 2, the $\eta_b(1S)$ might be detected in two-photon events [404,405]. The η_b is fully reconstructed with four, six, or eight charged decay products and possibly a π^0. In the expected mass range, for which estimates are listed in Table 3.17, the corresponding invariant mass distribution is rapidly decreasing, and the background from τ pairs can be kept small.

Table 3.21 summarizes the results for ALEPH, L3, and DELPHI. The search by ALEPH [419] in an 800 MeV/c^2 window turned up one candidate, shown in Fig. 3.24, with an excellent mass resolution of 30 MeV/c^2 at a mass of 9.30 ± 0.03 GeV/c^2. The signal expectation is about 1.6 events over one background event.

Table 3.21: 95% C.L. upper limits on the η_b two-photon partial width times branching ratio into various hadronic states from searches at LEP.

Expt	final state	$\Gamma_{\gamma\gamma} \times \mathcal{B}$ (keV)	Ref
ALEPH	4 charged	< 0.048	[419]
	6 charged	< 0.132	[419]
L3	$K^+K^-\pi^0$	< 2.83	[420]
	4 charged	< 0.21	[420]
	4 charged π^0	< 0.50	[420]
	6 charged	< 0.33	[420]
	6 charged π^0	< 5.50	[420]
	$\pi^+\pi^-\eta'$	< 3.00	[420]
DELPHI	4 charged	< 0.093	[421]
	6 charged	< 0.270	[421]
	8 charged	< 0.780	[421]

L3 has reported an analysis, considered close to final, in six decay modes [420]. Six candidates are found, compatible with an expected background of 2.5 events. The mass measurement is dominated by the detector resolution of about 300 MeV/c^2.

Recently, DELPHI has also reported preliminary results [421]. A total of seven candidates are found in a search window of 400 MeV/c^2. The expected background level is 5.5 events, and the mass resolution roughly 120 MeV/c^2.

[37] Authors: A. Böhrer, T. Ferguson, J. Tseng

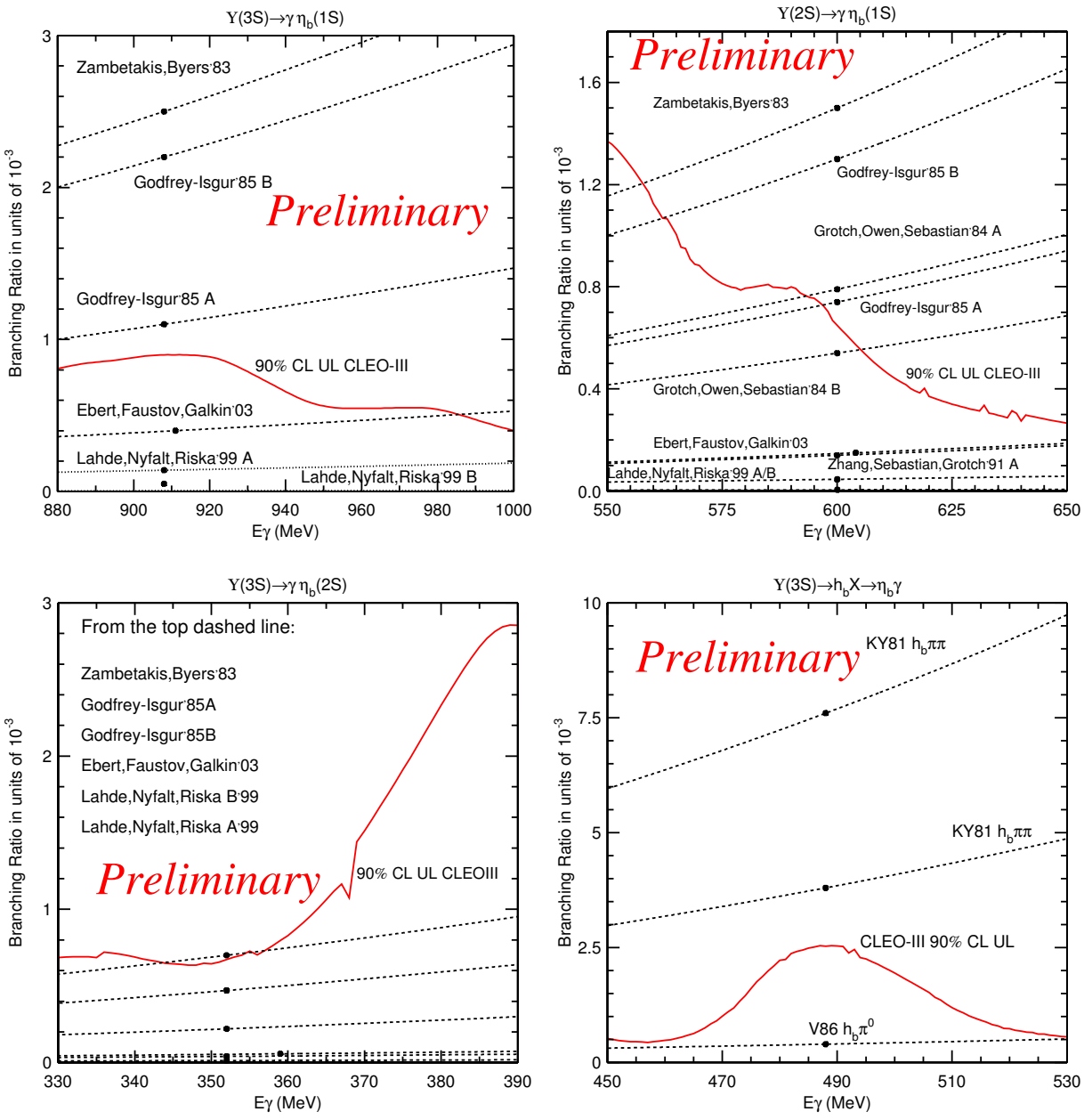

Fig. 3.23: CLEO 90% C.L. upper limits on $\mathcal{B}(\Upsilon(3S) \to \eta_b\gamma)$ (top left), $\mathcal{B}(\Upsilon(2S) \to \eta_b\gamma)$ (top right), $\mathcal{B}(\Upsilon(3S) \to \eta_b'\gamma)$ (bottom left), and $\mathcal{B}(\Upsilon(3S) \to h_b\pi^0, h_b\pi^+\pi^-) \times \mathcal{B}(h_b \to \eta_b\gamma)$ (bottom right) as a function of the photon energy E_γ, along with various theoretical predictions [206, 400–403].

Made on 2-Mar-2001 09:59:55 by boehrer with DALI_E2.
Filename: DC055136_002499_010302_0959.PS

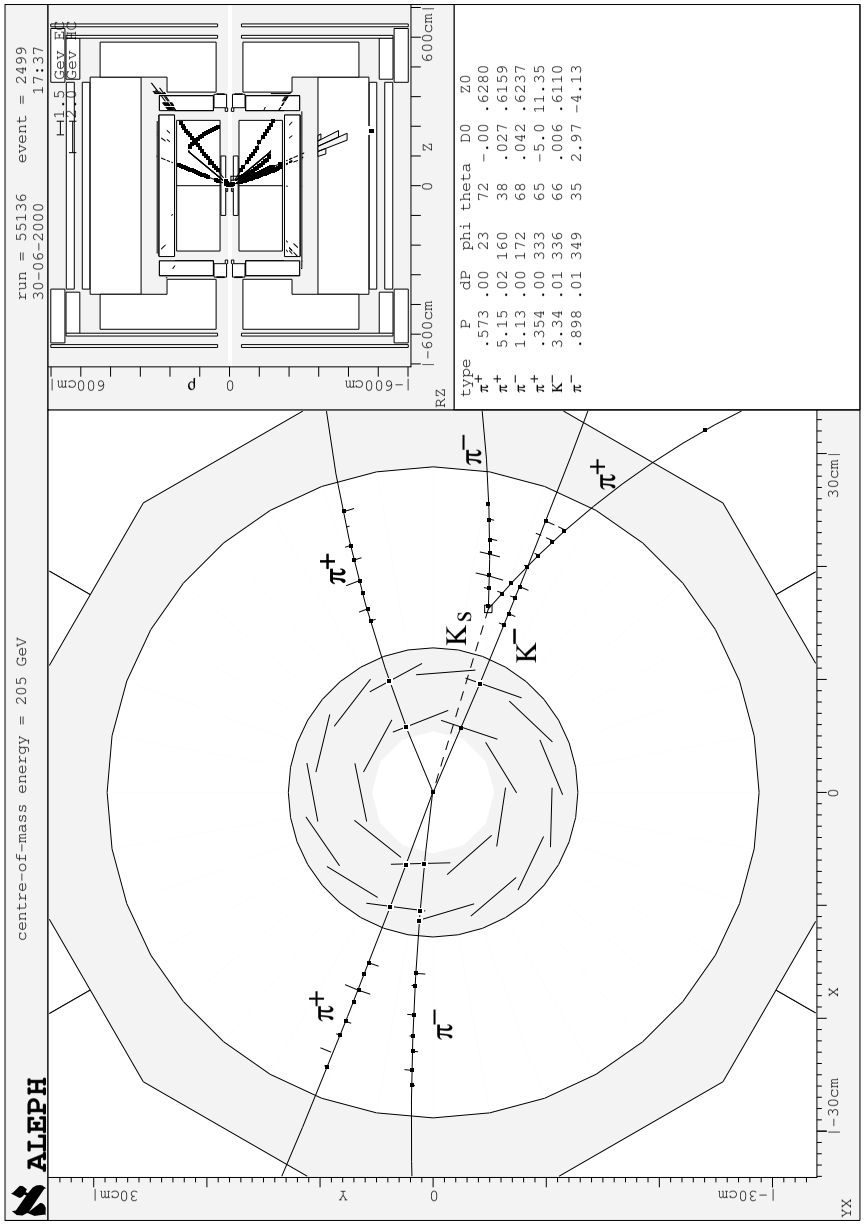

Fig. 3.24: $\eta_b \to K^0_S K^- \pi^+ \pi^+ \pi^-$ candidate at ALEPH, with a reconstructed mass of 9.30 ± 0.03 GeV/c^2.

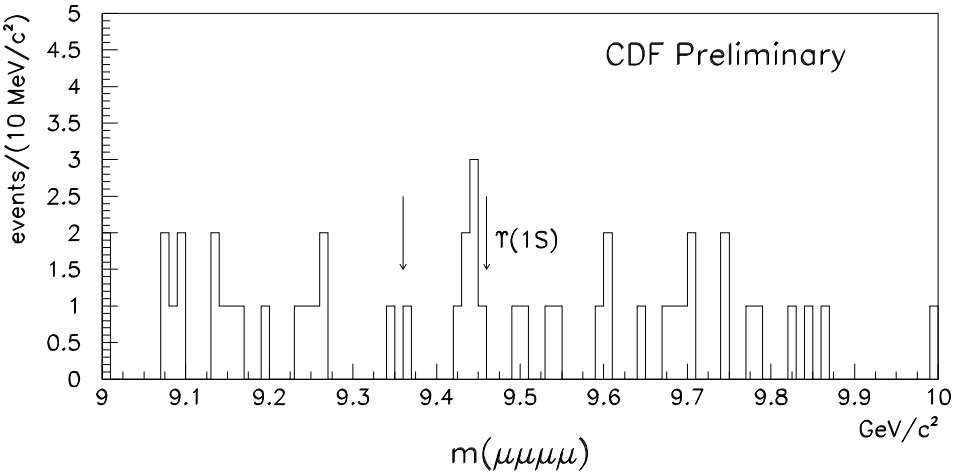

Fig. 3.25: The 4-muon invariant mass distribution from $J/\psi J/\psi$ events in CDF Run 1 data. The search window, the upper side of which is the world-averaged $\Upsilon(1S)$ mass [245], is marked by arrows.

CDF has searched for the exclusive decay $\eta_b \to J/\psi J/\psi$, where both J/ψ's decay to muon pairs, in the full 1992–96 "Run 1" data sample of about 100 pb^{-1} [422]. The mass spectrum is shown in Fig. 3.25; in this region, the mass resolution is about 10 MeV/c^2. A small cluster of seven events can be seen, where 1.8 events are expected from background. The statistical significance of the cluster is estimated to be 2.2σ. A simple fit to the mass distribution gives $9445 \pm 6(stat)$ MeV/c^2 as the mass of the cluster, where the error is only statistical. The mass difference relative to $\Upsilon(1S)$ is well to the low side of the theoretical expectation. If this cluster is due to η_b decay, then the product of its production cross-section and decay branching fractions is near the upper end of expectations [423].

The existence of the η_b is a solid prediction of the quark model, and its mass one of the most tractable to calculate. Both its existence and mass remain, for the present time, open questions. Some data at completed experiments remain to be published, however, while Run 2 is well underway at the Fermilab Tevatron.

7.3 h_c: searches[38]

The search of the singlet state of P wave charmonium (dubbed $h_c(1P)$) poses a unique experimental challenge for a variety of reasons:

- it cannot be resonantly produced in e^+e^-annihilation;
- it cannot be reached via E1 radiative transitions from $\psi\,'$; C-parity conservation forbids the transition from a 1^{--} to a $1^{+}-$ state.
- its production in $\psi\,'$ hadronic decays to $h_c(1P)\pi^0$ is isospin violating and has a small phase space available (if $M_{h_c(1P)} = M_{COG}$, $p_{\pi^0} = 86$ MeV/c; the two Doppler broadened photons will have and energy between 30 and 100 MeV in the $\psi\,'$ rest frame. In e^+e^-machines, the sensitivity on slow pions is not just affected by the physical backgrounds from other $\psi\,'$ decays, but also by the large combinatorial background with low energy uncorrelated photons from the beam.
- its production in B decays via the intermediate state $\eta_c(2S)$, which can decay radiatively (E1) to $h_c(1P)$, is suppressed by the large hadronic width of the $\eta_c(2S)$.
- its detection in the $J/\psi\pi^0$ decay mode, from $\psi\,'$ and B decays, as well as in hadroproduction, is shadowed by the more copious decay $\chi_{c1,2}\to\gamma J/\psi$, with an extra photon accidentally matching

[38] Authors: R. Mussa, D. Besson

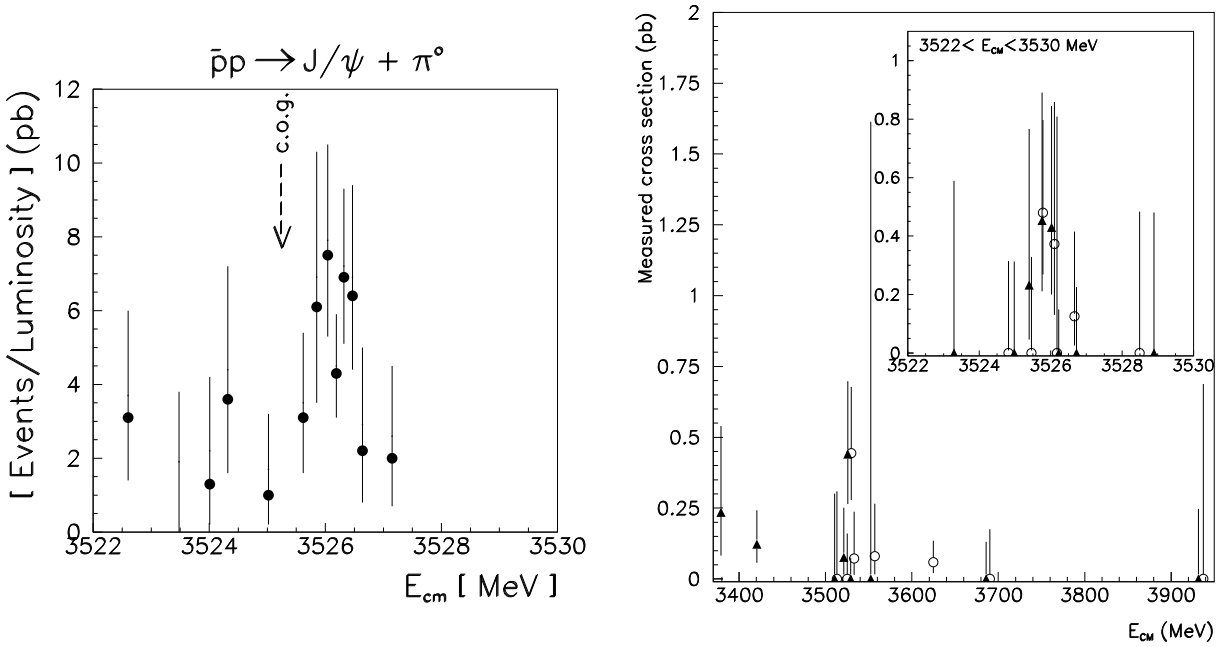

Fig. 3.26: Cross-section (black dots) observed by E760(left) for the reaction $p\bar{p}\rightarrow J/\psi\pi^0$ in the COG region; E835 could not confirm this evidence and observed the hint on the right in the $\gamma\eta_c\rightarrow 3\gamma$ channel.

the π^0 mass; this is also the most likely explanation of the signal seen in $J/\psi\pi^0$ by experiment E705, in 300 GeV/c $\pi^{\pm}$ and proton interactions on a lithium target [426].

– its formation in $p\bar{p}$ annihilation *may* be suppressed by helicity selection rule, but the same rule would forbid χ_{c0} and η_c formation , against the experimental evidence.
– its production in exclusive B decays *may* be suppressed as $\mathcal{B}(B\rightarrow\chi_{c0}K)$; if such selection mechanism does not apply, a search of $h_c(1P)$ via its E1 decay to η_c may soon give positive results.

Such elusive state was extensively searched for in formation from $p\bar{p}$ annihilations: searching for a resonance which has a width expected to be between the ψ and χ_{c1} but with an expected $\mathcal{B}$ to detectable EM decay channels of interests which is 100 to 1000 times weaker than the radiative decay of χ_{c1}, i.e., expected cross-sections between 1 and 10 picobarns. Experiment R704 at CERN [424] observed the signal:

$$\Gamma(h_c(1P)\rightarrow p\bar{p})\times\mathcal{B}(h_c(1P)\rightarrow J/\psi+X)\times\mathcal{B}(J/\psi\rightarrow e^+e^-)=0.14^{+0.15}_{-0.06}\text{ eV}$$

at a nominal mass of 3525.4±0.8±0.5 , which should be shifted down 0.8 MeV/c^2after comparing the χ_c measurements done by the two experiments.

Experiment E760 at Fermilab [425] observed the signal:

$$\Gamma(h_c(1P)\rightarrow p\bar{p})\times\mathcal{B}(h_c(1P)\rightarrow J/\psi+\pi^0)\times\mathcal{B}(J/\psi\rightarrow e^+e^-)=0.010\pm0.003\text{ eV}$$

at a nominal mass of 3526.2 ± 0.15, and did not see events in the channels $J/\psi\pi^+\pi^-$, $J/\psi\pi^0\pi^0$ E760 also determined a level of continuum for the inclusive reaction which was consistent with the one observed by R704.

In channels with such low statistics, a large amount of integrated luminosity taken to precisely quantify the background level is crucial. Such an issue was taken very seriously in E760, and even more in E835. To complicate the experimental situation, the signal observed by E760 is expected to be comparable to the $J/\psi\pi^0$ continuum, as predicted in reference [427], from soft pion radiation. It is hard to predict how interference between the resonant and continuum amplitude can distort the lineshape.

E835 took 6 times more data with respect to E760, to confirm the observation of $h_c(1P)$ and possibly measure the width as well as its decay ratios to other channels:the probably dominant decay mode to $\eta_c\gamma$ was studied, relying upon the rare η_c decays to $\gamma\gamma$. The first data set, 50 pb^{-1} taken in 1996, proved lately to be affected by an anomaly in the beam positioning system, which prevented to determine the absolute energy calibration of the machine better than 200 KeV. A second data taking period in year 2000 allowed to accumulate a comparable sample of data, but with 150 KeV resolution on the CM energy determination.

The E835 experiment, despite the 6 times larger statistics, could not confirm the $J/\psi\pi^0$ evidence observed by E760. On the other side, a hint of a signal is observed in the 3γ channel [428] Very tight cuts were applied in order to reject hadronic backgrounds from reactions with two neutral mesons in the final state. In the 3γ Dalitz plot, invariant masses of all pairs were requested to be above 1 GeV$/c^2$, to reject backgrounds from $\pi^0, \eta, \eta', \omega$. As the recoil photon angular distribution is expected to behave as $\sin\theta^2_{CM}$ on the resonance, a cut at $\cos\theta_{CM} < 0.5$ was imposed. This allowed to suppress most of the two meson background, which is prevalently forward-backward peaked. 13 events out of 29 pb^{-1} are observed in a $\delta M = 0.5$ MeV$/c^2$ wide bin between 3.5257 and 3.5262 MeV$/c^2$, while 3 events are observed in the remaining data between the χ_{c1} and the χ_{c2} (87 pb^{-1}). The statistical significance of the excess is between 1 and 3×10^{-3}, with different hypotheses on the resonance width. If the excess is not a statistical fluctuation, assuming a total width of 0.5 MeV, it is possible to measure $\Gamma(h_c\to p\bar{p})\mathcal{B}(h_c\to\eta_c\gamma) = 10.4\pm 3.7 \pm 3.4$ eV, where the systematic error comes from the statistical error on $\mathcal{B}(\eta_c\to\gamma\gamma)$), at a mass $M(h_c) = 3525.8 \pm 0.2 \pm 0.2$ MeV$/c^2$. The CLEO Collaboration has preliminary evidence [429] for the spin singlet h_c (1^1P_1) in looking at $\sim 3 \times 10^6$ decays of the ψ'(3686). This state is seen in two independent analyses, both of which use the decay chain $\psi'\to\pi^0 h_c$ followed by $h_c\to\gamma\eta_c$: one analysis is *in*clusive and the other uses six dominant *ex*clusive decays of the η_c.

The inclusive analysis shows an enhancement at over 3σ significance at a mass of $3524.4 \pm 0.7_{stat}$ MeV. The systematic uncertainty is $\sim$ 1 MeV. The left plot in Fig. 3.27 shows the fit of the data to the resolution function from Monte Carlo simulation and an "ARGUS" background shape.

Shown in the right panel of that figure is the exclusive analysis, with a statistical significance of $\sim 5\sigma$. The figure shows the data with, again, a fit to an ARGUS background and detector resolution function. Also shown are the events from the sideband of the invariant mass spectrum of the η_c reconstruction and the spectrum from a ψ' Monte Carlo simulation that does not include the h_c decay chain. Further checks on backgrounds peaking in the signal region are under way. The mass from the exclusive analysis is $3524.4 \pm 0.9_{stat}$ Mev, with systematic studies ongoing. All of these CLEO results on the h_c are considered preliminary. As a final remark, we can comment that the 20 years old search for this state is not over yet, and its evidence is still weak. It is therefore necessary to (a) consolidate the evidence for such a state from either B or $\psi(2S)$ decays , (b) to measure its mass at better than 1–2 MeV, (c) to prove its coupling to $p\bar{p}$, before planning to precisely measure its mass, total width and partial widths in formation from $p\bar{p}$ annihilations.

8 STATES CLOSE TO OPEN FLAVOUR THRESHOLDS

8.1 R values between 3.7 and 5 GeV[39]

The R value to be discussed in this section is one of the most fundamental quantities in particle physics that is defined as,

$$R = \frac{\sigma(e^+e^- \to hadrons)}{\sigma(e^+e^- \to \mu^+\mu^-)} \tag{3.46}$$

R value is expected to be constant so long as the centre-of-mass (c.m.) energy E_{cm} does not overlap with resonances or the threshold of production of a new quark flavour. A thorough review of R

[39] Author: Z. Zhao

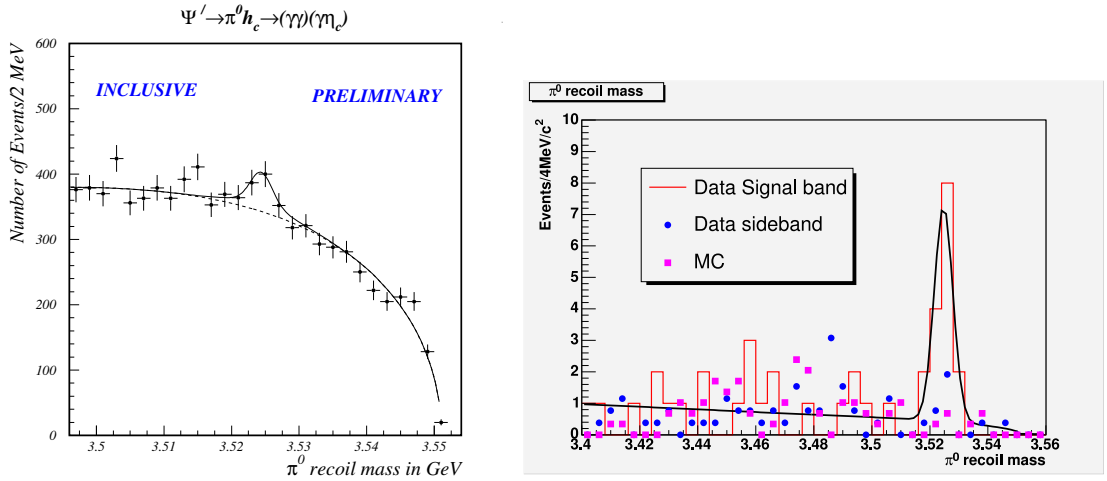

Fig. 3.27: The preliminary evidence from CLEO for the h_c singlet. On the left is the recoil mass spectrum against the π^0 in the *in*clusive analysis that only uses that pion and the photon in the $E1$ decay $h_c \to \gamma\eta_c$. To the right is the same variable for the *ex*clusive analysis in which six of the dominant η_c decay modes are used. In both cases the fits are to an ARGUS background and a resolution function from Monte Carlo studies. The exclusive plot also shows data events from the η_c sideband region and Monte Carlo simulation events of other ψ' decays.

measurements on the full energy range can be found in Chapter 6, while this subsection focuses on its complex structure in the energy region between 3.7 GeV and 5 GeV.

The most striking feature of the R values below 5 GeV is the complex structure in the energy region between 3.7 GeV and 4.5 GeV. Besides the resonance of $\psi(3770)$, broad resonance like structures peaking at around 4.04, 4.1 and 4.41 GeV have not been well understood in terms of their components and decay channels. These resonances near the charm threshold were observed more than 20 years ago [439–445, 447]. Table 3.22 lists the resonance parameters reported by these experiments.

8.1.1 PLUTO measurement between 3.1 and 4.8 GeV

The PLUTO Collaboration measured R values with the magnetic detector PLUTO at the e^+e^- storage ring DORIS between 3.1 and 4.8 GeV c.m. energy. A superconducting coil procedures a 2T magnetic field parallel to the beam axis. Inside coil there are 14 cylindrical proportional wire chambers and two lead converter, a 2 mm converter at radius 37.5 cm and a 9 mm converter at radius 59.4 cm. Two or more charged tracks are triggered and selected as hadronic event candidates. The background from beam–gas interaction and cosmic ray events is subtracted using the distribution of reconstructed event vertices alone the beam direction. Monte Carlo events are generated according to isotropic phase space to determine the detection efficiency for the hadronic events. An external luminosity monitor system is employed to observe the beam luminosity. The uncertainty of the luminosity measurement is about $\pm 5\%$. The systematic error in R values is estimated to be about 12%. PLUTO results agree with those of the SLAC–LBL group within systematic errors, but is about 10–15% lower than those of SLAC–LBL on the narrow J/ψ resonance and higher energies. However, the agreement on the energy dependence and the structure of the R values is quite good. The accuracy of PLUTO's measurement is limited by systematic error, which amount to almost one unit in R in the broad resonance region. The resonance parameters of the broad resonances cannot be determined with such a limited accuracy and energy points.

8.1.2 DASP measurement between 3.6 and 5.2 GeV

DASP Collaboration measured R values at c.m. energy between 3.6 and 5.2 GeV with a non magnetic inner detector of the double arm spectrometer DASP, which has similar trigger and detection efficiencies

Table 3.22: Resonance parameters measured for the broad structures between 3.7 and 4.5 GeV

Resonance	Experiment	Mass(MeV)	Γ_{tot}(MeV)	Γ_{ee}(eV)
$\psi(3770)$	MARK I	3772 ± 6	28 ± 8	345 ± 85
	DELCO	3770 ± 6	24 ± 5	180 ± 60
	MARK II	3764 ± 5	24 ± 5	276 ± 50
	BES([456])	3772.7 ± 1.6	24.4 ± 4.3	190 ± 25
$\psi(4040)$	DASP	4040 ± 10	52 ± 10	750 ± 150
	BES([456])	4050.4 ± 4.3	98.5 ± 12.8	1030 ± 110
	BES([246])	4040 ± 1	89 ± 6	911 ± 130
	CB([246])	4037 ± 2	85 ± 10	880 ± 110
$\psi(4160)$	DASP	4159 ± 20	78 ± 20	770 ± 230
	BES([456])	4166.5 ± 6.1	55.9 ± 12.3	370 ± 81
	BES([246])	4155 ± 5	107 ± 16	840 ± 130
	CB([246])	4151 ± 4	107 ± 10	830 ± 80
$\psi(4415)$	DASP	4417 ± 10	66 ± 15	490 ± 130
	MARK I	4414 ± 7	33 ± 10	440 ± 140
	BES([456])	4429.4 ± 8.5	86.0 ± 20.9	390 ± 74
	BES([246])	4429 ± 9	118 ± 35	640 ± 230
	CB([246])	4425 ± 6	119 ± 16	720 ± 110

for photon and charged particles. The inner detector of DASP is mounted between the two magnet arms of DASP. It is azimuthally divided into eight sectors, six of which consist of scintillation counters, proportional chambers, lead scintillator sandwiches and tube chambers, and the remaining two facing the magnet aperture, have only scintillation counter and proportional chambers. Tracks are recorded over solid angle of 62% for photon and 76% of 4π for charged particles. DASP collected a total integrated luminosity of 7500 nb^{-1}, which was determined by small angle Bhabha scattering measured by four identical hodoscopes with an uncertainty of 5%. The additional normalization uncertainty is estimated to be 15%. The uncertainties of the detection efficiencies for the hadronic events is about 12%. Three peaks centred around 4.04, 4.16 and 4.42 are observed. The data are insufficient to resolve structures between 3.7 and 4.5 GeV. By making a simplifying assumption that the cross-section can be described by an incoherent sum of Breit–Wigner resonances and a non resonant background, DASP reported resonance parameters as listed in Table 3.22.

8.1.3 SLAC–LBL measurement between 2.6 and 7.8 GeV

SLAC–LBL group did a R scan with MARK I at SPEAR which operated at c.m. energy between 2.6 and 7.8 GeV with peak luminosity between 10^{29} and 10^{31} cm^{-2} sec^{-1}. MARK I was a general purpose collider detector of the first generation. Its solenoidal magnet provide a near uniform magnetic field of 3891 ± 1 G over a volume 3.6 m long and 3.3 m in diameter. A pipe counter consisting of four hemicylindrical plastic counters surrounding the vacuum pipe were used to reduce the trigger rate of cosmic ray. Two sets of proportional wire chambers on the outside of the pipe counters had spacial resolution of 700 μm. Four modules of concertric cylindrical wire spark chambers were the main tracking elements of the detector, which gave a spacial resolution in the azimuthal direction of 340 μm, 1.0 and 0.5 cm for the 2^0 and 4^0 stereo gaps, respectively. Outside the spark chamber was an array of 48 plastic scintillation counters with a width of 20 cm each. The time-of-flight for this system was about 480 psec. An array of 24 shower counters made of five layers, each consisting of 0.64 cm of pilot F scintillator and 0.64 cm of lead. The energy resolution measured with Bhabha events was $\Delta E/E = 35\%/\sqrt{E}$. The

muon-identification spark chamber, the end-cap spark chamber, and the photon-detection capabilities of the shower counters were not used in this analysis. The R values and the corresponding resonance parameters in the energy region between 3.4 and 5.5 GeV is plotted together with those from PLUTO and DASP in Fig. 3.28 (right).

MARK I studied exclusive decay channels on the resonance at 4040 MeV and reported [446] $PsPs : PsV : VV = 0.05 \pm 0.03 : 1 : 32 \pm 12$, where Ps represents D meson and V stands for D^* meson. These early results stimulated a variety of theoretical interpretations.

8.1.4 BES measurement between 2 to 5 GeV

BES Collaboration has done a R scan with updated Beijing Spectrometer (BES II) at Beijing Electron–Positron Collider(BEPC).

The trigger efficiencies, measured by comparing the responses to different trigger requirements in R scan data and special runs taken at the J/ψ resonance, are determined to be 99.96%, 99.33% and 99.76% for Bhabha, dimuon and hadronic events, respectively.

BES's measurement first selects charged tracks, then hadronic events with charged tracks equal and greater than two. The number of hadronic events and the beam-associated background level are determined by fitting the distribution of event vertices along the beam direction with a Gaussian for real hadronic events and a polynomial of degree two for the background.

The subtraction of the beam-associated backgrounds is cross checked by applying the same hadronic event selection criteria to separated-beam data.

A new Monte Carlo event generator called LUARLW is developed together with LUND group for the determination of detection efficiencies of the hadronic events [450]. LUARLW removes the extreme-high-energy approximations used in JETSET's string fragmentation algorithm. The final states simulated in LUARLW are exclusive in contrast to JETSET, where they are inclusive. In addition, LUARLW uses fewer free parameters in the fragmentation function than JETSET. Above 3.77 GeV, the production of charmed mesons is included in the generator according to the Eichten Model [451, 452].

Different schemes for the radiative corrections were compared [355, 453–455]. Below charm threshold the four different schemes agree with each other to within 1%. Above charm threshold, where resonances are important, the agreement is within 1 to 3%. The formalism of Ref. [455] is used in our calculation, and differences between it and the schemes described in Ref. [355] are included in the systematic errors. In the calculation of the radiative correction above charm threshold, where the resonances are broad and where the total width of the resonance is related to the energy, we take the interference between resonances into account. The integrated luminosity is determined to a precision of 2–3% from the number of large-angle Bhabha events selectedusing only the BSC energy deposition. Figure 3.28 (right) shows the BES R scan results between 3.6 and 4.6 GeV.

Previously, BES Collaboration measured cross-section for charm meson production, using 22.3 pb^{-1} of e^+e^- data collected with BES I at $\sqrt{S}$=4.03 and 15 pb^{-1} at 4.14 GeV [460]. The charmed mesons used in this measurement are D^0 and D^+, of which the number of signal events are selected by fitting the inclusive $K^-\pi^+$ and $K^-\pi + \pi^+$ invariant mass distribution with Gaussian as signal plus a third order of polynomial background. Taking into account the detection efficiency, the correction of initial state radiation, and quote the corresponding braching ratio from PDG1998, BES reported their results as shown in Table 3.23, together with that predicted by the coupled channel model.

8.1.5 Remarks and prospects

DASP data agree with those of PLUTO resonabl well in shape but exceed their cross-sections by about half a unit in R above 4 GeV. In magnitude DASP's data are in closer agreement with those of SLAC–

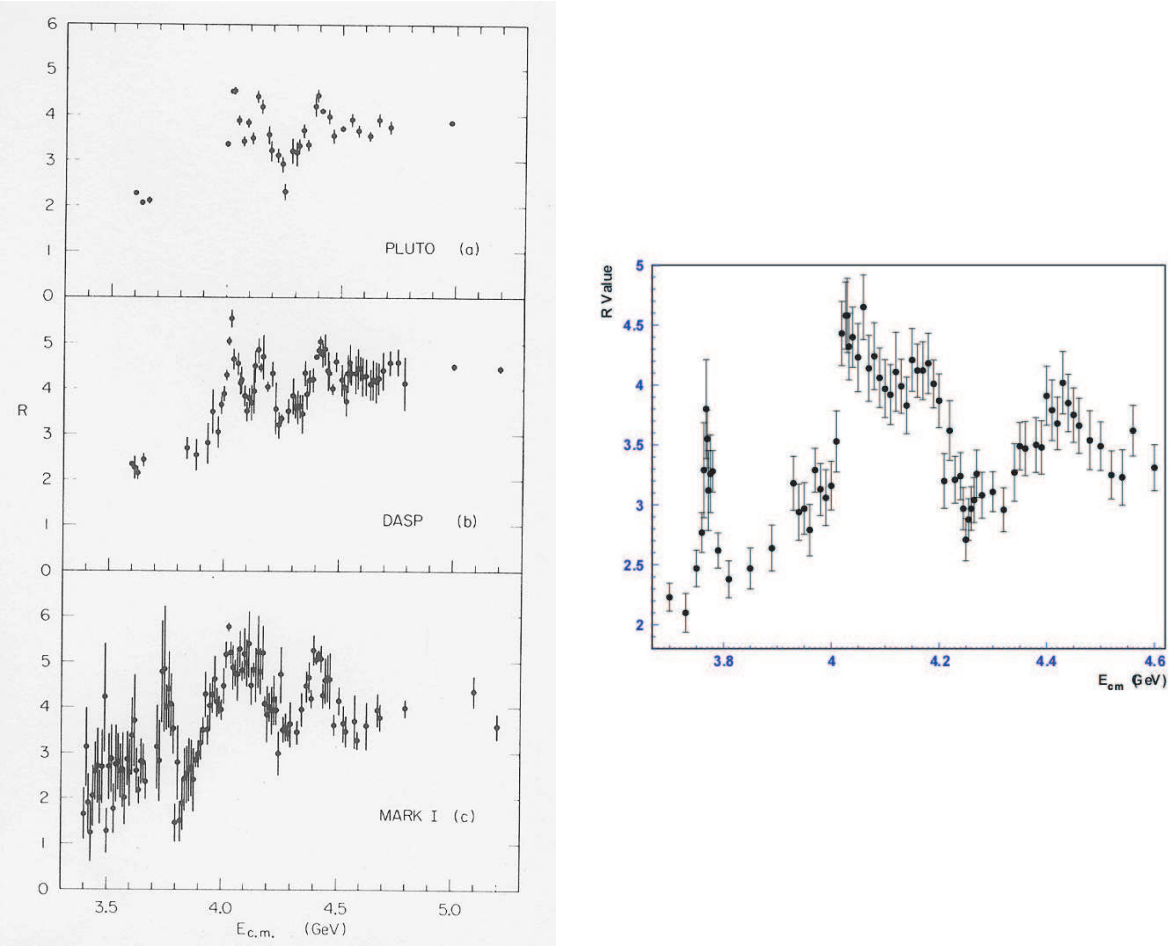

Fig. 3.28: R Values between 3.7 and 5 GeV from PLUTO, DASP and MARKI (left), and BES (right) experiments.

Table 3.23: Comparison of tree level cross-section measurement of BES with predictions of the coupled channel model. experimental D_s cross-section is taken from early work.

$\sqrt{s}$=4.03 GeV	Experiment	Coupled channel model
$\sigma_{D^0}+\sigma_{\bar{D}^0}$	19.9±0.6±2.3 nb	18.2 nb
$\sigma_{D^+}+\sigma_{D^-}$	6.5±0.2±0.8 nb	6.0 nb
$\sigma_{D_s^+}+\sigma_{D_s^-}$	0.81±0.16±0.27 nb	11.6 nb
σ_{charm}	13.6±0.3 ±1.5 nb	12.9 nb
$\sqrt{s}$=4.14 GeV	Experiment	Coupled channel model
$\sigma_{D^0}+\sigma_{\bar{D}^0}$	9.3±2.1±1.1 nb	15.1 nb
$\sigma_{D^+}+\sigma_{D^-}$	1.9±0.9±0.2 nb	4.5 nb
$\sigma_{D_s^+}+\sigma_{D_s^-}$	1.64± 0.39± 0.42 nb	1.85 nb
σ_{charm}	6.4±1.2±0.7 nb	10.7 nb

LBL but show some difference in the finer details of the energy dependence. For example, SLAC–LBL data didn't resolve the structure at 4.16 GeV. The total width measured by SLAC–LBL is smaller than that of DASP measurement. Despite of these discrepances, the difference observed among the three experiments are within the systmatic errors quoted.

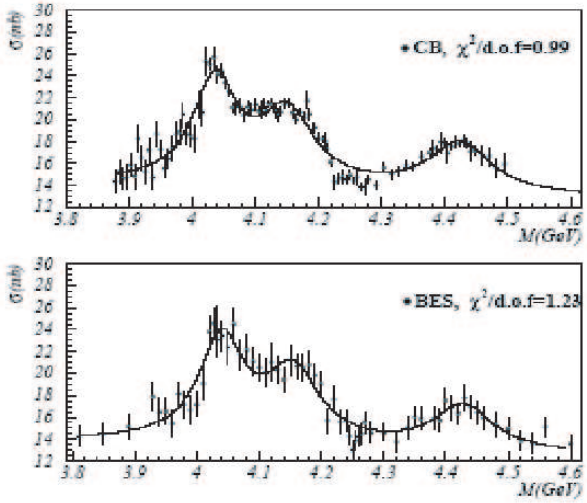

Fig. 3.29: Refit the R data of CB and BES II.

BES's R scan is done with a newer generation detector and e^+e^- collider as compared with the previous measurements, and has about 80 points in the energy region from 3.7 to 5 GeV. Because of this fine scan in this energy region that contributes most to the precision evaluation of $\alpha_{QED}(M_Z)$.

BES also fitted resonances as a Breit–Wigner shape with different continue background and takes into account the energy-dependence of resonance width and the coherence of the resonance [457]. BES's preliminary results are consistent with those of previous measurements for the peak positions at 3.77, 4.04, 4.16 and 4.42 GeV, and show larger Γ_{tot} of the resonances at 4.04 and 4.42 GeV and smaller Γ_{ee} of the resonaces at 3.77 and 4.16 GeV.

Fitting BES's R data between 3.7 and 4.6 GeV (75 data points) with Breit–Wigner resonances and none resonant background based on perturbative QCD [456], one obtain resonance parameters as listed in Table 3.22. The results from this fit has similar conclusion as the one from BES's, except that Γ_{tot} is no longer larger than the other measurements of the resonance at 4.42 GeV.

Recently, Kamal K. Seth refitted resonance parameters of the higher vector states of charmonium with existing R data [246]. Three Breit–Wigner resonances plus background that is parametrized with a linear function. He shows that the Crystal Ball (CB) and BES measurements are in excellent agreement. The analysis of the CB and BES data leads to consistent resonance parameters for the three vector resonances above the $D\bar{D}$ threshold. The masses of the three resonances determined by him in general agree with PDG, but have much smaller errors. However, the total widths of these three resonances determined by this work are about 67%, 37% and 179% larger than those adopted by PDG. The corresponding electron widths determined by this work are 23%, 8% and 51% larger with about a factor of 2 less errors. Figure 3.29 shows the fits to CB and BES data.

A factor of 2 to 3 reduction in uncertainty in the energy region of 3–5 GeV significantly improved the experimental situation, providing an opportunity to directly test QCD sum role where the notion of quark–hadron duality (QHD) plays a dominant role [456], and evaluate charm quark mass via experimental data to a precision below 10%. However, BES's data is still not enough, in terms of both statistics and systematic error restriction, to provide a clear picture of the broad resonance structures. To fully understand the complicated structures at the energies between 3.7 and 4.5 GeV, one needs to:

– perform the R scan with smaller energy steps and higher statistic in the entire energy region to a precision around 2–3%.
– collect data at the peak positions with high enough statistics to study the exclusive decay channels of the resonances.

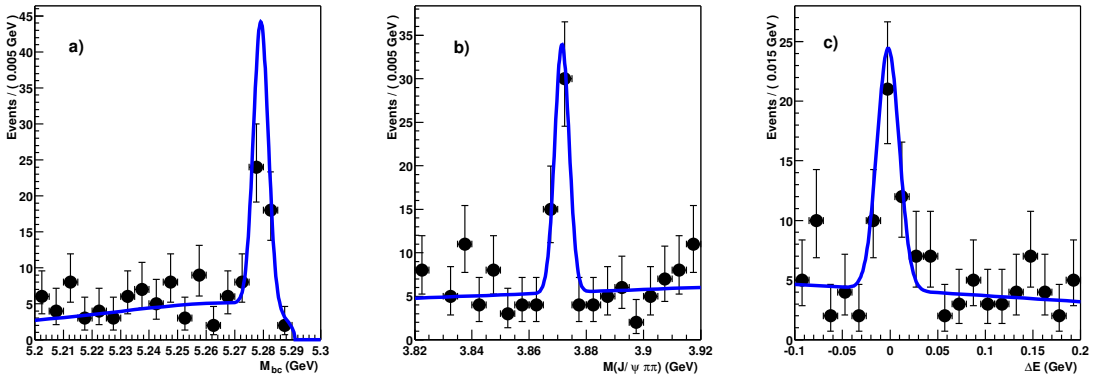

Fig. 3.30: From the Belle discovery paper [211]: projections of the data (points with error bars) and the results of an unbinned maximum likelihood fit (solid curve) for the $X(3872)\to\pi^+\pi^- J/\psi$ signal region. The variables (a) beam-constrained mass $M_{bc} = \sqrt{E^2_{\rm beam} - p^2_B}$, (b) invariant mass $M_{\pi^+\pi^- J/\psi}$, and (c) energy difference $\Delta E = E_B - E_{\rm beam}$, are those used in the fit; E_B and p_B are the energy and momentum of the $B^\pm\to K^\pm\pi^+\pi^- J/\psi$ candidate, and $E_{\rm beam}$ the energy of either $e^\pm$ beam, in the e^+e^- centre-of-mass system.

These could be the important physics topics for CLEO-c at CESR-c and BES III at BEPC II [458, 459]. Both CLEO-c and BES III may have the ability to clarify the ambiguity that has been bothering physicists for over 20 years.

8.2 X(3872): discovery and interpretations[40]

The $X(3872)$ is a narrow state decaying into $\pi^+\pi^- J/\psi$, with a mass $M_X \sim 3872\,\mathrm{MeV}$. Given the observed final state and the observed mass, in the charmonium region, it is natural to assume that the $X(3872)$ is itself a charmonium state. It has however proved difficult to identify the $X(3872)$ with any of the expected narrow $c\bar{c}$ mesons, leading to suggestions that it may be a more exotic particle. In this section, we briefly review the discovery and known properties of the $X(3872)$, and the difficulties they create for its interpretation.

8.2.1 Discovery, confirmation, and properties

The $X(3872)$ was discovered by the Belle collaboration in a study of $B^\pm\to K^\pm\pi^+\pi^- J/\psi$ decays [211]. In addition to the well-known ψ', a second peak was seen in the $M(\pi^+\pi^- J/\psi)$ distribution; the results of an unbinned maximum likelihood fit to the $X(3872)$ signal region in M, and two other variables which peak in the case of $B^\pm\to K^\pm\pi^+\pi^- J/\psi$ decay, are shown in Fig. 3.30. A yield of 35.7 ± 6.8 events was observed, with high significance (10.3σ), and the width of the mass peak was found to be consistent with the detector resolution. As the measured mass is well above the $D\overline{D}$ open charm threshold, the narrow width implies that decays to $D\overline{D}$ are forbidden; Belle [461] reports $\Gamma(X(3872) \to D\overline{D})/\Gamma(X(3872) \to\pi^+\pi^- J/\psi) < 7$ (90% CL), to be compared with a corresponding value > 160 for the $\psi(3770)$ [462]. Comparing decays via the $X(3872)$ to those via the ψ', Belle finds a considerable production rate in B decays, with product branching ratio

$$\frac{\mathcal{B}(B^+\to K^+ X(3872)) \times \mathcal{B}(X(3872)\to\pi^+\pi^- J/\psi)}{\mathcal{B}(B^+\to K^+\psi') \times \mathcal{B}(\psi'\to\pi^+\pi^- J/\psi)} = 0.063 \pm 0.012\,(\mathrm{stat}) \pm 0.007\,(\mathrm{syst}). \quad (3.47)$$

The observation has been confirmed in inclusive $p\overline{p}$ collisions by CDF [463] and D0 [464], as shown in Fig. 3.31, and in exclusive B meson decays by BaBar [465], shown in Fig. 3.32. The observed masses

[40] Author: B. Yabsley

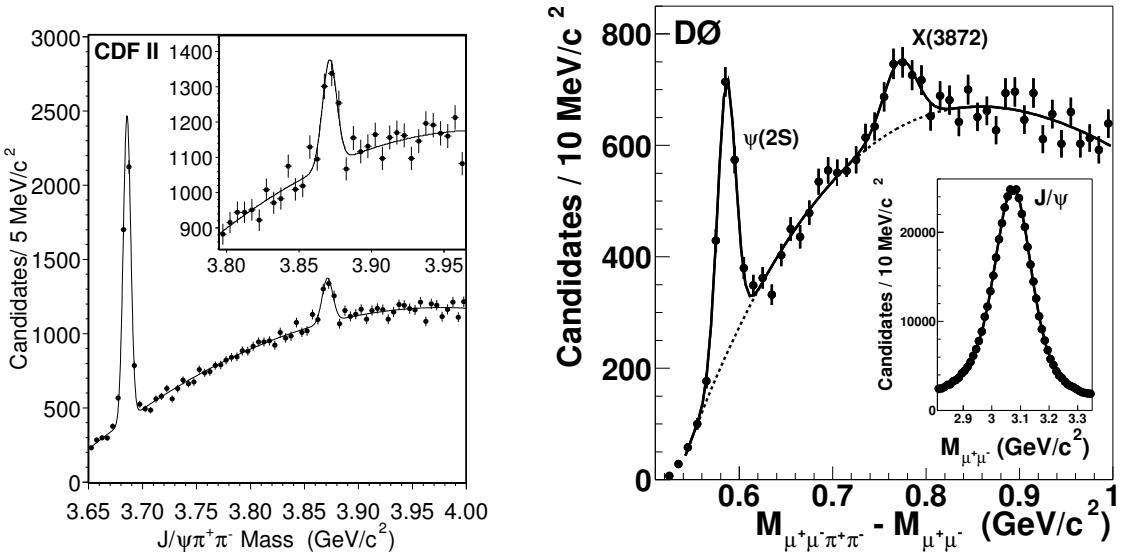

Fig. 3.31: Confirmation of the $X(3872)$ in inclusive $p\overline{p}$ collisions by CDF [463] (left) and D0 [464] (right). In each case peaks due to ψ' and $X(3872)\to\pi^+\pi^- J/\psi$ can be clearly seen; the insets show (left) an enlargement of the $X(3872)$ region and (right) the mass distribution for the $J/\psi\to\mu^+\mu^-$ candidates used in the analysis.

are consistent, with a weighted average value

$$M_X = (3871.9 \pm 0.5)\,\mathrm{MeV} \tag{3.48}$$

across the four experiments [211,463–465]. Each of CDF, D0, and BaBar likewise find a width consistent with the detector resolution; the only limit is that inferred by Belle [211],

$$\Gamma_X < 2.3\,\mathrm{MeV}\ (90\%\ \mathrm{CL}). \tag{3.49}$$

Belle finds a $M(\pi^+\pi^-)$ distribution concentrated at the kinematic boundary [211], coinciding with the ρ mass (Fig. 3.33). This is confirmed by CDF [463], who find little signal with $M(\pi^+\pi^-) < 500\,\mathrm{MeV}$; BaBar report that their statistics are too small to allow a clear conclusion, but do not exclude a concentration at the boundary [465].

8.2.2 Decay modes and interpretation of the $X(3872)$

The Belle collaboration has performed searches for various decay modes [211, 466] and an angular distribution study [466], to compare $X(3872)$ properties with those of predicted, but so far unseen, charmonium states. They restrict their attention to states with

1. expected masses [401] within 200 MeV of $M_X \simeq 3872\,\mathrm{MeV}$;
2. unnatural quantum numbers $J^P = 0^-,\ 1^+,\ 2^-,\ \ldots$ since decays to $D\overline{D}$ are not seen; and
3. spin angular momentum $J < 3$, since the state is seen in exclusive $B\to K X(3872)$ production with a significant rate, making high J unlikely (*cf.* $B^+\to K^+\chi_{c2}$, still not observed, and $B^+\to K^+\chi_{c0}$ and $K^+\chi_{c1}$ with branching fractions $(6 \sim 7)\times 10^{-4}$).

The 1^3D_3 state, ψ_3, is also studied following suggestions [187,188] that the rate for $\psi_3\to D\overline{D}$, suppressed by an $L = 3$ angular momentum barrier, may be low.

The search therefore includes the $C = -1$ states ψ_2, h_c', and ψ_3, and the $C = +1$ states η_{c2}, χ_{c1}', and η_c''. The observation of decays to $\pi^+\pi^- J/\psi$ favors $C = -1$, for which this mode is isospin-conserving; this would imply $\Gamma(X\to\pi^0\pi^0 J/\psi) \simeq \frac{1}{2}\Gamma(X\to\pi^+\pi^- J/\psi)$. On the other hand, the observed

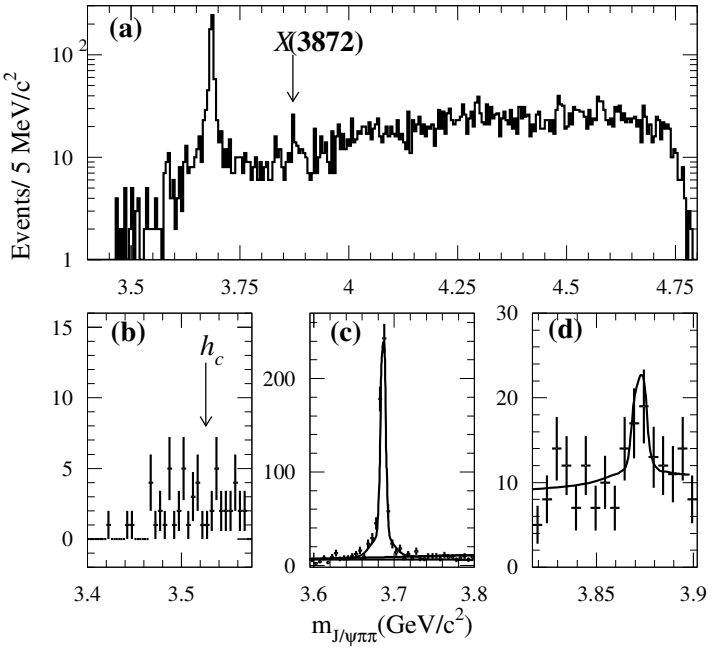

Fig. 3.32: Confirmation of the $X(3872)$ in $B^{\pm}\to K^{\pm}\pi^+\pi^- J/\psi$ decay from BaBar [465]. Distributions of the $\pi^+\pi^- J/\psi$ invariant mass are shown for B candidates in (a) the B-signal region, together with expanded views of the (b) h_c, (c) $\psi(2S)$, and (d) $X(3872)$ mass regions. In (c) and (d), the results of an unbinned maximum likelihood fit to the data are superimposed as a solid curve.

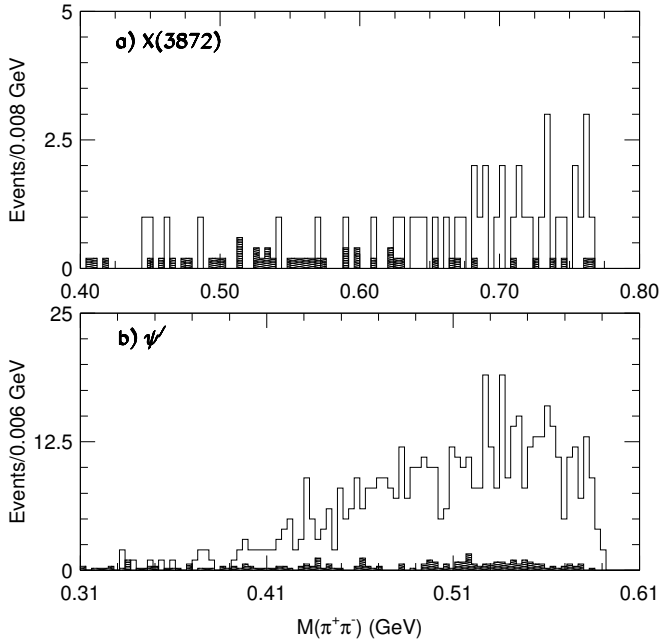

Fig. 3.33: From [211]: $M(\pi^+\pi^-)$ distribution for events in the (a) $M(\pi^+\pi^- J/\psi) = 3872\,\mathrm{MeV}$ signal region and (b) the ψ' region in Belle data. The shaded histograms are sideband data normalized to the signal-box area. Note the different horizontal scales.

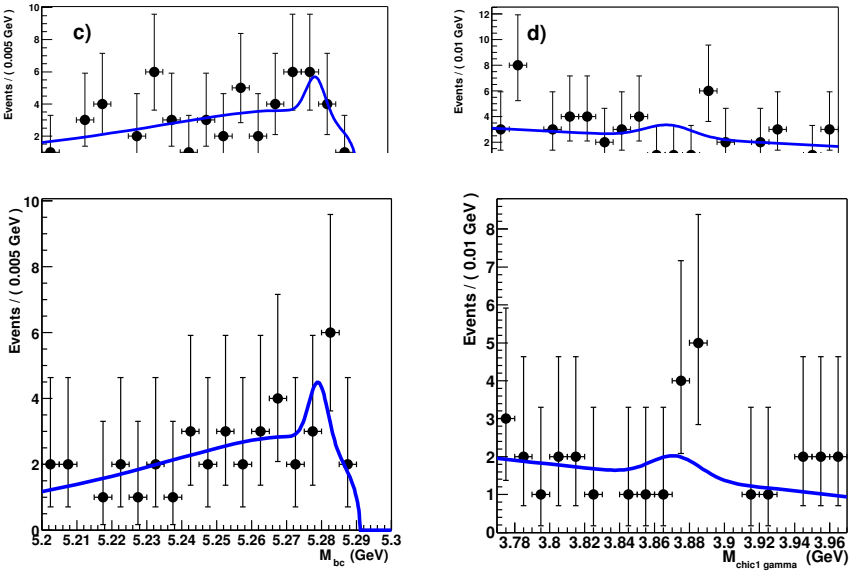

Fig. 3.34: (Upper plots) Signal band projections for the beam-constrained (B-candidate) mass M_{bc}, and charmonium candidate mass $M_{\gamma\chi_{c1}}$, in the Belle search for decays $B^+\to K^+X(3872)$, $X\to\gamma\chi_{c1}$ [211]; the results of an unbinned maximum likelihood fit are superimposed. The signal yield, $3.7 \pm 3.7 \pm 2.2$, is consistent with zero. (Lower plots) Similar distributions in the search for decays to $\gamma\chi_{c2}$ [466]; the fitted yield is $2.9 \pm 3.0 \pm 1.5$ events.

concentration of events at $M(\pi^+\pi^-) \approx m_\rho$ suggests that the decay may proceed via $X(3872)\to\rho J/\psi$, an isospin-violating process; this requires $C = +1$ and forbids the decay to $\pi^0\pi^0 J/\psi$. A study of the $\pi^0\pi^0 J/\psi$ final state is therefore important.

8.2.3 Searches for radiative decays

If the $X(3872)$ is identified with the 1^3D_2 (ψ_2) state, the decay to $\gamma\chi_{c1}$ is an allowed E1 transition with a large partial width, calculated to be $\Gamma(X\to\gamma\chi_{c1}) \simeq 210\,\text{keV}$ in potential models, taking coupled channel effects into account [187,188]. Similarly, the partial width for 1^3D_3 (ψ_3)$\to\gamma\chi_{c2}$ is calculated to be $\sim 300\,\text{keV}$. This is to be compared to the partial width for $\psi_{2,3}\to\pi^+\pi^- J/\psi$, expected to be equal to the $\psi(3770)$ partial width for both states. Ref. [466] conservatively assumes $\Gamma(\psi(3770)\to\pi^+\pi^- J/\psi) < 130\,\text{keV}$, leading to predictions $\Gamma(X\to\gamma\chi_{cJ})/\Gamma(X\to\pi^+\pi^- J/\psi) > 1.6$ for $\psi_2\to\gamma\chi_{c1}$ and > 2.3 for $\psi_3\to\gamma\chi_{c2}$ respectively. Belle has performed searches for $X(3872)$ decays to these final states (see Fig. 3.34), setting upper limits on the branching ratios (at 90% CL) of 0.89 for $\gamma\chi_{c1}$ [211], and 1.1 for $\gamma\chi_{c2}$ [466], below these expectations. Other considerations disfavor these states. If the X is the ψ_2, its separation from the $\psi(3770)$, $\Delta M = 102\,\text{MeV}$, is larger than present theory can accomodate [188]. The ψ_3 mass is expected to be similar. Production $B^+\to K^+\psi_3$ is also expected to be suppressed relative to other $K^+(c\bar{c})$ decays, due to the high spin $J = 3$, whereas the data implies a comparable rate if $X(3872) = \psi_3$ [466].

Another radiative decay search, for $X(3872)\to\gamma J/\psi$, tests the $X(3872) = 2^3P_1$ (χ'_{c1}) assignment [466]. The partial width $\Gamma(\chi'_{c1}\to\gamma J/\psi)$, for $M_{\chi'_{c1}} = 3872\,\text{MeV}$, is expected to be 11 KeV in the potential model [187], possibly reduced by coupled channel effects [188]. To estimate the partial width for the isospin-violating process $\chi'_{c1}\to\pi^+\pi^- J/\psi$, we take the isospin-violating hadronic charmonium transition $\psi'\to\pi^0 J/\psi$, with $\Gamma \simeq 0.3\,\text{keV}$: the ratio $\Gamma(X\to\gamma J/\psi)/\Gamma(X\to\pi^+\pi^- J/\psi)$ should then be $\mathcal{O}(10)$. The Belle search places an upper limit of 0.40 (90% CL) on this ratio, inconsistent with the expected value. The χ'_{c1} mass is predicted [187, 188] to be $3930 \sim 3990\,\text{MeV}$ or greater, likewise inconsistent with the $X(3872)$.

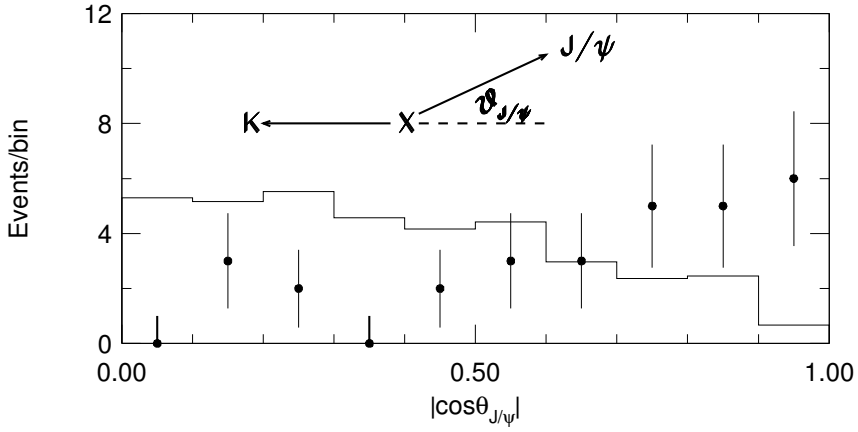

Fig. 3.35: From [466]: $|\cos^2\theta_{J/\psi}|$ distribution for $X(3872)\to\pi^+\pi^- J/\psi$ events in the data (points with error bars), and assuming $J^{PC} = 1^{+-}$ in the Monte Carlo (histogram); background events, determined using sidebands, are included in the Monte Carlo.

8.2.4 Studies of angular distributions

The $X(3872)$ will be produced polarized in the reaction $B^{\pm}\to K^{\pm}X(3872)$ for any spin $J_X > 0$, as both the initial state B and the accompanying K mesons are spin zero. Angular distributions of the final state particles can therefore distinguish between different quantum number assignments J^{PC} for the $X(3872)$. If the X is the h_c', with $J^{PC} = 1^{+-}$, decays should be distributed as $(1-\cos^2\theta_{J/\psi})\mathrm{d}\cos\theta_{J/\psi}$ [467], where $\theta_{J/\psi}$ is the angle between the J/ψ and the negative of the K momentum vectors in the $X(3872)$ rest frame. In the Belle study [466], the data tend to peak near $\cos\theta_{J/\psi} = 1$, where the 1^{+-} expectation is zero; both the data and expectation are shown in Fig. 3.35. The poor fit to the data ($\chi^2/dof = 75/9$) rules out any 1^{+-} assignment for the $X(3872)$, including the h_c'; this state in any case has an expected mass well above 3872 MeV. Further angular studies of other modes are foreseen.

8.2.5 Other searches

If $X(3872) = 1^1D_2$ (η_{c2}), the isospin conserving transition $\eta_{c2}\to\pi^+\pi^-\eta_c$ should be much more common than $\eta_{c2}\to\pi^+\pi^- J/\psi$, which is isospin violating; the branching fraction $\mathcal{B}(X\to\pi^+\pi^- J/\psi)$ would be $\mathcal{O}(1\%)$ or less, implying a large $B\to KX(3872)$ rate. This seems unlikely but can be tested by searching for the $X(3872)\to\pi^+\pi^-\eta_c$ decay.

Similar considerations apply if $X(3872) = \eta_c''$: the branching fraction to $\pi^+\pi^- J/\psi$ should be small, although in this case (with the η_c'' below open charm threshold) the dominant decay would be into two gluons, less convenient for a search. Assuming that such a state would have a similar width to the η_c (17 ± 3 MeV) [245], which also predominantly decay via two gluons, it is already disfavored by the 2.3 MeV upper limit on the $X(3872)$ width. Given $M_{\psi(3S)} = (4040 \pm 10)$ MeV, $M_{\eta_c''} = 3872$ MeV also implies a large $\psi(3S) - \eta_c''$ mass splitting, ~ 168 MeV, contrary to the expectation that the splitting will decrease with increasing radial quantum number (*cf.* $M_{\psi'} - M_{\eta_c'} = 48$ MeV [391] and $M_{\psi} - M_{\eta_c} = 117$ MeV) [245].

8.2.6 Summary

The status of the six candidates considered by Belle [466] is summarized in Table 3.24: some are already excluded by the data, and none is a natural candidate. Significant further information is expected once searches for other decays become available; the search for $X(3872)\to\pi^0\pi^0 J/\psi$ is particularly important. Already however the lack of a natural charmonium candidate that fits the data suggests two possibilities: (1) that the theory used to predict charmonium properties is flawed, or (2) that the $X(3872)$ is not a

Table 3.24: From [466]: Some properties of candidate charmonium states for the $X(3872)$, and a summary of the comparison with data. Mass predictions are taken from [401], and width predictions computed from [187], using a 3872 MeV mass value; the predicted width for the η_c'' is taken to be the same as the η_c width. Masses and widths are shown in MeV.

state	alias	J^{PC}	$M_{\rm pred}$	$\Gamma_{\rm pred}$	comment
1^3D_2	ψ_2	2^{--}	3838	0.7	Mass wrong; $\Gamma_{\gamma\chi_{c1}}$ too small
2^1P_1	h_c'	1^{+-}	3953	1.6	Ruled out by $\lvert\cos\theta_{J/\psi}\rvert$ distribution
1^3D_3	ψ_3	3^{--}	3849	4.8	M, Γ wrong; $\Gamma_{\gamma\chi_{c2}}$ too small; J too high
1^1D_2	η_{c2}	2^{-+}	3837	0.9	$\mathcal{B}(\pi^+\pi^- J/\psi)$ expected to be very small
2^3P_1	χ_{c1}'	1^{++}	3956	1.7	$\Gamma_{\gamma J/\psi}$ too small
3^1S_0	η_c''	0^{-+}	4060	~ 20	Mass and width are wrong

conventional $(c\bar{c})$ state. As the $X(3872)$ mass is very close to the $M_{D^0}+M_{D^{*0}}$ threshold, a $D\overline{D}^*$ bound state is a natural candidate [212, 467–472].

9 THE OBSERVATION OF THE B_c MESON AT CDF AND D0[41]

The CDF Collaboration has observed the ground state of the bottom-charm meson $B_c^\pm$ via the decay mode $B_c^\pm \to J/\psi l^\pm \nu$ and measured its mass, lifetime and production cross-section [39, 473]. The measurement was done at the Tevatron, in Run I, at $\sqrt(s) = 1.8$ TeV. Figure 3.36a shows the mass spectra for the combined $J/\psi e$ and $J/\psi\mu$ candidate samples, the combined backgrounds, and the fitted contribution from the $B_c^\pm \to J/\psi l^\pm \nu$ decay. The fitted number of B_c events is $20.4^{+6.2}_{-5.5}$, out of which $12.0^{+3.8}_{-3.2}$ come for the electron sample and $8.4^{+2.7}_{-2.4}$ from the muon sample.A fit to the same distribution with background alone was rejected at the level of 4.8 standard deviations. The $B_c^\pm$ mass was measured to be equal to 6.40±0.39(stat.)±0.13(syst.) GeV/c^2.

A measure of the time between production and decay of a $B_c^\pm$ meson is

$$ct^* \equiv \frac{M(J/\psi l)\cdot L_{xy}(J/\psi l)}{|p_T(J/\psi l)|} \tag{3.50}$$

where L_{xy} is the distance between the beam centroid and the decay point of the $B_c^\pm$ candidate in the transverse plane and projected along the $J/\psi l$ direction, and $p_T(J/\psi l)$ is the tri-lepton transverse momentum. Figure 3.36b shows the ct^* distribution for the data, the signal and the background distributions. The mean proper decay length $c\tau$ and hence the lifetime τ of the $B_c^\pm$ meson was obtained from the above distribution. It was determined that $c\tau = 137^{+53}_{-49}(\text{stat.})\pm 9(\text{syst.})$ μm or $\tau = 0.46^{+0.18}_{-0.16}(\text{stat.})\pm 0.03(\text{syst.})$ ps.

Recently [474] the D0 collaboration has reported the observation of a B_c signal in the decay mode $B_c^\pm \to J/\psi\mu^\pm\nu$, from a sample of 210 pb^{-1} of data taken during Run II, at $\sqrt{s} = 1.96$ TeV. The dimuon coming from J/ψ was required to be within 0.25 from the J/ψ mass, and a third muon track was required to come from the same vertex. The analysis yielded 95±12±11 events, at a mass $M(B_c^\pm) = 5.95^{+0.14}_{-0.13}(\text{stat.})\pm 0.34(\text{syst.})$ GeV/c^2. The lifetime was calculated to be $\tau(B_c^\pm) = 0.448^{+0.123}_{-0.096}$ (stat.) ± 0.121(syst.) ps. Fitted mass and lifetime are found to be uncorrelated. Figure 3.37(left) shows the invariant mass and pseudo-proper time distributions of the events. The analysis accounts for the possible contribution from $B_c \to \psi(2S)\mu^\pm\nu$ on the inclusive sample. As shown in Fig. 3.37(right), it is estimated that about 15 events are due to this component, and the systematic errors are obtained by

[41] Author: V. Papadimitriou

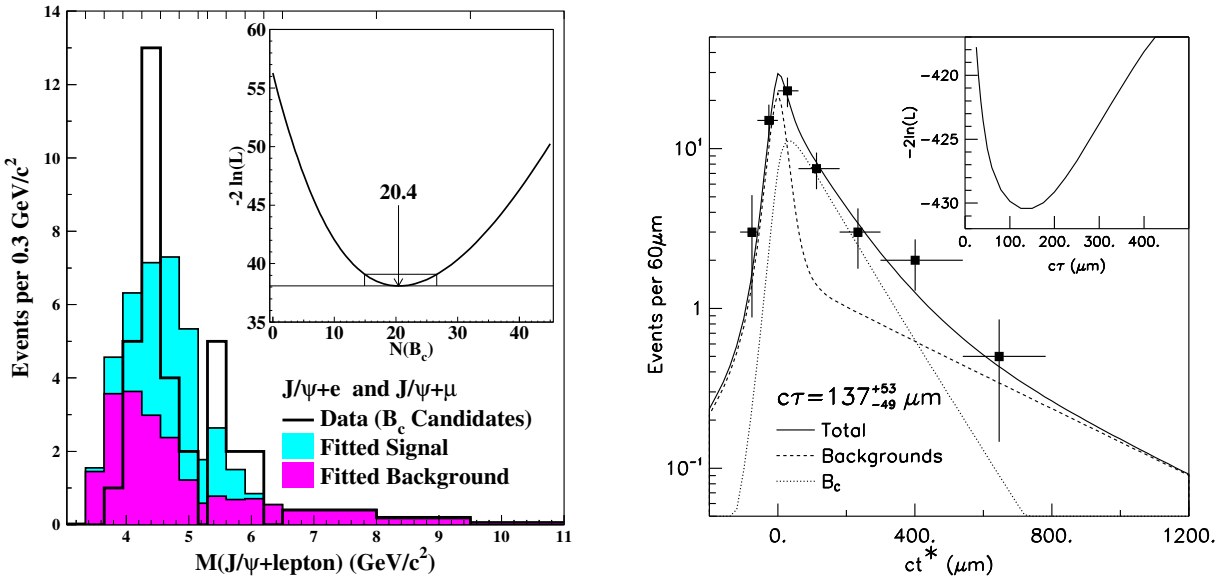

Fig. 3.36: On the left, (a) the histogram of the $J/\psi l$ mass that compares the signal and background contributions determined in the likelihood fit to the combined data for $J/\psi e$ and $J/\psi\mu$. The mass bins, indicated by tick marks at the top, vary in width. The total $B_c^{\pm}$ contribution is $20.4^{+6.2}_{-5.5}$ events. The inset shows the behavior of the log-likelihood function -2Ln(L) vs the number of B_c mesons. On the right, (b) the distribution in ct^* for the combined $J/\psi e$ and $J/\psi\mu$ data along with the fitted curve and contributions to it from signal and background. The inset shows the log-likelihood function vs $c\tau$ for the B_c meson.

varying this contribution from 0 to 30 events. In the near future, the mass uncertainty can be improved to better than 5(50) MeV/c^2 by CDF(D0) by using hadronic exclusive decay channels.

10 Evidence for doubly charmed baryons at SELEX[42]

The addition of the charmed quark to the (uds) triplet extends the flavour symmetry of the baryon octet and decuplet from SU(3) to SU(4). There is strong experimental evidence for all the predicted baryon states which contain zero or one valence charmed quark [245]. We review here the first experimental evidence for one of the six predicted baryon states which contain two valence charmed quarks, the doubly charmed baryons. There have been many predictions of the masses and other properties of these states [475–478]. The properties of doubly charmed baryons provide a new window into the structure of baryonic matter.

10.1 The SELEX experiment

The SELEX experiment uses the Fermilab 600 GeV/c charged hyperon beam to produce charm particles in a set of thin foil targets of Cu or diamond. The three-stage magnetic spectrometer is shown elsewhere [479, 481]. The most important features are: (a) the high-precision, highly redundant, silicon vertex detector that provides an average proper time resolution of 20 *fs* for single-charm particle decays, (b) a 10 m long Ring-Imaging Cherenkov (RICH) detector that separates π from K up to 165 GeV/c [480], and (c) a high-resolution tracking system that has momentum resolution of $\sigma_P/P < 1\%$ for a 200 GeV/c reconstructed Λ_c^+.

The experiment selected charm candidate events using an online secondary vertex algorithm which required full track reconstruction for measured fast tracks. An event was written to tape if all the fast

[42] Author:P. Cooper

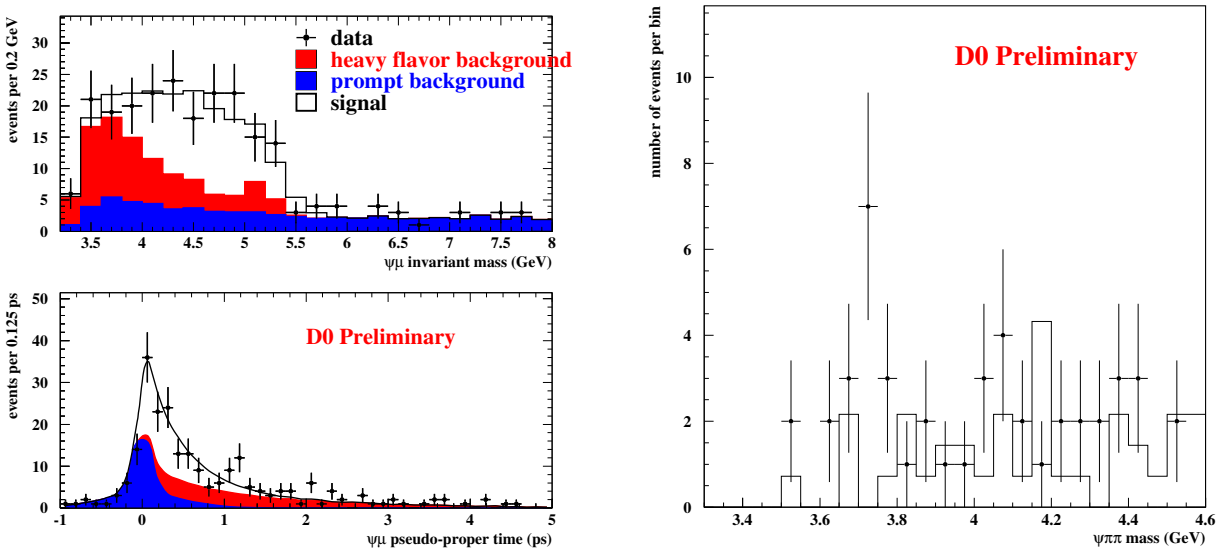

Fig. 3.37: The $J/\psi\mu$ invariant mass (top left) and pseudo-proper time distributions (bottom left) of the $B_c \to J/\psi\mu X$ candidates (points with error bars) from D0. The signal MonteCarlo events, generated with a mass of 5.95 GeV$/c^2$, as well as the most likely background sources are shown as solid histograms. The right plot shows the $J/\psi\pi^+\pi^-$ invariant mass of $J/\psi\pi^+\pi^-\mu X$ events that have M($J/\psi\pi^+\pi^-\mu$) between 4 and 6 GeV$/c^2$. The background (solid histogram) is estimated from events outside this mass range.

tracks in the event were inconsistent with having come from a single primary vertex. This filter passed 1/8 of all interaction triggers and had about 50% efficiency for otherwise accepted charm decays. The experiment recorded data from 15.2×10^9 inelastic interactions and wrote 1×10^9 events to tape using both positive and negative beams. 67% of events were induced by Σ^-, 13% by π^-, and 18% by protons.

10.2 Search strategy

A Cabibbo-allowed decay of a doubly charmed baryon must have a net positive charge and contain a charmed quark, a strange quark and a baryon. We chose to search for decay modes like $\Xi_{cc}^+ \to \Lambda_c^+ K^-\pi^+$ with an intermediate $K^-\pi^+$secondary vertex between the primary vertex and the Λ_c^+vertex and $\Xi_{cc}^+ \to pD^+K^-$ with an intermediate pK^- secondary vertex between the primary vertex and the D^+ .

Events were analyzed for evidence of a secondary vertex composed of an opposite-signed pair between the primary and the single charm decay point. We used all tracks not assigned to the single charm candidate in the search. The new secondary vertex had to have an acceptable fit χ^2 and a separation of at least 1σ from the new primary. These cuts were developed and fixed in previous searches for short-lived single-charm baryon states. We have applied them here without change. As a background check we also kept wrong-sign combinations in which the mass assignments are reversed.

10.3 $\Xi_{cc}^+ \to \Lambda_c^+ K^-\pi^+$ Search results and significance

The signal and wrong-sign backgrounds are shown in Fig. 3.38. There is a obvious peak at a mass of 3519 ± 2MeV$/c^2$. The number of events in the signal region shown is 22 events. We estimate the number of expected background events in the signal region from the sidebands as 6.1 ± 0.5 events. This determination has a (Gaussian) statistical uncertainty, solely from counting statistics. The single-bin significance of this signal is the excess in the signal region divided by the total uncertainty in the background estimate: $15.9/\sqrt{6.1 + 0.5^2} = 6.3\sigma$. The Poisson probability of observing at least this excess, including the Gaussian uncertainty in the background, is 1.0×10^{-6}. The overall probability of

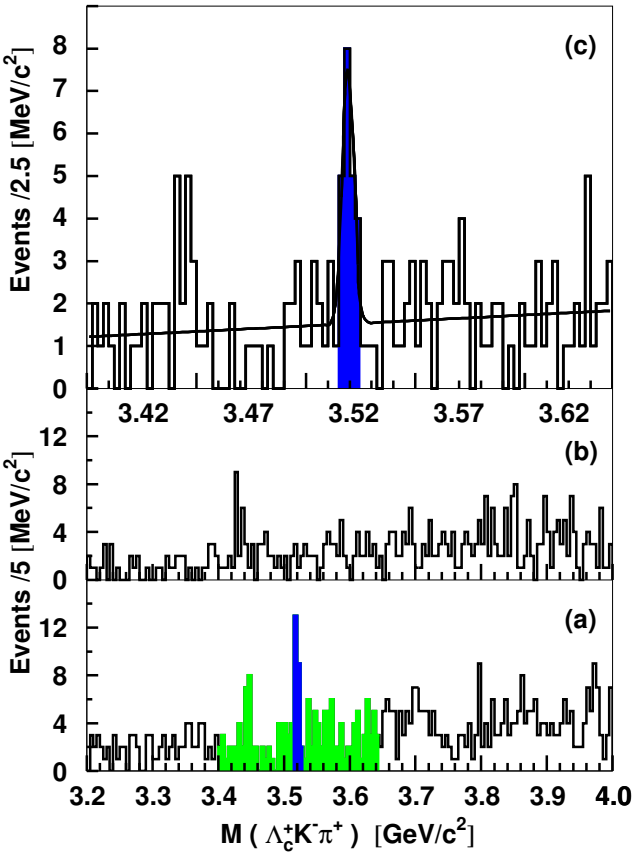

Fig. 3.38: (a) The $\Lambda_c^+ K^- \pi^+$ mass distribution in 5 MeV$/c^2$ bins. The shaded region 3.400–3.640 GeV$/c^2$ contains the signal peak and is shown in more detail in (c). (b) The wrong-sign combination $\Lambda_c^+ K^+ \pi^-$ mass distribution in 5 MeV$/c^2$ bins. (c) The signal (shaded) region (22 events) and sideband mass regions with 162 total events in 2.5 MeV$/c^2$ bins. The fit is a Gaussian plus linear background.

observing an excess at least as large as the one we see anywhere in the search interval is 1.1×10^{-4}. This result is published in reference [481].

10.4 $\Xi_{cc}^+ \to pD^+K^-$ search

After the discovery and publication of the $\Xi_{cc}^+ \to \Lambda_c^+ K^- \pi^+$ signal we sought to confirm the discovery in another decay mode which was likely to have a significant branching ratio. Obvious choices were $\Xi_c^+ \pi^+ \pi^-$ and $\Xi_{cc}^+ \to pD^+K^-$. Since the SELEX D^+ signal is large and well studied we began with it.

A similar analysis technique [482] resulted in the signal and wrong-sign background shown in Fig. 3.39. In this new decay mode we observe an excess of 5.4 events over an expected background of 1.6 ± 0.35 events. The Poisson probability that a background fluctuation can produce the apparent signal is less than 1.5×10^{-5}. The observed mass of this state is 3518 ± 3 MeV$/c^2$, consistent with the published result. Averaging the two results gives a mass of 3518.7 ± 1.7 MeV$/c^2$. The observation of this new weak decay mode confirms the previous suggestion that this state is a double charm baryon. The relative branching ratio $\Gamma(\Xi_{cc}^+ \to pD^+K^-)/\Gamma(\Xi_{cc}^+ \to \Lambda_c^+ K^- \pi^+) = 0.078 \pm 0.045$.

The lifetime of this state in both decay modes is very short; less than 33 *fs* at 90% confidence. The properties of these two signals are consistent with each other. SELEX reports an independent confirmation of the double charm baryon Ξ_{cc}^+, previously seen in the $\Xi_{cc}^+ \to \Lambda_c^+ K^- \pi^+$ decay mode, via the observation of its decay $\Xi_{cc}^+ \to pD^+K^-$.

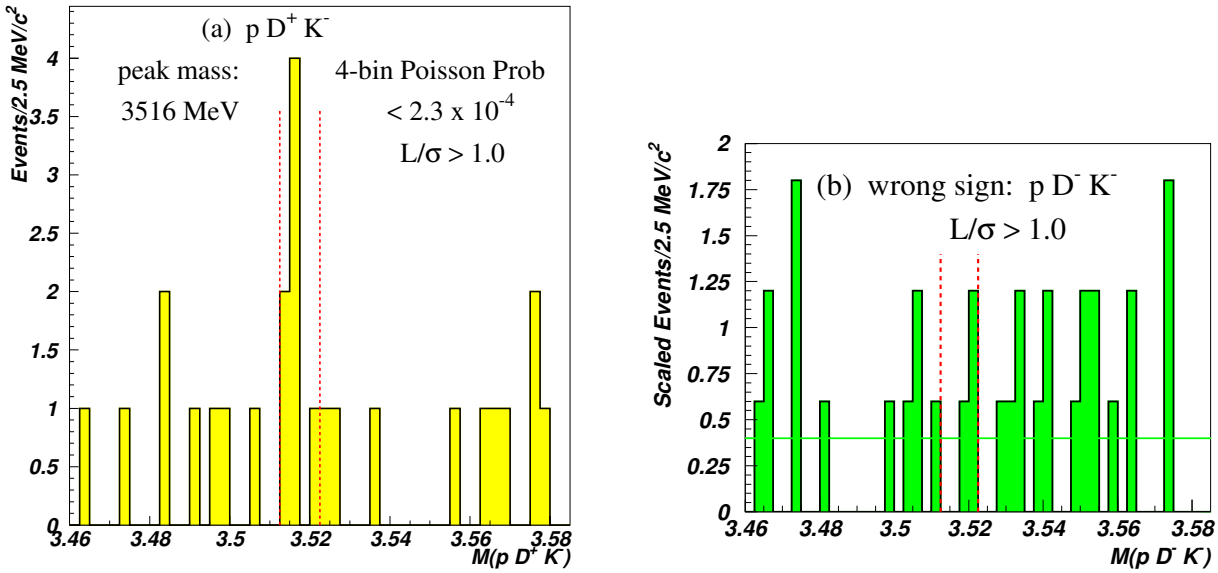

Fig. 3.39: (a) $\Xi_{cc}^{+} \to pD^{+}K^{-}$ mass distribution for right-sign mass combinations. (b) Wrong-sign events with a $D^{-}K^{+}$, scaled by 0.6. The line shows a maximum likelihood fit to occupancy.

10.5 Conclusions

The $\Xi_{cc}^{+}(ccd)$ doubly charmed baryon has now been observed by SELEX in two decay modes at a mass of 3518.7 ± 1.7 MeV$/c^2$with a lifetime less than 33 *fs* at 90% confidence. Analysis continues with SELEX data to searchfor additional decays modes for this state and to search for the two other doubly-charmed baryons ground states expected: $\Xi_{cc}^{++}(ccu)$ and $\Omega_{cc}^{+}(ccs)$.

11 SUMMARY AND OUTLOOK[43]

It took few years , after the discovery of the J/ψ, to sketch the spectroscopical pattern of the narrow ortocharmonium and ortobottomonium states: the experimental determination of such energy levels is extremely good, all states are know with precisions better than 1 MeV. On the other side, the experimental history of spin singlet states has started to clear up only in the recent years, but open puzzles remain:

- the total width of the $\eta_c(1S)$ (the ground state of charmonium) is as large as the one of the $\psi(3770)$, which can decay to open charm:
- after 16 years, the real $\eta_c(2S)$ has been observed, disconfirming an evidence by Crystal Ball that misled theory calculations on hyperfine splittings for more than a decade.
- two compatible evidences of the h_c state have been found in the last year, and may bring to an end the saga of the spin singlet P state; a concrete strategy to consolidate this observation is now needed.
- none of the 5 spin singlet states in the bottomonium system has been found yet; given the absence of scheduled running time on narrow Υ states in the near future, it is necessary to elaborate smarter search strategies to spot these states at asymmetric B-factories or hadron colliders .

The quest to complete the experimental spectra is now extending to the higher excitations:

- the search for narrow D-states resulted in the discovery of the $\Upsilon(1D)$ states in CLEO III, and to the observation of the intriguing X(3872) meson by Belle; while the bottomonium state falls well in the expected pattern, there is a wide variety of speculations on the nature of the X(3872).

[43] Authors: G. Bali, N. Brambilla, R. Mussa, J. Soto

– the need to achieve a deeper understanding of the region just above open charm threshold, together with the improvement of the experimental tools, will allow to disentangle each single contribution to the R ratio, hopefully clarifying the puzzles opened by the pioneering studies of Mark II.

As we have seen in this chapter the application of EFTs of QCD to heavy quarkonium has considerably increased our understanding of these systems from a fundamental point of view. NRQCD has allowed, on the one hand, for efficient lattice calculations of the masses of the bottomonium and charmonium states below open heavy flavour threshold. On the other hand, it has paved the way to pNRQCD, which provides, in the strong coupling regime, a rigorous link from QCD to potential models for states below open heavy flavour threshold. In the weak coupling regime, pNRQCD has allowed to carry out higher-order calculations and to implement renormalization group resummations and renormalon subtractions in a systematic way. This regime appears to be applicable at least for the $\Upsilon(1S)$ and $\eta_b(1S)$. Interestingly, as discussed in Section 2.3.1 (Tables 3.2 and 3.3) even some excited states can be reproduced in perturbation theory (inside the errors of the perturbative series).

The most challenging theoretical problem at present is the description of states above open heavy flavour threshold. The recent discovery of $X(3872)$ has made clear that potential models suffer from large systematic uncertainties in this region and that the inclusion of, at least, heavy-light meson degrees of freedom is necessary. Although NRQCD holds in this region, extracting information from it on the lattice is not simple, since besides heavy quarkonium, heavy-light meson pairs and hybrid states populate it. It would be important to develop theoretical tools in order to bring current phenomenological approaches into QCD based ones.

In order to stimulate progress in heavy quarkonium spectroscopy, we shall try to pose a number of questions, and try to provide what we believe to be reasonable answers to them, from the theory and experimental point of view.

• **Q.** What does theory need from experiment?

A1(*TH:)* Discovery and good mass measurements of the missing states below open heavy flavour threshold.

A1(*EXP:)* Concerning triplet S and P states of neutral heavy quarkonia, experimental measurements are mature and ahead of theory. Concerning the singlet S and P states, charmonia are under very active investigation at present, and probably will be nailed down to less than .5 MeV/c^2 in the near future, with an active cooperation amid experimental groups. In bottomonium, the situation looks less promising: only Tevatron experiments have currently some chance to detect the missing (narrow?) states, while CLEO III searches turned out no plausible candidates, and showed that more luminosity is needed at $\Upsilon(1,2,3S)$, but none of the active B-factories is planning to shift out of $\Upsilon(4S)$.

The experimental study of the spectrum of the charged heavy quarkonium, the B_c, has not started yet. The ground state has been seen by CDF and confirmed by D0, but via its semileptonic decay, which yield still very wide uncertainties on the mass (0.4 GeV/c^2). The experimental search for an exclusive, non leptonic mode is under way and will allow to know this state with accuracies better than 5 MeV/c^2 in the near future. Beyond this, most experimental efforts will be focused on finding the dominant decay modes of the ground state. The search for the B_c^*, which decays dominantly to B_c via M1 radiation of a soft photon , will be extremely challenging for current Tevatron experiments, due to the high combinatorial background and to the low efficiency on low energy photons. Same can be said for the P states , which are expected to decay to $B_c^{(*)}$ via dipion emission. It is hard to predict whether the hadronic B-factories, BTEV and LHCB, will be able to contribute to these spectroscopical studies. The issue should be discussed in Chapter 9.

A2(*TH:)* Thorough analysis of the region above open heavy flavour threshold in search for quarkonium states, hybrid states, molecules and other exotica.

A2(*EXP:)* The BES II R scan and the surprises from the asymmetric B-factories (X(3872) and double $c\bar{c}$ production) have ignited new experimental and theoretical interest in this physics region. The CLEO-c running at $\psi(3770)$ and above $D_s\bar{D}_s$ threshold has a very large physics potential for heavy quarkonium studies. At the same time, B factories can benefit from a large variety of techniques to identify new charmonium states: (a) inclusive ones , such as J/ψ and $\psi\,'$ recoil in double $c\bar{c}$, or K recoil in tagged B decays; (b) exclusive ones , such as $B\to(\psi,\eta_c)XK^{(*)}$ (for narrower states), $B\to D^{(*)}\bar{D^{(*)}}K^{(*)}$ (for wider states).

Some discovery potential is to be expected also from hadron colliders, where the large, very clean samples of D mesons can be used as starting point to search for peaks in $D\bar{D}$ invariant mass combinations.

• **Q.** What does experiments need from theory?

A1(*EXP:)* In spectroscopy, two are the crucial issues in the search of missing states: (a) a good understanding of the production/formation mechanisms; (b) a comprehensive set of decay channels, with solid predictions on the partial widths. The two issues are related between each other, and to the hot topics of the next chapter.

There is NOT an infinite number of ways to produce charmonium, less for bottomonium, much less for B_c: these couplings deserve a higher level of understanding, both theoretically and experimentally. This is much more important, when we do want to understand whether we can get some deeper insight from the non observation of a missing state. It must be noticed that most production mechanisms are not fully understood, and/or lead to wrong predictions.

A limited set of processes, then, deserve deeper theoretical understanding:

- M1 hindered radiative transitions: relativistic corrections are dominant in these processes that are the main gateways to η_b's.
- isospin violating hadronic transitions: it is now very important to establish a physical relation between $\psi(2S)\to h_c\pi^0$ and $h_c\to J/\psi\pi^0$. This can help clarifying the consistency between the two (still weak) evidences.
- factorization in B decays: exclusive B decays to K+$c\bar{c}$ were expected to yield $0^{-+},1^{--},1^{++}$ charmonia, and, in smaller quantities, $0^{++},2^{++}$. The prediction holds for the second, but χ_{c0}'s are produced as copiously as χ_{c1}'s . The understanding of the effective selection rules can help to set limits on the h_c production, and to find the possible quantum numbers of the X(3872) meson.
- coupling to exclusive $p\bar{p}$: helicity selection rule in perturbative QCD forbids the formation of η_c, χ_{c0}, h_c from $p\bar{p}$ annihilations; no suppression is observed in the first two cases, and the third is under active investigation. It is auspicable that recent developments in NRQCD can help to explain the $p\bar{p}$ coupling and make testable predictions on the coupling to $\eta_c(2S)$ and X(3872).
- the double $c\bar{c}$ selection rules are not yet clear: so far only scalars and pseudoscalars were observed recoiling against the J/ψ . This process has already allowed an indipendent confirmation of the $\eta_c(2S)$ observation. By understanding the dynamics, one can converge more rapidly on the determination of the quantum numbers of any bump that shows up in the J/ψ recoil spectrum.

Within theory one may ask the following questions:

• **Q.** What does the phenomenological approach need from the theoretical one?

A $*$ That the theory clearly points out the most relevant feautures that should be implemented in phenomenological models.

• **Q.** What does the theoretical approach need from the phenomenological one?

A $*$ To point out shortcomings in models which are relevant to experimental observations.

Within the theoretical approach:

• **Q.** What does EFTs need from lattice?

∗ Calculation of the correlators which parameterize nonperturbative effects in the weak coupling regime of pNRQCD.

∗ Calculation of the various potentials which enter pNRQCD in the strong coupling regime.

• **Q.** What does lattice need from EFT?

∗ Calculation of the NRQCD matching coefficients in lattice regularizations.

∗ Chiral extrapolations.

Let us next describe the future development which are desirable within each particular approach.

From the side of the EFT the priority "to-do" list is:

- Develop a suitable EFT for the region above open heavy flavour threshold.
- Include the effects of virtual pions. Pions should be included in the strong coupling regime of pNRQCD as ultrasoft degrees of freedom and their effect on the spectrum should be investigated.
- A systematic investigation of the structure of the renormalon subtractions in NRQCD matching coefficients and in the perturbative potentials.

For what concerns lattice calculations the priority practical lattice "to-do list" is:

- Further investigations of sea quark effects, in particular on charmonia and also in bottomonia, including charm mass effects.
- Calculation of threshold effects in charmonia and bottomonia, first using lattice potentials, then a multichannel analysis in lattice NRQCD/QCD.
- Further investigations of OZI suppressed contributions, in particular in the PS charm-sector.
- Mixing of charmonia and would-be glueballs.
- Doubly charmed baryons.
- QQq potentials.

From the side of phenomenological models the wish list includes:

- The major deficiency of these models is that they only include the $q\bar{q}$ components of the Fock space expansion and totally neglect higher Fock space components which can be included as coupled channel effects. These are expected to be most prominent for states close to threshold.

From the side of experiments we need:

- to clarify the nature of the X(3872) state, fully exploiting the four running experiments that see this state.
- to strengthen the h_c evidence , by asking for an active collaboration between experiments , in order to intensify the checks which certify the compatibility between the two recent evidences.
- to support further cross checks on the systematic errors on the masses of pseudoscalar charmonia: both BaBar and Belle should already have a large sample of $\gamma\gamma \to \eta_c(1, 2S)$, to measure with high precision both states.
- to search for doubly charmed baryons in asymmetric B-factories, as well as at the Tevatron.
- to measure, at CLEO-c, the coupling of the $\psi(3770)$ and the $\Upsilon(1, 2, 3S)$ states to $p\bar{p}$, to quantify the perspectives to study charmonium at open charm threshold and bottomonium with antiproton beams.
- to support further η_b searches at the Tevatron, and to strengthen the physics case for further running at narrow bottomonium energies.

REFERENCES

[1] W. E. Caswell and G. P. Lepage, Phys. Lett. B **167**, 437 (1986).

[2] B. A. Thacker and G. P. Lepage, Phys. Rev. D **43**, 196 (1991).

[3] G. T. Bodwin, E. Braaten and G. P. Lepage, Phys. Rev. D **51**, 1125 (1995) [Erratum-ibid. D **55**, 5853 (1997)] [arXiv:hep-ph/9407339].

[4] A. Pineda and J. Soto, Nucl. Phys. Proc. Suppl. **64**, 428 (1998) [arXiv:hep-ph/9707481].

[5] N. Brambilla, A. Pineda, J. Soto and A. Vairo, Nucl. Phys. B **566**, 275 (2000) [arXiv:hep-ph/9907240].

[6] M. E. Luke, A. V. Manohar and I. Z. Rothstein, Phys. Rev. D **61**, 074025 (2000) [arXiv:hep-ph/9910209].

[7] A. X. El-Khadra, A. S. Kronfeld and P. B. Mackenzie, Phys. Rev. D **55**, 3933 (1997) [arXiv:hep-lat/9604004].

[8] X. Liao and T. Manke, Phys. Rev. D **65**, 074508 (2002) [arXiv:hep-lat/0111049].

[9] M. Okamoto *et al.* [CP-PACS Collaboration], Phys. Rev. D **65**, 094508 (2002) [arXiv:hep-lat/0112020].

[10] S. Choe *et al.* [QCD-TARO Collaboration], JHEP **0308**, 022 (2003) [arXiv:hep-lat/0307004].

[11] P. Chen, Phys. Rev. D **64**, 034509 (2001) [arXiv:hep-lat/0006019].

[12] X. Liao and T. Manke, arXiv:hep-lat/0210030.

[13] C. J. Morningstar and M. J. Peardon, Phys. Rev. D **60**, 034509 (1999) [arXiv:hep-lat/9901004].

[14] B. Lucini and M. Teper, JHEP **0106**, 050 (2001) [arXiv:hep-lat/0103027].

[15] G. S. Bali, K. Schilling, A. Hulsebos, A. C. Irving, C. Michael and P. W. Stephenson [UKQCD Collaboration], Phys. Lett. B **309**, 378 (1993) [arXiv:hep-lat/9304012].

[16] R. Sommer, Nucl. Phys. B **411**, 839 (1994) [arXiv:hep-lat/9310022].

[17] G. S. Bali, Eur. Phys. J. A **19**, 1 (2004) [arXiv:hep-lat/0308015].

[18] C. McNeile and C. Michael [UKQCD Collaboration], Phys. Rev. D **70**, 034506 (2004) [arXiv:hep-lat/0402012].

[19] P. de Forcrand *et al.* [QCD-TARO Collaboration], JHEP **0408**, 004 (2004) [arXiv:hep-lat/0404016].

[20] C. McNeile, C. Michael and K. J. Sharkey [UKQCD Collaboration], Phys. Rev. D **65**, 014508 (2002) [arXiv:hep-lat/0107003].

[21] T. Struckmann *et al.* [TχL Collaboration], Phys. Rev. D **63**, 074503 (2001) [arXiv:hep-lat/0010005].

[22] P. Boyle [UKQCD Collaboration], arXiv:hep-lat/9903017; P. Boyle [UKQCD Collaboration], Nucl. Phys. Proc. Suppl. **63**, 314 (1998) [arXiv:hep-lat/9710036].

[23] C. W. Bernard *et al.* [MILC Collaboration], Phys. Rev. D **56**, 7039 (1997) [arXiv:hep-lat/9707008].

[24] M. di Pierro *et al.*, Nucl. Phys. Proc. Suppl. **129**, 340 (2004) [arXiv:hep-lat/0310042]; M. Di Pierro *et al.*, Nucl. Phys. Proc. Suppl. **119**, 586 (2003) [arXiv:hep-lat/0210051]; A. X. El-Khadra, S. Gottlieb, A. S. Kronfeld, P. B. Mackenzie and J. N. Simone, Nucl. Phys. Proc. Suppl. **83**, 283 (2000).

[25] N. Brambilla, arXiv:hep-ph/0012026; A. Pineda, Nucl. Phys. Proc. Suppl. **93**, 188 (2001) [arXiv:hep-ph/0008327]; A. H. Hoang, arXiv:hep-ph/0204299.

[26] B. Grinstein, Int. J. Mod. Phys. A **15**, 461 (2000) [arXiv:hep-ph/9811264]; A. V. Manohar and I. W. Stewart, Nucl. Phys. Proc. Suppl. **94**, 130 (2001) [AIP Conf. Proc. **618**, 381 (2002)] [arXiv:hep-lat/0012002].

[27] N. Brambilla, A. Pineda, J. Soto and A. Vairo, arXiv:hep-ph/0410047.

[28] A. S. Kronfeld, Phys. Rev. D **62**, 014505 (2000) [arXiv:hep-lat/0002008].

[29] C. T. H. Davies *et al.* [HPQCD, Fermilab Lattice, MILC, and UKQCD Collaborations], Phys. Rev. Lett. **92**, 022001 (2004) [arXiv:hep-lat/0304004].

[30] C. W. Bernard *et al.*, Phys. Rev. D **64**, 054506 (2001) [arXiv:hep-lat/0104002].

[31] G. P. Lepage, Phys. Rev. D **59**, 074502 (1999) [arXiv:hep-lat/9809157].

[32] S. A. Gottlieb, Nucl. Phys. Proc. Suppl. **128**, 72 (2004) [Nucl. Phys. Proc. Suppl. **129**, 17 (2004)] [arXiv:hep-lat/0310041].

[33] A. Gray *et al.* [HPQCD collaboration], Nucl. Phys. Proc. Suppl. **119**, 592 (2003) [arXiv:hep-lat/0209022]. C. Davies *et al.*, Nucl. Phys. Proc. Suppl. **119**, 595 (2003) [arXiv:hep-lat/0209122].

[34] C. Aubin *et al.* [MILC Collaboration], Nucl. Phys. Proc. Suppl. **129**, 227 (2004) [arXiv:hep-lat/0309088].

[35] G. P. Lepage *et al.*, Phys. Rev. D **46**, 4052 (1992) [arXiv:hep-lat/9205007]; C. T. H. Davies *et al.*, Phys. Rev. D **50**, 6963 (1994) [arXiv:hep-lat/9406017].

[36] G. S. Bali and P. Boyle, Phys. Rev. D **59**, 114504 (1999) [arXiv:hep-lat/9809180].

[37] M. A. Nobes and H. D. Trottier, Nucl. Phys. Proc. Suppl. **129**, 355 (2004) [arXiv:hep-lat/0309086].

[38] M. B. Oktay, A. X. El-Khadra, A. S. Kronfeld, P. B. Mackenzie and J. N. Simone, Nucl. Phys. Proc. Suppl. **119**, 464 (2003) [arXiv:hep-lat/0209150]; M. B. Oktay, A. X. El-Khadra, A. S. Kronfeld and P. B. Mackenzie, Nucl. Phys. Proc. Suppl. **129**, 349 (2004) [arXiv:hep-lat/0310016].

[39] F. Abe *et al.* [CDF Collaboration], Phys. Rev. Lett. **81**, 2432 (1998) [arXiv:hep-ex/9805034].

[40] H. P. Shanahan, P. Boyle, C. T. H. Davies and H. Newton [UKQCD Collaboration], Phys. Lett. B **453**, 289 (1999) [arXiv:hep-lat/9902025].

[41] R. A. Bertlmann and A. Martin, Nucl. Phys. B **168**, 111 (1980).

[42] S. Nussinov and M. A. Lampert, Phys. Rept. **362**, 193 (2002) [arXiv:hep-ph/9911532].

[43] I. F. Allison, C. T. H. Davies, A. Gray, A. S. Kronfeld, P. B. Mackenzie and J. N. Simone [HPQCD, Fermilab Lattice, and UKQCD Collaborations], arXiv:hep-lat/0411027.

[44] I. F. Allison *et al.* [HPQCD, Fermilab Lattice, and UKQCD Collaborations], arXiv:hep-lat/0409090.

[45] A. S. Kronfeld, Nucl. Phys. Proc. Suppl. **129** (2004) 46 [arXiv:hep-lat/0310063].

[46] K. J. Juge, J. Kuti and C. J. Morningstar, Phys. Rev. Lett. **82**, 4400 (1999) [arXiv:hep-ph/9902336].

[47] K. J. Juge, J. Kuti and C. Morningstar, Phys. Rev. Lett. **90**, 161601 (2003) [arXiv:hep-lat/0207004].

[48] N. Brambilla, A. Pineda, J. Soto and A. Vairo, Phys. Rev. D **63**, 014023 (2001) [arXiv:hep-ph/0002250]; A. Pineda and A. Vairo, Phys. Rev. D **63**, 054007 (2001) [Erratum-ibid. D **64**, 039902 (2001)] [arXiv:hep-ph/0009145].

[49] C. T. H. Davies, K. Hornbostel, G. P. Lepage, A. Lidsey, P. McCallum, J. Shigemitsu and J. H. Sloan [UKQCD Collaboration], Phys. Rev. D **58**, 054505 (1998) [arXiv:hep-lat/9802024].

[50] T. Burch and D. Toussaint [MILC Collaboration], Phys. Rev. D **68**, 094504 (2003) [arXiv:hep-lat/0305008].

[51] G. S. Bali *et al.* [TχL Collaboration], Phys. Rev. D **62**, 054503 (2000) [arXiv:hep-lat/0003012].

[52] C. McNeile, C. Michael and P. Pennanen [UKQCD Collaboration], Phys. Rev. D **65**, 094505 (2002) [arXiv:hep-lat/0201006].

[53] G. S. Bali, Phys. Rept. **343**, 1 (2001) [arXiv:hep-ph/0001312].

[54] C. Alexandrou, P. De Forcrand and A. Tsapalis, Phys. Rev. D **65**, 054503 (2002) [arXiv:hep-lat/0107006]; C. Alexandrou, P. de Forcrand and O. Jahn, Nucl. Phys. Proc. Suppl. **119**, 667 (2003) [arXiv:hep-lat/0209062].

[55] T. T. Takahashi, H. Suganuma, Y. Nemoto and H. Matsufuru, Phys. Rev. D **65**, 114509 (2002) [arXiv:hep-lat/0204011]; H. Suganuma, T. T. Takahashi and H. Ichie, arXiv:hep-lat/0312031.

[56] F. Okiharu and R. M. Woloshyn, Nucl. Phys. Proc. Suppl. **129-130**, 745 (2004) [arXiv:hep-lat/0310007].

[57] V. G. Bornyakov *et al.* [DIK Collaboration], Phys. Rev. D **70**, 054506 (2004) [arXiv:hep-lat/0401026].

[58] R. Lewis, N. Mathur and R. M. Woloshyn, Phys. Rev. D **64**, 094509 (2001) [arXiv:hep-ph/0107037].

[59] N. Mathur, R. Lewis and R. M. Woloshyn, Phys. Rev. D **66**, 014502 (2002) [arXiv:hep-ph/0203253].

[60] J. M. Flynn, F. Mescia and A. S. B. Tariq [UKQCD Collaboration], JHEP **0307**, 066 (2003) [arXiv:hep-lat/0307025].

[61] N. Brambilla, D. Gromes and A. Vairo, Phys. Lett. B **576**, 314 (2003) [arXiv:hep-ph/0306107].

[62] Y. Schröder, Phys. Lett. B **447**, 321 (1999) [arXiv:hep-ph/9812205].

[63] M. Peter, Phys. Rev. Lett. **78**, 602 (1997) [arXiv:hep-ph/9610209].

[64] N. Brambilla, A. Pineda, J. Soto and A. Vairo, Phys. Rev. D **60**, 091502 (1999) [arXiv:hep-ph/9903355].

[65] G. S. Bali and A. Pineda, Phys. Rev. D **69**, 094001 (2004) [arXiv:hep-ph/0310130].

[66] M. Baker and R. Steinke, Phys. Rev. D **63**, 094013 (2001) [arXiv:hep-ph/0006069]; M. Baker and R. Steinke, Phys. Rev. D **65**, 094042 (2002) [arXiv:hep-th/0201169].

[67] B. A. Kniehl, A. A. Penin, M. Steinhauser and V. A. Smirnov, Phys. Rev. D **65** (2002) 091503 [arXiv:hep-ph/0106135].

[68] B. A. Kniehl, A. A. Penin, V. A. Smirnov and M. Steinhauser, Nucl. Phys. B **635**, 357 (2002) [arXiv:hep-ph/0203166].

[69] N. Brambilla, A. Pineda, J. Soto and A. Vairo, Phys. Lett. B **470**, 215 (1999) [arXiv:hep-ph/9910238].

[70] A. Pineda and J. Soto, Phys. Lett. B **495**, 323 (2000) [arXiv:hep-ph/0007197].

[71] T. Appelquist, M. Dine and I. J. Muzinich, Phys. Rev. D **17**, 2074 (1978).

[72] T. Appelquist, M. Dine and I. J. Muzinich, Phys. Lett. B **69**, 231 (1977).

[73] W. Fischler, Nucl. Phys. B **129**, 157 (1977).

[74] A. Billoire, Phys. Lett. B **92**, 343 (1980).

[75] M. Melles, Phys. Rev. D **62**, 074019 (2000) [arXiv:hep-ph/0001295].

[76] M. Melles, Nucl. Phys. Proc. Suppl. **96**, 472 (2001) [arXiv:hep-ph/0009085].

[77] A. H. Hoang, arXiv:hep-ph/0008102.

[78] S. Recksiegel and Y. Sumino, Phys. Rev. D **65**, 054018 (2002) [arXiv:hep-ph/0109122].

[79] B. A. Kniehl and A. A. Penin, Nucl. Phys. B **563**, 200 (1999) [arXiv:hep-ph/9907489].

[80] F. A. Chishtie and V. Elias, Phys. Lett. B **521**, 434 (2001) [arXiv:hep-ph/0107052].

[81] A. Pineda, JHEP **0106**, 022 (2001) [arXiv:hep-ph/0105008].

[82] G. Cvetic, J. Phys. G **30**, 863 (2004) [arXiv:hep-ph/0309262].

[83] A. Pineda, Ph.D. Thesis, Barcelona 1998.

[84] A. H. Hoang, M. C. Smith, T. Stelzer and S. Willenbrock, Phys. Rev. D **59**, 114014 (1999) [arXiv:hep-ph/9804227].

[85] M. Beneke, Phys. Lett. B **434**, 115 (1998) [arXiv:hep-ph/9804241].

[86] I. I. Y. Bigi, M. A. Shifman, N. G. Uraltsev and A. I. Vainshtein, Phys. Rev. D **50**, 2234 (1994) [arXiv:hep-ph/9402360]; M. Beneke, Phys. Lett. B **344**, 341 (1995) [arXiv:hep-ph/9408380];

M. Beneke and V. M. Braun, the Nucl. Phys. B **426**, 301 (1994) [arXiv:hep-ph/9402364]; M. Neubert and C. T. Sachrajda, Nucl. Phys. B **438**, 235 (1995) [arXiv:hep-ph/9407394]; G. Martinelli and C. T. Sachrajda, Nucl. Phys. B **478**, 660 (1996) [arXiv:hep-ph/9605336].

[87] U. Aglietti and Z. Ligeti, Phys. Lett. B **364**, 75 (1995) [arXiv:hep-ph/9503209].

[88] Y. Sumino, Phys. Rev. D **65**, 054003 (2002) [arXiv:hep-ph/0104259].

[89] S. Necco and R. Sommer, Phys. Lett. B **523**, 135 (2001) [arXiv:hep-ph/0109093].

[90] A. Pineda, J. Phys. G **29**, 371 (2003) [arXiv:hep-ph/0208031].

[91] S. Recksiegel and Y. Sumino, Eur. Phys. J. C **31**, 187 (2003) [arXiv:hep-ph/0212389].

[92] T. Lee, Phys. Rev. D **67**, 014020 (2003) [arXiv:hep-ph/0210032].

[93] N. Brambilla, Y. Sumino and A. Vairo, Phys. Lett. B **513**, 381 (2001) [arXiv:hep-ph/0101305].

[94] Y. Sumino, Phys. Lett. B **571**, 173 (2003) [arXiv:hep-ph/0303120].

[95] N. Brambilla, Y. Sumino and A. Vairo, Phys. Rev. D **65**, 034001 (2002) [arXiv:hep-ph/0108084].

[96] S. Recksiegel and Y. Sumino, Phys. Rev. D **67**, 014004 (2003) [arXiv:hep-ph/0207005].

[97] N. Brambilla and A. Vairo, Phys. Rev. D **62**, 094019 (2000) [arXiv:hep-ph/0002075].

[98] A. Pineda and F. J. Yndurain, Phys. Rev. D **58**, 094022 (1998) [arXiv:hep-ph/9711287].

[99] S. Titard and F. J. Yndurain, Phys. Rev. D **51**, 6348 (1995) [arXiv:hep-ph/9403400].

[100] M. Beneke and V. A. Smirnov, Nucl. Phys. B **522**, 321 (1998) [arXiv:hep-ph/9711391].

[101] A. Pineda, Phys. Rev. D **65**, 074007 (2002) [arXiv:hep-ph/0109117].

[102] A. H. Hoang and I. W. Stewart, Phys. Rev. D **67**, 114020 (2003) [arXiv:hep-ph/0209340].

[103] A. A. Penin and M. Steinhauser, Phys. Lett. B **538**, 335 (2002) [arXiv:hep-ph/0204290].

[104] N. Brambilla and A. Vairo, arXiv:hep-ph/0411156.

[105] J. Pantaleone and S. H. H. Tye, Phys. Rev. D **37**, 3337 (1988).

[106] S. Recksiegel and Y. Sumino, Phys. Lett. B **578**, 369 (2004) [arXiv:hep-ph/0305178].

[107] B. A. Kniehl, A. A. Penin, A. Pineda, V. A. Smirnov and M. Steinhauser, Phys. Rev. Lett. **92**, 242001 (2004) [arXiv:hep-ph/0312086].

[108] A. A. Penin, A. Pineda, V. A. Smirnov and M. Steinhauser, Phys. Lett. B **593**, 124 (2004) [arXiv:hep-ph/0403080].

[109] A. Vairo, IFUM-816-FT.

[110] A. V. Manohar and I. W. Stewart, Phys. Rev. D **62**, 014033 (2000) [arXiv:hep-ph/9912226].

[111] A. V. Manohar and I. W. Stewart, Phys. Rev. D **63**, 054004 (2001) [arXiv:hep-ph/0003107].

[112] A. H. Hoang, A. V. Manohar, I. W. Stewart and T. Teubner, Phys. Rev. Lett. **86**, 1951 (2001) [arXiv:hep-ph/0011254]; Phys. Rev. D **65**, 014014 (2002) [arXiv:hep-ph/0107144].

[113] A. H. Hoang, A. V. Manohar and I. W. Stewart, Phys. Rev. D **64**, 014033 (2001) [arXiv:hep-ph/0102257].

[114] A. Pineda, Phys. Rev. D **66**, 054022 (2002) [arXiv:hep-ph/0110216].

[115] A. H. Hoang, Phys. Rev. D **69**, 034009 (2004) [arXiv:hep-ph/0307376].

[116] A. Pineda, Acta Phys. Polon. B **34**, 5295 (2003) [arXiv:hep-ph/0404225].

[117] A. A. Penin, A. Pineda, V. A. Smirnov and M. Steinhauser, arXiv:hep-ph/0406175.

[118] A. Pineda, Acta Phys. Polon. B **34**, 5295 (2003) [arXiv:hep-ph/0404225].

[119] M. B. Voloshin, Nucl. Phys. B **154**, 365 (1979).

[120] H. Leutwyler, Phys. Lett. B **98**, 447 (1981).

[121] Y. Kiyo and Y. Sumino, Phys. Lett. B **535**, 145 (2002) [arXiv:hep-ph/0110277].

[122] A. Pineda, Nucl. Phys. B **494**, 213 (1997) [arXiv:hep-ph/9611388].

[123] I. I. Balitsky, Nucl. Phys. B **254**, 166 (1985).

[124] N. Brambilla, eConf **C030614**, 029 (2003) [arXiv:hep-ph/0312142].

[125] N. Brambilla, D. Eiras, A. Pineda, J. Soto and A. Vairo, Phys. Rev. D **67**, 034018 (2003) [arXiv:hep-ph/0208019]; N. Brambilla, D. Eiras, A. Pineda, J. Soto and A. Vairo, Phys. Rev. Lett. **88**, 012003 (2002) [arXiv:hep-ph/0109130].

[126] J. Gasser and H. Leutwyler, Annals Phys. **158** (1984) 142; Nucl. Phys. B **250** (1985) 465.

[127] N. Brambilla, D. Gromes and A. Vairo, Phys. Rev. D **64**, 076010 (2001) [arXiv:hep-ph/0104068].

[128] A. Barchielli, N. Brambilla and G. M. Prosperi, Nuovo Cim. A **103**, 59 (1990).

[129] D. Gromes, Z. Phys. C **26**, 401 (1984).

[130] K. G. Wilson, Phys. Rev. D **10**, 2445 (1974); L. Susskind, in Les Houches, Session XXIX, ed. R. Balian and C.H. Llewellyn Smith (North-Holland Publishing Company, Amsterdam, 1977).

[131] E. Eichten and F. Feinberg, Phys. Rev. D **23**, 2724 (1981).

[132] Y. Q. Chen, Y. P. Kuang and R. J. Oakes, Phys. Rev. D **52**, 264 (1995) [arXiv:hep-ph/9406287].

[133] M. E. Peskin, in Proc. 11th SLAC Institute, SLAC Report No. 207, 151, ed. P. Mc Donough (1983); A. Barchielli, E. Montaldi and G. M. Prosperi, Nucl. Phys. B **296**, 625 (1988) [Erratum *ibid.* B **303**, 752 (1988)]; N. Brambilla, P. Consoli and G. M. Prosperi, Phys. Rev. D **50**, 5878 (1994) [arXiv:hep-th/9401051]; A. P. Szczepaniak and E. S. Swanson, Phys. Rev. D **55**, 1578 (1997) [arXiv:hep-ph/9609525]; F. Jugeau and H. Sazdjian, Nucl. Phys. B **670**, 221 (2003) [arXiv:hep-ph/0305021].

[134] N. Brambilla and A. Vairo, arXiv:hep-ph/9904330; F. J. Yndurain, arXiv:hep-ph/9910399.

[135] G. S. Bali, K. Schilling and A. Wachter, Phys. Rev. D **56**, 2566 (1997) [arXiv:hep-lat/9703019].

[136] G. S. Bali, N. Brambilla and A. Vairo, Phys. Lett. B **421**, 265 (1998) [arXiv:hep-lat/9709079].

[137] M. Baker, N. Brambilla, H. G. Dosch and A. Vairo, Phys. Rev. D **58**, 034010 (1998) [arXiv:hep-ph/9802273]; N. Brambilla and A. Vairo, arXiv:hep-ph/0004192; N. Brambilla and A. Vairo, Phys. Rev. D **55**, 3974 (1997) [arXiv:hep-ph/9606344]; M. Baker, J. S. Ball, N. Brambilla, G. M. Prosperi and F. Zachariasen, Phys. Rev. D **54**, 2829 (1996) [arXiv:hep-ph/9602419]; M. Baker, J. S. Ball, N. Brambilla and A. Vairo, Phys. Lett. B **389**, 577 (1996) [arXiv:hep-ph/9609233]; M. Baker, J. S. Ball and F. Zachariasen, Phys. Rev. D **56**, 4400 (1997) [arXiv:hep-ph/9705207]; H. G. Dosch and Y. A. Simonov, Phys. Lett. B **205**, 339 (1988); M. Schiestl and H. G. Dosch, Phys. Lett. B **209**, 85 (1988); Y. A. Simonov, Nucl. Phys. B **324**, 67 (1989).

[138] N. Brambilla, arXiv:hep-ph/9809263; N. Brambilla, G. M. Prosperi and A. Vairo, Phys. Lett. B **362**, 113 (1995) [arXiv:hep-ph/9507300].

[139] N. Brambilla, A. Pineda, J. Soto and A. Vairo, Phys. Lett. B **580**, 60 (2004) [arXiv:hep-ph/0307159].

[140] G. P. Lepage, arXiv:nucl-th/9706029.

[141] A. Czarnecki, K. Melnikov and A. Yelkhovsky, Phys. Rev. A **59**, 4316 (1999) [arXiv:hep-ph/9901394].

[142] A. Czarnecki, K. Melnikov and A. Yelkhovsky, Phys. Rev. Lett. **82**, 311 (1999) [arXiv:hep-ph/9809341].

[143] B. Bolder *et al.*, Phys. Rev. D **63**, 074504 (2001) [arXiv:hep-lat/0005018].

[144] A. Pineda, arXiv:hep-ph/0310135.

[145] S. Necco and R. Sommer, Nucl. Phys. B **622**, 328 (2002) [arXiv:hep-lat/0108008].

[146] S. Capitani, M. Lüscher, R. Sommer and H. Wittig [ALPHA Collaboration], Nucl. Phys. B **544**, 669 (1999) [arXiv:hep-lat/9810063].

[147] M. Lüscher, K. Symanzik and P. Weisz, Nucl. Phys. B **173**, 365 (1980).

[148] M. Lüscher and P. Weisz, JHEP **0207**, 049 (2002) [arXiv:hep-lat/0207003].

[149] M. Caselle, M. Pepe and A. Rago, JHEP **0410**, 005 (2004) [arXiv:hep-lat/0406008].

[150] M. Luscher and P. Weisz, JHEP **0407**, 014 (2004) [arXiv:hep-th/0406205].

[151] K. J. Juge, J. Kuti, C. Morningstar, Nucl. Phys. (Proc. Suppl.) **129**, 686 (2004) [arXiv:hep-lat/0310039].

[152] K. J. Juge, J. Kuti, C. Morningstar, [arXiv:hep-lat/0401032].

[153] M. Foster and C. Michael [UKQCD Collaboration], Phys. Rev. D **59**, 094509 (1999) [arXiv:hep-lat/9811010].

[154] H. G. Dosch, M. Eidemuller and M. Jamin, Phys. Lett. B **452**, 379 (1999) [arXiv:hep-ph/9812417].

[155] G. S. Bali, K. Schilling and C. Schlichter, Phys. Rev. D **51**, 5165 (1995) [arXiv:hep-lat/9409005].

[156] K. J. Juge, J. Kuti, C. Morningstar, [arXiv:hep-lat/0312019].

[157] N. Brambilla, T. Rösch, A. Vairo "QCD Effective Lagrangians for Heavy Baryons" IFUM-808-FT; T. Rösch, Diploma thesis, Heidelberg 2003.

[158] J. Soto, arXiv:hep-ph/0301138.

[159] J. P. Ma and Z. G. Si, Phys. Lett. B **568**, 135 (2003) [arXiv:hep-ph/0305079].

[160] J. J. Aubert *et al.*, Phys. Rev. Lett. **33**, 1404 (1974).

[161] J. E. Augustin *et al.*, Phys. Rev. Lett. **33**, 1406 (1974).

[162] G. S. Abrams *et al.*, Phys. Rev. Lett. **33**, 1453 (1974).

[163] T. Appelquist and H. D. Politzer, Phys. Rev. Lett. **34**, 43 (1975).

[164] A. De Rujula and S. L. Glashow, Phys. Rev. Lett. **34**, 46 (1975).

[165] T. Appelquist, A. De Rujula, H. D. Politzer and S. L. Glashow, Phys. Rev. Lett. **34**, 365 (1975).

[166] E. Eichten, K. Gottfried, T. Kinoshita, J. B. Kogut, K. D. Lane and T. M. Yan, Phys. Rev. Lett. **34**, 369 (1975) [Erratum-ibid. **36**, 1276 (1976)].

[167] S. W. Herb *et al.*, Phys. Rev. Lett. **39**, 252 (1977); W. R. Innes *et al.*, Phys. Rev. Lett. **39**, 1240 (1977) [Erratum-ibid. **39**, 1640 (1977)].

[168] Some earlier reviews on this subject are: V. A. Novikov, L. B. Okun, M. A. Shifman, A. I. Vainshtein, M. B. Voloshin and V. I. Zakharov, Phys. Rept. **41**, 1 (1978); W. Kwong, J. L. Rosner and C. Quigg, Ann. Rev. Nucl. Part. Sci. **37**, 325 (1987); W. Lucha, F. F. Schoberl and D. Gromes, Phys. Rept. **200**, 127 (1991).

[169] E. Eichten, K. Gottfried, T. Kinoshita, K. D. Lane and T. M. Yan, Phys. Rev. Lett. **36**, 500 (1976).

[170] E. Eichten, K. Gottfried, T. Kinoshita, K. D. Lane and T. M. Yan, Phys. Rev. D **17**, 3090 (1978) [Erratum-ibid. D **21**, 313 (1980)]; Phys. Rev. D **21**, 203 (1980).

[171] S. Godfrey and N. Isgur, Phys. Rev. D **32**, 189 (1985).

[172] D. P. Stanley and D. Robson, Phys. Rev. D **21** (1980) 3180.

[173] D. Ebert, R.N. Faustov and V.O. Galkin, Phys. Rev. D **67**, 014027 (2003) [hep-ph/0210381].

[174] S.S. Gershtein, V. V. Kiselev, A. K. Likhoded and A. V. Tkabladze, Phys. Rev. D **51**, 3613 (1995) [arXiv:hep-ph/9406339].

[175] L. P. Fulcher, Phys. Rev. D **44**, 2079 (1991).

[176] L. P. Fulcher, Phys. Rev. D **60**, 074006 (1999) [arXiv:hep-ph/9806444].

[177] L. P. Fulcher, Phys. Rev. D **50**, 447 (1994).

[178] S. N. Gupta, J. M. Johnson, W. W. Repko and C. J. I. Suchyta, Phys. Rev. D **49**, 1551 (1994) [arXiv:hep-ph/9312205].

[179] S. N. Gupta and J. M. Johnson, Phys. Rev. D **53**, 312 (1996) [arXiv:hep-ph/9511267].

[180] J. Zeng, J. W. Van Orden and W. Roberts, Phys. Rev. D **52**, 5229 (1995) [arXiv:hep-ph/9412269].

[181] F. J. Llanes-Estrada, S. R. Cotanch, A. P. Szczepaniak and E. S. Swanson, Phys. Rev. C **70**, 035202 (2004) [arXiv:hep-ph/0402253]; F. J. Llanes-Estrada and S. R. Cotanch, Nucl. Phys. A **697**, 303 (2002) [arXiv:hep-ph/0101078].

[182] M. Baldicchi and G. M. Prosperi, Phys. Rev. D **66**, 074008 (2002) [arXiv:hep-ph/0202172]; M. Baldicchi and G. M. Prosperi, Phys. Rev. D **62**, 114024 (2000) [arXiv:hep-ph/0008017]; P. Maris and C. D. Roberts, Int. J. Mod. Phys. E **12**, 297 (2003) [arXiv:nucl-th/0301049]; N. Brambilla and A. Vairo, Phys. Rev. D **56**, 1445 (1997) [arXiv:hep-ph/9703378]; N. Brambilla and A. Vairo, Phys. Lett. B **407**, 167 (1997) [arXiv:hep-ph/9703377]. N. Brambilla, E. Montaldi and G. M. Prosperi, Phys. Rev. D **54**, 3506 (1996) [arXiv:hep-ph/9504229];

[183] T. J. Allen, T. Coleman, M. G. Olsson and S. Veseli, Phys. Rev. D **67**, 054016 (2003) [arXiv:hep-ph/0207141]; T. J. Allen, M. G. Olsson and S. Veseli, Phys. Rev. D **62**, 094021 (2000) [arXiv:hep-ph/0001227].

[184] C. D. Roberts, Lect. Notes Phys. **647**, 149 (2004) [arXiv:nucl-th/0304050].

[185] N. Brambilla and G. M. Prosperi, Phys. Lett. B **236**, 69 (1990).

[186] N. Brambilla, Nuovo Cim. A **105**, 949 (1992); N. Brambilla and G. M. Prosperi, Phys. Rev. D **46**, 1096 (1992) [Erratum-ibid. D **46**, 4105 (1992)].

[187] T. Barnes and S. Godfrey, Phys. Rev. D **69**, 054008 (2004) [arXiv:hep-ph/0311162].

[188] E. J. Eichten, K. Lane and C. Quigg, Phys. Rev. D **69**, 094019 (2004) [arXiv:hep-ph/0401210].

[189] S. Jacobs, M. G. Olsson and C. I. Suchyta, Phys. Rev. D **33**, 3338 (1986) [Erratum-ibid. D **34**, 3536 (1986)].

[190] J. L. Richardson, Phys. Lett. B **82**, 272 (1979).

[191] W. Buchmüller and S. H. H. Tye, Phys. Rev. D **24**, 132 (1981).

[192] V. B. Berestetskij, E. M. Lifschitz, and L. P. Pitaevskij, *Relativistic Quantum Theory*, (Oxford, New York, Pergamon Press 1971) pp 280-286.

[193] D. Ebert, R. N. Faustov and V. O. Galkin, Phys. Rev. D **62**, 034014 (2000) [arXiv:hep-ph/9911283].

[194] S. Godfrey and R. Kokoski, Phys. Rev. D **43**, 1679 (1991).

[195] This is discussed in more detail in Appendix A of T. Barnes, N. Black and P. R. Page, Phys. Rev. D **68**, 054014 (2003) [arXiv:nucl-th/0208072].

[196] E.J.Eichten and C.Quigg, Phys. Rev. D **49**, 5845 (1994) [hep-ph/9402210].

[197] S. N. Gupta and S. F. Radford, Phys. Rev. D **24** (1981) 2309; Phys. Rev. D **25** (1982) 3430; S. N. Gupta, S. F. Radford and W. W. Repko, Phys. Rev. D **26**, 3305 (1982); J. Pantaleone, S. H. H. Tye and Y. J. Ng, Phys. Rev. D **33**, 777 (1986).

[198] A. H. Hoang and A. V. Manohar, Phys. Lett. B **483**, 94 (2000) [arXiv:hep-ph/9911461].

[199] D. Eiras and J. Soto, Phys. Lett. B **491**, 101 (2000) [arXiv:hep-ph/0005066].

[200] D. Ebert, R. N. Faustov and V. O. Galkin, Phys. Rev. D **66**, 037501 (2002) [ar2002rbXiv:hep-ph/0204204].

[201] N. Isgur, Phys. Rev. D **60**, 054013 (1999) [arXiv:nucl-th/9901032].

[202] T. Barnes and G. I. Ghandour, Phys. Lett. B **118**, 411 (1982).

[203] S. E. Csorna *et al.* [CLEO Collaboration], arXiv:hep-ex/0207060.

[204] S. Godfrey and J. L. Rosner, Phys. Rev. D **64**, 097501 (2001) [Erratum-ibid. D **66**, 059902 (2002)] [arXiv:hep-ph/0105273].

[205] S. Godfrey and J. L. Rosner, Phys. Rev. D **64**, 074011 (2001) [Erratum-ibid. D **65**, 039901 (2002)] [arXiv:hep-ph/0104253].

[206] S. Godfrey and J. L. Rosner, Phys. Rev. D **66**, 014012 (2002) [arXiv:hep-ph/0205255].

[207] S. K. Choi *et al.* [BELLE collaboration], Phys. Rev. Lett. **89**, 102001 (2002) [Erratum-ibid. **89**, 129901 (2002)] [arXiv:hep-ex/0206002].

[208] K. Abe *et al.* [Belle Collaboration], Phys. Rev. Lett. **89**, 142001 (2002) [arXiv:hep-ex/0205104].

[209] J. Ernst *et al.* (CLEO), CLEO-CONF-03-05, hep-ex/0306060.

[210] G. Wagner [BABAR Collaboration], arXiv:hep-ex/0305083.

[211] S. K. Choi *et al.* [Belle Collaboration], Phys. Rev. Lett. **91**, 262001 (2003) [arXiv:hep-ex/0309032].

[212] E. S. Swanson, Phys. Lett. B **598**, 197 (2004) [arXiv:hep-ph/0406080]; E. Braaten, M. Kusunoki and S. Nussinov, Phys. Rev. Lett. **93**, 162001 (2004) [arXiv:hep-ph/0404161].

[213] Y. Q. Chen and Y. P. Kuang, Phys. Rev. D **46**, 1165 (1992) [Erratum-ibid. D **47**, 350 (1993)]; S. M. Ikhdair and R. Sever, Int. J. Mod. Phys. A **19**, 1771 (2004) [arXiv:hep-ph/0310295].

[214] S. S. Gershtein, V. V. Kiselev, A. K. Likhoded and A. V. Tkabladze, Phys. Usp. **38**, 1 (1995) [Usp. Fiz. Nauk **165**, 3 (1995)] [arXiv:hep-ph/9504319].

[215] I. P. Gouz, V. V. Kiselev, A. K. Likhoded, V. I. Romanovsky and O. P. Yushchenko, arXiv:hep-ph/0211432.

[216] S. Godfrey, arXiv:hep-ph/0406228.

[217] F. Abe *et al.* [CDF Collaboration], Phys. Rev. D **58**, 112004 (1998) [arXiv:hep-ex/9804014].

[218] V. A. Novikov, L. B. Okun, M. A. Shifman, A. I. Vainshtein, M. B. Voloshin and V. I. Zakharov, Phys. Rev. Lett. **38**, 626 (1977) [Erratum-ibid. **38**, 791 (1977)].

[219] M. B. Voloshin, Sov. J. Nucl. Phys. **36**, 143 (1982) [Yad. Fiz. **36**, 247 (1982)].

[220] Y. I. Azimov, Y. L. Dokshitzer and V. A. Khoze, Sov. J. Nucl. Phys. **36**, 878 (1982) [Yad. Fiz. **36**, 1510 (1982)].

[221] M. B. Voloshin and Y. M. Zaitsev, Sov. Phys. Usp. **30**, 553 (1987) [Usp. Fiz. Nauk **152**, 361 (1987)].

[222] V. V. Kiselev, Mod. Phys. Lett. A **10**, 2113 (1995) [arXiv:hep-ph/9401339].

[223] G. S. Bali, T. Duessel, T. Lippert, H. Neff, Z. Prkacin and K. Schilling, arXiv:hep-lat/0409137; T. Lippert *et al.* (SESAM Collaboration) talk given at Lattice 2004, Fermilab, June 2004, to appear in the Proceedings.

[224] I. Tamm, J. Phys. (Moscow) **9**, 449 (1945); S. M. Dancoff, Phys. Rev. **78**, 382 (1950).

[225] E. Braaten and M. Kusunoki, Phys. Rev. D **69**, 074005 (2004) [arXiv:hep-ph/0311147].

[226] A. De Rujula, H. Georgi and S. L. Glashow, Phys. Rev. Lett. **38**, 317 (1977).

[227] A. De Rujula and R. L. Jaffe, MIT-CTP-658 *Presented at 5th Int. Conf. on Meson Spectroscopy, Boston, Mass., Apr 29-30, 1977*

[228] A. Le Yaouanc, L. Oliver, O. Pene and J. C. Raynal, Phys. Rev. D **8**, 2223 (1973).

[229] A. Le Yaouanc, L. Oliver, O. Pene and J. C. Raynal, Phys. Rev. D **9**, 1415 (1974).

[230] A. Le Yaouanc, L. Oliver, O. Pene and J. C. Raynal, Phys. Rev. D **12**, 2137 (1975) [Erratum-ibid. D **13**, 1519 (1976)].

[231] L. Micu, Nucl. Phys. B **10**, 521 (1969).

[232] T. Barnes, F. E. Close, P. R. Page and E. S. Swanson, Phys. Rev. D **55**, 4157 (1997) [arXiv:hep-ph/9609339].

[233] S. Godfrey and J. Napolitano, Rev. Mod. Phys. **71**, 1411 (1999) [arXiv:hep-ph/9811410].

[234] A. Le Yaouanc, L. Oliver, O. Pene and J. C. Raynal, Phys. Lett. B **71**, 397 (1977).

[235] N. Isgur and J. Paton, Phys. Rev. D **31**, 2910 (1985).

[236] R. Kokoski and N. Isgur, Phys. Rev. D **35**, 907 (1987).

[237] T. Barnes, arXiv:hep-ph/0406327.

[238] E. S. Ackleh, T. Barnes and E. S. Swanson, Phys. Rev. D **54**, 6811 (1996) [arXiv:hep-ph/9604355].

[239] Y. A. Simonov, Phys. Atom. Nucl. **66**, 2045 (2003) [Yad. Fiz. **66**, 2095 (2003)] [arXiv:hep-ph/0211410].

[240] A. Martin and J. M. Richard, Phys. Lett. B **115**, 323 (1982).

[241] A. Martin and J. M. Richard, CERN Cour. **43N3**, 17 (2003).

[242] E. J. Eichten, K. Lane and C. Quigg, Phys. Rev. Lett. **89**, 162002 (2002) [arXiv:hep-ph/0206018].

[243] J. L. Rosner, Phys. Rev. D **64**, 094002 (2001) [arXiv:hep-ph/0105327].

[244] J. L. Rosner, arXiv:hep-ph/0405196.

[245] S. Eidelman *et al.* [Particle Data Group Collaboration], Phys. Lett. B **592**, 1 (2004).

[246] K. K. Seth, arXiv:hep-ex/0405007.

[247] E. Eichten, Phys. Rev. D **22**, 1819 (1980).

[248] K. Heikkila, S. Ono and N. A. Tornqvist, Phys. Rev. D **29**, 110 (1984) [Erratum-ibid. D **29**, 2136 (1984)].

[249] N. Byers and E. Eichten, UCLA/89/TEP/56 *in Proc. of Europhysics Conf. on High Energy Physics, Madrid, Spain, Sep 6-13, 1989.*

[250] N. Byers, arXiv:hep-ph/9412292.

[251] C. Quigg, arXiv:hep-ph/0403187.

[252] M. K. Gaillard, B. W. Lee and J. L. Rosner, Rev. Mod. Phys. **47**, 277 (1975).

[253] A. De Rujula, H. Georgi and S. L. Glashow, Phys. Rev. D **12**, 147 (1975).

[254] S. Fleck and J. M. Richard, Prog. Theor. Phys. **82**, 760 (1989).

[255] S. Fleck and J. M. Richard, Part. World **1**, 67 (1990).

[256] M. J. Savage and M. B. Wise, Phys. Lett. B **248**, 177 (1990).

[257] M. J. Savage and R. P. Springer, Int. J. Mod. Phys. A **6**, 1701 (1991).

[258] E. Bagan, H. G. Dosch, P. Gosdzinsky, S. Narison and J. M. Richard, Z. Phys. C **64**, 57 (1994) [arXiv:hep-ph/9403208].

[259] R. Roncaglia, D. B. Lichtenberg and E. Predazzi, Phys. Rev. D **52**, 1722 (1995) [arXiv:hep-ph/9502251].

[260] B. Silvestre-Brac, Few Body Syst. **20**, 1 (1996).

[261] S. S. Gershtein, V. V. Kiselev, A. K. Likhoded and A. I. Onishchenko, Phys. Rev. D **62**, 054021 (2000).

[262] V. V. Kiselev and A. E. Kovalsky, Phys. Rev. D **64**, 014002 (2001) [arXiv:hep-ph/0005019].

[263] S. P. Tong, Y. B. Ding, X. H. Guo, H. Y. Jin, X. Q. Li, P. N. Shen and R. Zhang, Phys. Rev. D **62**, 054024 (2000) [arXiv:hep-ph/9910259].

[264] B. A. Gelman and S. Nussinov, Phys. Lett. B **551**, 296 (2003) [arXiv:hep-ph/0209095].

[265] J. M. Richard, Phys. Rept. **212**, 1 (1992).

[266] W. Ponce, Phys. Rev. D **19**, 2197 (1979).

[267] D. Ebert, R. N. Faustov, V. O. Galkin and A. P. Martynenko, Phys. Rev. D **66**, 014008 (2002) [arXiv:hep-ph/0201217].

[268] W. A. Bardeen, E. J. Eichten and C. T. Hill, Phys. Rev. D **68**, 054024 (2003) [arXiv:hep-ph/0305049].

[269] R. L. Jaffe, Phys. Rev. Lett. **38**, 195 (1977) [Erratum-ibid. **38**, 617 (1977)].

[270] H. J. Lipkin, Phys. Lett. B **195**, 484 (1987).

[271] C. Gignoux, B. Silvestre-Brac and J. M. Richard, Phys. Lett. B **193**, 323 (1987).

[272] A. Chodos, R. L. Jaffe, K. Johnson, C. B. Thorn and V. F. Weisskopf, Phys. Rev. D **9**, 3471 (1974).

[273] J. L. Rosner, Phys. Rev. D **33**, 2043 (1986).

[274] G. Karl and P. Zenczykowski, Phys. Rev. D **36**, 2079 (1987).

[275] S. Fleck, C. Gignoux, J. M. Richard and B. Silvestre-Brac, Phys. Lett. B **220**, 616 (1989).

[276] A. Gal, Nucl. Phys. A **721**, 945 (2003) [arXiv:nucl-th/0211070].

[277] G. Karl and P. Zenczykowski, Phys. Rev. D **36**, 3520 (1987).

[278] J. Leandri and B. Silvestre-Brac, Phys. Rev. D **40**, 2340 (1989).

[279] R. L. Jaffe and F. Wilczek, Phys. Rev. Lett. **91**, 232003 (2003) [arXiv:hep-ph/0307341].

[280] I. W. Stewart, M. E. Wessling and M. B. Wise, Phys. Lett. B **590**, 185 (2004) [arXiv:hep-ph/0402076].

[281] Y. R. Liu, A. Zhang, P. Z. Huang, W. Z. Deng, X. L. Chen and S. L. Zhu, Phys. Rev. D **70**, 094045 (2004) [arXiv:hep-ph/0404123].

[282] S. L. Zhu, Int. J. Mod. Phys. **LA19**, 3439 (2004) [arXiv:hep-ph/0406204].

[283] M. Oka, Prog. Theor. Phys. **112**, 1 (2004) [arXiv:hep-ph/0406211].

[284] J. Pochodzalla, arXiv:hep-ex/0406077.

[285] F. Stancu, Phys. Rev. D **58**, 111501 (1998) [arXiv:hep-ph/9803442].

[286] J. P. Ader, J. M. Richard and P. Taxil, Phys. Rev. D **25**, 2370 (1982).

[287] L. Heller and J. A. Tjon, Phys. Rev. D **32**, 755 (1985).

[288] L. Heller and J. A. Tjon, Phys. Rev. D **35**, 969 (1987).

[289] J. Carlson, L. Heller and J. A. Tjon, Phys. Rev. D **37**, 744 (1988).

[290] S. Zouzou, B. Silvestre-Brac, C. Gignoux and J. M. Richard, Z. Phys. C **30**, 457 (1986).

[291] H. J. Lipkin, Phys. Lett. B **172**, 242 (1986).

[292] D. M. Brink and F. Stancu, Phys. Rev. D **49**, 4665 (1994).

[293] D. M. Brink and F. Stancu, Phys. Rev. D **57**, 6778 (1998).

[294] D. Janc and M. Rosina, Few Body Syst. **31**, 1 (2001) [arXiv:hep-ph/0007024].

[295] D. Janc, M. Rosina, D. Treleani and A. Del Fabbro, Few Body Syst. Suppl. **14**, 25 (2003) [arXiv:hep-ph/0301115].

[296] A. Mihaly, H. R. Fiebig, H. Markum and K. Rabitsch, Phys. Rev. D **55**, 3077 (1997).

[297] C. Michael and P. Pennanen [UKQCD Collaboration], Phys. Rev. D **60**, 054012 (1999) [arXiv:hep-lat/9901007]; P. Pennanen, C. Michael and A. M. Green [UKQCD Collaboration], Nucl. Phys. Proc. Suppl. **83**, 200 (2000) [arXiv:hep-lat/9908032].

[298] A. M. Green and P. Pennanen, Phys. Lett. B **426**, 243 (1998) [arXiv:hep-lat/9709124].

[299] A. M. Green and P. Pennanen, Phys. Rev. C **57**, 3384 (1998) [arXiv:hep-lat/9804003].

[300] N. A. Törnqvist, Phys. Rev. Lett. **67**, 556 (1991).

[301] N. A. Törnqvist, Z. Phys. C **61**, 525 (1994) [arXiv:hep-ph/9310247].

[302] A. V. Manohar and M. B. Wise, Nucl. Phys. B **399**, 17 (1993) [arXiv:hep-ph/9212236].

[303] T. E. O. Ericson and G. Karl, Phys. Lett. B **309**, 426 (1993).

[304] D. Bressanini, G. Morosi, L. Bertini and M. Mella, Few-Body Syst. **31**, 199 (2002).

[305] CLEO Collaboration, R. Balest *et al.*, Phys. Rev. D **52**, 2661 (1995).

[306] Belle Collaboration (K. Abe *et al.*), Phys. Rev. Lett. **88**, 031802 (2002).

[307] BABAR Collaboration, (B. Aubert *et al.*), Phys. Rev. D **67**, 032002 (2003) [hep-ex/0207097]. See also Phys. Rev. Lett. **90**, 091801 (2003).

[308] BABAR Collaboration (B. Aubert *et al.*), Phys. Rev. D **65**, 032001 (2002).

[309] BABAR Collaboration (B. Aubert *et al.*), hep-ex/0203040.

[310] R. C. Giles and S.-H. H. Tye, Phys. Rev. D **16**, 1079 (1977).

[311] F. E. Close, I. Dunietz, P. R. Page, S. Veseli and H. Yamamoto, Phys. Rev. D **57**, 5653 (1998).

[312] G. Chiladze, A. F. Falk and A. A. Petrov, Phys. Rev. D **58**, 034013 (1998).

[313] A detailed account with more complete references is given by F. E. Close and S. Godfrey, Phys. Lett. B **574**, 210 (2003) [arXiv:hep-ph/0305285].

[314] J. Merlin and J. Paton, Phys. Rev. D **35**, 1668 (1987).

[315] T. Barnes, F. E. Close and E. S. Swanson, Phys. Rev. D **52**, 5242 (1995) [arXiv:hep-ph/9501405].

[316] T. Barnes, Nucl. Phys. B **158**, 171 (1979); P. Hasenfratz, R. Horgan, J. Kuti, and J. Richard, Phys. Lett. B **95**, 299 (1980); T. Barnes and F. E. Close, Phys. Lett. B **116**, 365 (1982); M. Chanowitz and S. Sharpe, Nucl. Phys. B **222**, 211 (1983); T. Barnes, F. E. Close and F. de Viron, Nucl. Phys. B **224**, 241 (1983); M. Flensberg, C. Peterson, and L. Skold, Z. Phys. C **22**, 293 (1984).

[317] S. Perantonis and C. Michael, Nucl. Phys. B **347**, 854 (1990); L. A. Griffiths, C. Michael and P. E. Rakow, Phys. Lett. B **129**, 351 (1983).

[318] K. J. Juge, J. Kuti and C. J. Morningstar, arXiv:hep-ph/9711451; Nucl. Phys. Proc. Suppl. **63**, 326 (1998) [arXiv:hep-lat/9709131].

[319] D. Horn and J. Mandula, Phys. Rev. D **17**, 898 (1978). Y. S. Kalashnikova and Y. B. Yufryakov, Phys. Atom. Nucl. **60**, 307 (1997) [Yad. Fiz. **60N2**, 374 (1997)] [arXiv:hep-ph/9510357].

[320] N. Isgur, R. Kokoski and J. Paton, Why They Are Missing And Where To Find Them," Phys. Rev. Lett. **54**, 869 (1985).

[321] F. E. Close and P. R. Page, Nucl. Phys. B **443**, 233 (1995) [arXiv:hep-ph/9411301].

[322] P. R. Page, E. S. Swanson and A. P. Szczepaniak, Phys. Rev. D **59**, 034016 (1999) [arXiv:hep-ph/9808346]. E. S. Swanson and A. P. Szczepaniak, Phys. Rev. D **56**, 5692 (1997) [arXiv:hep-ph/9704434].

[323] F. E. Close, Phys. Lett. B **342**, 369 (1995) [arXiv:hep-ph/9409203].

[324] P. R. Page, Phys. Lett. B **402**, 183 (1997) [arXiv:hep-ph/9611375].

[325] Y. P. Kuang and T. M. Yan, Phys. Rev. D **24**, 2874 (1981).

[326] F. E. Close and P. R. Page, Phys. Rev. D **52**, 1706 (1995) [arXiv:hep-ph/9412301].

[327] F. E. Close and J. J. Dudek, Phys. Rev. Lett. **91**, 142001 (2003) [arXiv:hep-ph/0304243].

[328] An estimate of the $\Gamma(\eta_c' \to \text{light hadrons})$ is given by S. Godfrey and J. L. Rosner, Phys. Rev. D **66**, 014012 (2002).

[329] G. T. Bodwin, E. Braaten, T. C. Yuan, and G. P. Lepage, Phys. Rev. D **46**, R3703 (1992).

[330] M. Beneke, F. Maltoni and I. Z. Rothstein, Phys. Rev. D **59**, 054003 (1999) [arXiv:hep-ph/9808360].

[331] P. Ko, J. Lee and H. S. Song, Phys. Rev. D **53**, 1409 (1996) [arXiv:hep-ph/9510202]; P. Ko, Phys. Rev. D **52**, 3108 (1995).

[332] F. Yuan, C. F. Qiao and K. T. Chao, Phys. Rev. D **56**, 329 (1997) [arXiv:hep-ph/9701250].

[333] P. w. Ko, J. Lee and H. S. Song, Phys. Lett. B **395**, 107 (1997) [arXiv:hep-ph/9701235].

[334] A. A. Zholents *et al.*, Phys. Lett. B **96**, 214 (1980).

[335] J. Z. Bai *et al.* [BES Collaboration], Phys. Rev. Lett. **69**, 3021 (1992).

[336] V.M. Aulchenko et al., Phys. Lett. B573 (2003) 63.

[337] V. M. Aulchenko *et al.* [KEDR Collaboration], Phys. Lett. B **573**, 63 (2003) [arXiv:hep-ex/0306050].

[338] A. A. Sokolov and I. M. Ternov, Phys. Dokl. **8**, 1203 (1964).

[339] A. D. Bukin *et al.*, in: Vth Int. Symposium on High Energy Physics and Elementary Particle Physics, Warsaw, 1975, p.138.

[340] A. S. Artamonov *et al.*, Phys. Lett. B **118**, 225 (1982).

[341] A. S. Artamonov *et al.*, Phys. Lett. B **173**, 272 (1984).

[342] A. S. Artamonov *et al.*, Phys. Lett. B **137**, 272 (1984).

[343] S. E. Baru *et al.*, Z. Phys. C **56**, 547 (1992).

[344] A. S. Artamonov *et al.* [OLYA Collaboration], Phys. Lett. B **474**, 427 (2000) [arXiv:hep-ex/0001040].

[345] W. W. MacKay *et al.* [CUSB Collaboration], Phys. Rev. D **29**, 2483 (1984).

[346] D. P. Barber *et al.* [ARGUS Collaboration], Phys. Lett. B **135**, 498 (1984).

[347] T. A. Armstrong *et al.* [E760 Collaboration], Phys. Rev. D **47**, 772 (1993).

[348] R. Assmann *et al.*, Eur. Phys. J. C **6**, 187 (1999).

[349] A. N. Skrinsky and Y. M. Shatunov, Sov. Phys. Usp. **32**, 548 (1989) [Usp. Fiz. Nauk **158**, 315 (1989)].

[350] C. Bernardini *et al.*, Phys. Rev. Lett. **10**, 407 (1963).

[351] V. E. Blinov *et al.*, Nucl. Instrum. Meth. A **494**, 81 (2002).

[352] V. V. Anashin *et al.*, Nucl. Instrum. Meth. A **478**, 420 (2002).

[353] Y. S. Derbenev, A. M. Kondratenko, S. I. Serednyakov, A. N. Skrinsky, G. M. Tumaikin and Y. M. Shatunov, Part. Accel. **10**, 177 (1980).

[354] S. E. Baru *et al.*, Z. Phys. C **30**, 551 (1986) [Erratum-ibid. C **32**, 622 (1986)].

[355] E. A. Kuraev and V. S. Fadin, Sov. J. Nucl. Phys. **41**, 466 (1985) [Yad. Fiz. **41**, 733 (1985)].

[356] J. D. Jackson and D. L. Scharre, Nucl. Instrum. Meth. **128**, 13 (1975).

[357] A. A. Zholents *et al.*, Yad. Fiz. **34**, 1471 (1981).

[358] E. R. Cohen and B. N. Taylor, J. Phys. Chem. Ref. Data **2**, 664 (1973).

[359] E. R. Cohen and B. N. Taylor, Rev. Mod. Phys. **59**, 1121 (1987) [Europhys. News **18**, 65 (1987)].

[360] T. A. Armstrong *et al.* [E760 Collaboration], Nucl. Phys. B **373**, 35 (1992).

[361] S. Bagnasco *et al.* [Fermilab E835 Collaboration], Phys. Lett. B **533**, 237 (2002).

[362] D. P. McGinnis, G. Stancari, S. J. Werkema, Nucl. Instrum. Methods A **506**, 205 (2003).

[363] M. Andreotti *et al.* [Fermilab E835 Collaboration], Phys. Rev. Lett. **91**, 091801 (2003) [arXiv:hep-ex/0308055].

[364] M. Andreotti *et al.* [Fermilab E835 Collaboration], in preparation.

[365] J. Z. Bai *et al.* [BES Collaboration], Phys. Rev. D **60**, 072001 (1999) [arXiv:hep-ex/9812016].

[366] J. Z. Bai *et al.* [BES Collaboration], Phys. Rev. Lett. **81**, 3091 (1998) [arXiv:hep-ex/9807001].

[367] S. W. Herb *et al.* [E288], Phys. Rev. Lett. **39**, 252 (1977); W. R. Innes *et al.* [E288], Phys. Rev. Lett. **39**, 1240 (1977); *erratum* **39**, 1640 (1977).

[368] C. Berger *et al.* [PLUTO], Phys. Lett. B**76**, 243 (1978); C. W. Darden *et al.* [DASP], Phys. Lett. B**76**, 246 (1978); J. K. Bienlein *et al.* [LENA], Phys. Lett. B**78**, 360 (1978).

[369] K. Han *et al.* [CUSB], Phys. Rev. Lett. **49**, 1612 (1982).

[370] G. Eigen *et al.* [CUSB], Phys. Rev. Lett. **49**, 1616 (1982).

[371] C. Klopfenstein *et al.* [CUSB], Phys. Rev. Lett. **51**, 160 (1983); F. Pauss *et al.* [CUSB], Phys. Lett. B **130**, 439 (1983).

[372] P. Haas *et al.*[CLEO], Phys. Rev. Lett. **52**, 799 (1984).

[373] R. Nernst *et al.* [Crystal Ball], Phys. Rev. Lett. **54**, 2195 (1985); W. S. Walk *et al.* [Crystal Ball], Phys. Rev. D **34**, 2611 (1986).

[374] H. Albrecht *et al.*[ARGUS], Phys. Lett. B **160**, 331 (1985).

[375] T. Skwarnicki *et al.* [Crystal Ball], Phys. Rev. Lett. **58**, 972 (1987).

[376] R. Morrison *et al.* [CLEO-II], Phys. Rev. Lett. **67**, 1696 (1991); U. Heintz *et al.* [CUSB-II], Phys. Rev. D **46** 1928 (1992); G. Crawford *et al.* [CLEO-II], Phys. Lett. B **294**, 139 (1992).

[377] K. W. Edwards *et al.* [CLEO Collaboration], Phys. Rev. D **59**, 032003 (1999) [arXiv:hep-ex/9803010].

[378] M. Artuso *et al.* [CLEOIII], CLNS 04/1897, CLEO 04-16 (2004), *submitted to PRL.*

[379] S. B. Athar *et al.* [CLEO Collaboration], arXiv:hep-ex/0408133.

[380] G. Bonvicini *et al.* [CLEO Collaboration], Phys. Rev. D **70**, 032001 (2004) [arXiv:hep-

ex/0404021].

[381] W. Kwong and J. L. Rosner, Phys. Rev. D **38**, 279 (1988).

[382] J. L. Rosner, Phys. Rev. D **67**, 097504 (2003) [arXiv:hep-ph/0302122].

[383] J. Z. Bai *et al.* [BES Collaboration], Phys. Rev. D **62**, 072001 (2000) [arXiv:hep-ex/0002006].

[384] D. Bisello *et al.* [DM2 collaboration], Nucl. Phys. B **350**, 1 (1991).

[385] Z. Bai *et al.* [MARK-III Collaboration], Phys. Rev. Lett. **65**, 1309 (1990).

[386] R. M. Baltrusaitis *et al.* [Mark-III Collaboration], Phys. Rev. D **33**, 629 (1986).

[387] J. Ernst *et al.*, [CLEO Collaboration], arXiv:hep-ex/0306060. Contributed to Europhysics Conference, July, 2003, Aachen, Germany;

[388] D. M. Asner *et al.* [CLEO Collaboration], Phys. Rev. Lett. **92**, 142001 (2004) [arXiv:hep-ex/0312058].

[389] B. Aubert *et al.* [BABAR Collaboration], arXiv:hep-ex/0311038.

[390] Edwards *et al.*, Phys. Rev. Lett. **48**, 70 (1982).

[391] T. Skwarnicki, Int. J. Mod. Phys. A **19**, 1030 (2004) [arXiv:hep-ph/0311243].

[392] B. Aubert *et al.* [BABAR Collaboration], Nucl. Instrum. Meth. A **479**, 1 (2002) [arXiv:hep-ex/0105044].

[393] F. Fang *et al.* [Belle Collaboration], Phys. Rev. Lett. **90** (2003) 071801 [arXiv:hep-ex/0208047].

[394] K. Abe *et al.* [Belle Collaboration], arXiv:hep-ex/0306015.

[395] T. Barnes, T. E. Browder and S. F. Tuan, Phys. Lett. B **385**, 391 (1996) [arXiv:hep-ph/9605278].

[396] B. Aubert *et al.* [BABAR Collaboration], Phys. Rev. D **70**, 011101 (2004) [arXiv:hep-ex/0403007].

[397] H. C. Huang *et al.* [Belle Collaboration], Phys. Rev. Lett. **91**, 241802 (2003).

[398] J. Z. Bai *et al.* [BES Collaboration], Phys. Lett. B **578**, 16 (2004) [arXiv:hep-ex/0308073].

[399] S. B. Athar *et al.* [CLEO Collaboration], arXiv:hep-ex/0408133.

[400] V. Zambetakis and N. Byers, Phys. Rev. D **28**, 2908 (1983).

[401] S. Godfrey and N. Isgur, Phys. Rev. D **32**, 189 (1985).

[402] T. A. Lahde, C. J. Nyfalt and D. O. Riska, Nucl. Phys. A **645**, 587 (1999) [arXiv:hep-ph/9808438].

[403] D. Ebert, R. N. Faustov and V. O. Galkin, Phys. Rev. D **67**, 014027 (2003) [arXiv:hep-ph/0210381].

[404] A. Boehrer, arXiv:hep-ex/0106020.

[405] A. Boehrer, arXiv:hep-ex/0305029.

[406] A. X. El-Khadra, arXiv:hep-ph/9508266.

[407] L. Marcantonio, P. Boyle, C. T. H. Davies, J. Hein and J. Shigemitsu [UKQCD Collaboration], Nucl. Phys. Proc. Suppl. **94**, 363 (2001) [arXiv:hep-lat/0011053].

[408] C. T. H. Davies, private communication, as cited in [419].

[409] A. Spitz *et al.* [TXL Collaboration], Phys. Rev. D **60**, 074502 (1999) [arXiv:hep-lat/9906009].

[410] T. Manke *et al.* [CP-PACS Collaboration], Phys. Rev. D **62**, 114508 (2000) [arXiv:hep-lat/0005022].

[411] G. S. Bali, K. Schilling and A. Wachter, Phys. Rev. D **56**, 2566 (1997) [arXiv:hep-lat/9703019].

[412] N. Brambilla, private communication, as cited in [419].

[413] S. Narison, Phys. Lett. B **387**, 162 (1996) [arXiv:hep-ph/9512348].

[414] J. L. Rosner, in S. J. Lindenbaum, ed., *Experimental Meson Spectroscopy - 1983*, AIP Conference Proceedings No. 113 (New York: AIP, 1984), p. 46.

[415] T. Barnes, F. E. Close, private communication, as cited in [419].

[416] T. Barnes, arXiv:hep-ph/0103142.

[417] E. J. Eichten and C. Quigg, Phys. Rev. D **49**, 5845 (1994) [arXiv:hep-ph/9402210].

[418] D. Ebert, R. N. Faustov and V. O. Galkin, arXiv:hep-ph/0006186.

[419] A. Heister *et al.* [ALEPH Collaboration], Phys. Lett. B **530**, 56 (2002) [arXiv:hep-ex/0202011].

[420] M. Levtchenko [L3 Collaboration], Nucl. Phys. Proc. Suppl. **126**, 260 (2004).

[421] A. Sokolov, Nucl. Phys. Proc. Suppl. **126**, 266 (2004).

[422] J. Tseng [CDF collaboration], FERMILAB-CONF-02-348-E *Presented at 5th International Conference on Quark Confinement and the Hadron Spectrum, Gargnano, Brescia, Italy, 10-14 Sep 2002*

[423] E. Braaten, S. Fleming and A. K. Leibovich, Phys. Rev. D **63**, 094006 (2001) [arXiv:hep-ph/0008091].

[424] C. Baglin *et al.* [R704 Collaboration], Phys. Lett. B **171**, 135 (1986).

[425] T. A. Armstrong *et al.*, Phys. Rev. Lett. **69**, 2337 (1992).

[426] L. Antoniazzi *et al.* [E705 Collaboration], Phys. Rev. D **50**, 4258 (1994).

[427] M. K. Gaillard, L. Maiani and R. Petronzio, Phys. Lett. B **110**, 489 (1982).

[428] C. Patrignani [for the E835 collaboration], arXiv:hep-ex/0410085.

[429] A. Tomaradze [for the CLEO collaboration], arXiv:hep-ex/0410090.

[430] B. Pietrzyk, "Fit of Standard Model: results on $\alpha_{QED}(M_Z)$ and influence on m_H", Proceeding of "Workshop on Hadron Cross-Section at Low Energies", Pisa, Italy, October 8-10, 2003.

[431] F. Jegerlehner, arXiv:hep-ph/0312372.

[432] B. Lee Roberts, "Results and Prospects on the Measurement of g-2", Proceeding of "Workshop on Hadron Cross-Section at Low Energies", Pisa, Italy, October 8-10, 2003.

[433] M. Davier, "Hadronic contrubition to a_μ", Proceeding of "Workshop on Hadron Cross-Section at Low Energies", Pisa, Italy, October 8-10, 2003.

[434] M. Steinhauser, "The Impact of $\sigma(e^+e^- \to hadron)$ Measurement on the Parameters of Standard Model", Proceeding of "Workshop on Hadron Cross-Section at Low Energies", Pisa, Italy, October 8-10, 2003.

[435] R. R. Akhmetshin *et al.* [CMD-2 Collaboration], Phys. Lett. B **527**, 161 (2002) [arXiv:hep-ex/0112031].

[436] R. R. Akhmetshin *et al.* [CMD-2 Collaboration], Phys. Lett. B **578**, 285 (2004) [arXiv:hep-ex/0308008].

[437] J. Z. Bai *et al.* [BES Collaboration], Phys. Rev. Lett. **84**, 594 (2000) [arXiv:hep-ex/9908046].

[438] J. Z. Bai *et al.* [BES Collaboration], Phys. Rev. Lett. **88**, 101802 (2002) [arXiv:hep-ex/0102003].

[439] J. Burmester *et al.* [PLUTO Collaboration], Phys. Lett. B **66**, 395 (1977).

[440] R. Brandelik *et al.* [DASP Collaboration], Phys. Lett. B **76**, 361 (1978).

[441] J. Siegrist *et al.*, Phys. Rev. Lett. **36**, 700 (1976).

[442] P. A. Rapidis *et al.*, Phys. Rev. Lett. **39**, 526 (1977) [Erratum-ibid. **39**, 974 (1977)].

[443] I. Peruzzi *et al.*, Phys. Rev. Lett. **39**, 1301 (1977).

[444] J. Siegrist *et al.*, "Hadron Production By E+ E- Annihilation At Center-Of-Mass Energies Between Phys. Rev. D **26**, 969 (1982).

[445] G. S. Abrams *et al.*, Phys. Rev. D **21**, 2716 (1980).

[446] G. Goldhaber *et al.*, Phys. Lett. B **69**, 503 (1977).

[447] W. Bacino *et al.*, Phys. Rev. Lett. **40**, 671 (1978).

[448] A. Osterheld *et al.*, SLAC-PUB-4160.

[449] J. Z. Bai *et al.* [BES Collaboration], Nucl. Instrum. Meth. A **458**, 627 (2001).

[450] B. Andersson and H. m. Hu, arXiv:hep-ph/9910285.

[451] E. Eichten, K. Gottfried, T. Kinoshita, K. D. Lane and T. M. Yan, Phys. Rev. D **21**, 203 (1980).

[452] J. C. Chen, G. S. Huang, X. R. Qi, D. H. Zhang and Y. S. Zhu, Phys. Rev. D **62**, 034003 (2000).

[453] F. A. Berends and R. Kleiss, Nucl. Phys. B **178**, 141 (1981).

[454] G. Bonneau and F. Martin, Nucl. Phys. B **27**, 381 (1971).

[455] C. Edwards *et al.*, SLAC-PUB-5160.

[456] M. Eidemuller, J. Phys. G **29**, 1153 (2003) [arXiv:hep-ph/0210247].

[457] G. S. Huang *et al*, "Resonance parameters between $3.7 - 5.0$ GeV from BES data", BES analysis Memo.

[458] D. G. Cassel, "CLEOC and CESR-C: A new frontier of weak and strong interaction", Proceeding of LP2001, 23-28, July 2001, Rome, Italy.

[459] H. S. Chen, "BES III and BEPCII Project", Proceeding of ICHEP2002, 24-31, July 2002, Amsterdam, Holland.

[460] Z. Bai *et al.* [BES Collaboration], Phys. Rev. D **62**, 012002 (2000) [arXiv:hep-ex/9910016].

[461] K. Abe *et al.* [Belle Collaboration], Phys. Rev. Lett. **93**, 051803 (2004) [arXiv:hep-ex/0307061].

[462] J. Z. Bai *et al.* [BES Collaboration], arXiv:hep-ex/0307028.

[463] D. Acosta *et al.* [CDF II Collaboration], Phys. Rev. Lett. **93**, 072001 (2004) [arXiv:hep-ex/0312021].

[464] V. M. Abazov *et al.* [D0 Collaboration], Phys. Rev. Lett. **93**, 162002 (2004) [arXiv:hep-ex/0405004].

[465] B. Aubert *et al.* [BABAR Collaboration], arXiv:hep-ex/0406022.

[466] S. L. Olsen [Belle Collaboration], arXiv:hep-ex/0407033.

[467] S. Pakvasa and M. Suzuki, Phys. Lett. B **579**, 67 (2004) [arXiv:hep-ph/0309294].

[468] M. B. Voloshin, Phys. Lett. B **579**, 316 (2004) [arXiv:hep-ph/0309307].

[469] N. A. Tornqvist, Phys. Lett. B **590**, 209 (2004) [arXiv:hep-ph/0402237].

[470] F. E. Close and P. R. Page, Phys. Lett. B **578**, 119 (2004) [arXiv:hep-ph/0309253].

[471] C. Y. Wong, Phys. Rev. C **69**, 055202 (2004) [arXiv:hep-ph/0311088].

[472] E. Braaten and M. Kusunoki, Phys. Rev. D **69**, 114012 (2004) [arXiv:hep-ph/0402177].

[473] F. Abe *et al.* [CDF Collaboration], Phys. Rev. D **58**, 112004 (1998) [arXiv:hep-ex/9804014].

[474] D0 Collaboration, D0 note 4539-CONF.

[475] A. De Rujula, H. Georgi and S. L. Glashow, Phys. Rev. D **12**, 147 (1975).

[476] M. J. Savage and M. B. Wise, Phys. Lett. B **248**, 177 (1990).

[477] J. G. Korner, M. Kramer and D. Pirjol, Prog. Part. Nucl. Phys. **33**, 787 (1994).

[478] K. Anikeev *et al.*, arXiv:hep-ph/0201071, see references [111-124].

[479] M. Mattson, Ph.D. thesis (Carnegie Mellon University, 2002).

[480] J. Engelfried *et al.*, Nucl. Instrum. Meth. A **431**, 53 (1999).

[481] M. Mattson *et al.* [SELEX Collaboration], Phys. Rev. Lett. **89**, 112001 (2002) [arXiv:hep-ex/0208014].

[482] A. Ocherashvili *et al.* [SELEX Collaboration], arXiv:hep-ex/0406033.